Technical Progress Report: Year 2

Targeting Reserve Growth Opportunities in the Northern Gulf of Mexico Basin: Transferring Secondary Gas Recovery Technology to the Offshore Environment

by

M. V. De Angelo, T. F. Hentz, L. J. Wood, Hongliu Zeng, and R. E. Barba

assisted by

Eugene Kim, Ramiro Amaya, Adrian Badescu, Cem Kilic, Claudia Rassi, and Yujie Hu

prepared for

National Energy Technology Laboratory
U.S. Department of Energy

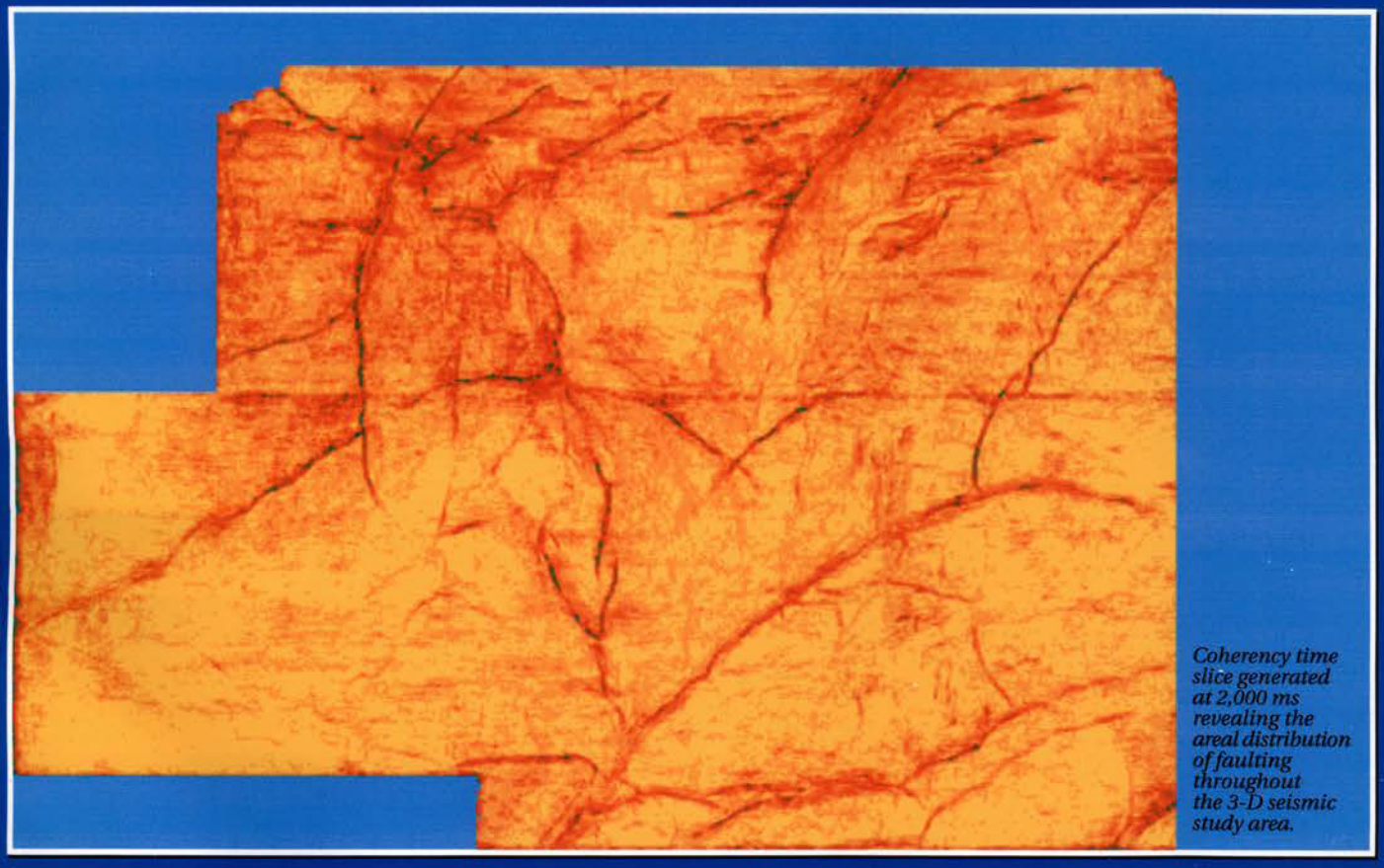

Coherency time slice generated at 2,000 ms revealing the areal distribution of faulting throughout the 3-D seismic study area.

Bureau of Economic Geology
Scott W. Tinker, Director
The University of Texas at Austin
Austin, TX 78713-8924

October 2000

Technical Progress Report: Year 2

Targeting Reserve Growth Opportunities in the Northern Gulf of Mexico Basin: Transferring Secondary Gas Recovery Technology to the Offshore Environment

by

M. V. De Angelo, T. F. Hentz, L. J. Wood, Hongliu Zeng, and R. E. Barba

assisted by

Eugene Kim, Ramiro Amaya, Adrian Badescu, Cem Kilic, Claudia Rassi, and Yujie Hu

prepared for

National Energy Technology Laboratory
U.S. Department of Energy
P.O. Box 10940, 626 Cochrans Mill Road
Pittsburgh, PA 15236-0940

under contract no. DE-FC26-98FT40136

Bureau of Economic Geology
Scott W. Tinker, Director
The University of Texas at Austin
Austin, TX 78713-8924

October 2000

EXECUTIVE SUMMARY

The Bureau of Economic Geology's (BEG) Offshore Secondary Gas Recovery is a multifiscal-year project funded by the U.S. Department of Energy, whose goal is to research new techniques for defining the structure, stratigraphy, and hydrocarbons in a mature area in the northern Gulf of Mexico and to utilize those multidisciplinary methods to identify additional gas resources, as well as predict regional trends in hydrocarbon accumulation. PHASES 1 and 2 of the project work plan (PROJECT PREPARATION and DATA GATHERING AND LOADING, respectively) are completed. PHASE 3 of the plan (DATA ANALYSIS) is 65 percent completed, with all third- and fourth-order key surfaces mapped in the log data. Sixty fourth-order and twelve third-order sequences have been defined using well data, and key flooding surfaces have been mapped in the seismic volume. Structural mapping of 13 key horizons is completed and provides a structural framework within which to look at production and reservoir development. The sequence framework is complete within and immediately between the two fields and provides a basis for examining hydrocarbon occurrence and distribution. Stratal slices of the seismic amplitude data volume have been completed at 4-ms intervals through the data, providing detailed maps of amplitude anomalies associated with quality reservoirs. The process of transforming the seismic attribute volume into a three-dimensional petrophysical volume is progressing, and the addition of an engineer in FY 2001 will initiate development of a fourth-order-level reservoir-flow model within a carefully chosen subset of the data volume. Biannual meetings and continual electronic communication between the BEG and the staff of industry partner, Texaco, have facilitated the exchange of information and ideas to the mutual benefit of both parties. The project scientists have contributed to several development locations, and some

have proven successful. The project is on track of its projected timeline, and it is currently focused on defining opportunities in specific new infield and intrafield play trends, petrophysical analysis of key reservoir units, identification of unperforated and underperforming reservoirs, evaluation of completion practices and suggestion of improvements in process, seismic mapping of third- and fourth-order unconformities, and defining both structural and stratigraphic play trends in these Miocene-age systems. Objectives in the next fiscal year are to map seismic unconformities throughout the 3-D volume; produce a library of isopach, structure, isolith and production maps on key producing horizons; examine migration into productive areas and fault-sealing capacity; produce a portfolio of resource-growth opportunities; and develop enhanced methods for quick interpretation and targeting of productive trends. The FY2001 work will include generating an inversion volume and interpreting general attributes of seismic data, as well as continuing log-facies and parasequence interpretation, fault-seal analysis, examination of resource distribution trends, and petrophysical and engineering analysis on the wells. Identification of new infield and intrafield play trends and un- or undertapped reservoir compartments will continue, and initial booking of additional resources will occur near the end of the year. In addition, work will intensify in investigating the upside potential of the deep (beneath 12,000 ft) portions of the section.

CONTENTS

EXECUTIVE SUMMARY iii
INTRODUCTION 1
Business Drivers for Secondary Gas Recovery 1
Summary of Project Objectives and Key Accomplishments 2
Summary of Progress 6
REGIONAL SETTING AND FRAMEWORK 7
Study Area 7
Regional Stratigraphic Framework 8
Regional Structural Context 9
Reservoir Framework 11
Resource Distribution 11
Sequence-Stratigraphic Framework 12
Sequences 14
Depositional Systems and Systems Tracts 17
GEOPHYSICAL DATA QUALITY AND REPROCESSING 28
Data Quality 28
Interpretation-Oriented Data Processing 29
3-D Seismic Structural Framework 31
Fault-Interpretation Methods 32
Observations 33
Surface Mapping Methods 33
Observations 34
Prospects 36
SEISMIC ATTRIBUTE ANALYSIS AND INTERPRETATION 41
Fluid Modeling 41
Seismic Sedimentology by Stratal Slicing 44
Seismic-Lithology Relationship 44
Stratal Slicing 45
Pattern Recognition and Facies Analysis 46
Seismic Sedimentology 49
Petrophysical Input to the Reservoir Characterization Process 50
Establishing a Petrophysical Model 50
Defining Unperforated and Underperforming Zones 52
Underperforming Pay: Example from Blocks 30 and 31, "Y" Sandstone 53
FY 2001 WORK PLAN 55
ACKNOWLEDGMENT 57
REFERENCES 57

Figures

1. U.S. natural gas demand and production forecasts showing a widening gap between demand and production, indicating needed growth in either imports or domestic production to fill demand.

2. Pie-chart diagrams showing the state of hydrocarbons in the GOM on the shelf, where 55 percent is nonassociated gas, to the deepwater, where only 25 percent is gas and that gas is associated with oil.

3. Gantt Chart of project timeline showing key project phases and events.

4. Map of the Vermilion and South Marsh Areas showing the study's primary target fields, Starfak and Tiger Shoal, as well as surrounding fields and the outline of the two major 3-D seismic surveys being used in this resource assessment.

5. Schematic diagram showing several opportunity types for reserve growth identified within the study area.

6. Schematic summary of structural and stratigraphic intrafield reserve growth opportunities preliminarily defined across the study area.

7. Regional cross section showing the main structural features and stratigraphic packages from northwest to southeast across the Gulf of Mexico.

8. Composite type log of Starfak and Tiger Shoal fields that displays gross stacking patterns, reservoir nomenclature, extinction horizons of invertebrate paleofauna, and stage boundaries.

9. Time-depth-structure map of the Rob. L-4 sand.

10. Structure map of MFS 25.

11. Bar graph of cumulative gas production from all primary sandstone-body reservoirs in Starfak and Tiger Shoal fields.

12. Bar graph of cumulative oil production from all primary sandstone-body reservoirs in Starfak and Tiger Shoal fields.

13. Bar graph of total hydrocarbon production from all primary sandstone-body reservoirs in Starfak and Tiger Shoal fields.

14. Pie charts illustrating relative percentage of oil, gas, and total hydrocarbons produced from specific reservoirs in Starfak and Tiger Shoal fields.

15. Well log cross section of the Rob. L sands, the deepest reservoirs in Starfak field.

16. Coastal-onlap curve of third-order sequences in the uppermost lower Miocene to upper Miocene succession, as interpreted from well log data from Starfak and Tiger Shoal fields.

17. Seismic isochron maps representing thickness between fourth-order maximum flooding surfaces within four successive upper Miocene third-order cycles.

18. Schematic diagram of regional stratal stacking patterns and systems tracts within a third-order sequence.

19. Depositional-dip-oriented cross section of the third-order lowstand systems tract comprising fourth-order SB 35 through 30 within third-order sequence 4 in Starfak field.

20. Amplitude stratal slice of the 12000A sand illustrating the lowstand deltaic wedge and incised-valley fill of third-order sequence 2 within the general area of Starfak and Tiger Shoal fields.

21. Amplitude stratal slice of the M sand illustrating the lowstand deltaic wedge and incised-valley fill of third-order sequence 7 within the general area of Starfak and Tiger Shoal fields.

22. Isochore map of fourth-order sequence 33 in Starfak field.

23. Isochore map of fourth-order sequence 34 in Starfak field.

24. Depositional-dip-oriented seismic profile A–A′ that transects Starfak field.

25. Depositional-dip-oriented seismic profile B–B′ located immediately east of Starfak field.

26. Depositional-dip-oriented seismic profile C–C′ located in the undrilled area between Starfak and Tiger Shoal fields.

27. Bar graph of cumulative gas production from the 10 third-order lowstand systems tracts in Starfak and Tiger Shoal fields.

28. Bar graph of cumulative oil production from the 10 third-order lowstand systems tracts in Starfak and Tiger Shoal fields.

29. Bar graph of total hydrocarbon production from the 10 third-order lowstand systems tracts in Starfak and Tiger Shoal fields.

30. Isochore map of fourth-order sequence 40 in Starfak field.

31. Map of the Vermilion Block 50 and south Marsh Island Areas showing the outline of the two major 3-D seismic surveys being used in this resource assessment.

32. Interpretive advantage of 90°-phase wavelet.

33. A 0°-phase (original) seismic section tied to wells in Starfak field.

34. A 90°-phase (reprocessed) seismic section tied to wells.

35. Continuity time slice at 2,100 ms showing a sharp and complete regional fault system in the shallower section.

36. Continuity time slice at 3,700 ms illustrating numerous small, subtle faults in the area between Starfak and Tiger Shoal fields and to the northwest of Starfak field in the deeper section.

37. Spectral balancing of deep data, before processing and after processing.

38. Coherency time slice generated at 2,000 ms revealing the areal distribution of faulting throughout the 3-D seismic study area.

39. Conventional time slice extracted from the 3-D seismic amplitude volume.

40. Vertical seismic profile showing structural (rollover), stratigraphic (bright spot), and fault interpretations of first- and second-order normal faults.

41. Vertical seismic profile showing an "hourglass" feature associated with transecting faults.

42. Time-structure map of maximum flooding surface 2 depicting the subsurface topography associated with the five major producing fields.

43. Time-structure map of the Robulus 4 sand with associated second-order fault swarms in Starfak field.

44. Prospect 1 location posted on a time-structure map of MFS16.

45. Vertical seismic cross section (A–A′) of prospect 1.

46. Prospect 2 and 21 locations posted on a time-structure map of MFS26.

47. Vertical seismic cross sections of prospect 2.

48. Prospect 3 and 6 locations posted on a time-structure map of the Robulus 2 sand.

49. Vertical seismic cross sections of prospect 3.

50. Prospect 4, 5, and 9 locations posted on a time-structure map of the Robulus 2 sand.

51. Vertical seismic cross sections of prospect 4.

52. Vertical seismic cross sections of prospect 5.

53. Vertical seismic cross sections of prospect 6.

54. Prospects 7 and 10 posted on a time-structure map of MFS30.

55. Vertical seismic cross sections of prospect 7.

56. Prospect 8 location posted on a time-structure map of MFS40.

57. Vertical seismic cross sections of prospect 8.

58. Vertical seismic cross sections of prospect 9.

59. Vertical seismic cross sections of prospect 10.

60. Prospect 11 location posted on a time-structure map of MFS24.

61. Vertical seismic cross sections of prospect 11.

62. Prospect 12 and 17 locations posted on a time-structure map of the Robulus 2 sand.

63. Vertical seismic cross sections of prospect 12.

64. Prospect 13 and 14 locations posted on a time-structure map of MFS16.

65. Vertical seismic cross sections of prospect 13.

66. Vertical seismic cross sections of prospect 14.

67. Prospect 15 location posted on a time-structure map of MFS26.

68. Vertical seismic cross sections of prospect 15.

69. Prospect 16 location posted on a time-structure map of the Robulus 2 sand.

70. Vertical seismic cross sections of prospect 16.

71. Vertical seismic cross sections of prospect 17.

72. Prospect 18 location posted on a time-structure map of MFS40.

73. Vertical seismic cross sections of prospect 18.

74. Prospect 19 location posted on a time-structure map of MFS13.

75. Vertical seismic cross sections of prospect 19.

76. Prospect 20 location posted on a time-structure map of MFS45.

77. Vertical seismic cross sections of prospect 20.

78. Vertical seismic cross sections of prospect 21.

79. P-velocity and density curves selected from wells 30-2 and 31-16.

80. P-velocity of clean sandstone and shale against depth with trend lines.

81. Bulk density of clean sandstone and shale against depth with trend lines.

82. Acoustic impedance trend lines of brine-saturated sandstones, shale, and hydrocarbon-saturated sandstones.

83. Reflection coefficient trend lines related to brine-saturated sandstones and hydrocarbon-saturated sandstones.

84. Acoustic impedance as an indicator of lithology.

85. Cross section A–A′ in Starfak field showing well-to-seismic correlation in two-way traveltime.

86. Amplitude stratal slices showing a Pliocene coastal plain, upper Miocene incised valley fill, and an upper Miocene highstand-shelf delta system.

87. A four-stratal-slice series showing the migration of IVF's in geologic time.

Tables

1. Distribution of reserves and production data by geologic age for the Gulf of Mexico, showing the Miocene-age reservoir resources leading all categories, including remaining proved reserves

2. Texaco-designated sandstone-body reservoirs in Starfak and Tiger Shoal fields

3. Cumulative gas production from all sandstone-body reservoirs in Starfak and Tiger Shoal fields

4. Cumulative oil production from all sandstone-body reservoirs in Starfak and Tiger Shoal fields.

5. Total hydrocarbons produced from all sandstone-body reservoirs in Starfak and Tiger Shoal fields

6. Cumulative gas production from all sandstone-body reservoirs within the third-order lowstand systems tracts in Starfak and Tiger Shoal fields

7. Cumulative oil production from all sandstone-body reservoirs within the third-order lowstand systems tracts in Starfak and Tiger Shoal fields

8. Total hydrocarbons produced from all sandstone-body reservoirs within the third-order lowstand systems tracts in Starfak and Tiger Shoal fields

9. Hydrocarbon properties from production data

10. Brine and rock properties

Plates

1. Detailed timeline and project task description for the offshore SGR Project ..... in pocket

2. West-east regional strike cross section of Starfak and Tiger Shoal fields, illustrating correlation of fourth-order sequence boundaries, maximum flooding surfaces, and transgressive surfaces between the two fields..... in pocket

INTRODUCTION

Business Drivers for Secondary Gas Recovery

Natural gas is projected by many analysts to surpass oil and liquid gas and dominate the market in the United States within the next decade, if not sooner (Hefner, 1993; Fisher, 1999). Recent projections by Lore and others (1999) show natural-gas demand reaching approximately 32 Tcf by 2015. Although production is also expected to increase, the gap between demand and production that must be filled by imports is projected to continue to widen (fig. 1) throughout the coming 20 yr. Projected declines in natural-gas production indicate that existing gas reserves in proven fields on OCS lands will be nearly depleted by 2020. In the absence of significant changes in resource estimates, technology, investment or discovery sizes, the U.S. Mineral Management Service has projected that the Federal OCS will be unable to maintain its current level of contribution toward meeting the Nation's demand for natural gas past the year 2020 (Lore, 1999).

The Gulf of Mexico (GOM) currently provides more than one-quarter of the natural gas produced in the United States and is projected to contain approximately 16 percent of the proven natural gas reserves nationwide (Lore and others, 1999). Within the GOM, Miocene-age strata contain the dominant share of original and remaining proven gas reserves (table 1; Lore and others, 1999). Of the 67.3 Tcf discovered to date, 54.6 Tcf has been produced and another 12.7 Tcf remains to be recovered. These reserves represent 41 percent of the total remaining proven recoverable reserve in the GOM and constitute a significant proven reserve waiting to be recovered. These Miocene-age resources are found almost exclusively in shelf water depths of less than 200 m amid existing infrastructure. Recent declines in per capita performance on the

GOM shelf and improvements in deep-drilling technology have spurred the movement of large companies to search for hydrocarbons in deep water. Oil is the dominant product in deep-water provinces, the majority of gas found in association with oil (fig. 2). Therefore, although 80 to 140 Tcf of gas is potentially producible over the next 50 yr from fields located in deep-water regions, its association with oil complicates the economics, cycle time, needed technology, and infrastructure associated with its development (Lore and others, 1999). Although a larger share of overall gas demand is expected to be met by deep-water fields over the next 15 yr, there is a significant need to arrest the slow decline in shelf-bound gas production if the outer continental shelf (OCS) is to continue viably contributing to the Nation's energy future. With more than 41 percent of proven, recoverable GOM natural-gas resources remaining to be produced from shelf-bound fields and more remaining to be booked as resources, there is a strong need for new play concepts to revitalize existing fields on the modern shelf. In addition, new process designs and imaging tools for reducing uncertainty in exploration and production will enable small and large companies to arrest the decline in capital performance on the GOM shelf and maintain their interests. Such objectives are inherent in the goals of the Secondary Gas Recovery research program.

Summary of Project Objectives and Key Accomplishments

The Offshore Secondary Gas Recovery (OSGR) project began October 1998 as a 4-yr joint research venture between the Bureau of Economic Geology (BEG) and the U.S. Department of Energy (DOE). The project is an outgrowth of a previous DOE-sponsored BEG project that produced the *Atlas of Northern Gulf of Mexico Gas and Oil Reservoirs, Volumes 1 and 2* (Hentz and others, 1997; Seni and others, 1997). The OSGR project is focused on practical application of products from the atlas study and providing owners of offshore GOM

leases a process-oriented road map for increasing hydrocarbon reserves and their asset base. The goals of the OSGR project are multifold and include research in new techniques and methods in defining the structure, stratigraphy, and hydrocarbon character in a major field in the northern GOM and to utilize those multidisciplinary techniques and methods to identify additional gas resources, as well as predict regional trends in hydrocarbon accumulation. The specific objectives of the project are to (1) increase reserves, (2) prioritize newly identified prospects and development opportunities, (3) develop and apply new technologies, (4) create transferable knowledge, and (5) achieve these objectives using quality products in a timely fashion. The objectives of the project will be achieved by completing a nine-phase work plan and the tasks associated with that work plan (fig. 3; plate 1).

The two fields under study are Tiger Shoal and Starfak fields in the Vermilion and South Marsh Island Areas, northern GOM (fig. 4). Although originally designed to look at data from a single field, the project has evolved to encompass two fields in detail, as well as to consider surrounding fields of Mound Point, Lighthouse Point, and Amber. This evolution reflects our desire to consider more regional applicability of research results: to move from the postage-stamp application of research results from a single field to the broader distribution of observations throughout the GOM Miocene. Phases 1 (PROJECT PREPARATION) and 2 (DATA GATHERING AND LOADING) of the project plan are completed. Significant progress has been made in DATA ANALYSIS (Phase 3), involving mapping of key horizons in seismic and well logs and the outgrowth of new play concepts and ideas in reservoir architecture. In addition, stratal-slice technology (Zeng, 1998a, b; 2000) has proved to be a quick-look tool of great value when bright-spot prospecting for valley fills, a major resource reservoir type across the study area. We are currently constructing approaches to quick-map reservoir bodies within

this data volume and to generate 3-D visualization of the reservoir/seal system. Two meetings were conducted this year with Texaco personnel in our Austin research facility. Ongoing interactions with Texaco's development team resulted in several successful development-well proposals and successfully drilled prospects. In addition, our staff petrophysicist and engineer traveled to Texaco's offices in New Orleans to facilitate obtaining production data. Texaco has been active in review meetings with DOE and has actively sought BEG staff input into drilling decisions. Texaco has been an excellent industry partner, proactive in providing information and receptive to all requests.

The team has achieved our Year Two project objective, reaching a point in the technical work and generation of technical products where we can begin providing input into ongoing development drilling for our industry partner. In addition, we are providing a portfolio of reserve growth opportunities to Texaco to facilitate development of Starfak and Tiger Shoal fields. A summary of preliminary resource-growth opportunities is included herein (Prospects) that include new interfield reservoirs, untapped reservoirs and compartments, and incompletely drained reservoirs and compartments, as well as new intrafield resource-growth opportunities (fig. 5). Production information from the fields suggests homogeneity within specific reservoir systems and horizons; however, preliminary assessment of the data suggests great opportunity for finding new intrafield reservoirs in the study areas. Previous researchers (Finley and Tyler, 1994) have suggested that new infield reservoirs provide the largest incremental resource-growth additions in secondary-resource-assessment studies. Intrafield resource play trends provide a whole new level of resource-growth opportunity and are defined herein as those existing outside the defined structural closure of existing fields, but between fields, and well within reach of existing infrastructure. Therefore, our focus includes both structural and stratigraphic

opportunities in this reserve growth prospect class, as well as analysis of infield new, untapped, and incompletely drained reservoir systems (fig. 5).

The Gantt Chart shown in plate 1 illustrates the current status of technical assessment in the study areas. The petrophysical and engineering analysis of unperforated and underperforming reservoirs is well under way and has yielded several opportunities that will be conveyed to our industry partner. In addition, identification of these opportunities lends insight into potential technology improvements for increasing performance and providing resource growth. Time-depth maps integrated with amplitude maps provide a basis for defining new inter- and intrafield opportunities, both structural and stratigraphic. Well log cross sections completed within, between, and extending outside of structural closures that define the two fields provide a basis for understanding reservoir distribution in structural opportunities and potential stratigraphic traps.

As the end of the calendar year approaches, we have begun to compile specific resource-growth opportunities associated with specific play trends unique to Miocene-age systems in the northern Gulf. These trends are summarized in fig. 6. Trends and specific opportunities will be compiled in a series of horizon-focused portfolio maps, each of which will document potential plays, prospects, and recompletion opportunities at those horizons and summarize the additional resource potential available at minimum, most likely, and maximum risk, as well as at certainty. In addition, we will devote increasing time to evaluating the upside potential that exists in the deeper strata and depositional facies of the area. Modeling will begin in earnest in the coming year through evaluation of software for integration of geophysical, geologic, and petrophysical data in a 3-D format and build toward an eventual flow simulation along high-priority horizons to be selected by the BEG and Texaco.

Summary of Progress

The project's technical analysis is currently on schedule with our project plan (fig. 1; plate 1). We have completed the populating, quality checking, and cleanup of the digital data bases, including all well log files. As stated in previous reports, our study area includes two target fields: Starfak and Tiger Shoal. In addition, we have requested (and Texaco has gladly provided) select, adjacent, regional well locations to aid in evaluating issues associated with regional sequence stratigraphy and intrafield resource potential. We are continuing to search for whole core, as well as downhole flow test data, to aid in petrophysical and engineering analysis. Upcoming drilling plans by Texaco offer additional opportunities for more data that will be included in the data base if possible. We have provided Texaco with a clean, searchable Oil Field Manager (OFM) data base, which is significantly improved from the original, and they will provide future updates using the improved OFM. Well log correlation of key lithostratigraphic and chronostratigraphic surfaces in both third- and fourth-order cycles has been completed to the systems-tract level, thought to be the level of stratigraphic control on hydrocarbon distribution. Third-order regional flooding surfaces have been integrated between the wells and the 3-D seismic and have been mapped throughout the data volume, providing structure maps at 13 key horizons. In addition, several of these flooding events provide the bounding surfaces for initial isopach mapping of third-order genetic sequences. Some more detailed mapping of fourth-order surfaces and isopaching of associated intervals have been initiated as a check on the level of map-defined detail available in the well logs and seismic data sets. We are attempting several approaches to quick-mapping the seismic attributes and stratal-slice data volumes, in hopes of providing improved methodology, which maximizes the value of these data.

Seismic modeling has been completed for defining seismic response to various fluids and pressures, and products are assisting in defining an approach to utilizing amplitude as an

indicator of lithology and fluid type within the data volume. Additional work is anticipated in this area as an outgrowth of ongoing petrophysical analysis. Initial seismic modeling indicates a close association between amplitude and grain size, as well as amplitude and product type above approximately 12,000 ft. This relationship, coupled with the high signal-to-noise ratio of the data, allows sharp delineation of sand-prone depositional elements, such as incised valleys, channels and lowstand prograding wedges, and bright-spot analysis, for hydrocarbons within favorable traps. Finally, the interpretation of deep structural and stratigraphic elements (> 3 s) is key to defining the deep-gas potential of the area. Much of the upside potential is thought by the team and our industry partners to reside in these deeper horizons. These areas will be the focus of continued mapping and reservoir assessment.

Texaco plans to provide the team with a current (ca. 1990) estimate of resources in the fields. The BEG team will appraise this estimate and provide new resource numbers following completion of the technical evaluation. In addition, Texaco's active drilling program throughout the coming year will provide much feedback on selected prospects and play types.

REGIONAL SETTING AND FRAMEWORK

Study Area

Starfak and Tiger Shoal fields are located in offshore Louisiana immediately north of the Salt Deformation Province. Although the area's large-scale structural folds are a product of deep salt movement, geologic conditions in the area are structurally simple as compared with the complex diapiric deformation that occurs to the south (fig. 7). The fields are associated with several subregional normal faults and associated antithetic faults that are responsible for

additional structural partitioning within these two large fields. The primary foci of this study, Starfak and Tiger Shoal fields, have been owned and operated by Texaco Exploration and Production, Inc., since the late 1950's. Current resource-in-place estimates for Starfak are approximately 316 Bcf gas and 13.3 MMbbl oil, and for Tiger Shoal estimates are 3.1 Tcf gas and 35.9 MMbbl oil. Reservoirs are Miocene-age facies of coastal-plain, shelf, slope and basin-floor depositional systems stacks in an overall shallowing-up succession 20,000 ft thick. Sinuous, digitate, and lobate geometries associated with the system's depositional elements are readily apparent on regional horizontal seismic-attribute slices. Abundant wells across the fields (155 total) provide ample quantitative petrophysical, production, and engineering data for constraining seismic and flow-unit correlations, assessing the influence of fluid, lithology, and pressure on seismic and well log response and accurately modeling past and future reservoir performance.

Regional Stratigraphic Framework

Starfak and Tiger Shoal fields produce hydrocarbons from sandstones in most of the Miocene Series (upper lower to upper Miocene), which in the two fields forms a dominantly regressive, progradational succession as much as 10,000 ft thick (fig. 8). The lower part of the reservoir-bearing interval (upper lower Miocene) is characterized by approximately 3,000 ft of mostly slope and basinal depositional facies: lowstand basin-floor fan, slope-fan, and lowstand-deltaic-wedge depositional facies. Shale-dominated slope-fan deposits, each deposit as much as about 1,000 ft thick, compose the major portion of this lower zone. At about 13,000 ft, this succession is overlain by a 7,000-ft-thick upper zone of a mostly on-shelf and significant, but volumetrically minor, off-shelf lowstand depositional facies that exhibits a grossly increasing abundance of sandstone upward (middle and upper Miocene). Cyclic distal highstand, distal

transgressive, and lowstand prograding-wedge and distal incised-valley-fill facies in the basal part of this upper zone grade upward into progressively more proximal, cyclic highstand, transgressive, and incised-valley-fill facies. A thick succession of aggradational fluvial coastal-plain deposits occur only a few hundred feet above the reservoir-bearing study interval. This upward-shallowing trend of depositional facies coincides with that of the entire Miocene interval in the offshore northern Gulf of Mexico (Seni and others, 1997). Paleontological data from selected wells indicate that the 10,000-ft section from the oldest reservoir (*Robulus* L-8 sand) at the base of the study interval to the uppermost reservoir (A sand) represents about 16.5 m.y. of deposition and ranges in age from early Miocene (~23 mya) to latest Miocene (~6.5 mya) (Fillon and others, 1997).

Regional Structural Context

Starfak and Tiger Shoal fields are located in the Oligocene-Miocene Detachment Province of the northern Gulf Coast continental margin (Diegel and others, 1995). This region is generally characterized by large-displacement, dominantly down-to-the-basin listric growth faults that sole on a regional detachment zone above the Oligocene section. Regional deformation is a product of salt mobilization. Its origin is either the level of the autochthonous Jurassic Louann Salt or the detachment zone for the growth faults represented by a salt weld that formerly contained a thick, allochthonous salt body (Diegel and others, 1995). A characteristic feature of this province is the great thickness of deltaic and other on-shelf sediments above the detachment zone, typically exceeding 3 mi. This remarkable stacking of deltaic/shelf sandstone reservoirs helps make this province one of the world's great petroleum provinces, of which Starfak and Tiger Shoal fields are part.

Geologic conditions in the greater two-field study area are structurally simple compared with those of the complex, diapirically deformed strata that occur to the south. The two fields are associated with several subregional normal growth faults and related ancillary faults that cause additional structural partitioning. One first-order growth fault transects Starfak and Tiger Shoal fields; however, at least five first-order, large-displacement faults occur in the entire area of seismic coverage. First-order growth faults, as opposed to second-order faults, are characterized by large apparent offsets (>500 ft of maximum offset), and they extend from near the seafloor to below the maximum depth of seismic coverage (4.4 s, ~18,000 ft). Second-order faults occur having both growth and nongrowth geometries and in typically much shorter segments having smaller amounts of apparent offset. A first-order, broadly arcuate, west-east-trending growth fault cuts the north part of the two fields and acted as a primary control on basin geometry and depositional-systems-track development during the early Miocene (figs. 9, 10). A narrow zone of second-order, north-south-trending growth faults roughly bisects Tiger Shoal field, generally separating primarily gas producing reservoirs in the west part of the field from primarily oil reservoirs in the east (fig. 10). Second-order, deep-seated, east-west-trending faults extend from Starfak field into a broad structural low (saddle) between the two fields (fig. 9).

Structurally, Starfak field is characterized by (1) the first-order, arcuate, west-east-trending growth fault with approximately 600 ft of apparent offset in the field and (2) by the deep-seated, east-west-trending faults that bound rotated fault blocks. The up-section termination of these smaller, lower offset faults is generally at about 11,500 ft; the basal soles of these normal faults are deeper than the range of seismic coverage. Structurally trapped hydrocarbons are being produced from rollover anticlines against the first-order growth fault and from deep

zones in the rotated fault blocks. In contrast, structural traps in Tiger Shoal field are generally anticlines cut by the second-order, north-south-trending faults.

Reservoir Framework

In all, 62 Texaco-designated reservoirs gas and oil reservoirs occur within Starfak and Tiger Shoal fields: 15 in Starfak and 47 in Tiger Shoal (table 2). In accordance with Texaco's established reservoir nomenclature, these sandstone-body reservoirs are named, in descending order, A through Z sands (some are variously subdivided using alphanumeric designations, such as T-1 sand and M-1 [lower] sand), 12000 A sand, 12000 B sand, and the *Robulus* L-1 through *Robulus* L-8 sands (fig. 8). Reservoir sandstones range in depth from about 6,200 to 16,200 ft in Starfak field and 6,000 to 15,400 ft in Tiger Shoal field.

Many of the Texaco-designated reservoir sandstones approximately coincide with key sequence-stratigraphic (chronostratigraphic) boundaries that are discussed in the section, Sequence-Stratigraphic Framework. Among other benefits, this coincidence greatly aided in the precise correlation of sandstone-bearing intervals across the 4-mi undrilled saddle between Starfak and Tiger Shoal fields (fig. 9). With only two exceptions, Texaco-designated reservoir sandstones are approximately correlative between the fields. The Texaco-designated E and L sand reservoirs in Starfak and Tiger Shoal fields are not time-stratigraphic equivalents between the two fields, although the true equivalents are within only 100 to 150 ft of the miscorrelated intervals.

Resource Distribution

Starfak field, discovered in 1975, comprises 53 wells, most of which are gas producers. Starfak produces gas from 13 primary reservoirs and oil from 12 reservoirs (figs. 11 through 13;

tables 3 through 5). Texaco differentiates 15 reservoirs in the field (table 2); however, for the purposes of simplification, the T-1A and T1-B reservoirs are herein consolidated into the T-1 reservoir. Tiger Shoal has produced gas and oil since 1958 from 103 wells. Oil wells are located primarily on the east side of the field, mainly in Block 217. Productive sandstones generally occur stratigraphically higher in Tiger Shoal wells than in Starfak wells. Tiger Shoal produces from 27 primary reservoirs. Of the 47 total reservoirs designated by Texaco (table 2) in Tiger Shoal, only these 27 primary units are represented in figures 11 through 13 because each has contributed more than about 3 percent of cumulative production. In Starfak, the 12000A, Rob L-2, and U sands have produced the most gas and oil, whereas the T-1, Y, and N sands are the most prolific hydrocarbon reservoirs in Tiger Shoal (fig. 14).

Sequence-Stratigraphic Framework

Paramount among the tasks of the project is construction of a detailed chrono- and sequence-stratigraphic framework for the 10,000-ft reservoir-bearing interval in Starfak and Tiger Shoal fields and recognition of the producing reservoirs within the systems-tract framework. This approach provides a firm genetic context for all other primary and ancillary phases of the project, including structural, geophysical, petrophysical, and various mapping phases. Moreover, it establishes the critical groundwork for focusing study on reservoir-specific attributes and the identification of previously undetected hydrocarbon prospects within both the two-field area and within the entire 3-D seismic volume. By providing a fundamental and accurate correlation framework based largely on chronostratigraphy, the sequence-stratigraphic approach promises an enhanced understanding of the spatial and temporal distribution of reservoir, seal, and potential source facies; reservoir compartmentalization; and pay continuity in the study area.

We reported on the initial results of the sequence-stratigraphic framework in our Technical Progress Report of the project's first year (Hentz and others, 1999). In the second year of the project, we solidified this framework by differentiating additional fourth-order (~0.2- to 0.5-m.y. duration) sequences, notably in the Robulus L sandstone succession (fig. 15), and by defining third-order sequences (~1.5 m.y. duration) for more precise correlation of genetic units between Starfak and Tiger Shoal fields. Third- and fourth-order sequence boundaries mark pronounced fieldwide erosional surfaces and their correlative surfaces of exposure. Delineating additional key chronostratigraphic (sequence boundaries) and regionally diachronous (maximum flooding surfaces and transgressive surfaces of erosion) has enabled us to more accurately identify sandstone-bearing depositional systems tracts within the reservoir-bearing succession, predict the areal geometry of sandstone-body reservoirs and reservoir flow units, and form a robust reference system within which all engineering, production, and petrophysical data can be placed. Moreover, this model allows correlation between the sequence framework and regional production data (see Relation of Production to Systems Tracts), interpolation of these key surfaces within and between the field areas, extrapolation of the maximum flooding surfaces within the 352-mi^2 area of seismic coverage, and prediction of field-scale and regional depositional attributes. The ability to extrapolate the maximum flooding surfaces throughout the area of seismic coverage is an especially critical achievement because it enables (1) accurate mapping of regional structure at numerous horizons that bound productive zones, thus defining trapping structures, and (2) correlation of the primary plays (identified in Starfak and Tiger Shoal fields) within the entire seismic area (for example, the prolific third-order lowstand systems tracts, discussed later). These accomplishments can extend our knowledge of hydrocarbon prediction in Miocene strata in other areas of the northern Gulf of Mexico. The sequence-

stratigraphic framework of the Miocene Series can be readily applied to surrounding offshore fields, especially if complemented by paleontological data to improve correlation confidence.

Sequences

Fourth Order

The 9,000- to 10,000-ft reservoir-bearing Miocene interval in Starfak and Tiger Shoal fields comprises at least 60 fourth-order sequences, each of which records an average of about 0.25 m.y. Thickness of fourth-order sequences ranges from less than 50 ft to approximately 500 ft. Thick, shale-dominated intervals (for example, between sequence boundaries [SB] 47 and 48, and 29 and 30) certainly contain additional, unidentified fourth-order sequences; however, the bounding surfaces of these sequences are not clearly resolvable using well log and seismic data. In almost all instances, fourth-order sequence boundaries occur at the top, base, or within the Texaco-designated reservoir sandstones (plate 2). Therefore, in the study area, fourth-order sequences best define reservoir-scale attributes. Details of the log character, depositional context, and further relations of these fourth-order sequences to the large-scale sequence-stratigraphic framework are discussed in following sections (Depositional Systems and Systems Tracts).

Third Order

The 10 third-order sequences in the study interval, which represent an average duration of about 1.5 m.y., are bounded by SB 59, 48, 41, 35, 28, 23, 19, 13, 11, and 4 (plate 2; fig. 16). Third-order parasequence stacking patterns in the two fields define coastal onlap that generally coincides with that of Exxon researchers (Haq and others, 1988). The agreement of most of these published basin-scale, time-stratigraphic boundaries and those independently derived for this study improves confidence in the designation of sequence boundaries in the two-field study area. However, we have delineated three third-order cycles between 10.5 and 8.2 m.y. (between

fourth-order SB 23 and 11), a time interval that Haq and others (1988) identified as representing one third-order cycle (fig. 16). Other researchers also independently concluded that there are multiple third-order cycles within this time range (Styzen, 1996; H. E. Denman, personal communication, 1999). The bases and tops of these additional cycles coincide with locally well developed fourth-order lowstand systems tracts (incised-valley fills) at SB 19, 13, and 11 (plate 2). Absolute ages of sequence boundaries and maximum flooding surfaces depicted in figure 16 are derived from Haq and others (1988), but they closely approximate ages derived from paleontological data collected from the two fields.

Seismic isochron maps (fig. 17) illustrate the overall progradation and basinward shift of on-shelf and basinal systems tracts within (and continuing throughout) the upper group of third-order cycles within the whole area of seismic coverage. Areas of thinnest sediment on the maps are inferred to represent primarily on-shelf, proximal highstand-delta deposits and starved-shelf and -basin sediments. Adjacent areas of south- and southeast-thickening strata record basinward expansion of medial and distal deltaic successions, although extensive lowstand incised-valley fills are also prominent components. Shelf-edge position was identified by amplitude stratal slicing. Progradation occurred during overall rising relative sea level, indicating that the high rate of sediment supply that characterizes deposition during the Miocene in the Gulf Coast Basin exceeded the rate of eustatic rise.

We have delineated the specific third-order sequences in the study interval, which vary from approximately 500 to 1,800 ft in thickness. They are designated 1 through 10 in plate 2. The well log expression of this low-order cyclicity is best illustrated within the distal and medial on-shelf portion of the study interval between SB 41 and 13 (sequences 3 through 7, plate 2). In this gross interval, each third-order sequence comprises (1) a series of relatively thin, closely

spaced fourth-order sequences at the base, commonly with pronounced lowstand-valley incision in the lowermost fourth-order sequences (plate 2); overlain by (2) an atypically thick (as much as 150 ft) transgressive systems tract; and (3) an upper section of typically two to four thick, fourth-order highstand systems tracts and interstratified thin transgressive systems tracts. Commonly these fourth-order highstand systems tracts decrease in thickness and become progressively more sandstone-rich upward. Third-order sequences 4 and 5 (between SB 35 to 28 and SB 28 to 23, respectively) best exemplify these features (plate 2). The basal series of thin, fourth-order sequences (bounding incised-valley fills and distal highstand and transgressive systems tracts) and laterally equivalent fourth-order lowstand prograding wedges (for example, SB 35 to 30 in sequence 4) collectively compose the third-order lowstand systems tract. The middle thick transgressive systems tract (between SB 30 and MFS 30) is the third-order transgressive systems tract, and the upper succession of thick fourth-order highstand systems tracts and interstratified thin transgressive systems tracts (between MFS 30 and SB 28) collectively represent the third-order highstand systems tract (fig. 18).

Variation of this most common third-order stacking pattern occurs in the basal part of the study interval (below ~12,700 ft), where distal-shelf, shelf-edge, and slope facies predominate, and in the uppermost part of the study interval, which is characterized by proximal on-shelf facies. The two basal sequences (sequences 1 and 2, plate 2) vary from the just-described, most common third-order stacking pattern because of their distal position relative to the basin profile. They contain mostly lowstand deposits (deltaic wedge and slope fan), which display different stacking patterns. Specifics about these deposits are discussed in a later section (Depositional Systems and Systems Tracts). In the uppermost part of the study interval (sequences 8 through 10, plate 2), proximal fourth-order sequences that compose the third-order sequences are thin and

richer in sandstone than the underlying sequences (plate 2), aspects that tend to obscure the separate progradational and retrogradational successions that are used to define systems tracts.

Second Order

SB 23 (base of the N-sand zone, which includes N-1 and N-2) also coincides with a second-order boundary of Haq and others (1988) (fig. 16). The N-sand zone consists of a pair of closely juxtaposed incised-valley-fill deposits that extend throughout Starfak and Tiger Shoal fields (plate 2). Seismic data indicate that they probably also record two major episodes of temporally closely spaced incision in the area of no well control between the fields. The middle Miocene N-sand valley fills collectively represent a maximum of more than 300 ft of incision and, therefore, apparent base-level fall in the medial on-shelf area.

Depositional Systems and Systems Tracts

Using the sequence-stratigraphic approach, we can identify systems tracts on at least two scales (third and fourth order), depending on the magnitude and duration of relative sea-level variation. Systems tracts comprise an array of depositional systems that we can interpret using log-facies patterns. No whole cores were available for this study. Systems tracts become increasingly more proximal upsection, grading from lowstand basin-floor-fan, slope-fan, and prograding-wedge deposits in the lower Miocene section to proximal lowstand incised-valley-fill, highstand, and transgressive accumulations in the upper Miocene section. Older, fourth-order sequences are approximately 100 to 500 ft thick and are inferred to be distal deltaic/strandplain systems within highstand and transgressive tracts and basin-floor-fan and overlying slope-fan deposits within lowstand prograding wedges. Locally thick (~250 ft) incised-valley fills contain inferred fluvial deposits and sandy transgressive bayhead-deltaic and shaly estuarine facies. Conversely, younger sequences, less than 50 to about 200 ft thick, exhibit

blockier, fluvial-dominated, lowstand incised-valley fills and proximal, sandy highstand and transgressive deltaic and strandplain systems.

Lowstand Systems Tract

The lowstand systems tract includes four depositional components: basin-floor fan, slope fan, lowstand deltaic wedge, and incised-valley fill. The first three components compose the lowstand prograding wedge. All four elements are collectively represented in Starfak and Tiger Shoal fields.

Basin-Floor Fan.—Sandstones that originated as inferred basin-floor fans are the stratigraphically lowest potential reservoir facies in the study interval. The bases of these fans coincide with at least one third-order sequence boundary at the boundary's most distal (basinward) extent. The fan sandstones occur exclusively in the Robulus L zone (third-order sequence 1, plate 2). Two sandstone-bearing, basin-floor-fan deposits can be correlated in Starfak field; they mark the bases of SB 59 (Rob. L-7) and SB 60 (Rob. L-8) (fig. 15). The well-developed Rob. L-7 sandstone at SB 59, which is as much as 230 ft thick, is inferred to be a major, third-order basin-floor fan at the base of the third-order sequence containing most of the Robulus L sands. The Rob. L-8 sandstone at SB 60 is also probably a third-order basin-floor fan; however, because this portion of the study interval is only sparsely penetrated by wells, no firm conclusions in this regard can be drawn. The overlying sandstones at SB 56 to 58 are inferred to represent fans of channel-levee complexes within slope deposits of the Robulus L third-order sequence (sequence 1, plate 2). They are thinner (20 to 60 ft thick) and more localized within Starfak field than the third-order fans. However, because they can be correlated throughout the field and commonly occur at the bases of large-scale (~200- to 300-ft-thick), upward-fining, shaly, slope-fan successions, they are inferred to mark fourth-order sequence boundaries.

Slope Fan.—Slope-fan deposits, which downlap on the basin-floor fan, include the thick (as much as 1,000 ft) shale-dominated successions in the bottom parts of the basal two third-order sequences (plate 2). These deposits compose the basal 30 percent of the drilled Miocene section in the deeper wells. Approximately 90 to 95 percent of these deposits are shale. Gamma-ray curves of these deposits display the characteristic broadly (over several hundreds of feet) sinusoidal log signature that records well penetration of upper, medial, and lower slope facies. Further details of this facies is presented the discussion of third-order sequence 1 below.

Lowstand Deltaic Wedge.— Lowstand deltaic wedges are composed of sandstone-dominated progradational units that are restricted seaward of the shelf edge and that onlap the slope of the underlying sequence. These wedges are well defined in the 3-D seismic volume and compose about 10 to 20 percent of the overall section in Starfak field. In the study area, wedges occur as distinct, single-event progradational units (fourth-order sequences) and as zones of stacked fourth-order progradational units that form portions of third-order lowstand prograding wedges (figs. 15, 19). Generally sandstone-rich progradational parasequence sets that range from 50 to 300 ft in thickness form the fourth-order deltaic wedges, which represent deltaic progradation at the lowstand shoreline located basinward of the preceding shelf edge. The transition zone between each wedge and its associated updip feeder fluvial system marks the approximate position of the contemporaneous shelf edge. Third-order wedges are as much as 1,700 ft thick (fig. 15) in the area of well coverage.

In contrast to Starfak field, lowstand deltaic wedges are absent in Tiger Shoal because Tiger Shoal is in a generally more proximal depositional position relative to Starfak. Isolated wells located south (basinward) of Tiger Shoal field exhibit inferred deltaic wedge sandstones in some of the same intervals that contain wedge deposits in the southern part of Starfak field.

Lowstand prograding wedges and other time-equivalent, distal-shelf to upper-slope successions typically overlie, or are cut by, numerous penecontemporaneous (growth) faults in Starfak field and in the untested area between the two fields. This relation suggests that movement on these faults influenced the position of the shelf edges and, therefore, the updip limits of lowstand prograding wedges (figs. 20, 21). Lowstand wedges generally exhibit a forward-stepping pattern, younger wedges being located progressively farther south. This pattern coincides with progressive southward shift in time of the regional Miocene shelf edge in response to overall Miocene progradation. In Starfak field, these faults represent at least two generations of syndepositional-faulting episodes that probably (1) controlled the positions of the shelf/slope break and, consequently, the location of lowstand-deltaic sedimentation and (2) enhanced accommodation rates for downdip-thickening, lowstand-deltaic deposits.

The existence of lowstand prograding wedges within the Miocene succession is one of the more significant findings of this study. Starfak field contains four third-order prograding wedges that can be clearly imaged using seismic data in areas outside of well control. Within the field, third-order sequences 1 (fig. 15) and 2 (plate 2) compose the distal portions of two well-developed successions composed of third-order basin-floor-fan, slope-fan, and deltaic-wedge deposits. In contrast, sequences 3 and 4 in Starfak, especially sequence 4 (fig. 19), capture the regional updip, proximal pinch-out of fourth-order deltaic wedges.

Because (1) the third-order lowstand prograding wedges in sequences 1 and 4 (plate 2) are key distal and proximal end-member portions, respectively, of these wedges in the area of well control and (2) they are the two best-developed prograding wedges in the well logs and in the seismic volume, they are herein described in more detail. The lowstand prograding wedge of sequence 1 includes most of the locally productive Robulus L sandstones (Rob. L-1 to Rob. L-7)

and is an excellent example of a complete third-order wedge succession. However, the internal geometry of the wedge is not well resolved on seismic profiles, possibly in part because of its occurrence within the overpressured zone (below ~13,000 ft). The base of the wedge is defined by basin-floor-fan sandstones overlying third-order SB 59 (Rob. L-7) (fig. 15). This deposit is overlain by as much as 700 ft of shale-dominated slope-fan deposits that contain SB 56 through 58, which mark the bases of thin sandstone units of inferred localized fans of channel-levee complexes within three fourth-order sequences. Shales originated as slope muds. Even thinner sandstone intervals within the shaly succession also represent inferred sandy fan-turbidite deposits that accumulated on the slope. The sandier 500- to 600-ft-thick section between SB 55 and transgressive surface (TS) 49 records at least two major progradational pulses (lowstand deltas) in an overall progradational succession: SB 55 to 54 (Rob. L-5 sand), SB 54 to TS 49 (Rob. L-4 to Rob. L-1). The Rob. L sand reservoirs are primarily structural traps within deep-seated, east-west-trending fault blocks in Starfak field (fig. 9).

The third-order lowstand systems tract, including deltaic-wedge facies, in the lower part of sequence 4 (plate 2) in Starfak field is also particularly noteworthy because it has produced the highest cumulative total of hydrocarbons in the study area (see Relation of Production to Systems Tracts). In the area of well control in Starfak field, this lowstand interval comprises six distinct fourth-order valley-fill/deltaic wedge units associated with SB 30 (T-1 sand), SB 31 (T-2 sand), the sandstone unit at SB 32, SB 33 (U sand), SB 34 (V sand), and the sandstone unit at SB 35 (fig. 19). The updip limits of the individual fourth-order deltaic wedges occur in the central part of Starfak field (figs. 22, 23). In three depositional-dip-oriented seismic profiles of the third-order lowstand prograding wedge (figs. 24 through 26), we define six seismically resolvable depositional episodes as seismic units 1 through 6. These six seismic units correlate only partly

with the six fourth-order depositional sequences defined on well logs. The top of the wedge (top of seismic unit 6) corresponds to the transgressive surface above the T-1 sand, the top of seismic unit 5 is the top of the T-2 zone, the top of seismic unit 4 is the top of the U-sand zone, and the top of seismic unit 3 is the top of the V-sand zone. However, the seismic stratigraphy of seismic unit 3 is complex; well log correlation with the seismic signature indicates that seismic unit 3 comprises fourth-order sequences 34 and 35, the basal sequences of the third-order wedge in the area of well control. The seismic profiles indicate that at least two additional seismic units (1 and 2) were deposited primarily south (downdip) and southeast of well control. We tentatively conclude that third-order SB 35 (base of third-order wedge in the area of well control) was a major sediment-bypass surface (unconformity) across which the sediments in seismic units 1 and 2 were transported. However, future work will involve examining the three-dimensional seismic architecture of the sequence-4 lowstand systems tract in more detail using work-station visualization software.

Sandstone zones that display prominent coastal-onlap geometry within the third-order lowstand systems tract of sequence 4 (plate 2) form potential stratigraphic traps for hydrocarbon accumulation in the untested region between Starfak and Tiger Shoal fields. Because this third-order lowstand prograding wedge is a proven producer in Starfak field (figs. 27 through 29) and seismic data indicate that the sandstone-rich wedge, with the similar internal sandstone geometries, extends to the east, we think that there is a high potential for new discoveries in the untested interfield area. For example, our preliminary assessment is that seismic unit 4 (U-sand zone) produces gas from the depositional-updip and upstructure termination of thick lowstand-delta sandstones in the central part of Starfak field (figs. 22, 24). The same onlap termination of the U sand exists in seismic profiles shot between Starfak and Tiger Shoal fields. Therefore, we

think that a high potential exists for further development and extension of this sequence-4 wedge play into this untested area. Similarly, the block-faulted lowstand systems tracts within deeper third-order sequences 1, 2, and 3 (plate 2), which also extend into the untested interfield area and are prominent producers in Starfak field (figs. 27 through 29), are also very likely candidates for new hydrocarbon discoveries (fig. 20). In contrast to the lowstand systems tract of sequence 4, these wedge systems are characterized primarily by structural hydrocarbon traps (rollover beds against faults).

Incised Valley Fill.— In Starfak and Tiger Shoal fields, facies of lowstand systems tracts in on-shelf successions consist of the basal, fluvial portions of incised-valley fills. On-shelf facies compose 50 to 60 percent of the study interval (A to T-1 sand). Erosional surfaces occur at the bases of thick (50 to 250 ft) blocky to spiky log facies that represent incised-valley fills composed of lowstand fluvial facies overlain by inferred estuarine and bayhead-delta deposits of transgressive systems tracts. Juxtaposition of fluvial facies over neritic on-shelf shales represents significant basinward shifts in coastal onlap. Sequence boundaries at surfaces of exposure that are equivalent to the erosional surfaces mark the tops of major upward-coarsening log motifs that record subaerial exposure of these progradational (late-highstand deltaic) deposits.

Changes in log motif (indicating changes in net-sandstone or sandstone/shale distribution) that characterize incised-valley-fill facies are associated with the spatial location of the lowstand valley relative to the proximal, medial, or distal paleoshelf. The magnitude of valley incision increases and valley fills generally thicken to the south, downdip on the paleoshelf. Log signatures of the valley fill in those reaches of the valleys incised into proximal and medial paleoshelf settings are blocky, blocky serrated, or upward fining. This character records well-developed (low-clay-content), high-porosity, stacked fluvial-channel architectural

elements. Minor gamma-ray highs (thin shale partings or shale-pebble lag conglomerates) separating individual fluvial-channel elements represent reactivation surfaces that may form localized reservoir flow barriers. These are dominantly lowstand fills inferred to have aggraded during late lowstand time when relative sea level was stable or slowly rising. Lowstand fluvial fills are overlain by valley-confined transgressive deposits (described in the following section). In contrast, thicker valley fills (as much as ~250 ft) are located in more distal shelf locations. These valleys form areally restricted topographic "notches" in the paleoshelf margin (fig. 30). Valleys are located immediately upslope of lowstand prograding wedges that were fed by sediments cannibalized from erosion of the underlying highstand shelf deposits as "knickpoints" eroded landward, forming the final lowstand river profiles.

Transgressive systems tract. The generally thin (10- to 40-ft) backstepping, progradational successions (retrogradational parasequence sets) that compose transgressive systems tracts disconformably overlie the transgressive surfaces (1) that lie within lowstand valley-fill deposits and at the top of nonincised lowstand prograding wedges and (2) that merge with the sequence boundaries in interfluve areas. These parasequence sets form stacked, upward-fining, log-facies successions that culminate in a high-gamma-ray zone (marine condensed section) signifying the maximum landward extent of the shoreline. In the most proximal portions of the study interval, the condensed section is difficult to recognize, being landward of the updip limit of deposition of marine shales. In these successions (~SB 1 to 7, plate 2), the surface of marine flooding is contained within a predominantly sandy section. In most of the study area, however, the condensed sections are composed of regionally correlatable organic-rich shales deposited under tranquil marine conditions during inundation of the shelf.

In Starfak and Tiger Shoal fields, transgressive systems tracts are generally 60 ft thick or less but locally attain thicknesses of as much as 180 ft (third-order transgressive systems tracts). Lateral thickness within any one systems tract systematically varies; transgressive deposits are commonly thicker and comprise more parasequences in the updip areas, reflecting increased lobe switching in the backstepping deposits as a function of steady decrease in accommodation space as the depositional systems moved more landward. Parasequences are also commonly sandier in the updip areas of the proximal and medial on-shelf deposits because of closer proximity to source area(s) and the increased reworking of deposits as one moves from high-accommodation locations near the lowstand shelf margin to low-accommodation proximal areas of the stable coastal plain. Sandstone content within parasequences of the transgressive systems tracts also increases upsection toward the most landward (proximal-shelf) depositional facies within the study interval.

Incised valleys in the proximal to medial shelf facies of the study interval generally contain fewer than about 50 percent transgressive-system-tract deposits, which are thinly interstratified silty sandstones and shales in an overall upward-fining interval. These transgressive sandstones and shales are interpreted to represent fine-grained estuarine and coarser grained bayhead-delta sediments, both of which are areally restricted to the confines of the physiographic incised valley. The more distal valleys that are incised into the upper slope and filled with late-lowstand sandstones separated by thin, intervening shales within a generally overall aggradational succession probably contain a somewhat lower percentage of transgressive fill, although the distinction between lowstand and transgressive deposits within these valley fills on well logs is not precise.

Highstand Systems Tract. Sediments of highstand systems tracts form progradational parasequence sets that generally display upward trends of parasequence thinning and increase in percentage of sandstone within parasequences. These upward-coarsening successions, typically 150 to 200 ft thick in most of the study interval, range from as thin as 60 ft in the most proximal shelf locations to as thick as 600 ft in the distal-shelf areas.

Sandstones within late-highstand parasequences, the uppermost parasequences of the progradational parasequence sets, represent delta-front deposits, locally developed distributary channel fills, delta-mouth bars, and interdeltaic shoreface facies. Early-highstand parasequences originated as more distal variations of these same deltaic and shoreface environments of deposition. Seismic stratal slices of highstand successions illustrate generally lobate and digitate aerial geometries.

Relation of Production to Systems Tracts

Within individual fourth-order systems tracts, hydrocarbons have been produced from (1) sandy lowstand incised-valley fills, (2) deltaic/strandplain sandstones of late-highstand systems tracts, (3) deltaic sandstones of late-lowstand deltaic wedges, and (4) transgressive bayhead deltaic sandstones. However, calculation of the vertical distribution of production in Starfak and Tiger Shoal fields indicates that the vast majority of gas and oil production is from the third-order lowstand systems tracts at the bases of the third-order cycles (figs. 27 through 29).

Within Starfak and Tiger Shoal fields (through July 1, 2000), 92.6 percent of all gas production, 98.0 percent of all oil production, and 92.6 percent of total hydrocarbon production have come from the lowstand systems tracts of the third-order sequences (tables 6 through 8). In each category, the T-1-to-V-sand lowstand systems tract (= lowstand systems tract of sequence 4

[plate 2]) has produced the most hydrocarbons, followed by the X-to-Y-sand lowstand systems tract (= lowstand systems tract of sequence 3).

Collectively the sequence-stratigraphic model and the overall genetic framework (plate 2) of the third-order lowstand systems tracts reveal the most likely reasons that they are the principal locations of hydrocarbon concentration in the two fields. The reservoir-rock quality of lowstand deposits is generally superior to that of sandstones within the other systems tracts (L. F. Brown, Jr., personal communication, 2000). The sandstones of basin-floor fans, prograding deltaic wedges, and incised-valley fills are typically the coarsest grained rocks in a basin because they accumulated directly from sediment transport of lowstand fluvial sands through contemporaneous incised valleys. Because of the tendency of these sandstones toward coarser texture, porosity and permeability values are typically higher than those of sandstones in the other systems tracts. Moreover, the clustering of relatively thin fourth-order systems tracts (that compose the third-order lowstand systems tracts at the bases of third-order sequences [plate 2]) below thick shales of third-order transgressive systems tracts creates optimal conditions for effective seal of hydrocarbons within the coarse lowstand sandstones. Similarly, the common juxtaposition of fluvial sandstones against neritic shales from lowstand incision creates potential for lateral seals at incised-valley margins. Finally, the areally restricted distribution of commonly thick, stacked deltaic-wedge sandstones within slope and basinal shales creates an ideal condition for potential hydrocarbon migration and entrapment.

The concentration of hydrocarbons within third-order lowstand systems tracts is a key finding of this study, and this observation has major implications for exploration of new hydrocarbon reserves within the area encompassed by the 3-D seismic volume. Extrapolation of key sequence-stratigraphic surfaces that bound the third-order lowstand systems tracts from the

fields throughout the seismic volume is an effective first step in defining the regional distribution of these proven hydrocarbon "pools." Subsequent seismic-structural mapping and 3-D seismic interpretation of internal lowstand-systems-tract geometries will help strategically target undeveloped reservoirs between fields.

GEOPHYSICAL DATA QUALITY AND REPROCESSING

Data Quality

The 3-D seismic data were acquired between 1994 and 1995 in an area approximately 352 mi^2. The data were merged from two surveys, OCS 310 (southwest) and SL 340 (northeast), covering five of Texaco's offshore fields: Starfak, Tiger Shoal, Mound Point, Lighthouse Point, and North Lighthouse Point (fig. 31). Both surveys are oriented NW-SE in the inline direction and SW-NE in the crossline direction. Western Geophysical Corporation (WGC) of New Orleans conducted the acquisition by using a cable crew with an airgun source. Both WGC and Texaco's New Orleans office were involved in the data processing. Although some acquisition problems (dead cable, time breaks, etc.) resulted in difficulties and delays, there is no evidence of significant problems in quality in the final product (Texaco Exploration and Production Inc., 1996).

From an interpreter's point of view, the 3-D seismic data set is of good quality. Dominant frequency varies from 40 Hz in the shallow section to 20 Hz in the deep section, many of the gas reservoirs or reservoir groups being clearly resolved. Visible direct seismic indicators of gas-bearing zones include bright spots on structural highs and against faults and significant velocity sag observed in the gas-bearing area of Tiger Shoal field. The signal-to-noise ratio is high, with

no multiples or other coherent noises, and no migration problems are apparent. The merged data volume, however, does show some subtle differences in dynamic characteristics between the OCS310 subvolume and the SMI subvolume. The potential effect of this difference on the project should, however, be minimal because both Starfak and Tiger Shoal fields are well within the OCS310 subvolume.

We have paid particular attention to the accurate tying of wells to seismic data. Five checkshots in Starfak field were loaded into the data base. Analysis of the checkshot curves resulted in an allocation of different time-depth (T-D) curves to different wells on the basis of their distance from checkshot wells and structural location. Although most sonic and density log curves are partly spurious because of borehole washout, we have been able to edit sonic/density logs in two wells to produce good-quality synthetic seismograms that show a reliable tie between well logs and nearby seismic traces. A constant shift was applied to the log curves from all other wells to match the tie with the two wells with good synthetics. Available log-interpreted picks of sequence boundaries and tops of main reservoir units (mainly in Starfak field) were then loaded into the data base and checked for consistency in correlation.

Interpretation-Oriented Data Processing

We applied three types of poststack processing to the 3-D volume to improve interpretability of the data. First, a 90°-phase shift was applied to the original, approximately zero-phase data. The shape of seismic wavelet determines which part of the wavelet is the most important for seismic response. It is well known that the zero-phase wavelet is symmetrical and has maximum energy in its central part. Its small side lobes make it better than minimum- and maximum-phase wavelets of the same frequency for detecting reservoirs vulnerable to the geological noise from both above and below. The main problem for interpreters, however, is that

for a single reservoir (layer) two seismic events (one peak and one trough) can be seen, which may cause confusion in identifying sandstones from shales when multiple reservoirs are involved in the interval of interest. In fact, for seismically thin layers, 90°-phase wavelet is better than its zero-phase counterpart for interpretation (fig. 32). For 90°-phase wavelet, one reservoir is reflected by one seismic event, which can be a peak or trough, depending on sand-shale acoustic relationship. It occurs at the middle of the reservoir, having two weak side lobes, which makes more sense for a geologist because the seismic section of 90° phase best matches its "inversion" or impedance section without an inversion actually being done. The resulting 90°-phase data, therefore, coincide better with impedance logs and, in turn, with gamma-ray, SP, and resistivity curves—those with which geologists are most familiar. For this reason, a 90°-phase data set was selected for most of the seismic interpretation in the project. The difference between the data of two phases and their influence on well-seismic correlation is shown in figures 33 and 34.

We then calculated continuity (Landmark) cubes from the original data to aid in fault interpretation and identification of stratigraphic features. The project's primary benefit of these cubes is that they can image numerous faults of different scales (from regional [tens of miles] to local [hundreds to thousands of feet]) and resolve important depositional features (for example, channel systems and slope fans). Benefit of the processing can easily be seen in continuity time slices (figs. 35, 36), which show a sharp and complete regional fault system in the shallower section (fig. 35, 1 to 3 s) and many small, subtle faults in the area between Starfak and Tiger Shoal fields and to the northwest of Starfak field in the deeper section (fig. 36, 3 to 4.5 s), which are otherwise difficult to pick.

Further, we conducted a processing of spectral balancing on deep data (3 s and deeper) to improve vertical seismic resolution. The deep section is an important hydrocarbon producing

zone (U-Y Sands, 12,000 Sands and Robulus Sands) and one of the critical targets of this research. However, compared with the higher frequency, shallower data (30- to 40-Hz dominant frequency in interval of 1 to 3 s), deeper data are characterized by a significantly lower dominant frequency (~20 Hz) and therefore much lower vertical resolution. To improve the interpretability of the seismic data, we enhanced the amplitude level of higher frequency components in the data, while keeping the lower, originally dominant frequency components intact. The range and enhancing scale of the higher frequency components were carefully selected and tested to avoid overamplifying the noise level of the data. The processing moved the dominant frequency of the data to the 30- to 40-Hz level (comparable to the shallower data). The resulting data reveal more stratigraphic details vertically (compare fig. 37a and 37b, especially the lowstand wedge). Judging by the good and sometimes even better correlation between well logs and seismic events in the processed data, these improvements are real and come from originally masked higher-frequency signals.

3-D Seismic Structural Framework

An integrated interpretational approach was utilized to refine the structural framework and identify potential bypassed hydrocarbon accumulations. In exploration areas, 3-D seismic is an invaluable tool that can provide detailed information about the subsurface geology within a study area. The 3-D seismic enables teams of geoscientists to identify and exploit reserve growth opportunities in a timely fashion. In mature fields such as Starfak and Tiger Shoal, 3-D seismic can improve the spatial resolution of the structural framework and identify potentially bypassed hydrocarbon accumulations. The 3-D seismic can extend reservoir understanding away from well control by identifying known seismic waveforms at producing reservoirs and then search the entire volume for similar seismic waveforms, which may produce the same results. The

interpreter can examine the 3-D seismic volume from many different perspectives, allowing detailed analysis of specific areas of interest.

Fault-Interpretation Methods

For this study, it was determined that a first pass of coherence time slices would be useful in the initial phase of the research. A major advantage of coherence attributes is that they allow a mathematical assessment of the 3-D seismic data volume without being biased by previous interpretation. Coherence calculations compare waveform similarity between adjacent traces within a specified time window, which are cross-correlated with neighboring traces. The lowest correlation coefficient calculated will be assigned to the central sample. Coherence values can range from +1 to –1. A value of +1 indicates a perfect match between adjacent traces, which is typical of where rock matrix has no lateral variations (no faulting or change in rock type). A value of –1 indicates significant trace similarity if the phase of one of the waveforms is inverted, which could be an indicator of offset (faulting) within the reference window. A coherence value of zero indicates no correlation between seismic reflection character. Lower coherence values (0 to –1) may indicate significant lateral changes in rock type, pore-fluid content, faulting, or any geologic variation that can affect seismic reflection waveshapes. Fault segments are more pronounced on the coherence time slices (fig. 38) than they are on the conventional amplitude time slices (fig. 39). Time slices of the coherency volume, starting at 2,000 ms, were generated at 100-ms intervals. Fault segments were identified and mapped at each 100-ms interval. Vertical sections oriented in dip direction were then extracted from the 3-D seismic amplitude volume for analysis. Afterward the fault segments identified from the coherence time slices were projected on the extracted dip sections. The interpreter can then determine whether the fault segments can be correlated to a particular fault line that may present itself in the vertical section (fig. 40).

Observations

Analysis of the 3-D seismic volume reveals the presence of numerous (60 +) normal faults throughout the study area. There are at least five first-order normal faults, extending from near the seafloor to below seismic depth coverage (fig. 40). The first-order growth faults are characterized by increasingly thicker sequences of sediments as depth increases. These five faults have many rollover features at depth, many of which have not been exploited. Numerous (60+) second-order faults were interpreted. Although second-order faults generally have less maximum offset (<200 ft) compared with that of first-order faults, significant reserve growth opportunities are associated with these important features.

Several hourglass features are observed throughout the study area. Hourglass features are characterized by a crosscutting of fault segments that appear as an X in a vertical seismic section, which are associated with transecting faults (fig. 41). Hourglass features form good structural traps, with a minimum of two sides bounded by faults. The next phase of the study was to map key lithostratigraphic horizons throughout the 3-D seismic volume.

Surface Mapping Methods

In order to transfer key strata to the proper 3-D image time, several synthetic seismograms were generated for well-to-seismic calibration. Wells with checkshot surveys were used as controls. Checkshot data were available only from wells in Vermilion Block 50 (Starfak) field. The resulting time-depth functions were then applied to the well information for proper well-to-seismic calibration. Key stratigraphic markers were then posted in the 3-D seismic volume. It was decided early in the planning stage that maximum flooding events would be the easiest events to map across the 3-D seismic volume. They are by definition regionally extensive and produce a strong reflection signal that is easily tracked throughout the study area. The

structural framework of this study area presented some obstacles for the interpreter. It became apparent early in the study that trying to map surfaces across the large first-order growth faults associated with paleoshelf edges would be difficult. Most attempts to correlate a largely displaced updip surface with the displaced equivalent downdip surface produced uncertain results. Fault regions of minimum displacement provided the highest level of correlation confidence. Consequently, mapping began in Vermilion Block 50 (Starfak) field, where key horizon correlations had been well established in well log data. The mapping surface was then correlated and mapped throughout Tiger Shoal field. Subsequent mapping continued to the north of study area and stopped at the major growth fault associated with the shelf edge. The surface was then correlated over the large growth fault in the northeast of the study area. Finally the surface was extended to the south and terminated in the south-central sector of the study area. All surfaces that were mapped in the 3-D seismic data followed this approach, allowing the interpreter to take advantage of areas of minimal offset across the larger first-order faults.

Observations

Time-structure maps revealed several structural high points within the study area (fig. 42). Tiger Shoal and Mound Point fields are structurally high, with a locally depressed block flanked by faults on each side, examples of classic graben features. Light House Point and North Light House Point dominate the central, northwestern portions of the study area. Within each of these fields normal faults play a significant roll in hydrocarbon trapping. In addition, Starfak field is a subregional high point in the south-southwestern portion of the study area. All of these topographical features are conformable to depth, having impact on possible structural plays even at depths corresponding to Robulus sands. These time-structural highs have been heavily targeted for hydrocarbon exploitation.

The study area is dominated by extensional normal faulting, with no evidence of compression. A significant first-order growth fault (A in fig. 42) runs east to west through the middle of the study area. This fault forms the northern boundary of Starfak and Tiger Shoal fields. In the area north of Starfak field, this fault has offsets greater than 350 ft. Producing reservoir sands are on the downthrown side of this fault. In addition, offsets decrease (<250 ft) in Tiger Shoal field, with reservoir-quality sands on both sides of the fault. A north-south-trending first-order fault (B in fig. 42) separates Light House Point and North Light House Point fields. It forms the western boundary of Light House Point field and has offsets greater than 350 ft. Mound Point field is bounded on the western edge by a first-order normal fault (C in fig. 42). The fault trends from the southwestern portion of Mound Point field and extends to the northeast beyond 3-D seismic coverage. Most reservoir-quality sands are on the downthrown side of the fault. Offsets exceed 350 ft at the 12000 A sand reservoir interval. Two first-order growth faults (D and E in fig. 42) separate important fault basins located in the southern and southeastern portions of the study area, from the five major prospects within the study area. These two faults, characterized by offsets (>500 ft) increasing with depth and thickening basinward deposits, are thought to define the shelf edge. Downdip deposits may offer good trend plays, targeting stratigraphically trapped (pinch-out) hydrocarbon accumulations that parallel the fault line (strike). Additional fault complexes are evident throughout the study area, each with potentially significant bypassed hydrocarbon accumulations.

First order growth faults have many associated rollover features (fig. 40). Rollovers are created when active normal faults drag beds of the downthrown block at a rate faster than that of the upthrown block, creating structural closure on a minimum of two sides. Rollovers are

excellent targets for hydrocarbon accumulations. These features are commonly found in the lower portions of first-order growth faults, where fault juxtapositioning is greatest.

Structure below maximum flooding surface 45 is more complex. First-order growth faults have significant offset (>600 ft) with depth and influence the channeling of reservoir-quality sediments into the south-southeastern portion of the study area. The seismic data reveal wedges thought to be deposited during a rapid eustatic fall. Several fault swarms (fig. 43) were interpreted in the south portion of Starfak field. They are characterized by closely spaced second-order normal faults with limited offset (<100 ft.) Many of the faults impact the lowstand systems tract wedges and may have significant influence on hydrocarbon mobility at these depths. In some cases, where offset is greater than sand thickness, they may form seals that impede the flow of hydrocarbons and form effective traps. In other cases, they may allow hydrocarbons to escape lowstand-wedge systems and move along the faulted rock matrix to shallower reservoir intervals.

Prospects

During the structural-interpretation phase of the study many preliminary prospects for hydrocarbon accumulation were identified, including traps such as rollovers, bright spots terminated against faults, flat spots, untested fault blocks, faulted anticlines, and pure stratigraphic traps. Each prospect has a structure-map view and dip/strike seismic cross section for visualization aids. Locations represent Louisiana State plane south cartographic projections. The preliminary prospects are summarized next.

Prospect 1

This prospect is located on the north-northwest edge of the study area (fig. 44). It is defined as a classic flat spot, at 2,200 ms, with velocity sag immediately below (fig. 45). This typically is a direct hydrocarbon indicator (DHI), where the flat seismic reflection can be

attributed to a fluid contact. The zone of interest corresponds with the L-sand. Location x: 1753690 y: 321320.

Prospect 2

Prospect 2 is located in the east-central portion (Block 228) of the study area (fig. 46). The trap is characterized as a rollover (downthrown) feature within an untested fault block with strong amplitudes (fig. 47). However, there is a possible spill point to the northeast. The P and Q sands are targeted. Location x: 1805138 y: 255761.

Prospect 3

This prospect (fig. 48) is located in Tiger Shoal field (Block 218). The trap is a structural high with high amplitudes truncated against a second-order normal fault (fig. 49). The deep Rob L sands are targeted. Location x: 1762551 y: 276774.

Prospect 4

Prospect 4 (fig. 50) is located in the saddle area between Starfak and Tiger Shoal fields (Block 219). This prospect is a faulted anticline, with an updip truncation against a second-order fault. There may be spill points to the east and west. The Rob L sands are targeted (fig. 51). Location x: 1744895 y: 281538.

Prospect 5

This prospect is located (fig. 50) in the saddle area between Starfak and Tiger Shoal fields (Block 219). The trap is a faulted anticline with rollover against a second-order fault to the south. There may be spill points to the east and west. The Rob L sands are targeted (fig. 52). Location x: 1745318 y: 283066.

Prospect 6

This prospect is located (fig. 48) in the southern portion of Tiger Shoal field (Block 218). The trap is a structural high (rollover) bounded by two second-order faults to the north and east. The prospect lies on the upthrown portion of the fault. The Rob L sands are targeted (fig. 53). Location x: 1764174 y: 275973.

Prospect 7

Prospect 7 is located (fig. 54) on the eastern edge of Tiger Shoal field (Block 217). There are two potential targets at different depths. The shallow T sands have strong amplitudes on the upthrown side of a first-order normal fault (fig. 55). This is also true for the deeper 12000 sands. Location x: 1769626 y: 283164.

Prospect 8

Prospect 8 lies (fig. 56) in the saddle area between Starfak and Tiger Shoal fields (Block 211). This prospect has high amplitudes that truncate against a north-bounding first-order normal fault. In addition, this prospect is within an hourglass feature (fig. 57). This area has significant amounts of Y sand, and there may be other locations that provide additional reserve growth opportunities. Location x: 1752547 y: 292110.

Prospect 9

Prospect 9 lies (fig. 50) on the southeastern edge of Starfak field (Block 219). This prospect is a lowstand wedge that has been faulted by numerous (swarms) second-order normal faults. These fault blocks are typically downthrown to the south. This fault block has three sides faulted and may have structural closure to the east. In addition, it is an untested fault block. The Rob L sands are targeted (fig. 58). Many more potential prospects at the Rob L interval are being analyzed. Location x: 1740240 y: 279194.

Prospect 10

This prospect is located (fig. 54) in the southern portion of Tiger Shoal field (Block 218). This is a bright spot forming on a structural high on the upthrown side of a second-order normal fault. The T sands are targeted (fig. 59). Location x: 1763585 y: 278521.

Prospect 11

This prospect is located (fig. 60) in the southeastern area of Tiger Shoal field (Block 217). This trap is a classic bright spot at 2,400 ms with velocity sag and is a pure stratigraphic play. The O sand is targeted (fig. 61). Location x: 1766920 y: 276222.

Prospect 12

This prospect is located (fig. 62) within Light House Point field. The trap is a rollover feature on the upthrown side of a first order normal fault. There are three-way structural closures with fault bounding on the southeast. The Rob L sands are targeted (fig. 63). Location x: 1770196 y: 314411.

Prospect 13

The prospect is located (fig. 64) in the south-central portion (Block 230) of the study area. It is an example of a trend play along the downthrown side of a first-order growth fault to the north. There are several rollover features that have the potential for hydrocarbon accumulations. The L sands are targeted (fig. 65). Location x: 1777872 y: 255609.

Prospect 14

This is an additional trend play (fig. 64) along the first-order growth fault (Block 231) associated with prospect 13. Again we are targeting the rollover features at the L sand interval (fig. 66). Location x: 1764263 y: 253888.

Prospect 15

This prospect is located (fig. 67) in the northwest portion of the study area. It consists of a bright spot rolling north to south with a stratigraphic pinch-out to the southwest (fig. 68). This is a good example of a combination stratigraphic-structural prospect. The Q1 sand is targeted. Location x: 1757987 y: 323419.

Prospect 16

This prospect (fig. 69) is targeting a flat spot with high amplitude. In addition, this prospect lies north of Tiger Shoal field (Block 211), within an untested fault block. It is structurally bounded by faults on the south and east. The Rob L sands are targeted (fig. 70). Location x: 1751688 y: 298097.

Prospect 17

This prospect is located (fig. 62) in the northwestern portion (Block 208) of the study area. It consists of an updip structural high bounded on the north and east by second-order growth faults. High amplitudes are terminated against the faults. The Rob L sands are targeted (fig. 71). Location x: 1761440 y: 314440.

Prospect 18

This prospect lies (fig. 72) in the saddle area (Block 211) between Starfak and Tiger Shoal fields. It is characterized by a structural high flanked by two first-order normal faults. The Y sand is targeted (fig. 73). Location x: 1754453 y: 291832.

Prospect 19

Prospect 19 is located (fig. 74) within Light House field. It is within a Tiger Shoal clone (faulted anticline) with two bright spots of interest. These bright spots are associated with the

B sand, which has a flat spot, and the deeper J sand, associated with an untested rollover feature (fig. 75). Location x: 1771400 y: 313992.

Prospect 20

This prospect (fig. 76) is near the easternmost extent of the Amber Complex (Blocks 236/237) in the southeastern portion of the study area. It is defined as an upthrown trap with two flanking faults to the north and east. The 12000 A & B sands are targeted (fig. 77). Location x: 1795204 y: 238723.

Prospect 21

This prospect is located (fig. 46) on the eastern edge (Block 227) of the study area. It is an upthrown trap flanked by two second-order normal faults. Strong amplitudes associated with the Q sand is targeted (fig. 78). Location x: 1814163 y: 247407.

Subsequent analysis is necessary for risk evaluation of each prospect. Prospects may be added or removed as additional information is integrated with these data. Rankings will be assigned to each prospect after integration with geological, stratigraphic, and petrophysical controls.

SEISMIC ATTRIBUTE ANALYSIS AND INTERPRETATION

Fluid Modeling

The most important data needed to study acoustic behavior of rocks are P-wave velocity and bulk density. Unfortunately in the study area there is no direct measurement of velocity and rock moduli from core, so sonic and density logs are the only source of available data. To make things worse, only two wells (30-2 and 31-16) have segments of both sonic and density logs of fair quality (fig. 79), with serious borehole washouts in all other wells. As a result, one can

conduct only a sandstone/shale trend analysis. More detailed, layer-by-layer analysis is not realistic, until new, high-quality well log data are available.

Data (excluding hydrocarbon-saturated sandstones) from the two wells were combined, and P-velocity and bulk density of sand and shale were plotted against depth, with trend lines added (fig. 80, 81). In general, for the interval of interest (6,000 to 15,000 ft, or A – Robulus Sands), sandstones have higher P-velocity (except where <7,000 ft) and lower bulk density (all depths) than shale. The abrupt changes of P-velocity and bulk density around 13,000 ft (above 12,000A Sand) reflect the top of the overpressure zone in the area. Because these trends are for water-saturated sandstone only, the hydrocarbon effect on response is as yet unknown.

Gassman's Equation was then used to calculate how much velocity change is expected if pore fluid in a sandstone were substituted with gas:

$$M = \rho V_p^2 = K_{drf} + \frac{4}{3}\sigma_{drf} + \frac{(1 - \frac{K_{drf}}{K_{ma}})^2}{\frac{1 - \phi - \frac{K_{drf}}{K_{ma}}}{K_{ma}} + \frac{\phi}{K_{fl}}},$$

where

M = P-wave modulus,

ρ = density of shaly sandstone,

V_p = P-wave velocity,

ϕ = effective porosity,

K_{drf} = bulk modulus of dry rock frame,

K_{ma} = bulk modulus of matrix,

K_{fl} = bulk modulus of pore fluid,

σ_{drf} = Poisson's ratio of dry rock.

On the basis of the production data derived from information for hydrocarbon properties, the ρ and Kfl values of gas calculated from Thomas and others (1970), the ρ and Kfl values of oil calculated from Wang and others (1988) (table 9), and some common assumptions of brine and rock moduli (table 10), K_{drf} can be calculated first by inputting V_p and ρ of a brine-saturated sandstone. The V_p of gas-saturated sandstone is then found by substituting the ρ, Kfl of brine-saturated sandstone, with that of gas-saturated sandstone. In the input parameters, hydrocarbon saturation was assigned 65 percent, a fair guess from petroleum engineering data.

Shaly sandstone $$\frac{1}{K_{ma}} = \frac{V_{sh}}{21.42} + \frac{\left(1-V_{sh}\right)}{36.47}$$

$$\sigma_{dry} = \begin{cases} 0.15 & V_{sh} \le 0.15^{*} \\ 0.88V_{sh} - 0.082 & 0.15 < V_{sh} \le 0.40 \\ 0.83V_{sh} + 0.082 & V_{sh} > 0.40 \end{cases}$$

* Formulated from Hilterman, 1990

The results were plotted as the acoustic impedance trend lines of hydrocarbon-saturated sandstones, together with brine-saturated sandstones and shale (fig. 82). The most dramatic effect on sandstone impedance comes from gas, shown by the most significant decrease of sandstone impedance compared with that of brine-saturated sandstone. Condensate-saturated sandstone shows a change in impedance very similar to, but slightly weaker than, that of gas-saturated sandstone. Oil saturation has a less sensitive influence on sandstone impedance (about halfway between gas line and water line, fig. 82). All hydrocarbon-saturated sandstones, however, show systematic decrease in magnitude of impedance change owing to the pressure increase with depth, which increases the values of ρfl and Kfl.

Converted to reflection coefficient trends (fig. 83), water-saturated sandstones below the shale show normal reflections of RC –0.05 – 0.10. In contrast, gas-saturated sandstones beneath the shale are characterized by a strong, negative reflection (RC<–0.05 or bright spots) in most of the depth range, except for 11,500 to 13,000 ft and 13,700 to 15,000 ft, where the gas signal becomes insignificant (RC –0.05 – 0.01) and is considered undetectable from surrounding reflections. Condensate-saturated sandstones are predicted to behave in a manner very similar to that of gas-saturated sandstones. As a result, they cannot be distinguished from each other in terms of seismic amplitude. The RC trend of oil-saturated sandstones is in between those of gas- and water-saturated sandstones, showing a potential of being bright spots only where it is shallower than 9,000 ft.

Seismic Sedimentology by Stratal Slicing

The 3-D seismic volume records an interval of Miocene-Pliocene sediments in a 0.4- to 4.0-s section, including all major hydrocarbon-producing zones in the area. Except for local Starfak and Tiger Shoal fields, however, most of the area has no well control. To reach the project goal of finding additional gas reserves between and beyond wells, workers must improve 3-D seismic interpretation so that sequence-stratigraphic and reservoir study can be extrapolated to the entire area, throughout the section of interest. An important step is to optimize depositional-facies mapping by automating depositional-surface picking in the 3-D volume and to link seismic-attribute patterns directly to sedimentary rocks and depositional processes.

Seismic-Lithology Relationship

Analysis of sonic and density logs is essential to revealing the acoustic relationship between sandstone and shale. A segment (upper Miocene) of sonic and density logs in a type

well was first converted to an impedance log (Z, product of velocity × bulk density) and then plotted against the effective porosity (ϕ_e, density porosity with clay effect removed, fig. 84). ϕ_e is here an indicator of lithology, with the highest ϕ_e (>0.3) being clean sandstone, the lowest ϕ_e (<0.1) being shale, and intervening values being shaly sandstone and sandy shale. Notice in figure 32 that, statistically, Z linearly decreases with ϕ_e. In other words, sandstone is characterized by a Z lower than shale. If bounded by thick shale, the top of the sandstone would be reflected as a seismic trough (zero-phase wavelet in SEG reverse polarity).

After careful depth-to-time conversion and seismic-phase adjustment, this acoustic separation of sandstone and shale can best be seen on a well-to-seismic tied section (fig. 85). More than 90 percent of the sandstones (middle Miocene-Pliocene) are tied to seismic trough events (red) without much ambiguity. Not only are regionally continuous sandstones confined to continuous seismic trough events (for example, B, I, and N sands, fig. 85), but many lenticular sand bodies also show excellent correlation to patchy seismic events (for example, a, b, and c, fig. 85). In contrast, most of the thin shales are characterized by seismic peak events (black). The only exception is some thick shaly units in the middle Miocene section that are reflected as complex peak-trough couplets, an indication of internal heterogeneity. The seismic amplitude (trough) can be safely used as an interpretation guideline to indicate sandstone directly. It can also be used to tie seismic to the sandstones in area wells.

Stratal Slicing

Seismic attributes must be picked on a depositional surface (geologic time surface) if they are to represent a genetic depositional unit. Such a seismic-surface display is called a stratal slice (Zeng, 1994). Time slices and horizon slices are currently the most commonly used seismic-surface displays to extract stratigraphic information. For depositional-facies analysis,

however, both methods have limitations. Their strict application conditions have prevented them from being used in complicated (for example, wedged) seismic sequences. Stratal slicing improves seismic-surface display mainly by making slices proportional between geologic time-equivalent seismic-reference events (for example, flooding surfaces). A comparison among different approaches will be presented in the poster. For more details refer to Zeng (1994), Zeng and others (1995), Posamentier and others, (1996), and Zeng and others (1998a, b).

A stratal-slice volume has been generated among 13 reference seismic events in the middle Miocene-Pliocene section. Among 776 stratal slices in the roughly 3.0-s data interval, 46 are highlighted on the well-to-seismic section (fig. 85) to show positions of representative stratal slices in two-way time and their relationship with seismic events, lithostratigraphic units, and well log characteristics. The highlighted slices demonstrate typical depositional facies images in different stages of basin development and will be shown in a stratal-slice movie in the poster. However, only selected slices are discussed herein for highlighting the methodology and the geologic interpretation of stratal slices.

Pattern Recognition and Facies Analysis

The interpretation of stratal slices is an integrated study of all available data. The key process is the pattern recognition of seismic-attribute (most commonly amplitude) images guided by depositional models. In some cases the patterns alone are enough for accurate facies identification (for example, a meandering fluvial system). In other situations, however, well-derived information is always helpful, especially when seismic patterns are complex. In this study, the following pieces of information are used in seismic-pattern/depositional-facies conversion:

- Pattern geometry: channel (shoestring), lobe, digitate, sheet/random, etc.

- Pattern texture: smooth, patchy (variable), wormlike, etc.
- GR/SP log pattern: upward fining, upward coarsening, blocky, serrate, straight, etc.
- Amplitude (seismic-lithology relationship): negative (thick/blocky sand), positive (shale/condensed section), low/variable (variable polarity, thin sand/shale), highly negative (gas sand).
- Relationships: regional setting, structure, sea level/systems tract inferred by sequence-stratigraphic study, etc.

For example, slice 1160 (fig. 86) illustrates some moderately sinuous, channellike features. Internal amplitudes are more smoothed as compared with those surrounding the features. On the basis of seismic-lithology modeling, negative amplitudes indicate thick sandstone trends. Wells that penetrate these features show that they are characterized by an upward-fining log pattern, supporting evidence of a fluvial channel fill. The slice is in the Pliocene section, an interval interpreted by sequence-stratigraphic study as developing primarily in a coastal-plain environment. Therefore, the best interpretation of these features would be coastal streams.

Slice 2248 (fig. 86) shows a markedly different channel type. Most of these features are subregional in size and typically straight with local bifurcation downstream. Internally smoothed, negative-amplitude patterns are visually striking as compared with surrounding sheetlike, mostly positive amplitude patterns. These features are composed of mostly blocky and blocky-serrate sandstones in the penetrating wells and can be interpreted as thick sandstone belts. Stratigraphically below the Pliocene coastal-plain deposits, these Miocene features represent incised valley fills (IVF's) that incise exposed shelf facies. The IVF's contain deposits of lowstand and transgressive systems tracts. Similar IVF's can be seen terminating updip in the

coastal plain (for example, fig. 86a), indicating that at least some of the IVF's also drain the landwardmost portion of the lowstand coastal plain.

Slice 2472 (fig. 86c) highlights generally lobate and digitate aerial geometries that have negative amplitudes that are inferred to be thick sandstone bodies. Each finger- or channellike feature grades downdip to low/variable-amplitude lobes, which have been confirmed by wells as being composed of thin, serrate sandstones. On the basis of its highstand position in the sequence-stratigraphic framework, the system has been interpreted as a highstand shelf delta.

In the interval studied, gas sandstone commonly shows as a bright spot. However, condensed sections and salt layers sometimes also generate bright spots that confuse interpreters. Facies analysis on stratal slices can help in reducing the ambiguity. For instance, F1 sand in Tiger Shoal field is gas producing in several wells. The reservoir is interpreted as an IVF sandstone and is reflected in figure 34 as a bright spot labeled BS I. Although in some incised-valley deposits, thickness changes can cause amplitude variability, here there is no indication (on the basis of combined seismic and well data) that this sand is characterized by any significant thickness change throughout the field area. Therefore, the amplitude change is interpreted to be a function of fluid content. Several other examples of undrilled, high-amplitude IVF's are shown labeled BS II-IV. These examples, associated with the F1 sand interval, appear bounded updip by faults, creating possible structural/stratigraphic gas traps.

Through this process, stratal slices can be used to map sequential depositional elements and to aid in the evaluation of exploration and infield drilling targets. The next step is to automate the procedure by applying Neural Networks in facies-pattern recognition.

Seismic Sedimentology

Like an air photo or satellite picture of a modern depositional system, stratal slices can be used in sedimentological study of ancient depositional systems. Stratal slices make full use of horizontal seismic resolution (limited to seismic bin size or a quarter seismic wavelength, whichever is larger), enough to depict most, if not all, depositional-facies changes meaningful in well-to-well-scale reservoir detection/description. Depositional facies cannot only be mapped areally in detail (as shown in fig. 86), but they can also be studied in geologic time to gain a sense of depositional history.

In the studied interval, expected stratigraphic resolution (at which two consecutive stratal slices show significant pattern changes) is around 5 m. In fact, as will be shown in the stratal slice movie, all fourth-order (30 to 130 m) and many fifth-order (5 to 30 m) depositional systems that can be recognized in well log correlation have been resolved by stratal slices. For example, figure 87 depicts four IVF's in a 100- to 200-m section all developed during fourth-order lowstand periods. Slices 2544 and 2560 are stratigraphically separated by a shale only 3 to 15 m thick. The four slices were selected from 28 stratal slices sliced proportionally through the interval, many of them depicting significant facies changes. The four-slice series highlights the migration of IVF's with geologic time by portraying their size, direction, and spatial distribution. Such generic information on the character and behavior of Miocene-Pliocene depositional systems can also be used to gain more regional understanding of targeting Mio-Pliocene exploration in the Gulf of Mexico.

Petrophysical Input to the Reservoir Characterization Process

The goals of the petrophysical analysis are to

- Identify unperforated zones and zones that are performing below their potential,
- Provide inputs for recompletion or infill-drilling opportunities,
- Examine primary completion designs and suggest improved designs for enhancing recovery, and .
- Provide quantitative estimates of petrophysical parameters to aid in mapping and estimate of gas resources.

To achieve these goals it is necessary to design an integrated petrophysical model that can be used to calculate various parameters on each well. These results will be coupled with seismic mapping and adjacent well and production data to target underperforated and underperforming zones in existing wells.

Establishing a Petrophysical Model

The petrophysical analysis of the two study fields should provide an estimate for each well of effective porosity, water saturation, permeability to air at surface conditions, net feet of permeable interval, permeability of gas at in situ conditions and net feet of gas pay. It is important that the model be calibrated to all available core information. The porosity calculated by the petrophysical model should match core effective porosity, and calculated permeability to air should be equal to core permeability to air. In addition, model and core effective porosity should match, model Sw should be 100 percent in water zones with no residual hydrocarbons, and the Sw should also be equal to core capillary-pressure data Swirr in zones that produce only gas. Finally, the model's permeability to gas should be equal to well-test permeability or net overburden stressed Klinkenberg corrected permeability.

This approach is complicated by several factors in this study. Only a single whole core exists in the study area, taken in the 31-6 through the Rob L Formation. This core has special core analysis (capillary pressure and net overburden permeability) on some of samples, but such limited amounts of whole core place some uncertainty on the derived model. These data are supplemented by a significant number of percussion sidewall core from area wells. The error bar around percussion core data is somewhat larger than that obtained using conventional or sidewall drilled core; however, this is the best information available in this field. An additional complication in building the petrophysical model is that open-hole porosity log data in the shales is of poor quality universally in all the hole conditions. To mitigate this later problem, the logs were compared with sidewall core porosities to help normalize the data. Several models were used to estimate porosity in every well, with the model that gave the best agreement with sidewall core porosity chosen. Models used included density-neutron crossplot, density, sonic, and an empirical porosity from core data and shale volume. Reasonably good agreement was attainable in all cases.

The focus of petrophysical work later in the calendar year has been in Starfak field. Starfak has an excellent distribution of porosity information, with logs in 56 wells. These data were analyzed and integrated with existing whole and sidewall core information, as well as a more regional analog data set of Miocene capillary pressure and permeability data to derive a set of final parameters and equations for calculating petrophysical parameters for Starfak field. These derivations are

- Rw 0.094 ohm-m at 77 F (from SP and Rmf) (northern Starfak wells)
- Rw 0.110 ohm-m at 77 F (from SP and Rmf) (southern Starfak wells)
- A = 0.81, m = 2, and n = 2

- Modified Simandoux model
- Temperature = 77 + 0.01 * depth
- $K^{air} = 10^{(1.663895E+01 * PHIEQ\ 2.449536)}$
- $K^{gas} = ((35.5 * PHIEQ^2 * ((PHIEQ-BVWQ)/BVWQ)))^2$
- $BVWI = (0.2552 * K^{air\ -0.2716})$
- SWI = BVWI/PHIEQ

Defining Unperforated and Underperforming Zones

With the petrophysical model currently in place, the identification of unperforated zones is relatively straightforward. If a zone has indications of reasonable hydrocarbon volume and permeability to hydrocarbons and there are no perforations in the zone within the zone's drainage area, it is unperforated pay. The identification of underperforming perforated zones is somewhat more involved. This determination can be done on two levels. The first level involves the calculation of volumetric reserves for the structural and stratigraphic compartment the completion is draining. A comparison of the current cumulative hydrocarbon production for the compartment with the volumetric reserves originally in place provides a good indication of the compartment's drainage. These reservoirs have well-documented recovery efficiencies in analog fields to estimate the amount of gas or oil that can be reasonably recovered. This information can be factored into a decision on whether a recompletion of an existing zone can recover the additional hydrocarbons or whether a new well is needed.

The second level of analysis involves a systems approach. The concept of NODAL analysis has been successfully applied in the Gulf of Mexico for the last 20 yr. The NODAL process provides an estimate of well performance as a function of drawdown pressure, near-well-bore skin damage, perforation efficiency, and tubing size. The three key inputs to this

process are effective permeability to hydrocarbons, reservoir pressure, and the magnitude of well-bore skin damage. All three of these can be obtained directly from a transient pressure well test. The most critical of the three is effective permeability to hydrocarbons. With the integration of well-test and well log data, this effective permeability value can be estimated from well log porosity and irreducible water saturation. The output of the analysis is an estimate of what the well should be producing with different completion options. The completion option of choice today in unconsolidated reservoirs is the "frac pack," where a gravel pack assembly is run in combination with a hydraulic fracture treatment. This was not widely used in the Miocene in the Gulf until the early to mid-1990's. At the time when most wells were drilled in Starfak and Tiger Shoal, the standard final completion procedure was either slightly overbalanced perforating in mud or underbalanced perforating. Both techniques have been shown since then to be ineffective in removing near-well-bore skin damage. These techniques normally result in high near-well-bore skin damage, with plus 10 to 15 very common. The "frac pack" procedure has resulted in significant productivity increases in high-permeability reservoirs, and it should be the procedure of choice for most of the sands in Starfak and Tiger Shoal. Negative skin values can be consistently obtained with this technique. In sands where water contacts are nearby, the preferred technique is extreme overbalanced perforating with tubing-conveyed perforating guns and resin for consolidation of the sands. This procedure has been successfully implemented on numerous high-permeability wells in the Gulf, with significant reductions in skin damage in all cases.

Underperforming Pay: Example from Blocks 30 and 31, "Y" Sandstone

All wells have been analyzed in Starfak field to date, and many wells with unperforated pay have been identified. A good example is the FS 40 sand (Y SS) in the southern portion of Block 30 and the northern portion of Block 31. FS 40 is present in most of the wells in the fault

block but has only produced from one well (8.5 Bcf from the 1-6 ST well). This area has been the focus of detailed analysis to assess potential resource addition.

During the initial log analysis it was observed that the 30-6 well had 59.5 ft of gas pay and the 30-5 well had 57.5 ft of gas pay, with no recorded production from either well following perforating. Both wells had been completed in late 1984. Upon further analysis it was observed that the 30-6 sidetrack twin to the 30-6 completed in 1997 was an excellent producer. The zone averaged 7.8 MMcf/d over the first 38 mo of production and was still making 6.6 MMcf/d with a 675 psi FTP in May of 2000. The 30-5 well is 2,300 ft away and the "Y" sand is of higher quality than the producing 30-6 ST well. The amplitude anomaly extends well to the west of the 30-5, and several locations should be available in addition to a workover in the 30-5. Pay is present in the 31-17 and 31-17ST to the south. The 30-5 has been plugged back to uphole zones; however, it was only making 200 Mcf/d in April of this year and may be a workover or sidetrack candidate soon if it is mechanically feasible.

Initial gas-in-place estimates are being refined according to the stratigraphic and structural interpretation. Rough numbers based on the pay thicknesses encountered in the four wells with "Y" sand pay indicate that between 91 and 259 Bcf of gas could be in place within the 2,050-acre amplitude anomaly. Only one well is currently draining this reservoir in the fault block. With only 8.5 Bcf recovered to date, this total represents between 3.3 and 9.3 percent of original gas in place.

The primary reason the initial completions did not produce was most likely the failure to remove formation damage. In 1984 the most advanced stimulation practice in the Gulf of Mexico was tubing-conveyed underbalanced perforating. The "Y" sand has below-average permeability for the Miocene in the Gulf (15 to 25 md), and it is normally pressured. Underbalanced perforating cannot remove damage in the permeability range observed in the "Y" sand.

Calculations based on laboratory data indicate that between 5,000 and 6,000 psi underbalance would be required to remove damage from the drilling and cementing process. Because these zones have only 5,000 psi reservoir pressure to begin with, such an undertaking is very difficult. In addition, if more than 500 psi underbalance is placed across unconsolidated sand faces, the formation can collapse. Analysis of production records indicates a lot of sand production from these wells, and it is highly likely that they would not remain competent under the underbalanced conditions required to remove damage.

Modern completion practices include hydraulic fracturing, combined fracturing and gravel packing ("frac-packs"), and extreme overbalanced perforating. The proper stimulation procedure for these zones would depend on the degree of consolidation of the formation and the proximity to water. In any case, the damage can be removed and production maximized.

FY 2001 WORK PLAN

The OSGR team met many of our original goals in FY 2000, including fault-plane and horizon interpretation of the seismic data volume, integrated depositional sequence analysis, detailed seismic and well-log facies analysis, fluid/seismic response analysis and initial assessment of prospects and resource distribution. We are well under way in completing tasks in well-by-well engineering, completion and production analysis, seismic attributes and hydrocarbon indicator analysis, risk evaluation, and prospecting for resource addition targets. Because the dynamics of this project involve interaction with Texaco's ongoing development activity, many of the project tasks will be ongoing throughout the life of the project. The OSGR project timeline is currently on track. The team (1) presented two papers at the 2000 AAPG Meeting in New Orleans and another at the Society of Exploration Geophysicists 2000

Development and Production Forum, (2) shared both fall and spring project planning reviews with Texaco, and (3) mentored six students working on Ph.D. theses using data related to the project. One of the students has finished his thesis titled *Evaluation of Risk Analyses and Their Application in Exploration and Production of an Offshore Petroleum and Gas Field,* and it will be submitted to the graduate school this fall. In addition, we formalized a new website for Offshore SGR (http://www.beg.utexas.edu/resprog/sgr/index.htm) to facilitate public dissemination of research results. Researchers also plan to submit several abstracts for presentation at the 2001 AAPG Meeting in Denver.

The FY 2001 work plan for the OSGR project focuses on continuing to build a model of the genetic hydrocarbon system in the area of primary well log control. This model will be transferable generically to other geographic areas and Miocene-age strata in the Gulf of Mexico. The next task in completing Phase 3 of the project is production of structure, isopach, isolith, paleogeographic, systems tract, and petrophysical maps on all third-order sequences and on fourth-order sequences representing main production intervals. Production data will be plotted for all log cross sections. A petrophysical model using all available information should be completed by fall and will be used to continue development of a transform for deriving petrophysical attributes from the seismic data. Now that the fault polygons have been mapped, quality checked, and finalized, their information can be loaded into a data base for fault analysis and seal evaluation. Seismic attribute and facies analysis will continue within the established framework of key surfaces. Plans are to test the application of neural-network-based facies-interpretation software as a tool for reducing cycle time in 3-D seismic interpretation. In addition, we will begin testing software in earnest and designing a process for incorporating this detailed information into a 3-D reservoir model for key units across the area. Analyses of all

these data will converge in FY 2001 into a preliminary portfolio of prospects and recompletion opportunities for the existing fields, assessment of intrafield opportunities, and an initial assessment of remaining reserves.

ACKNOWLEDGMENT

The Bureau of Economic Geology acknowledges support of the SGR Project by Landmark Geographics Corporation via the Landmark University Grant Program.

REFERENCES

Diegel, F. A., Karlo, J. F., Schuster, D. C., Shoup, R. C., and Tauvers, P. R., 1995, Cenozoic structural evolution and tectono-stratigraphic Framework of the northern Gulf Coast continental margin, *in* Jackson, M. P. A., Roberts, D. G., and Snelson, S., eds., Salt tectonics: a global perspective: American Association of Petroleum Geologists Memoir 65, p. 109–151.

Fillon, R. H., Lawless, P. N., and Lytton, R. G., III, 1997, Gulf of Mexico Oligocene-Miocene biostratigraphic and cycle chart: Texaco Exploration and Production, Inc.

Finley, R. J., and Tyler, N., 1994, Infield development for independent producers: Gulf Coast Association of Geological Societies, Short Course Notes No. 1, unpaginated.

Fisher, W. L., 1999, Energy and environment into the twenty-first century: the challenge to technology and ingenuity: Environmental Geosciences, v. 6, no. 4, p. 191–199.

Haq, B. U., Hardenbol, J., and Vail, P. R., 1988, Mesozoic and Cenozoic chronostratigraphy and cycles of sea-level change, *in* Wilgus and others, eds., Sea-level changes: an integrated approach: Society of Economic Paleontologists and Mineralogists Special Publication No. 42, p. 71–108.

Hefner, R.A., 1993, New thinking about natural gas, *in* The future of energy gases: U.S. Geological Survey Professional Paper 1570, p. 807–829.

Hentz, T. F., Seni, S. J., and Wermund, E. G., Jr., eds., 1997, Atlas of northern Gulf of Mexico gas and oil reservoirs: volume 2. Pliocene and Pleistocene reservoirs: The University of Texas at Austin, Bureau of Economic Geology, 78 p. + 3 pl.

Hentz, T. F., Zeng, H., Wood, L. J., Kilic, C., Yeh, J. S., Skolnakorn, J., and De Angelo, M., 1999, Targeting reserve growth opportunities in the northern Gulf of Mexico basin: transferring secondary gas recovery technology to the offshore environment: The University of Texas at Austin, Bureau of Economic Geology, technical progress report: year 1, prepared for U.S. Department of Energy, Federal Energy Technology Center, under contract no. DE-FC26-98FT40136, 40 p.

Hilterman, F., 1990, Is AVO the seismic signature of lithology? a case history of Ship Shoal-South Addition: The Leading Edge, v. 9, no. 6, p. 15–22.

Lore, G. L., Ross, K. M., Bascle, B. J., Nixon, L. D. and Klazynski, R. J., 1999, Assessment of conventional recoverable hydrocarbon resources of the Gulf of Mexico and Atlantic outer continental shelf; as of January 1, 1995: U.S. Department of the Interior, Minerals Management Service, Gulf of Mexico OCS Region, Office of Resource Evaluation, OCS Report MMS 99-0034, CD-Rom.

Posamentier, H. W., Dorn, G. A., Cole, M. J., Beierle, C. W., and Ross, S. P., 1996, Imaging elements of depositional systems with 3-D seismic data: a case study: Gulf Coast Section, Society of Economic Paleontologists and Mineralogists Foundation, 17th Annual Research Conference, p. 213–228.

Seni, S. J., Hentz, T. F., Kaiser, W. F., and Wermund, E. G., Jr., eds., 1997, Atlas of northern Gulf of Mexico gas and oil reservoirs: volume 1. Miocene and older reservoirs: The University of Texas at Austin, Bureau of Economic Geology, 199 p.

Styzen, M. J., compiler, 1996, A chart in two sheets of the Late Cenozoic chronostratigraphy of the Gulf of Mexico: Gulf Coast Section, Society of Economic Paleontologists and Mineralogists Foundation, 2 sheets.

Texaco Exploration and Production, Inc., 1996, South Marsh Island 3-D Survey Processing Report, project number 11036-3D.

Thomas, L. K., Hankinson, R. W., and Phillips, K. A., 1970, Determination of acoustic velocities for natural gas: Journal of Petroleum Technology, v. 22, no. 7, p. 889–892.

Wang, Z. J., Nur, A., and Batzle, M. L., 1988, Acoustic velocities in petroleum oils: Society of Petroleum Engineers Paper 18163.

Zeng, Hongliu, 1994, Facies-guided 3-dimensional seismic modeling and reservoir characterization: The University of Texas at Austin, Ph.D. dissertation, 164 p.

Zeng H., Backus, M. M., Barrow, K. T., and Tyler, N., 1995, Three-dimensional seismic modeling and seismic facies imaging: Gulf Coast Association of Geological Societies Transactions, v. 45, p. 621–628.

Zeng H., Backus, M. M., Barrow, K. T., and Tyler, N., 1998a, Stratal slicing, part I: realistic 3-D seismic model: Geophysics, v. 63, no. 2, p. 502–513.

Zeng H., Henry, S. C., and Riola, J. P., 1998b, Stratal slicing, part II: real seismic data: Geophysics, v. 63, no. 2, p. 514–522.

Zeng, H., Hentz, T., and Wood, L. J., 2000, Three-dimensional seismic facies imaging by stratal slicing of Miocene-Pleistocene sediments in the greater Vermilion block 50—Tiger Shoal field area, offshore Louisiana (ext. abs.): American Association of Petroleum Geologists Annual Convention, New Orleans, CD-Rom.

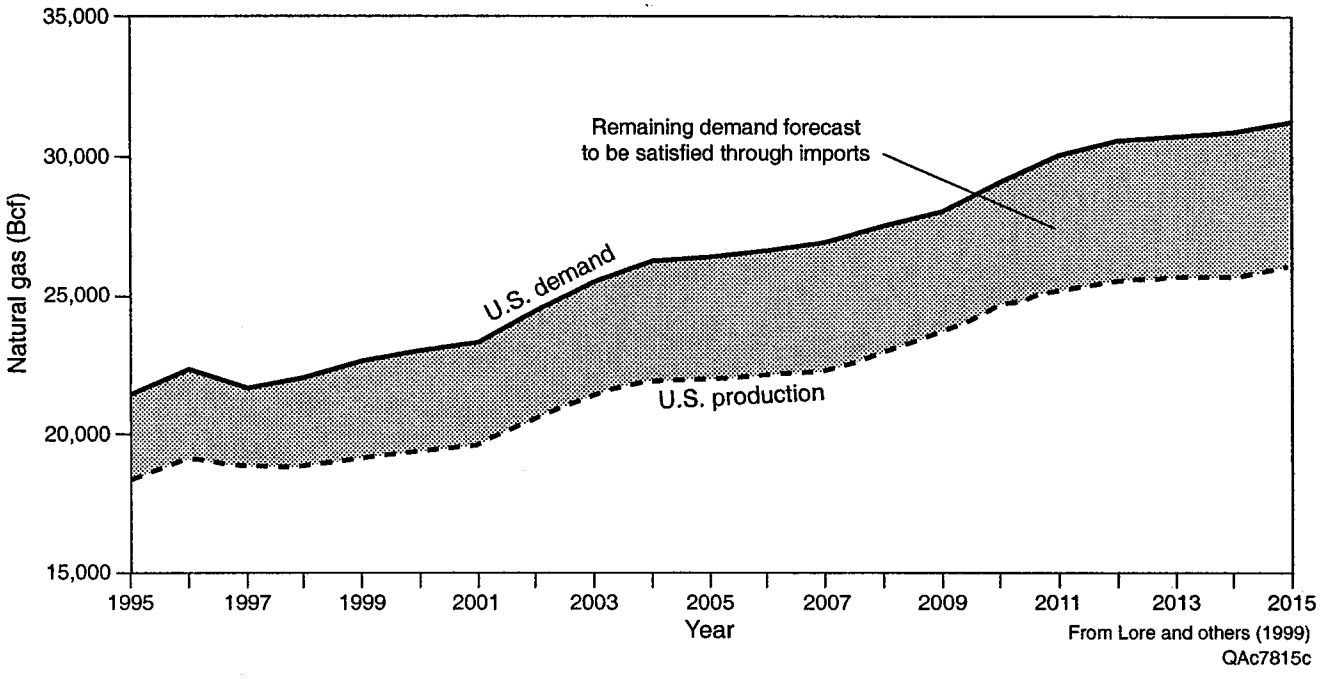

Figure 1. U.S. natural gas demand and production forecasts showing a widening gap between demand and production, indicating needed growth in either imports or domestic production to fill demand.

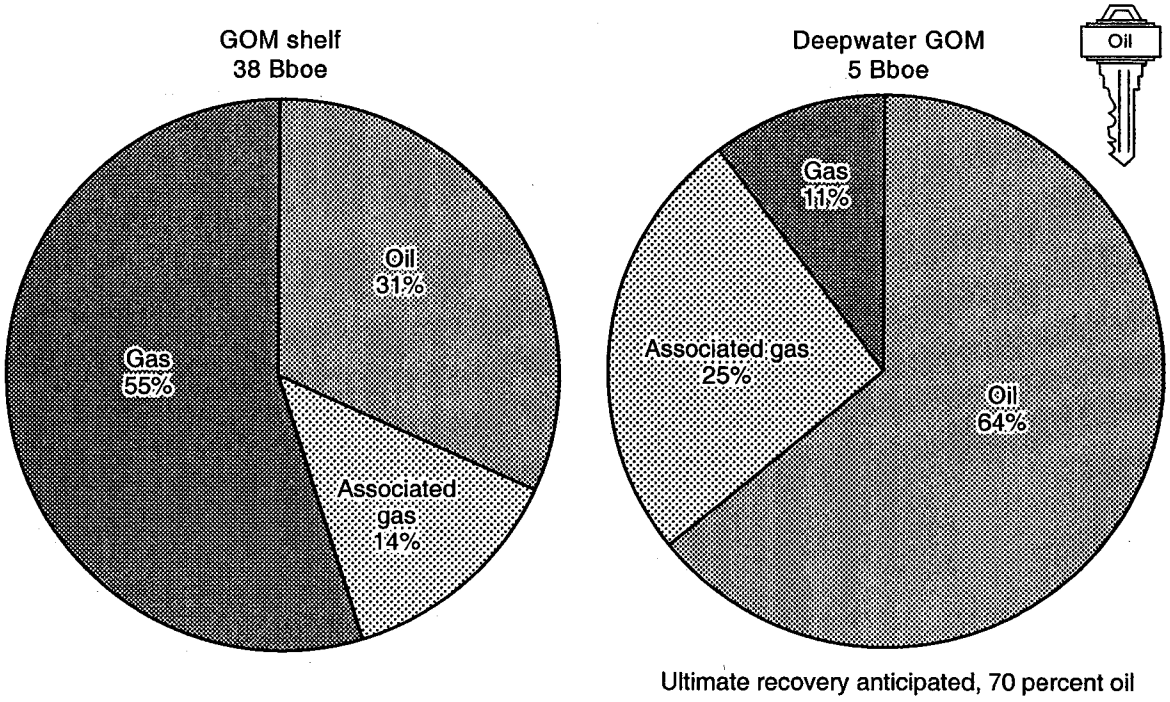

Figure 2. Pie-chart diagrams showing the state of hydrocarbons in the GOM on the shelf, where 55 percent is nonassociated gas, to the deepwater, where only 25 percent is gas and that gas is associated with oil.

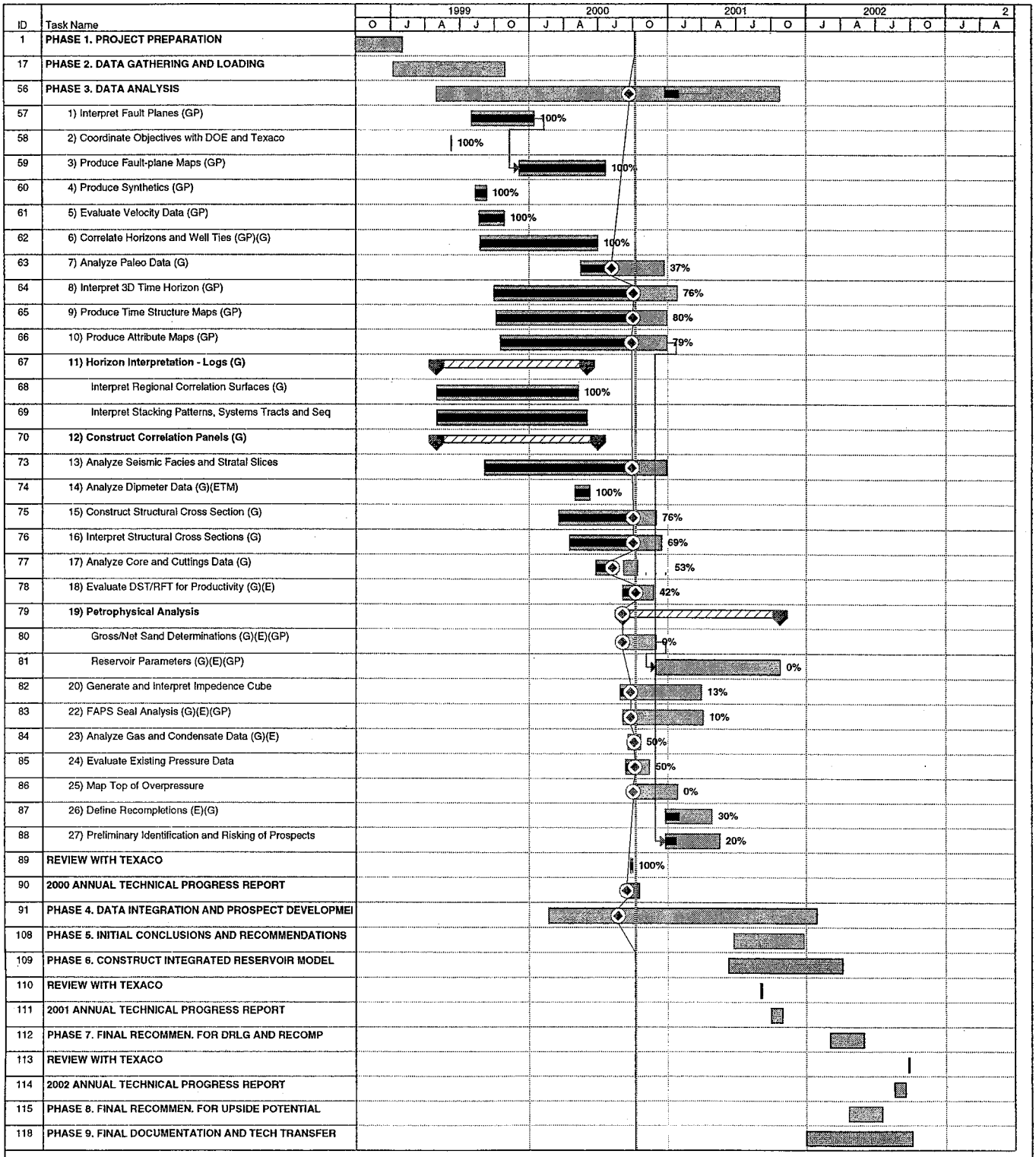

Figure 3. Gantt chart of project time line showing key project phases and events.

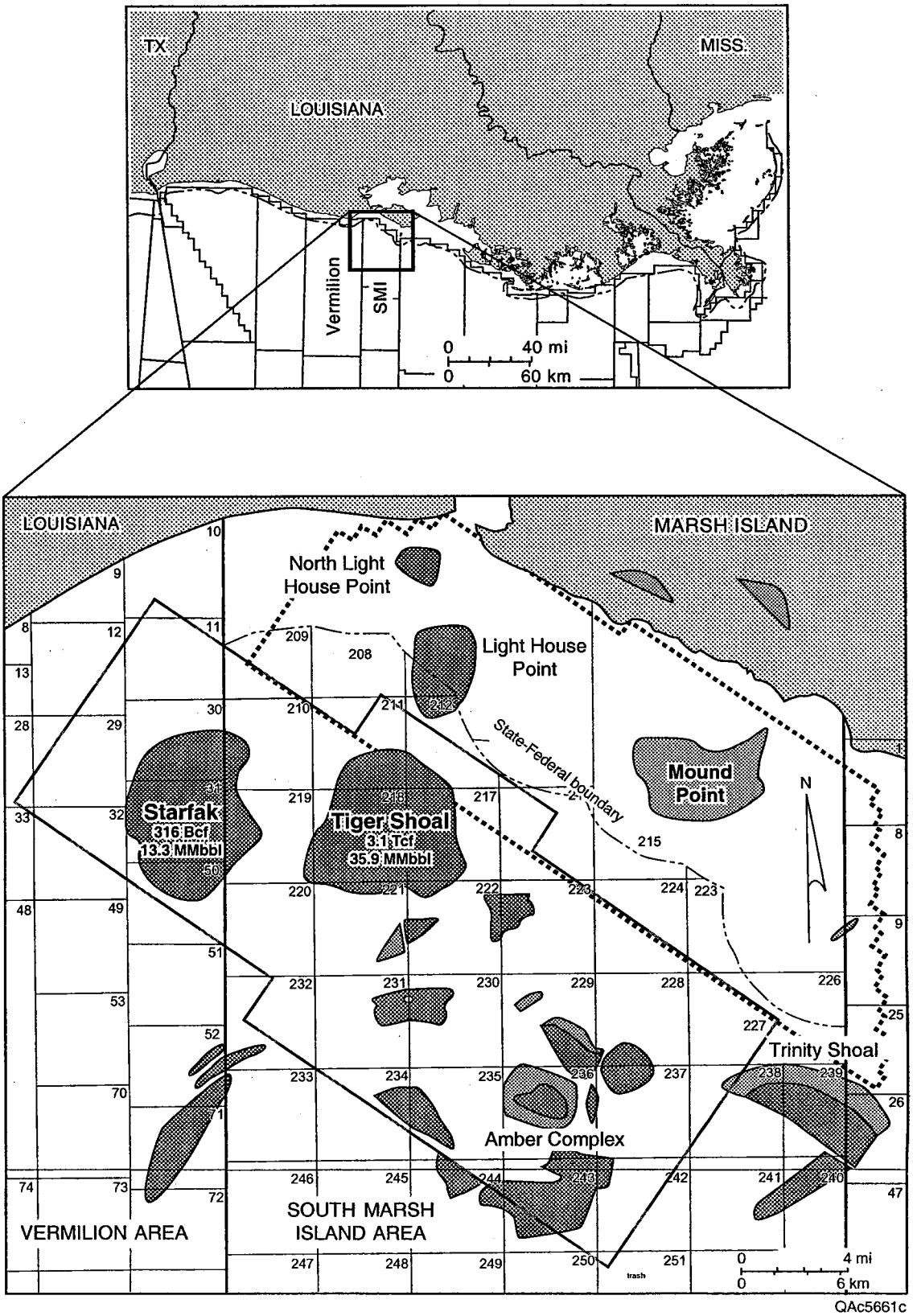

Figure 4. Map of the Vermilion and South Marsh Areas showing the study's primary target fields, Starfak and Tiger Shoal, as well as surrounding fields and the outline of the two major 3-D seismic surveys being used in this resource assessment.

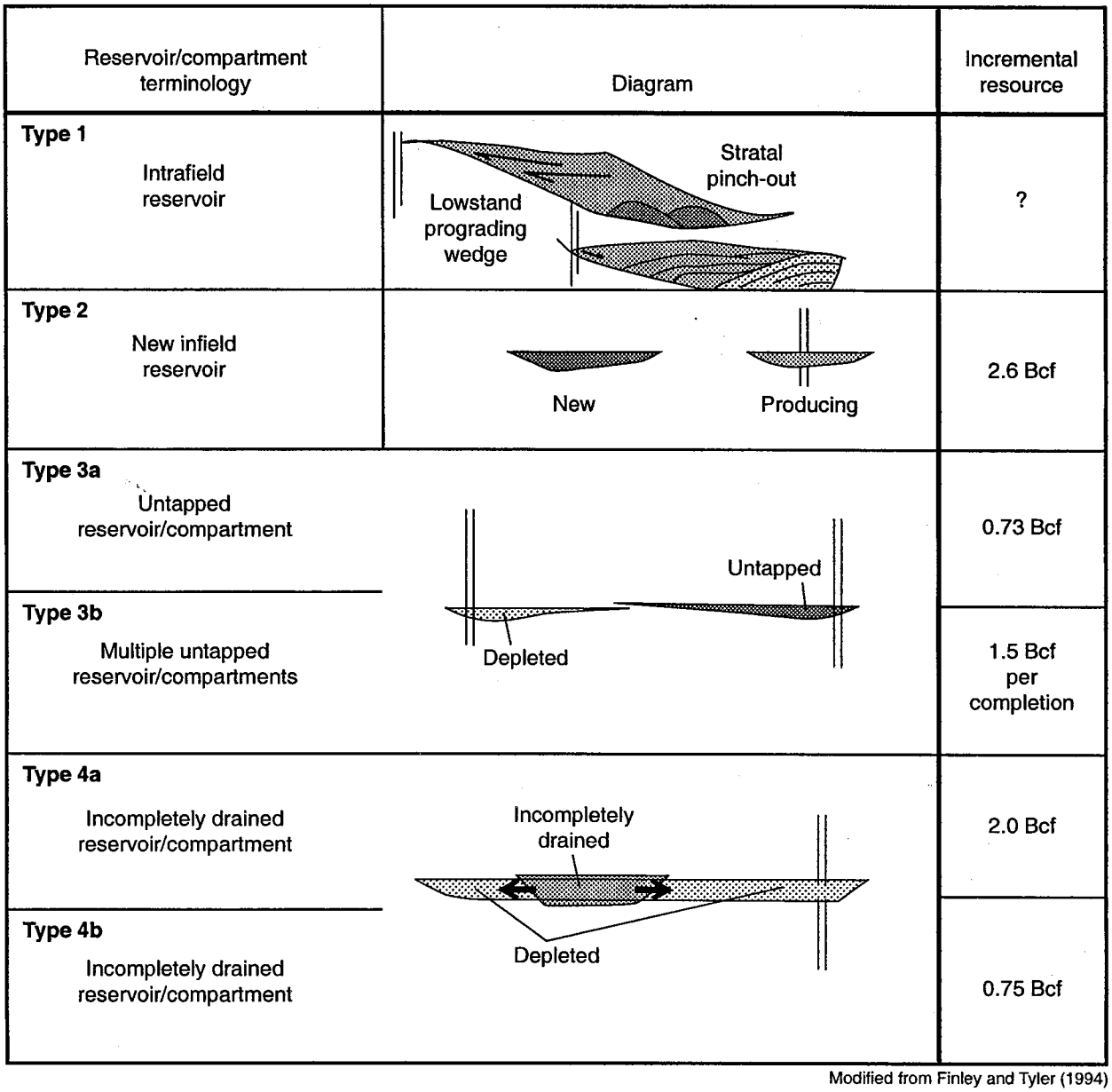

Figure 5. Schematic diagram modified from Finley and Tyler (1994) showing several opportunity types for reserve growth identified within the study area.

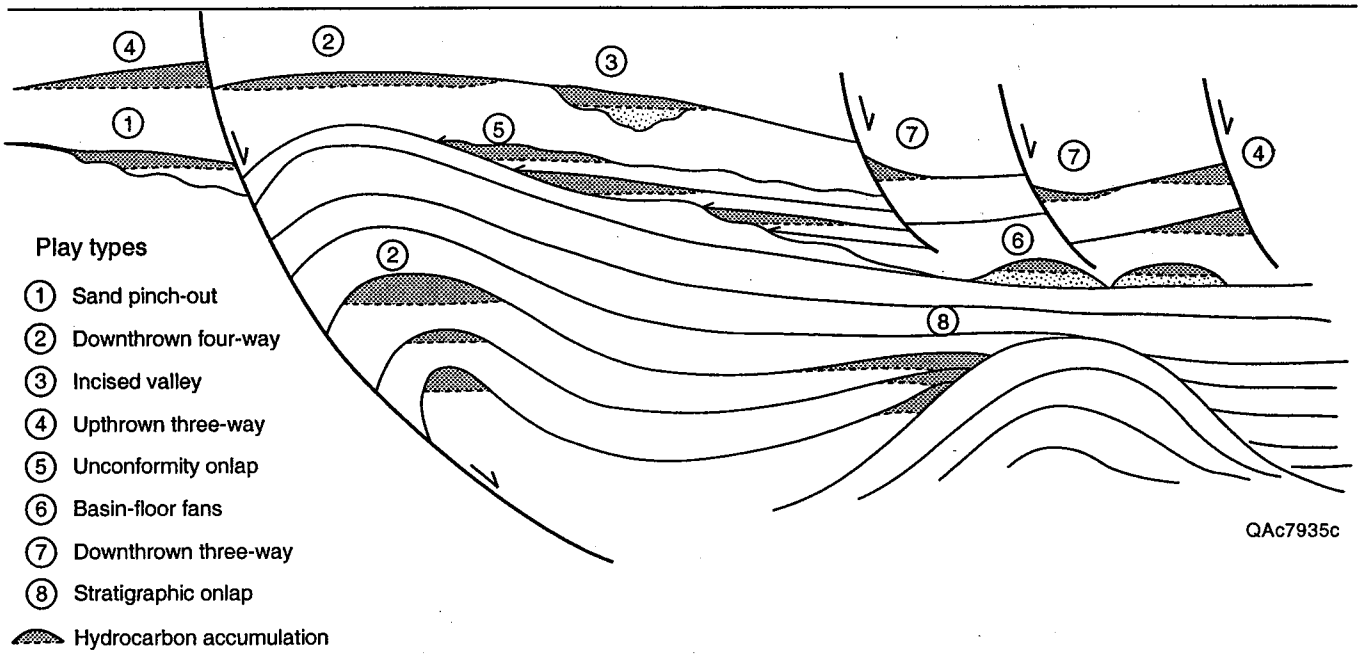

Figure 6. Schematic summary of structural and stratigraphic intrafield reserve growth opportunities (play types) preliminarily defined across the study area.

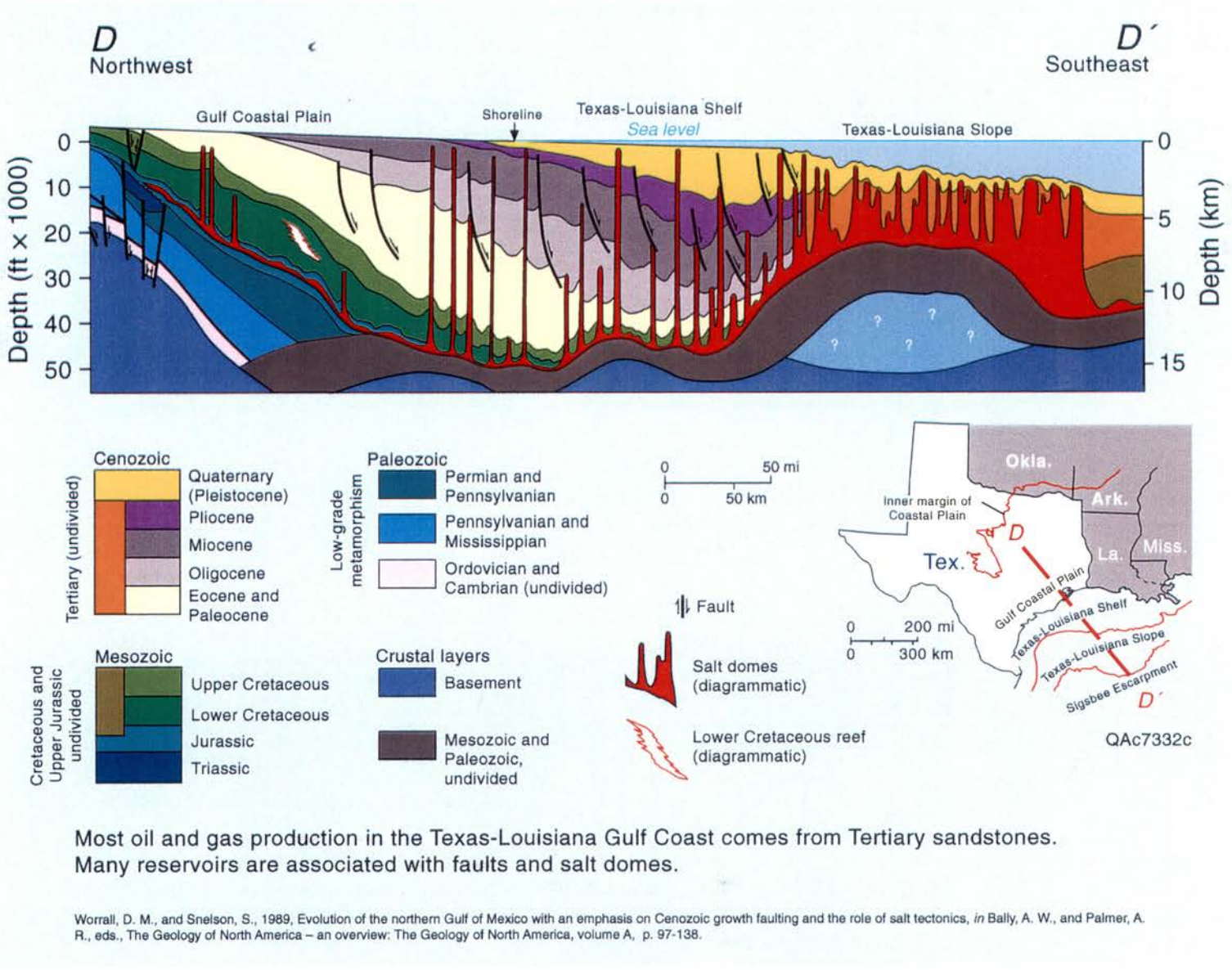

Figure 7. Regional cross section showing the main structural features and stratigraphic packages from northwest to southeast across the Gulf of Mexico. The study area is located along the Louisiana shelf, north of the main mobile salt province.

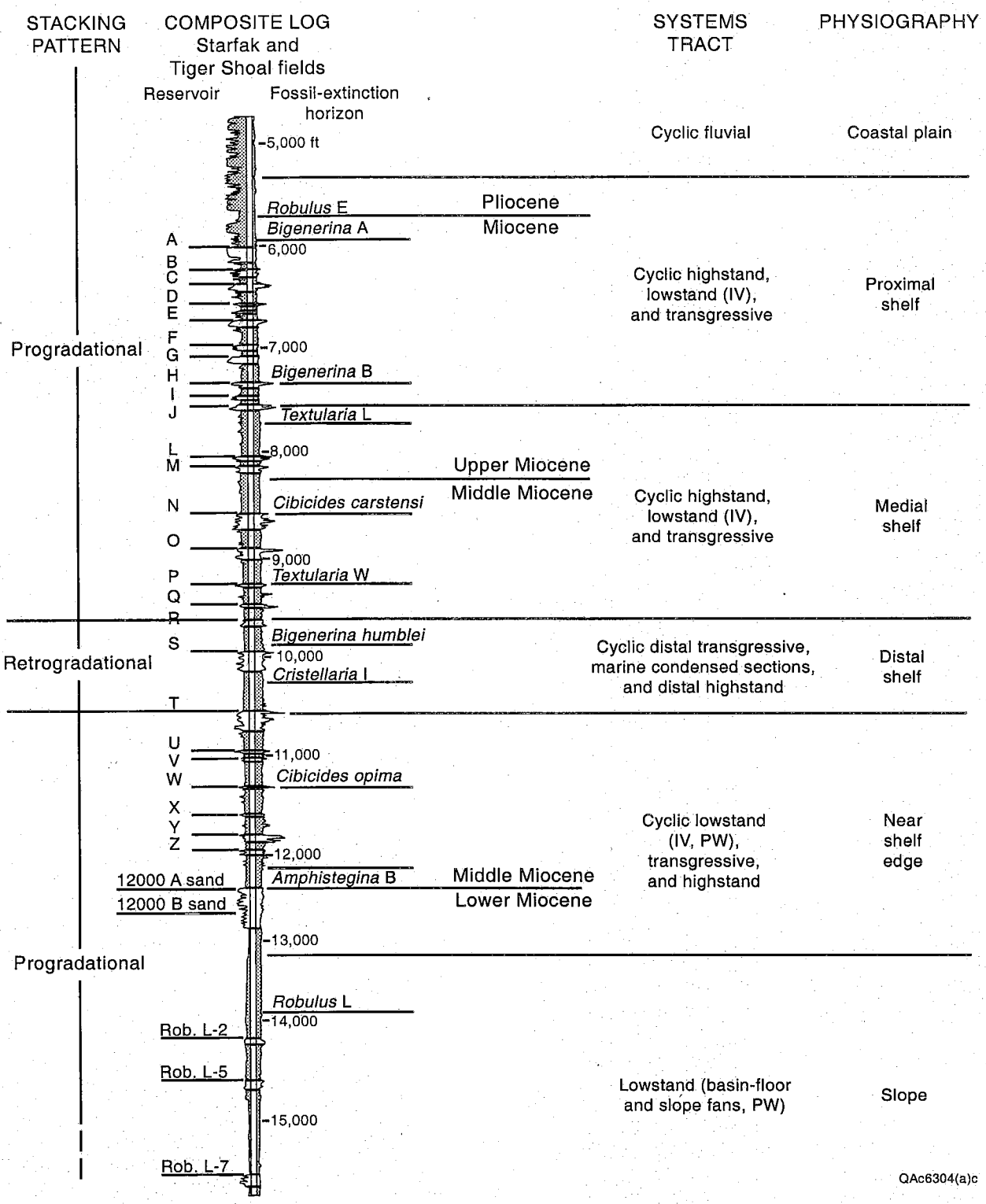

Figure 8. Composite type log of Starfak and Tiger Shoal fields that displays gross stacking patterns, reservoir nomenclature, extinction horizons of invertebrate paleofauna, and stage boundaries. Stage boundaries are approximate and are based on microfossils from several wells in each field. Interpretation of systems tracts and paleophysiography is based on wireline-log facies, inferred lateral facies relationships, facies-stacking patterns, and mapping using seismic data (primarily time-depth-structure and isochron maps and amplitude stratal slices).

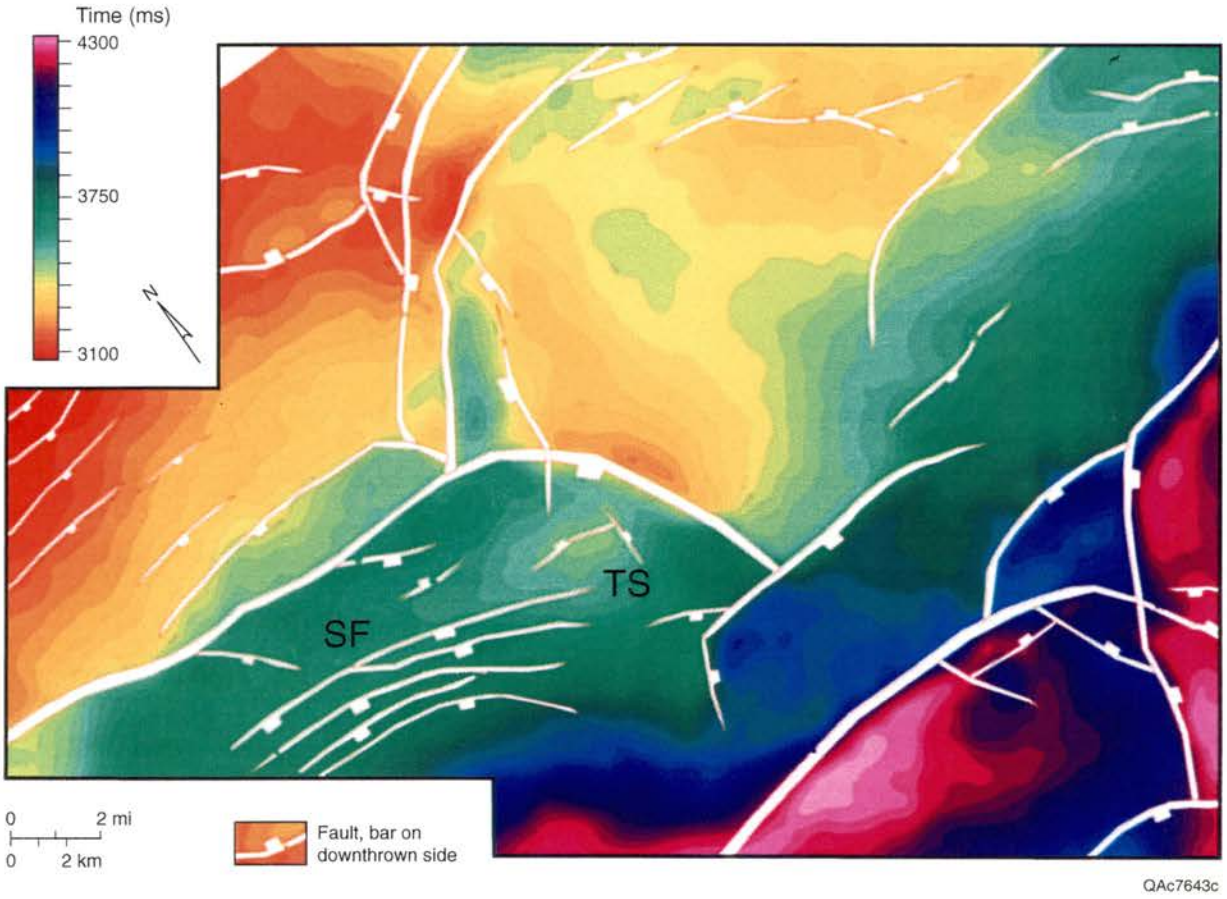

Figure 9. Time-depth-structure map of the Rob. L-4 sand (SB 54, plate 2). This unit occurs at approximately 14,700 ft in Starfak (SF) field. Note that the regional fault distribution varies from that of the shallower MFS 25 horizon (fig. 10). In particular, the deep-seated, east-west-trending faults that extend from Starfak field toward Tiger Shoal (TS) are absent at the shallower horizon.

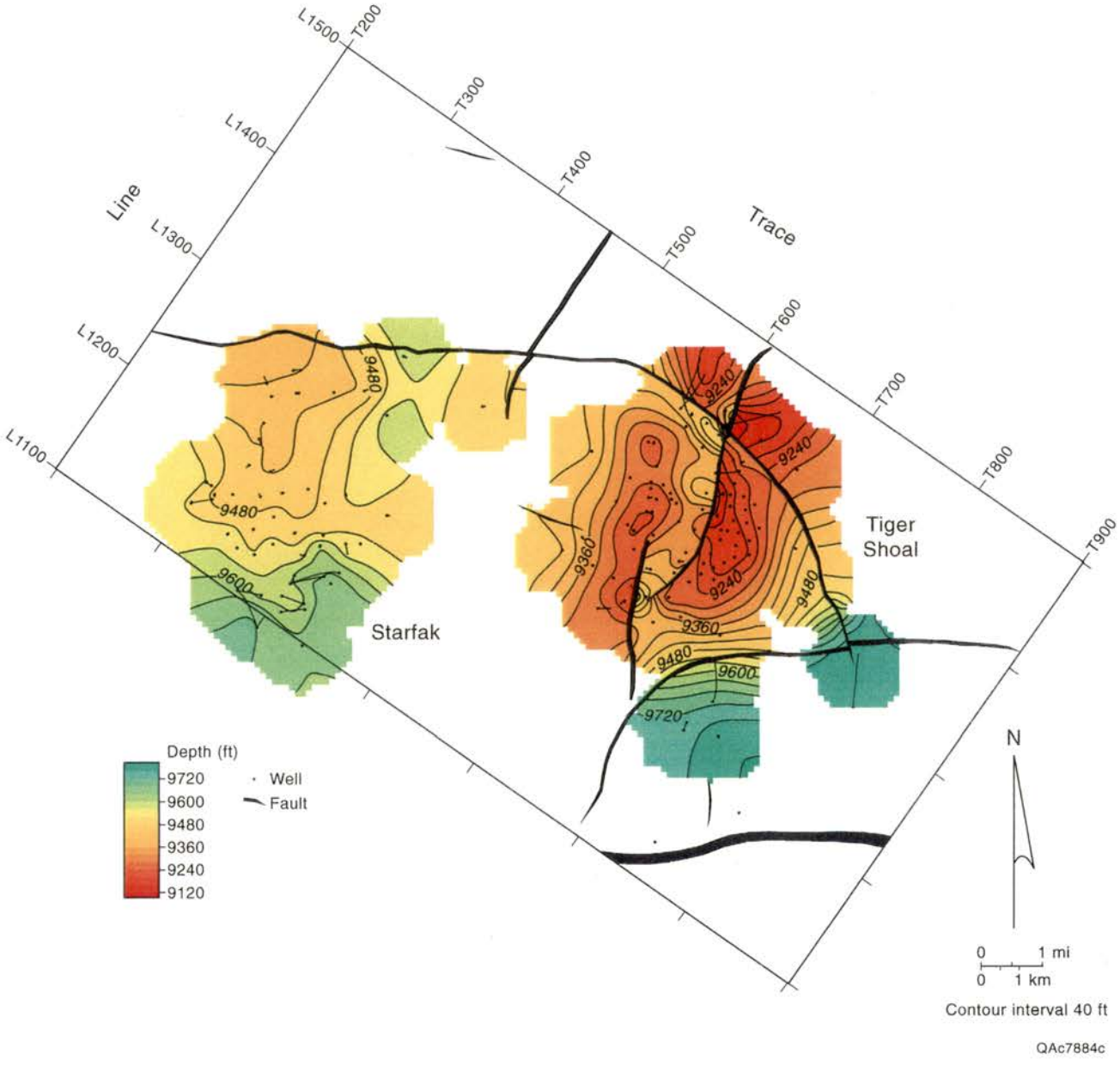

Figure 10. Structure map of MFS 25 (between O and P sands, plate 2) derived from well-log data. Fault traces derived from 3-D seismic interpretation.

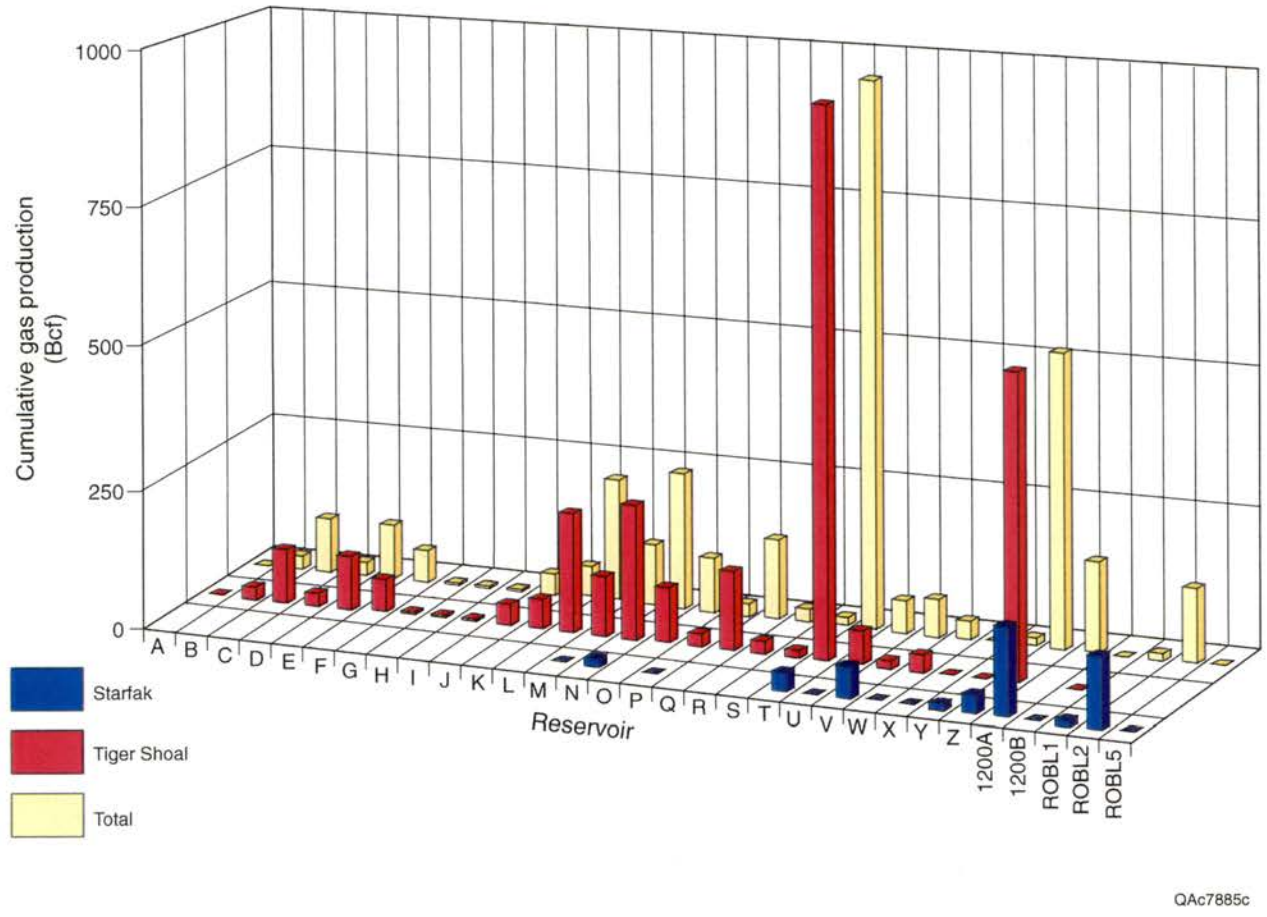

Figure 11. Bar graph of cumulative gas production (through 7/1/00) from all primary sandstone-body reservoirs in Starfak and Tiger Shoal fields.

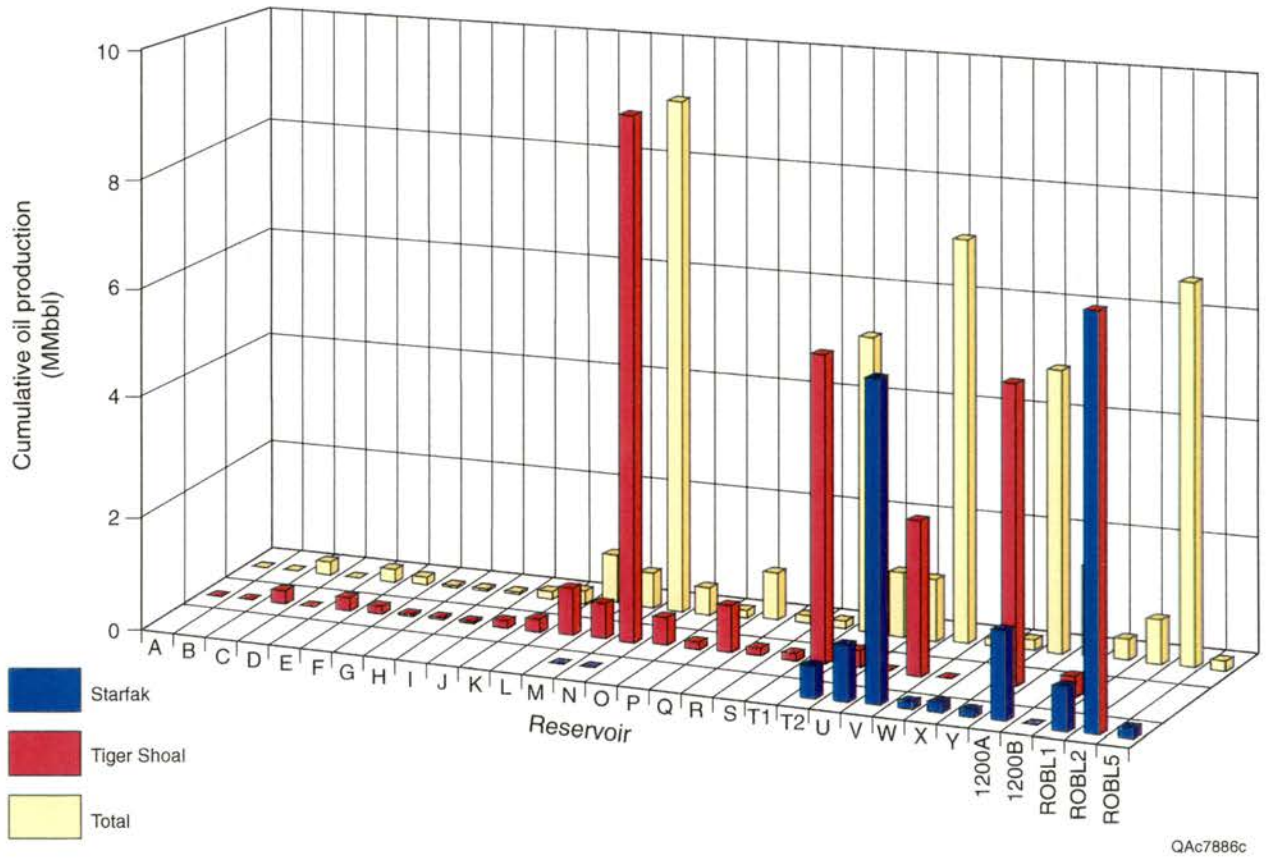

Figure 12. Bar graph of cumulative oil production (through 7/1/00) from all primary sandstone-body reservoirs in Starfak and Tiger Shoal fields.

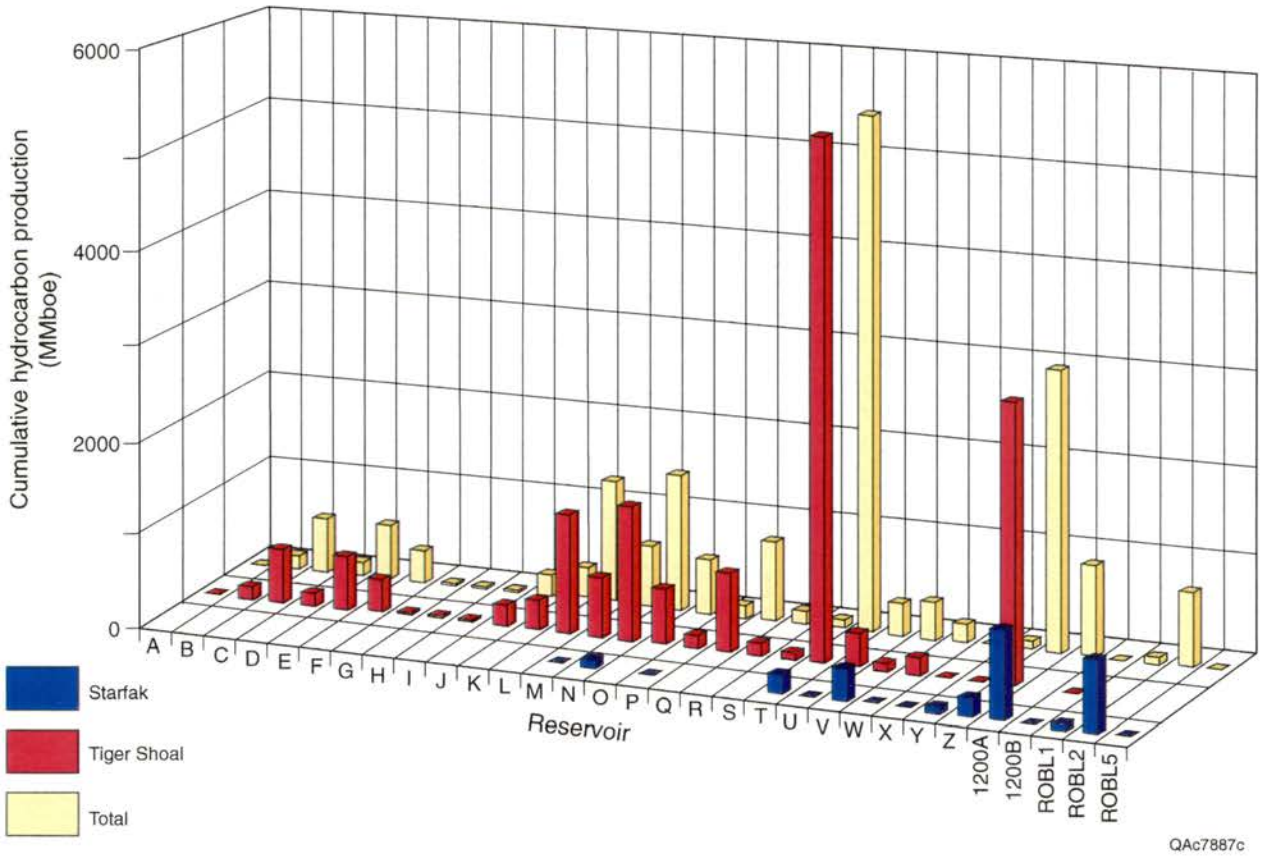

Figure 13. Bar graph of total hydrocarbon production (through 7/1/00) from all primary sandstone-body reservoirs in Starfak and Tiger Shoal fields. For conversion of gas-volume units into barrels-of-oil-equivalent (boe), we used the standard equation, 1 Mcf = 5.62 boe.

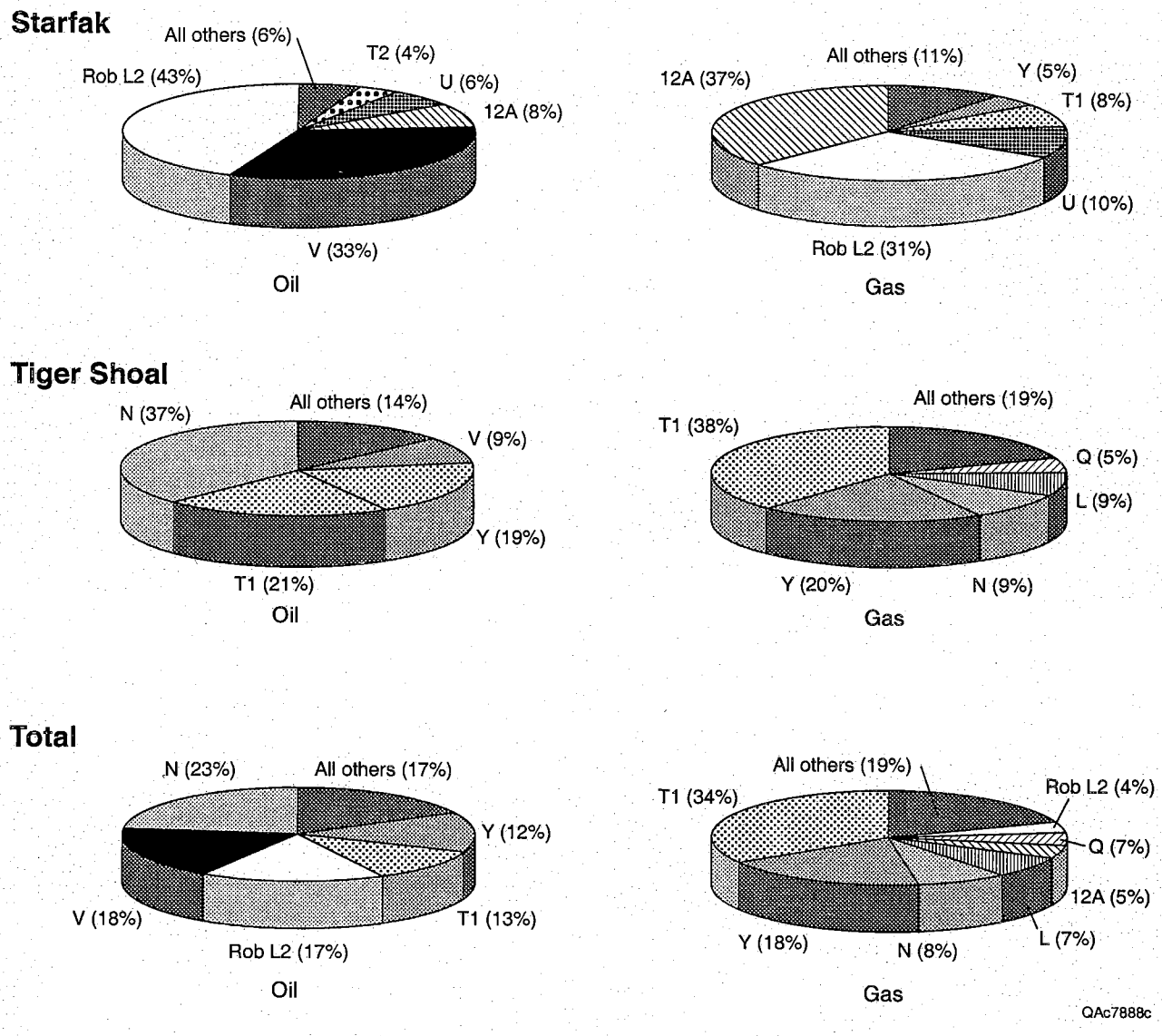

Figure 14. Pie charts illustrating relative percentage of oil, gas, and total hydrocarbons produced from specific reservoirs in Starfak and Tiger Shoal fields (through 7/1/00).

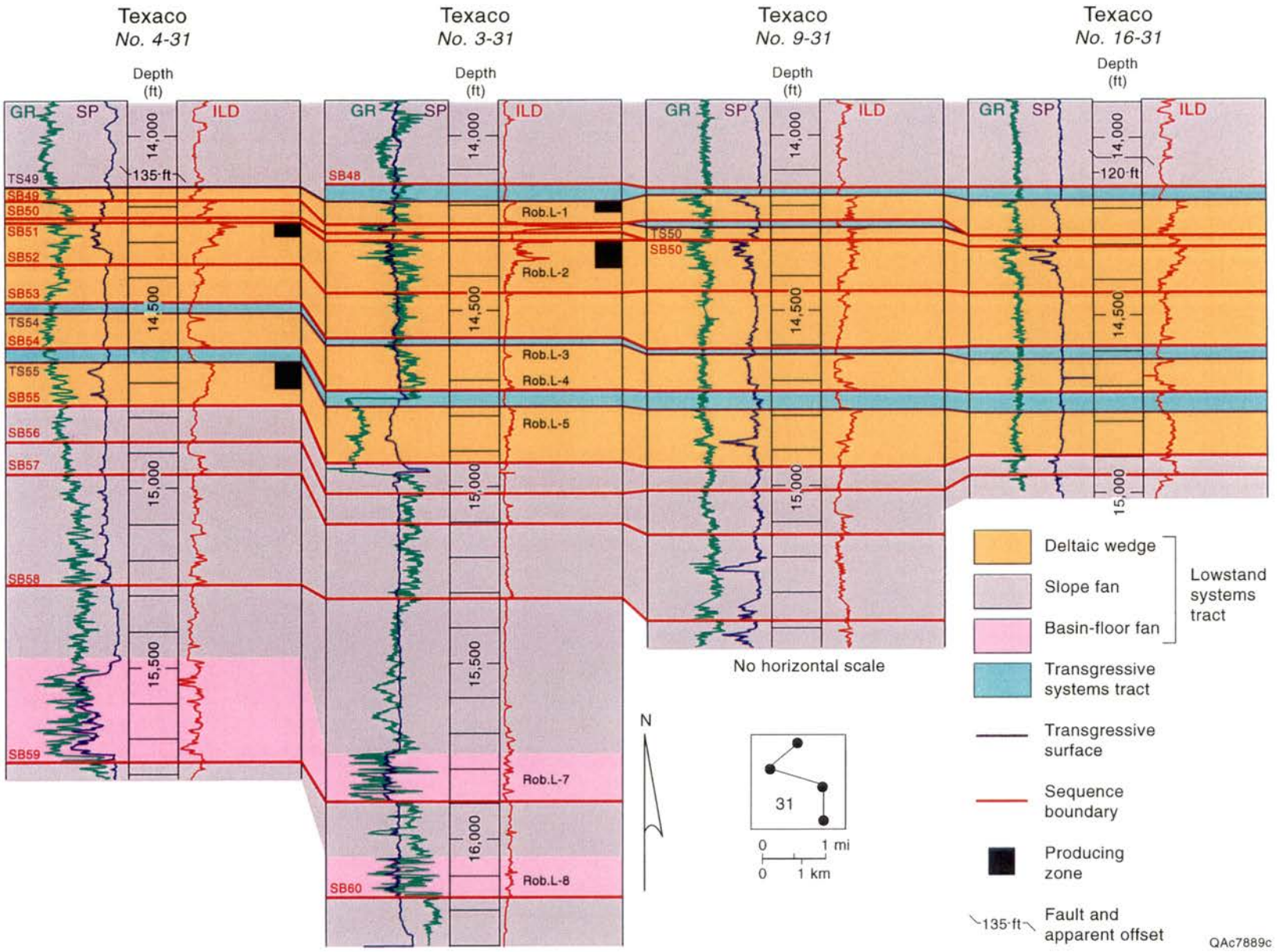

Figure 15. Well log cross section of the Rob. L sands, the deepest reservoirs in Starfak field. The succession between sequence boundaries (SB) 59 and 48 represents the distal portion of a third-order lowstand prograding wedge (lower part of third-order sequence 1 shown on plate 2).

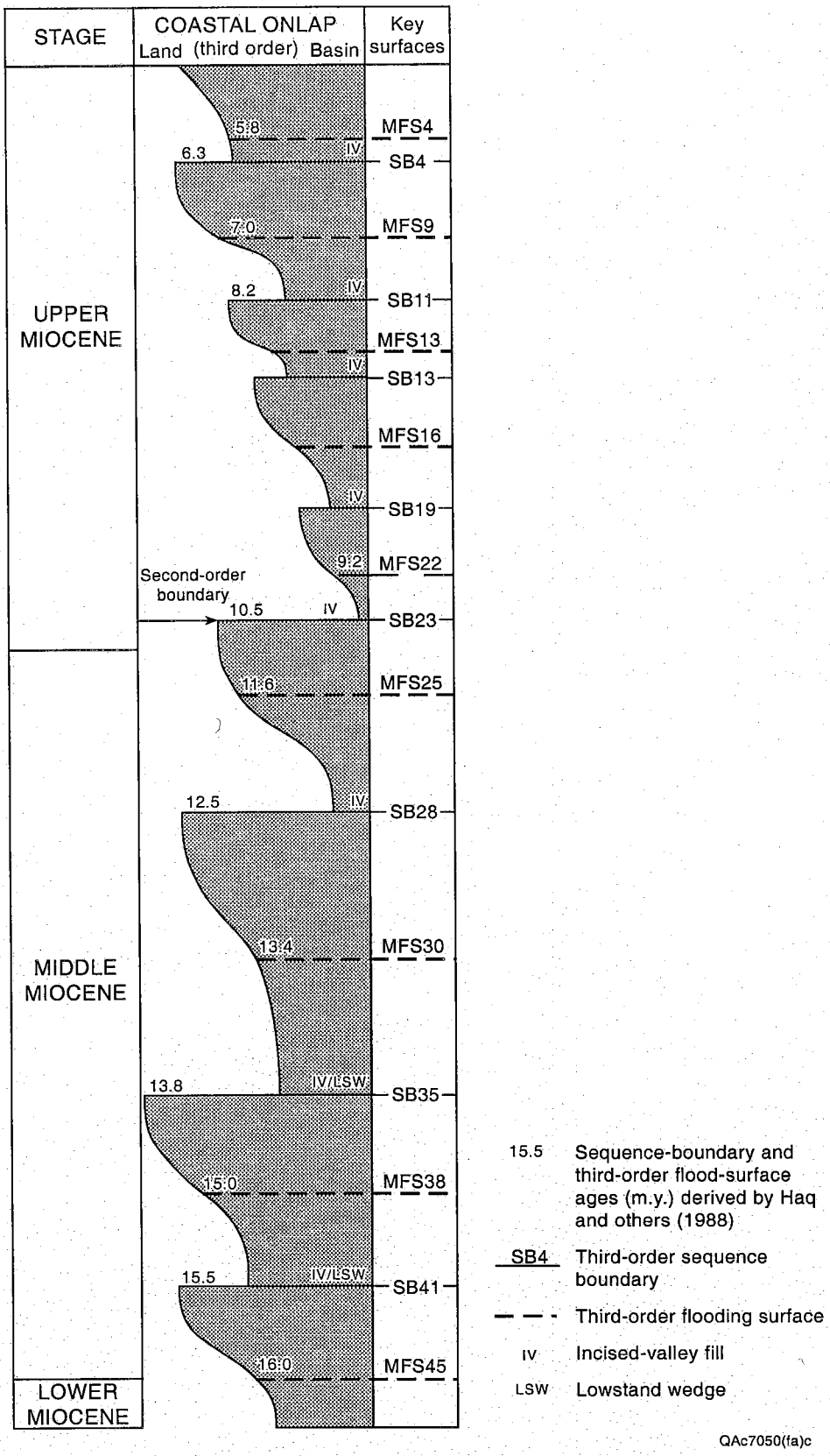

Figure 16. Coastal-onlap curve of third-order sequences in the uppermost lower Miocene to upper Miocene succession, as interpreted from well log data from Starfak and Tiger Shoal fields. Third-order sequence boundaries (SB) and maximum flooding surfaces (MFS) are represented. The succession represented is also that shown on plate 2 (upper part of third-order sequence 2 through sequence 10). After Haq and others (1988).

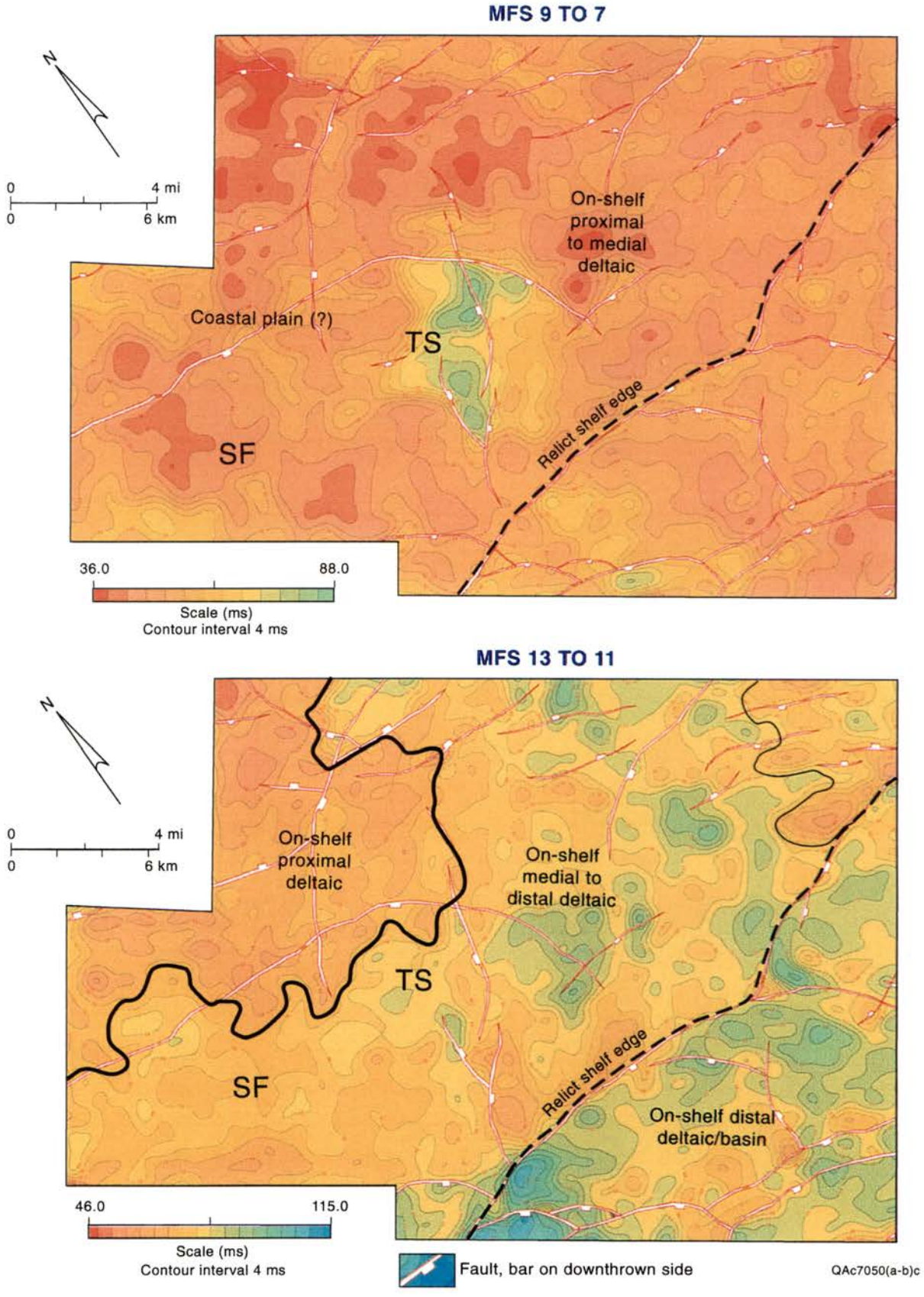

Figure 17. Seismic isochron maps representing thickness between fourth-order maximum flooding surfaces within four successive upper Miocene third-order cycles. Individual maximum flooding surfaces were initially correlated within the entire 3-D seismic cube after calibration with wireline logs in the two field areas. SF = Starfak, TS = Tiger Shoal.

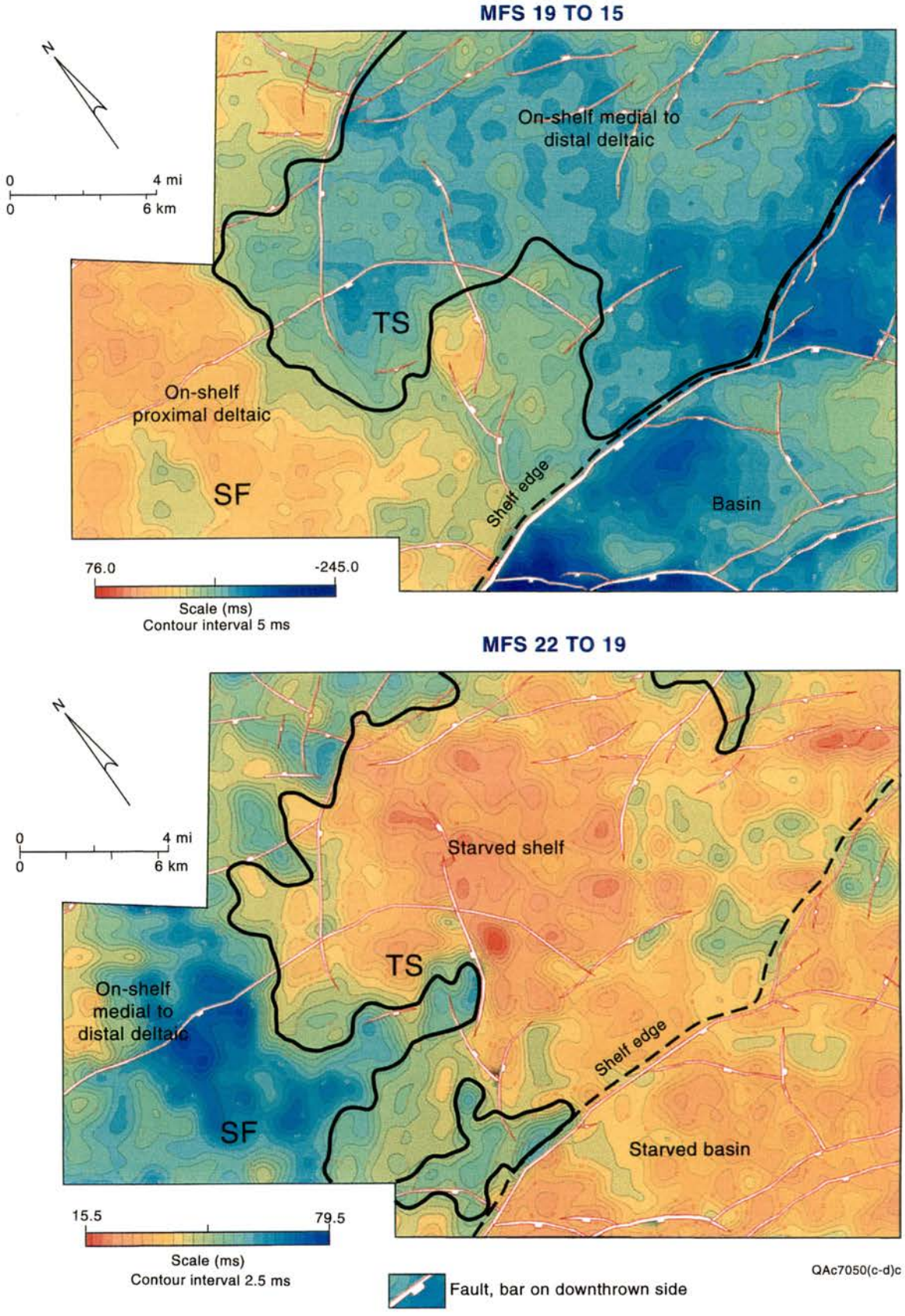

Figure 17. Continued.

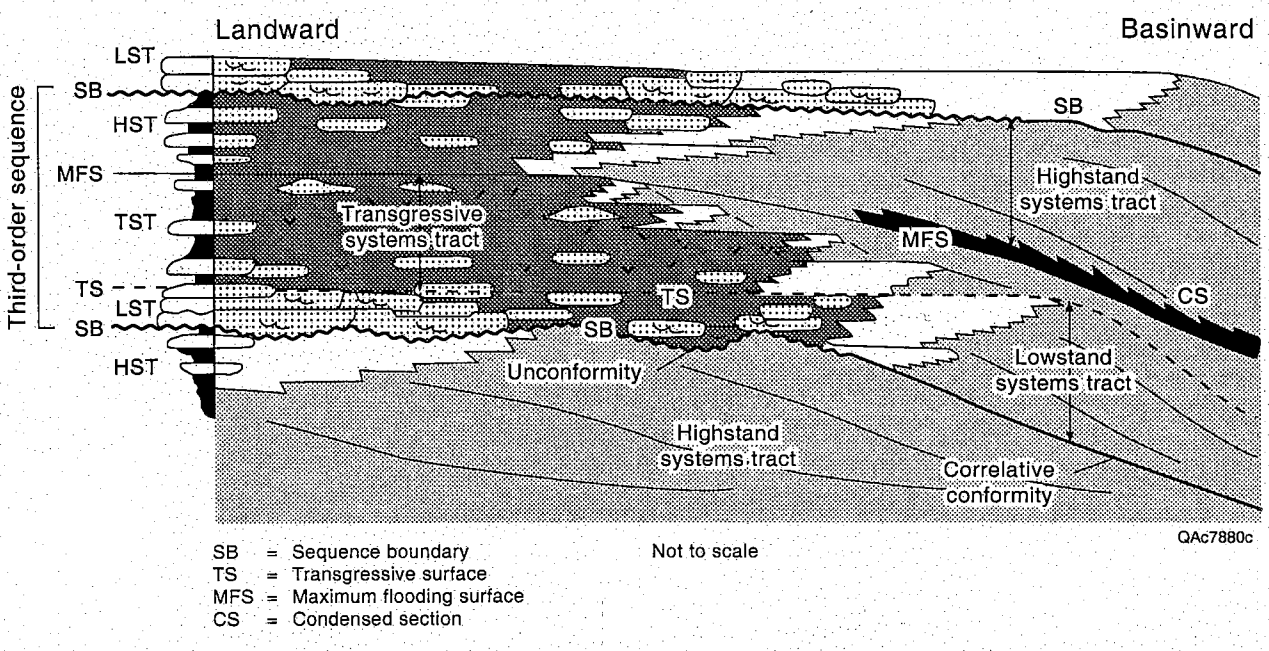

Figure 18. Schematic diagram of regional stratal stacking patterns and systems tracts within a third-order sequence.

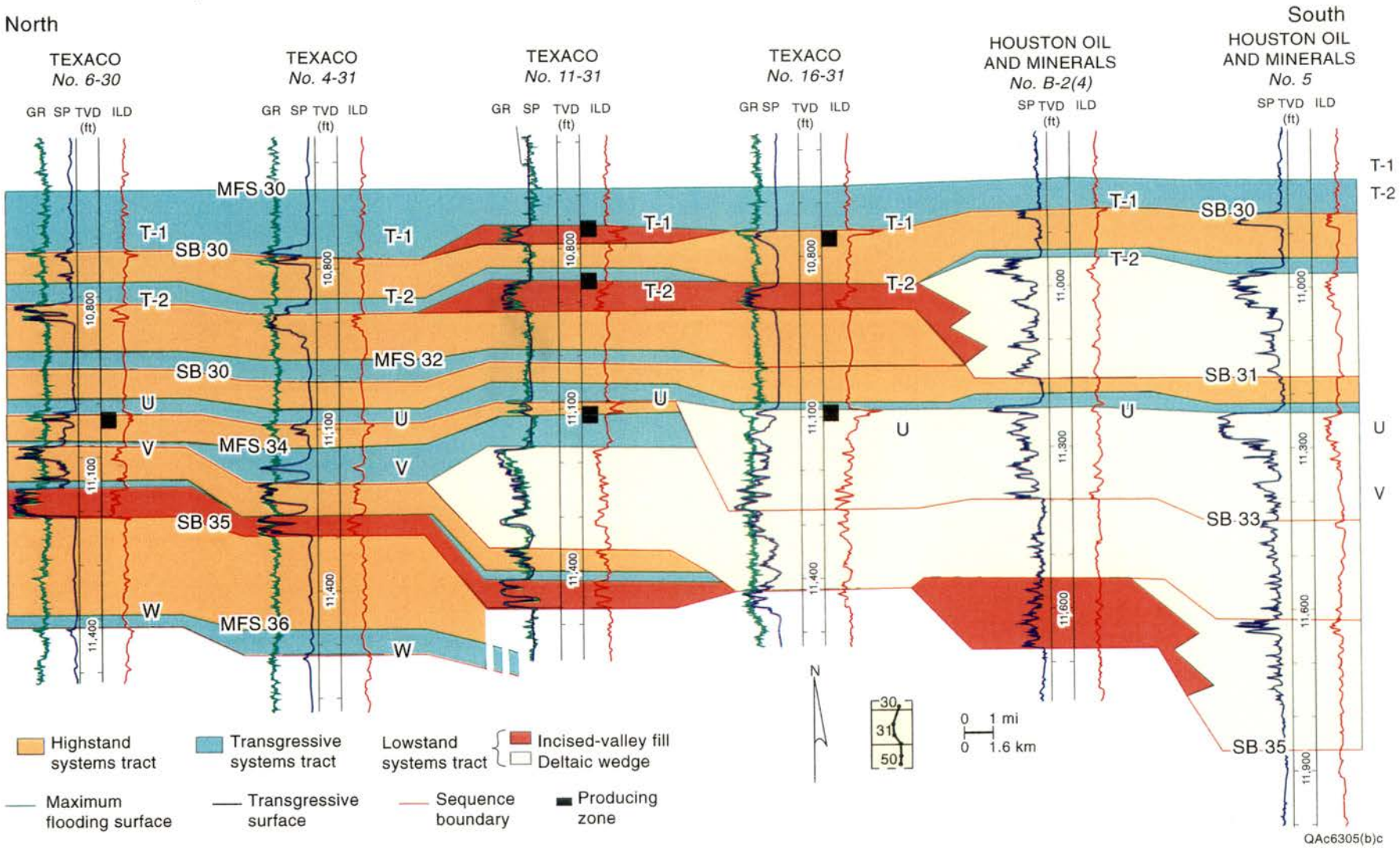

Figure 19. Depositional-dip-oriented cross section of the third-order lowstand systems tract comprising fourth-order SB 35 through 30 (T-1 to V sand) within third-order sequence 4 in Starfak field (plate 2). This transect portrays the regional updip, proximal pinch-out of fourth-order deltaic wedges within the field. Third-order lowstand systems tracts defined within the study interval are the intervals of greatest hydrocarbon production. Of all these, this lowstand systems tract has collectively produced the most hydrocarbons (see Relation of Production to Systems Tracts).

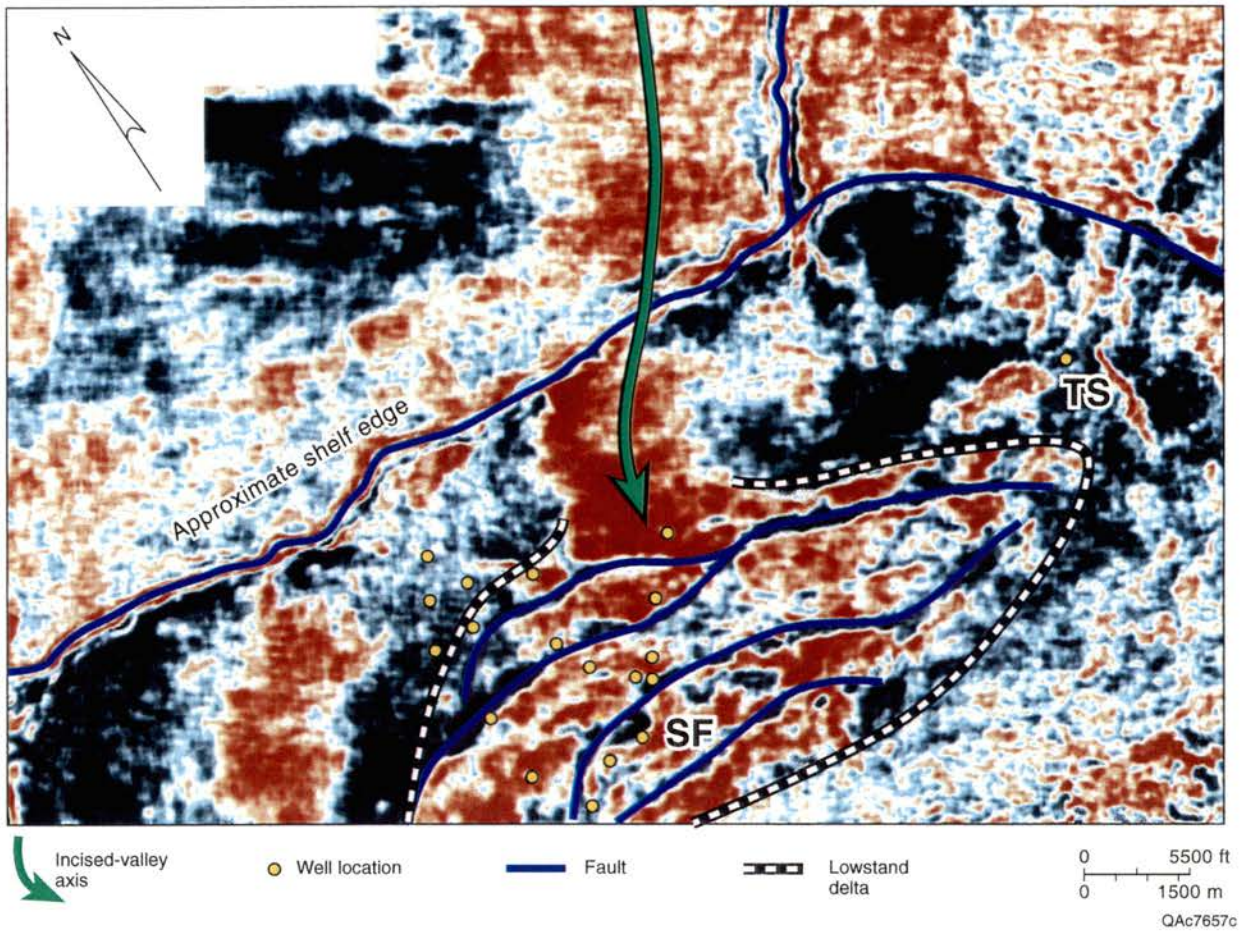

Figure 20. Amplitude stratal slice of the 12000A sand (SB 45) illustrating the lowstand deltaic wedge and incised-valley fill of third-order sequence 2 (plate 2) within the general area of Starfak (SF) and Tiger Shoal (TS) fields. The shelf edge of the preceding highstand systems tract, basinward of which relative sea level dropped immediately before wedge deposition, coincides with the first-order west-east-trending growth fault that transects the northern part of the two fields. This prominent paleophysiographic feature exerted significant control on the areal distribution of the lowstand systems tract. Syndepositional subsidence (growth) along the fault probably contributed significantly to creation of accommodation for the accumulation of the thick, lowstand-deltaic sands and associated slope-fan deposits. Note that the second-order, deep-seated, east-west-trending faults (fig. 9) that cut the wedge extend eastward from Starfak field into the undrilled area between the two fields, suggesting potential for new discoveries in this proven structural play.

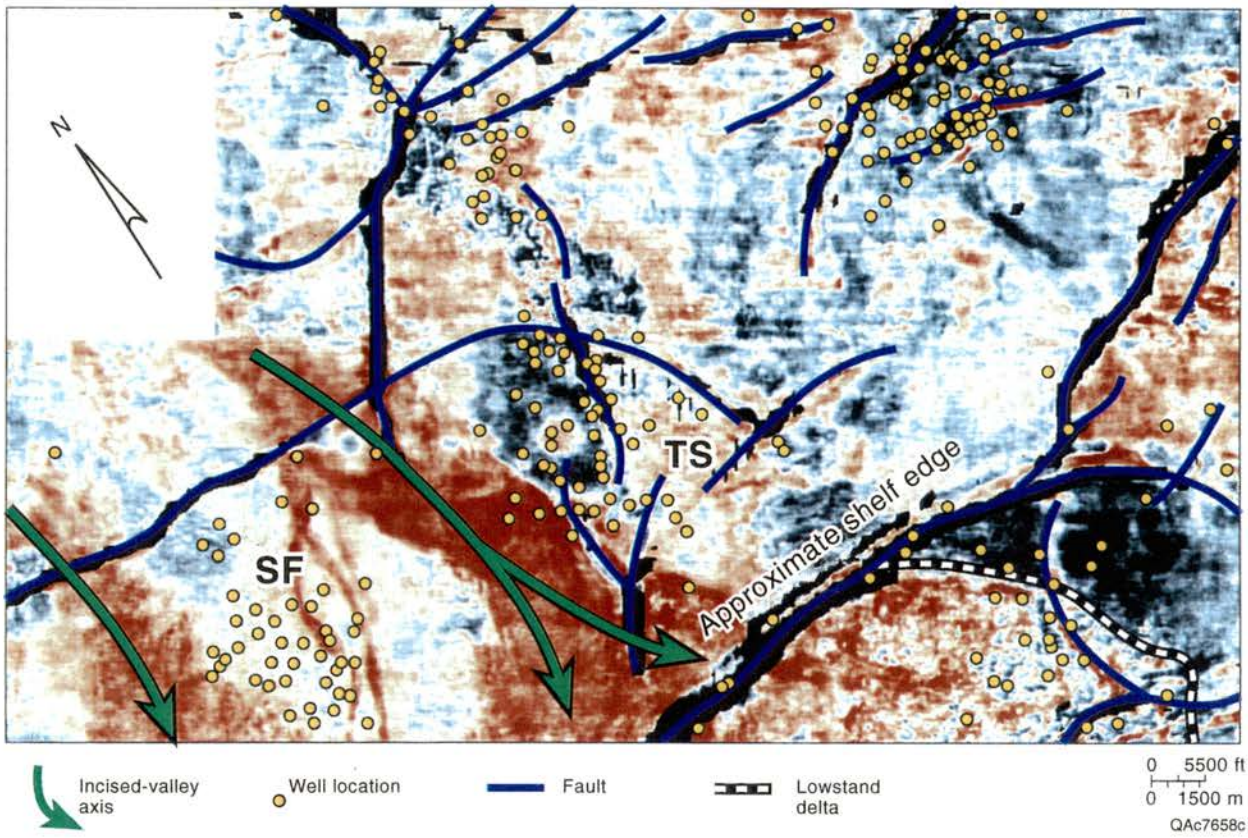

Figure 21. Amplitude stratal slice of the M sand (SB 18) illustrating the lowstand deltaic wedge and incised-valley fill of third-order sequence 7 (plate 2) within the general area of Starfak (SF) and Tiger Shoal (TS) fields. The stratal slice supports the interpretation from well log data in the two fields that the M sand coincides with incised-valley fills and correlative surfaces of exposure in the updip, on-shelf portion of the third-order lowstand systems tract in the field areas. The valley systems fed a lowstand deltaic wedge approximately 3.5 mi southeast of the fields. The shelf edge of the preceding highstand systems tract coincides with one of the five first-order syndepositional growth faults within the seismic area.

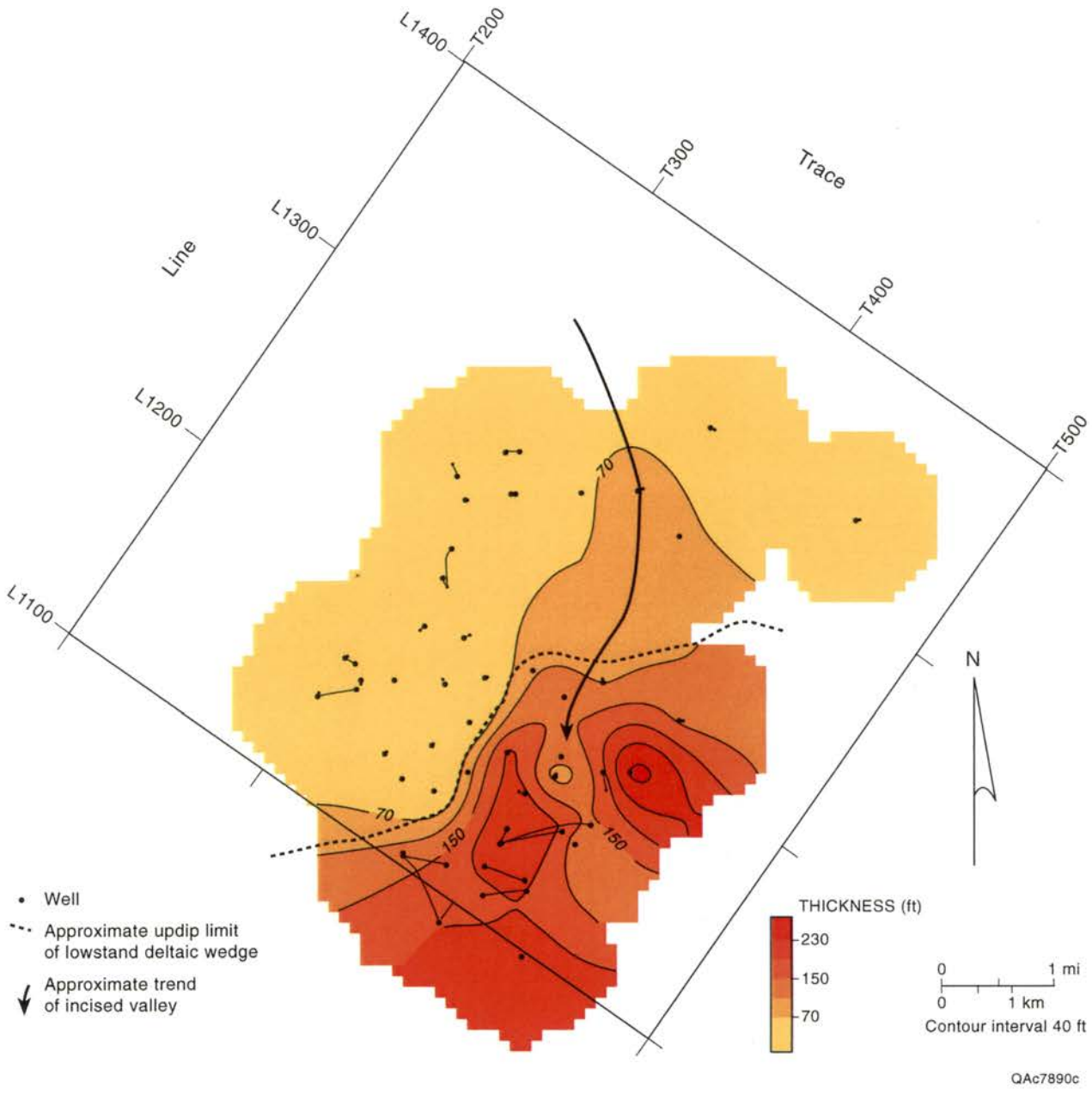

Figure 22. Isochore map of fourth-order sequence 33 (U sand) in Starfak field. The map illustrates the approximate trend of the incised-valley-fill feeder system and the pronounced southward thickening of the sequence, coinciding with deltaic-wedge development as shown on well logs (fig. 19).

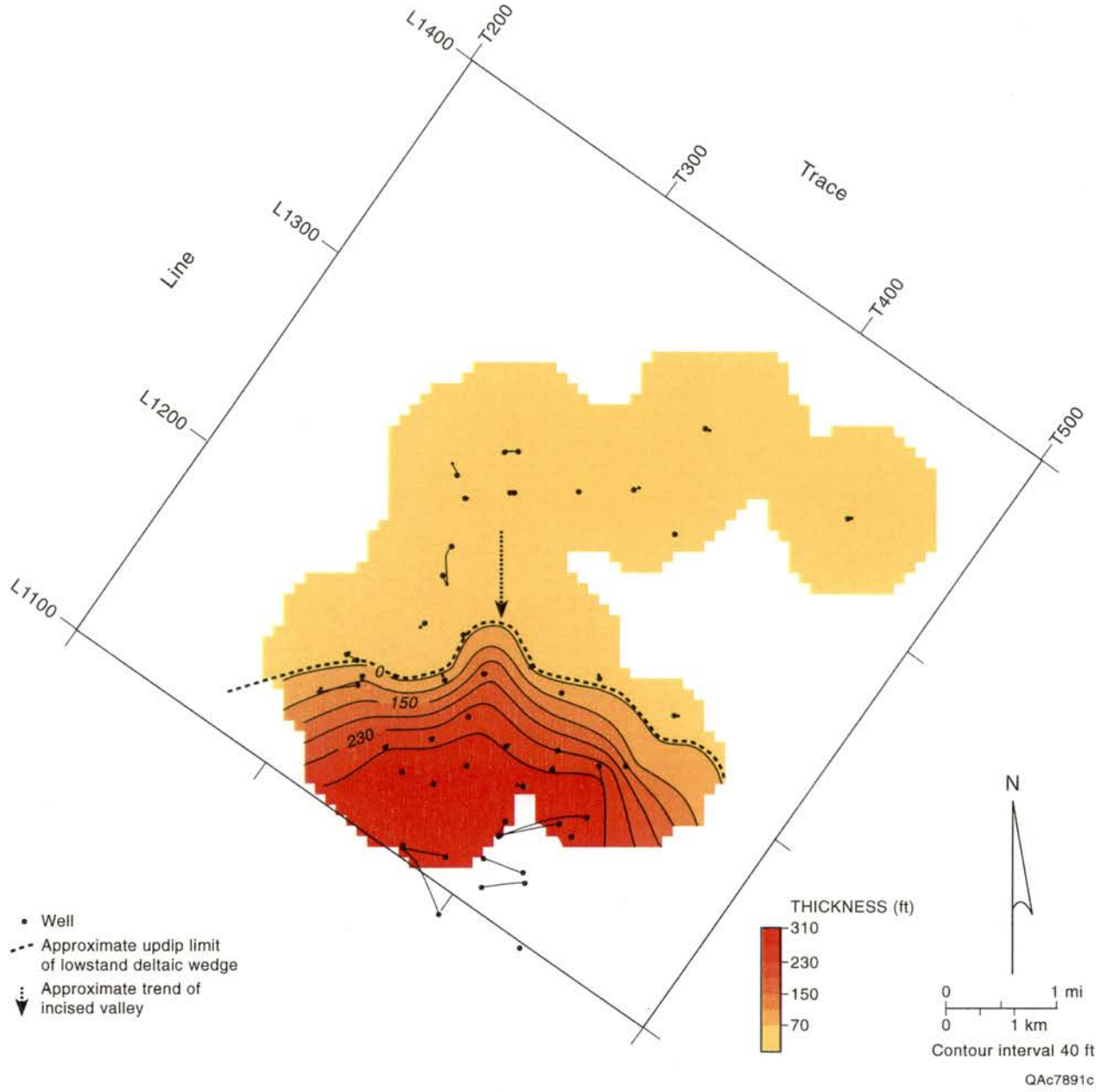

Figure 23. Isochore map of fourth-order sequence 34 (V sand) in Starfak field. The map illustrates the pronounced southward thickening of the sequence, coinciding with deltaic-wedge development as shown on well logs (fig. 19).

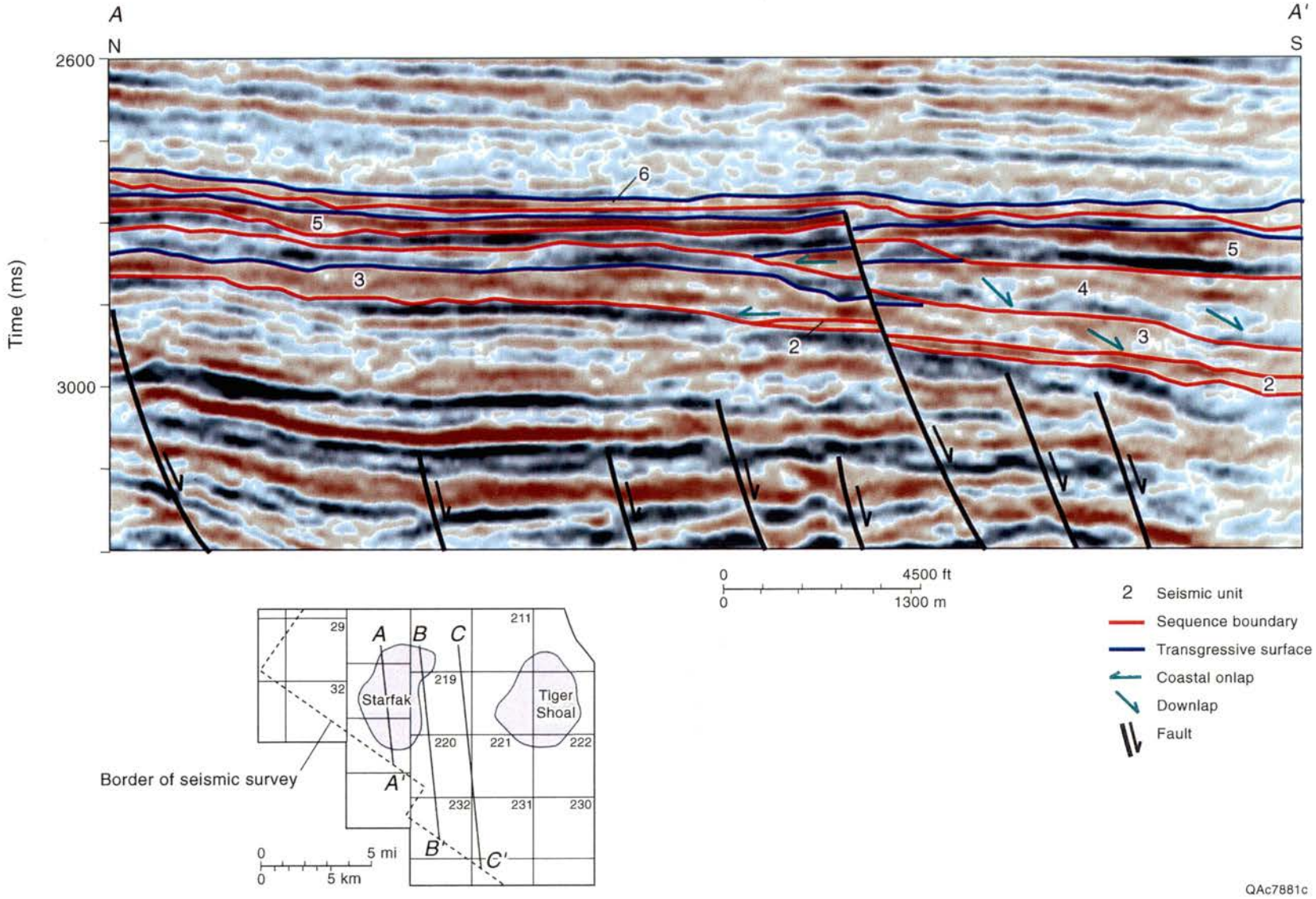

Figure 24. Depositional-dip-oriented seismic profile A–A′ that transects Starfak field.

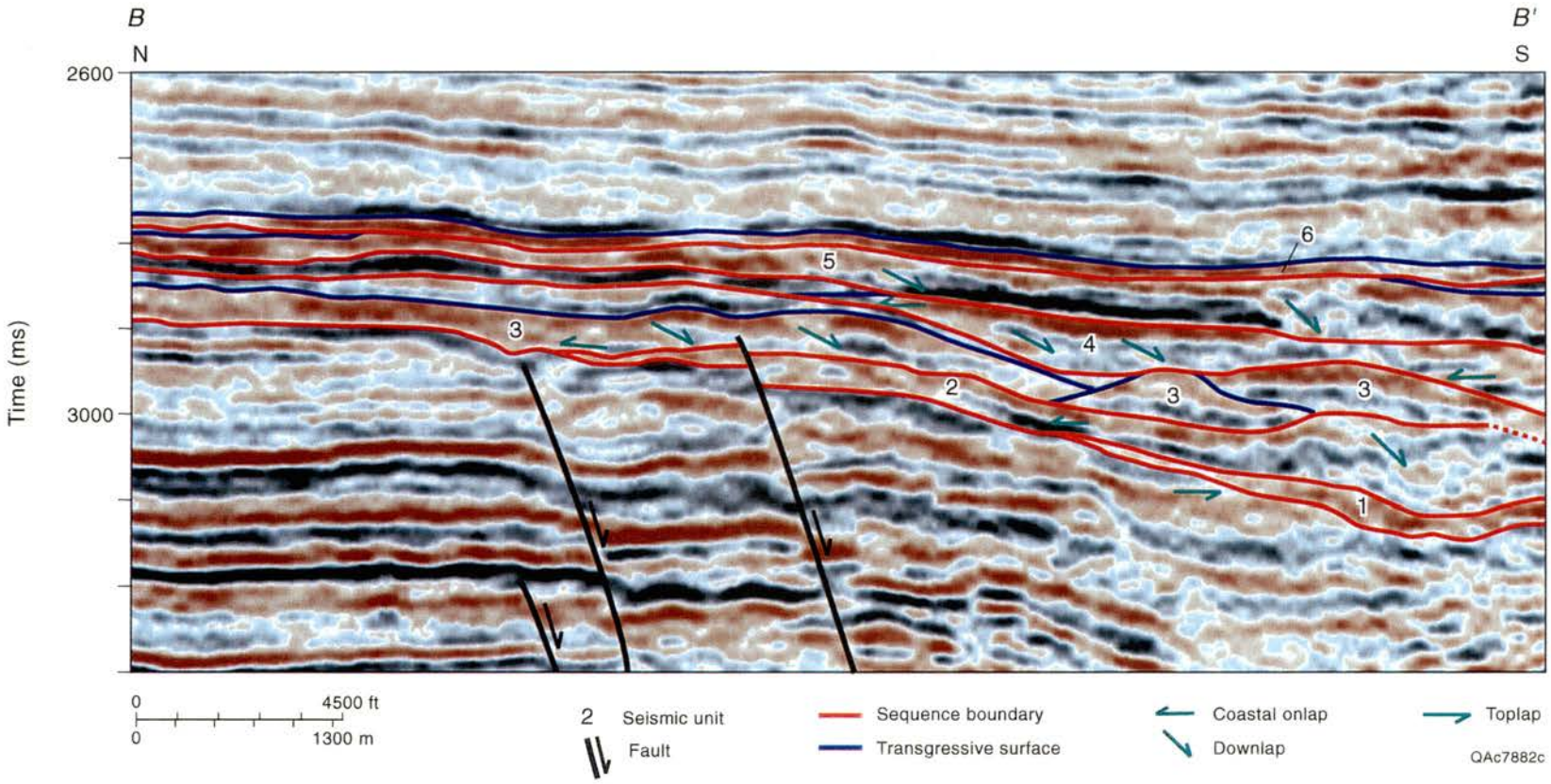

Figure 25. Depositional-dip-oriented seismic profile B–B′ located immediately east of Starfak field. Section line shown on figure 24.

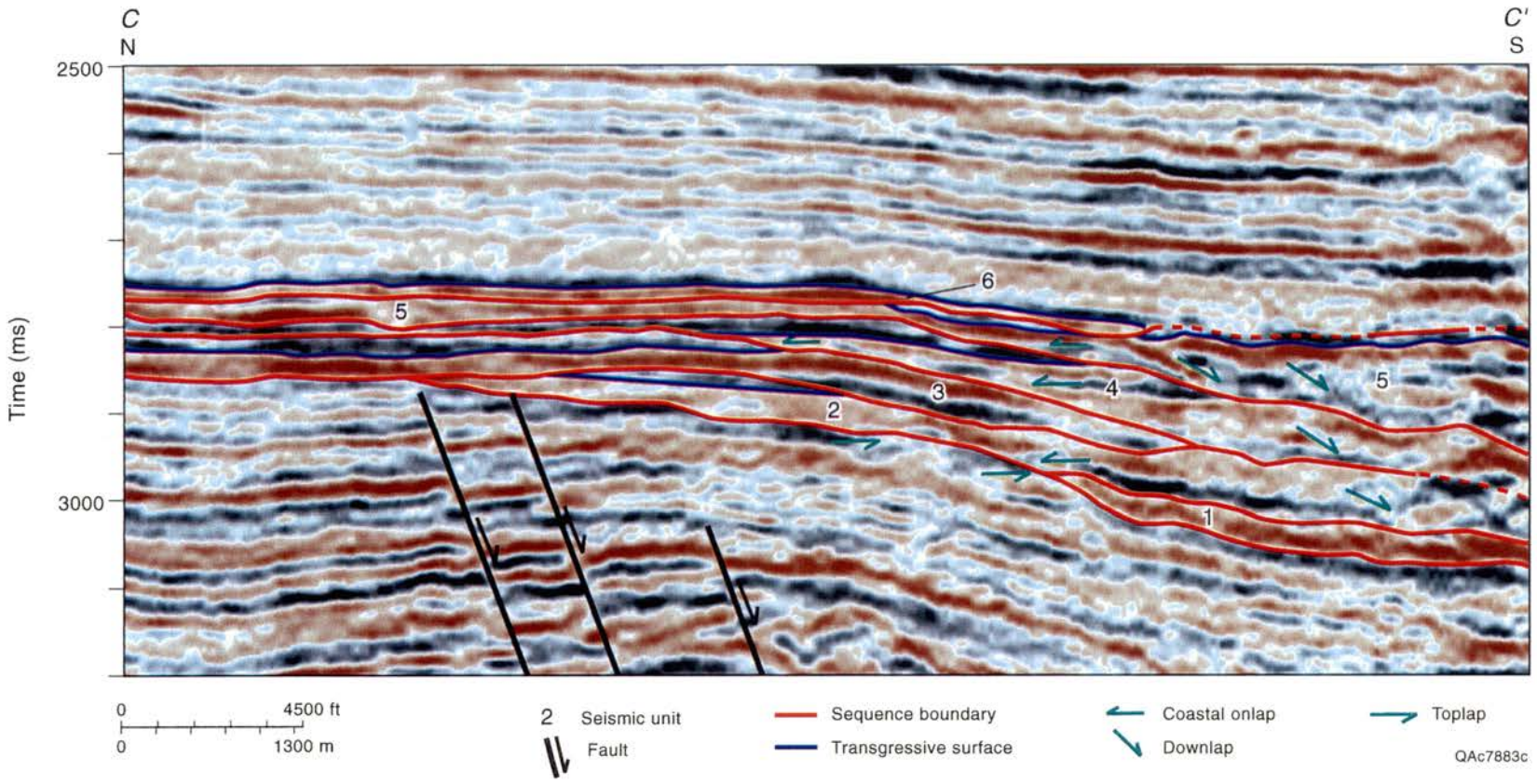

Figure 26. Depositional-dip-oriented seismic profile C–C′ located in the undrilled area between Starfak and Tiger Shoal fields. Section line shown in figure 24.

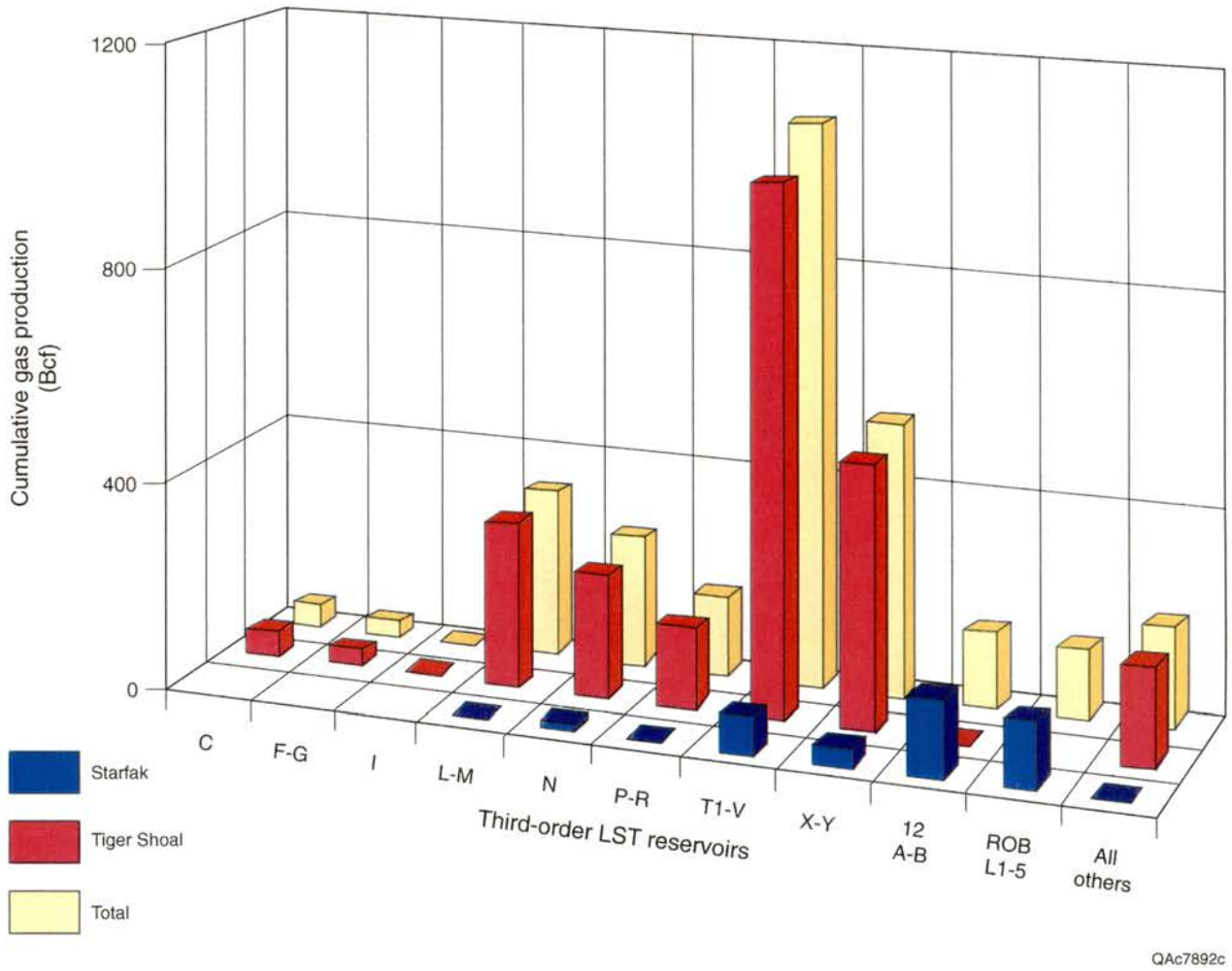

Figure 27. Bar graph of cumulative gas production (through 7/1/00) from the 10 third-order lowstand systems tracts in Starfak and Tiger Shoal fields. Each systems tract is named for its uppermost and lowermost (or only) sandstone-body reservoir for easier cross-referencing with the volumetrics of individual reservoirs (table 3). Within the body of this report, however, lowstand systems tracts C, F-G, I, L-M, N, P-R, T1-V, X-Y, 12A-B, and Rob L1-5 are designated by the third-order sequences of which they are a part: sequences 10 through 1, respectively, on plate 2. The category "All others" represents cumulative production from all reservoirs that do not occur in the 10 third-order lowstand systems tracts.

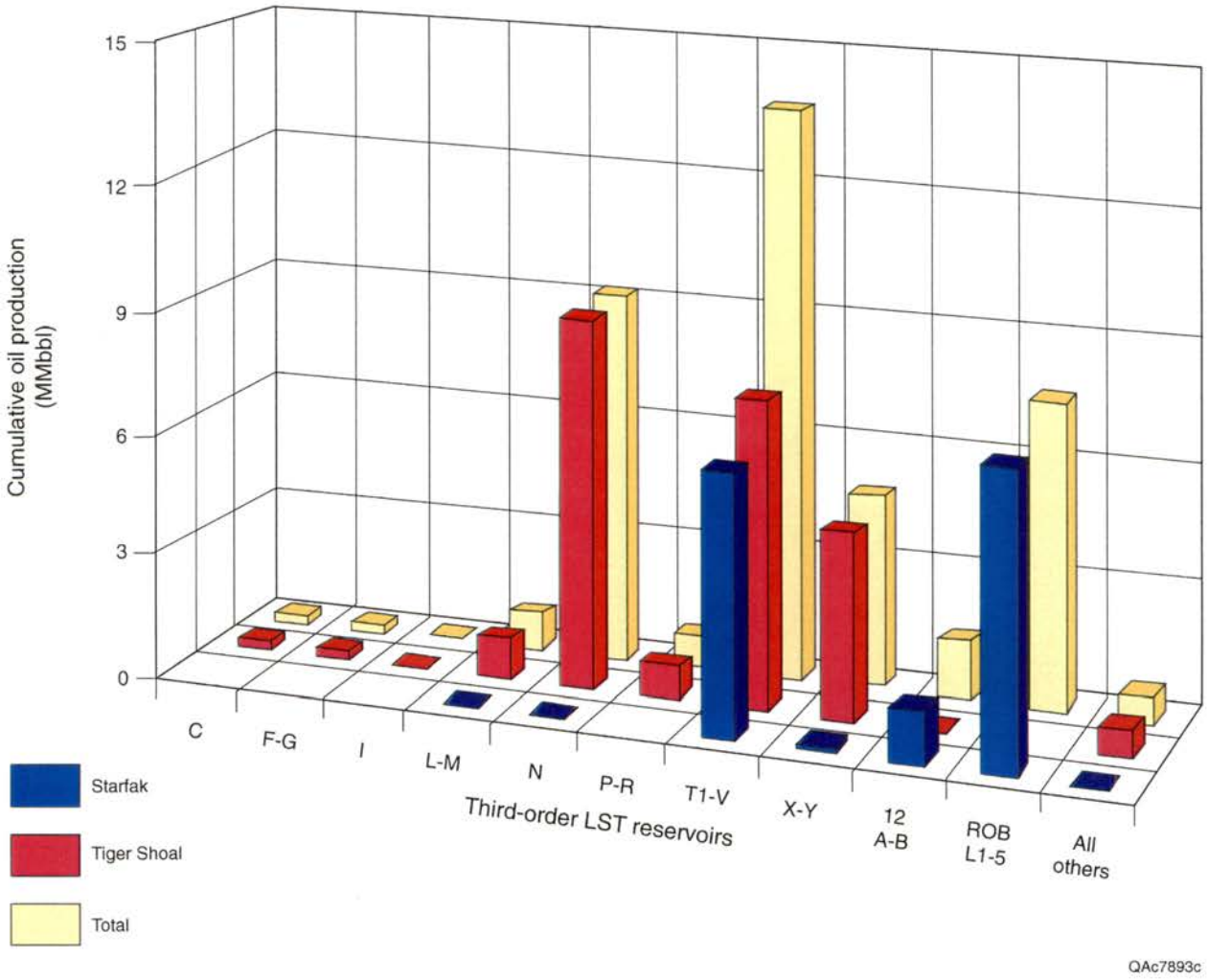

Figure 28. Bar graph of cumulative oil production (through 7/1/00) from the 10 third-order lowstand systems tracts in Starfak and Tiger Shoal fields. Each systems tract is named for its uppermost and lowermost (or only) sandstone-body reservoir for easier cross-referencing with the volumetrics of individual reservoirs (table 4). Within the body of this report, however, lowstand systems tracts C, F-G, I, L-M, N, P-R, T1-V, X-Y, 12A-B, and Rob L1-5 are designated by the third-order sequences of which they are a part: sequences 10 through 1, respectively, on plate 2. The category "All others" represents cumulative production from all reservoirs that do not occur in the 10 third-order lowstand systems tracts.

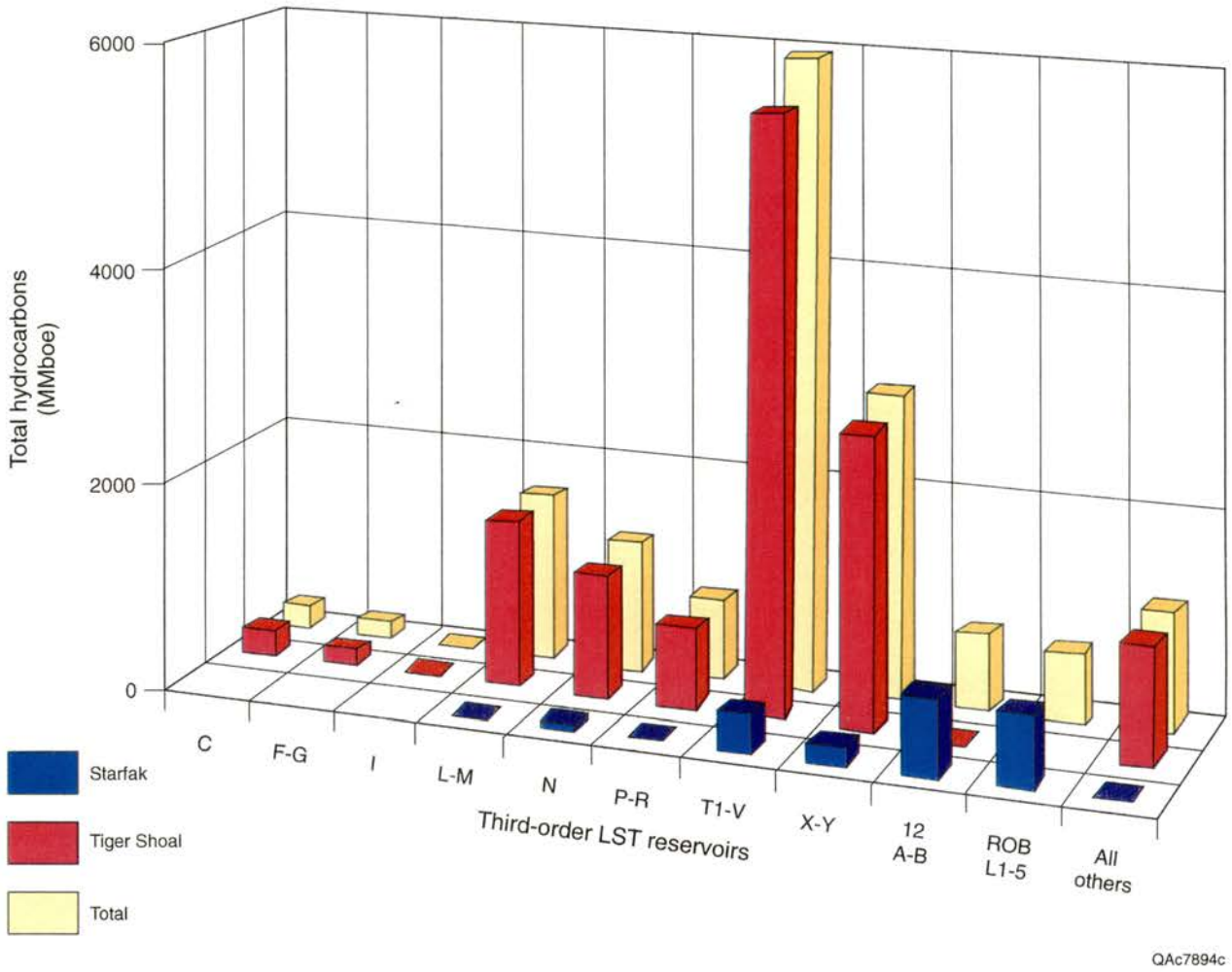

Figure 29. Bar graph of total hydrocarbon production (through 7/1/00) from the 10 third-order lowstand systems tracts in Starfak and Tiger Shoal fields. Each systems tract is named for its uppermost and lowermost (or only) sandstone-body reservoir for easier cross-referencing with the volumetrics of individual reservoirs (table 5). Within the body of this report, however, lowstand systems tracts C, F-G, I, L-M, N, P-R, T1-V, X-Y, 12A-B, and Rob L1-5 are designated by the third-order sequences of which they are a part: sequences 10 to 1, respectively, on plate 2. The category "All others" represents cumulative production from all reservoirs that do not occur in the 10 third-order lowstand systems tracts. For conversion of gas-volume units into barrels-of-oil-equivalent (boe), we used the standard equation, 1 Mcf = 5.62 boe.

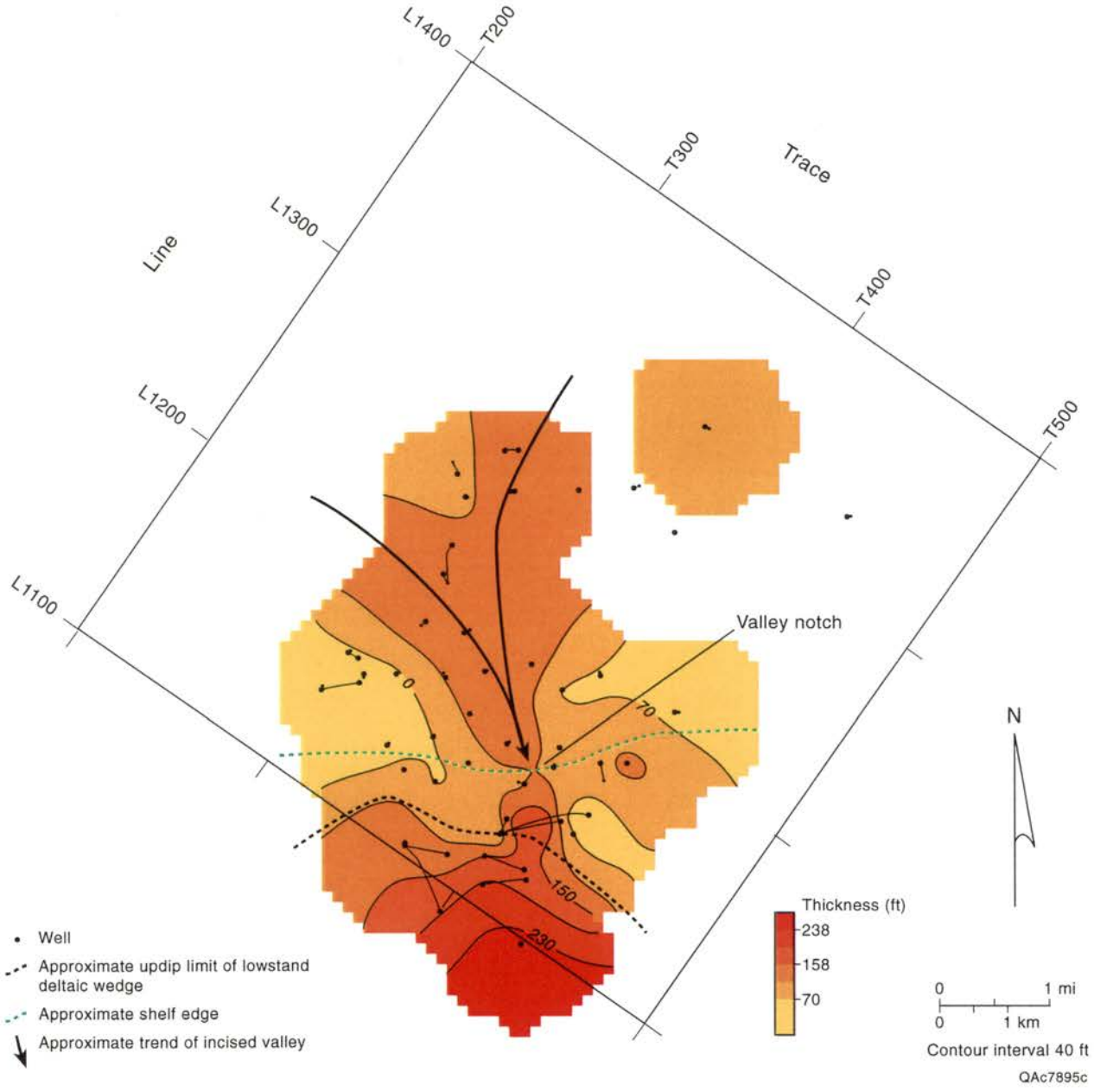

Figure 30. Isochore map of fourth-order sequence 40 (Y sand) in Starfak field. The map illustrates the pronounced southward thickening of the sequence, the trend of the incised-valley-fill feeder system, and the areal restriction of the incised valley, where it eroded through the exposed shelf edge of the preceding highstand systems tract (valley notch).

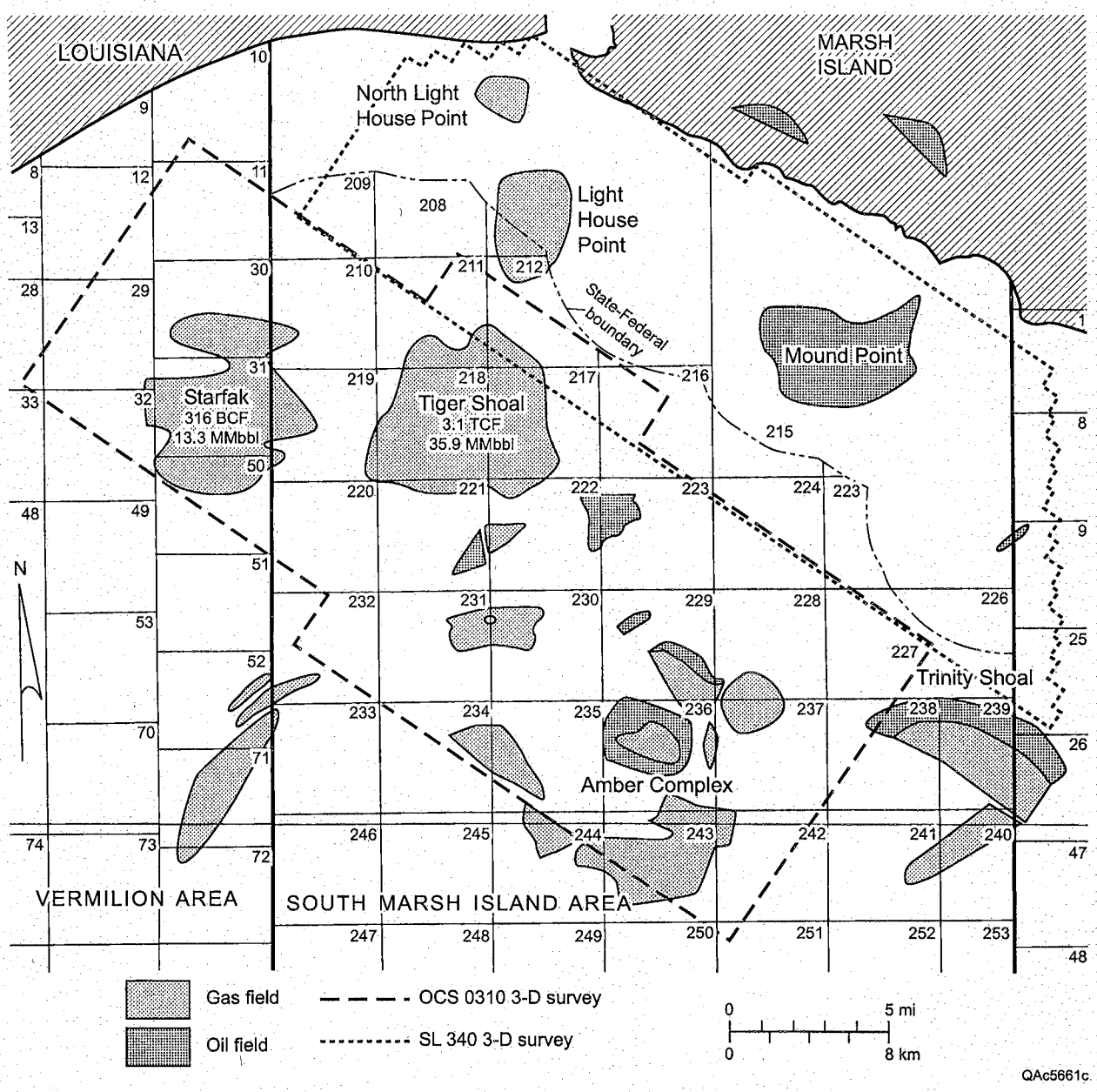

Figure 31. Map of the Vermilion Block 50 and south Marsh Island areas showing the outline of the two major 3-D seismic surveys being used in this resource assessment.

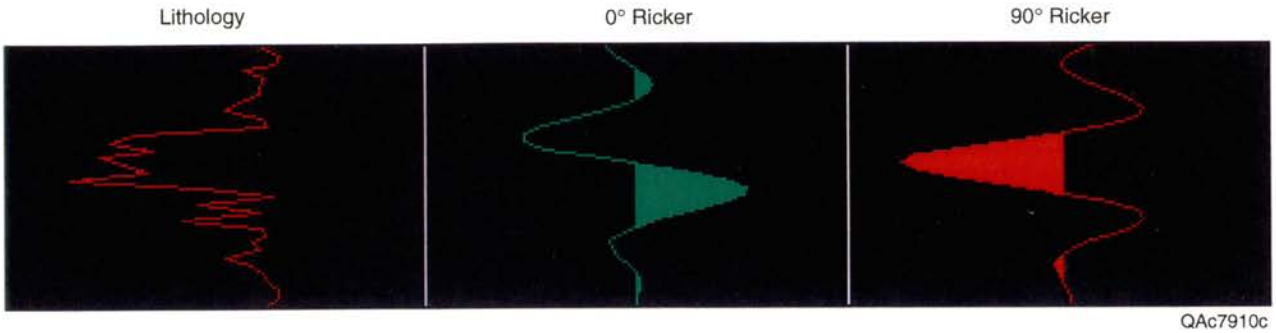

Figure 32. Interpretive advantage of 90°-phase wavelet. For seismically thin layers, one reservoir is reflected by one trough (peak) at top and one peak (trough) at base with 0°-phase wavelet, but only one main trough (peak) at middle if a 90°-phase wavelet is involved.

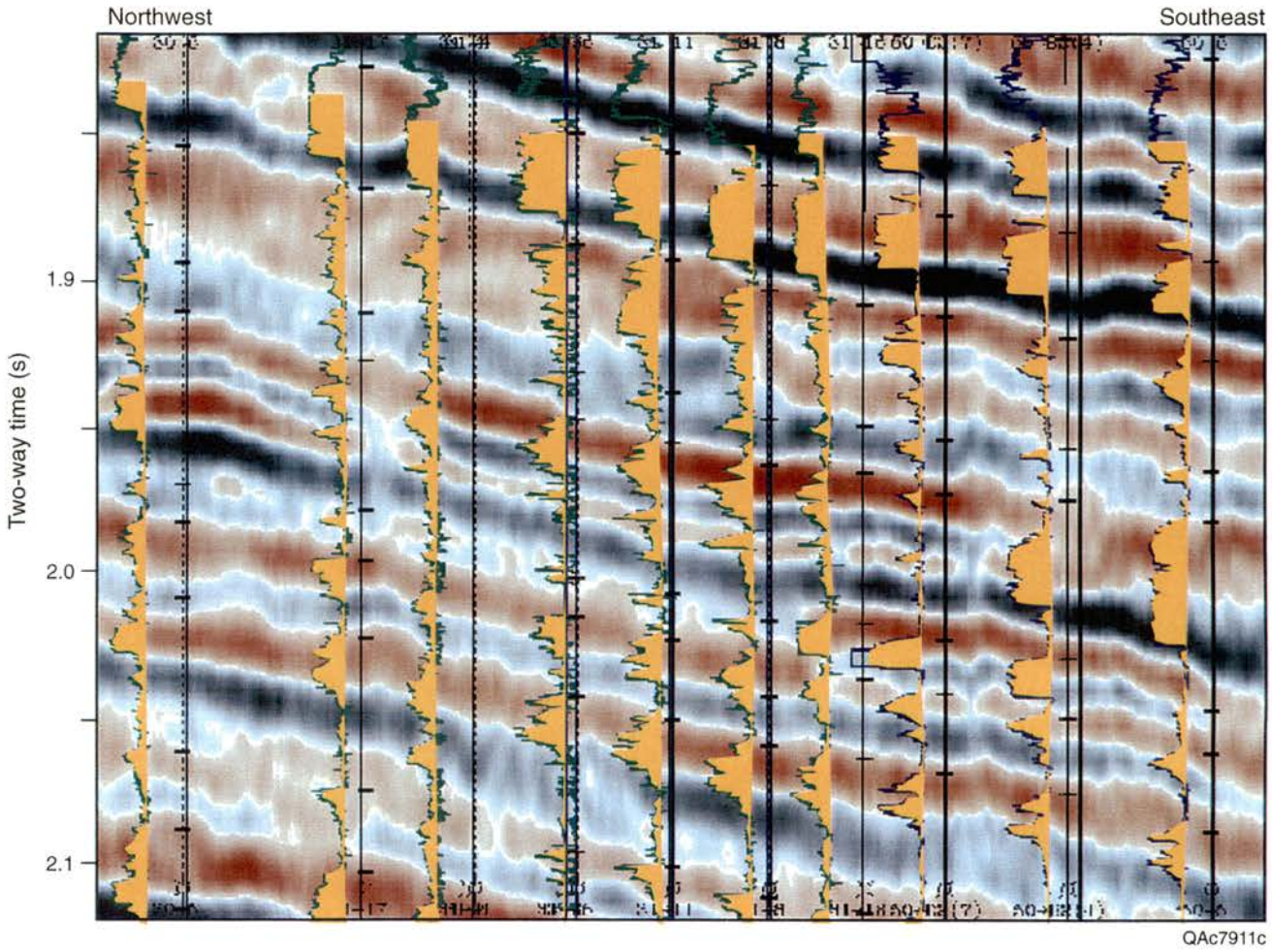

Figure 33. A 0°-phase (original) seismic section tied to wells (GR/SP) in Starfak field. Each sandstone ties to a pair of seismic events (trough or red at top and peak or black at bottom).

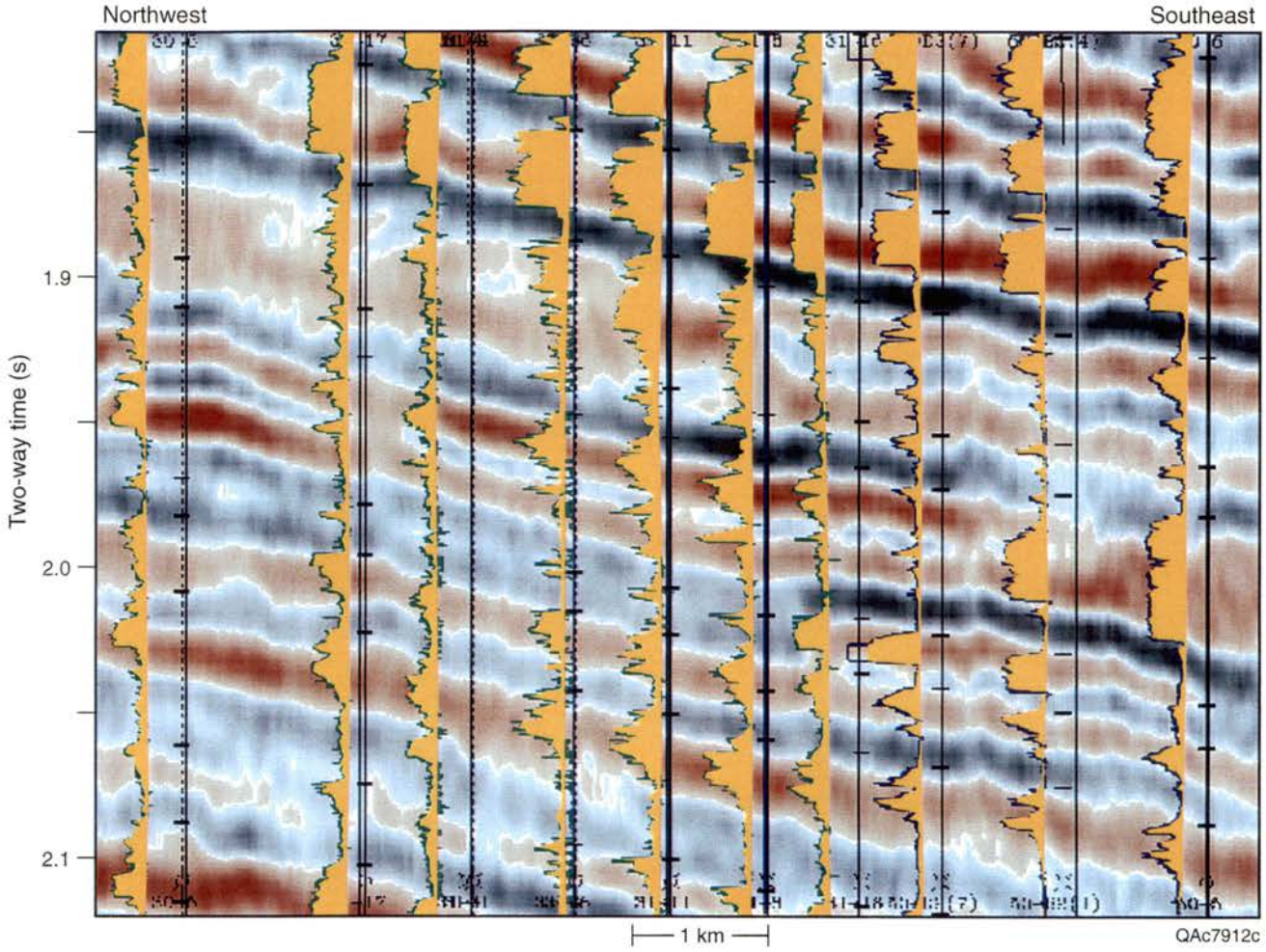

Figure 34. A 90°-phase (reprocessed) seismic section tied to wells (same as fig. 33). Each sandstone ties to one seismic event (trough or red at middle).

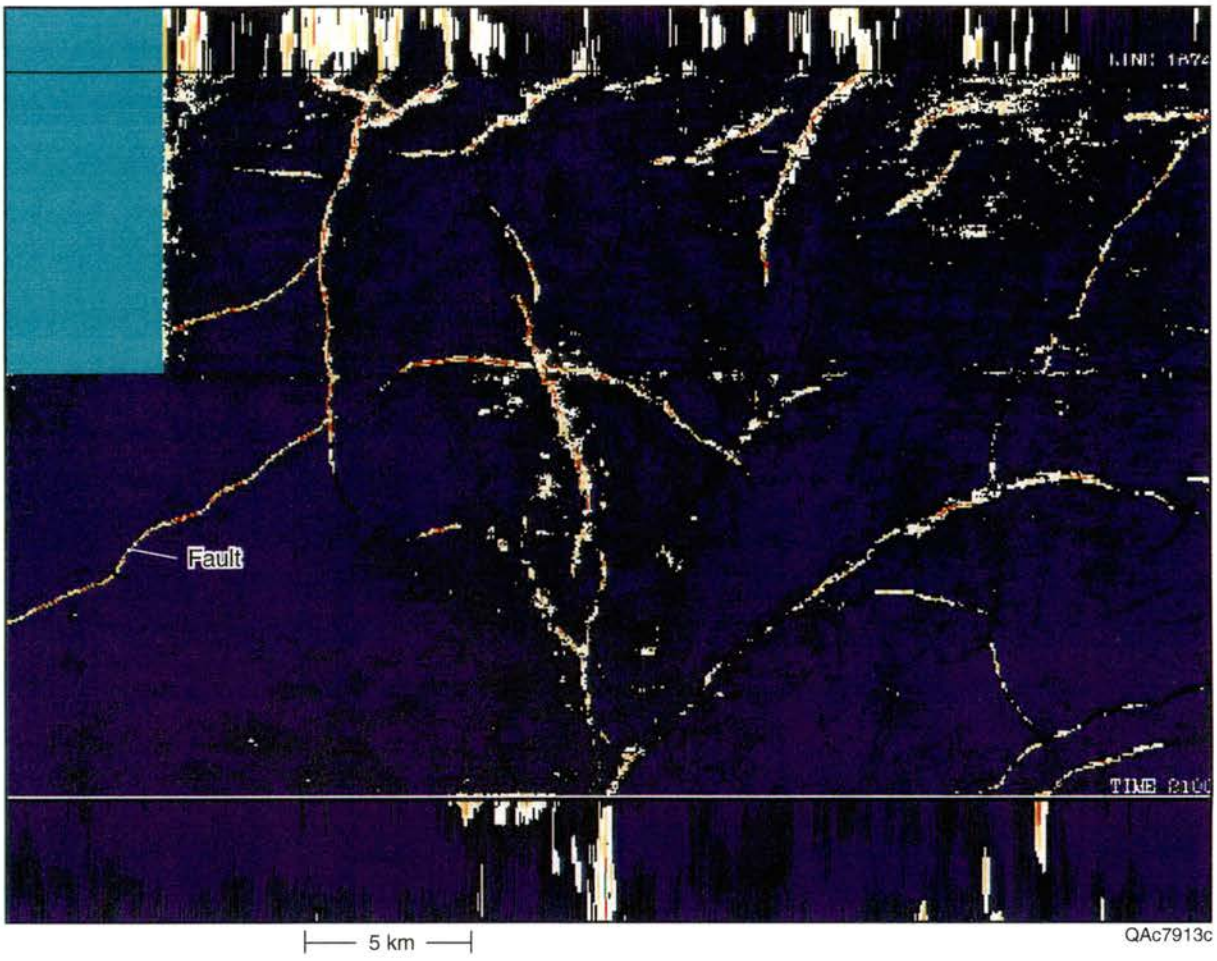

Figure 35. Continuity time slice at 2,100 ms (in chair map) showing a sharp and complete regional fault system in the shallower section.

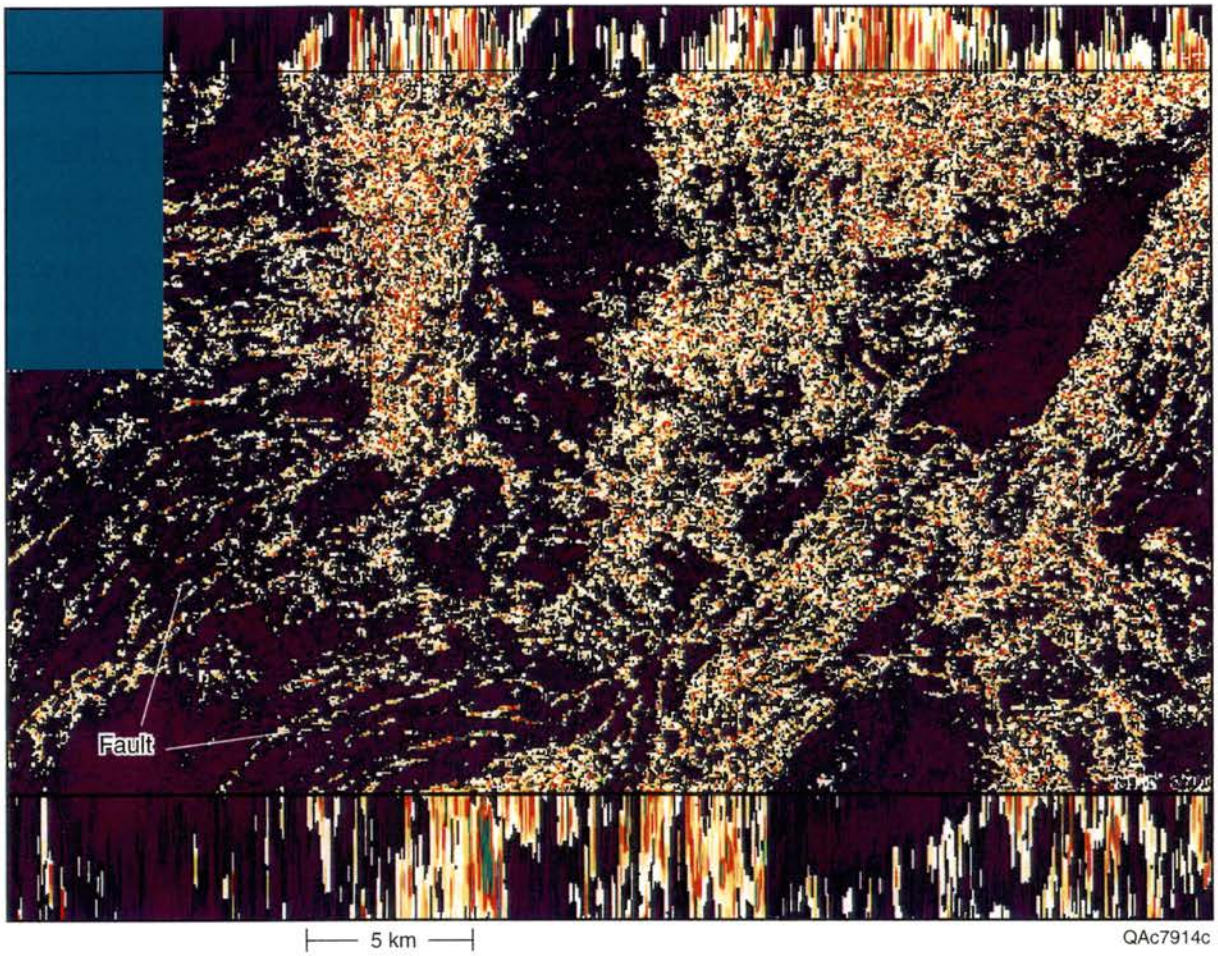

Figure 36. Continuity time slice at 3,700 ms (in chair map) illustrating numerous small, subtle faults in the area between Starfak and Tiger Shoal fields and to the northwest of Starfak field in the deeper section.

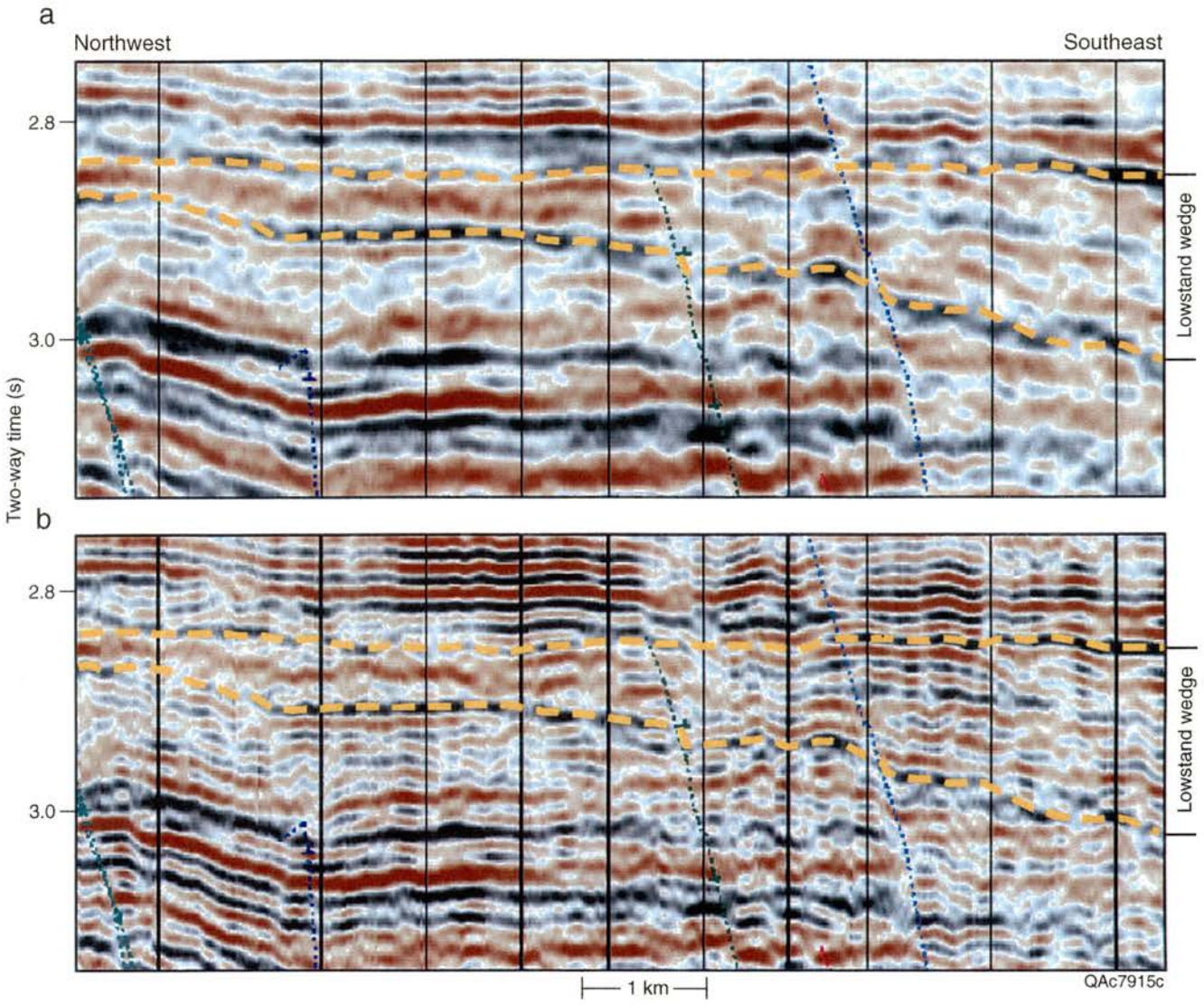

Figure 37. Spectral balancing of deep data (a) before processing and (b) after processing.

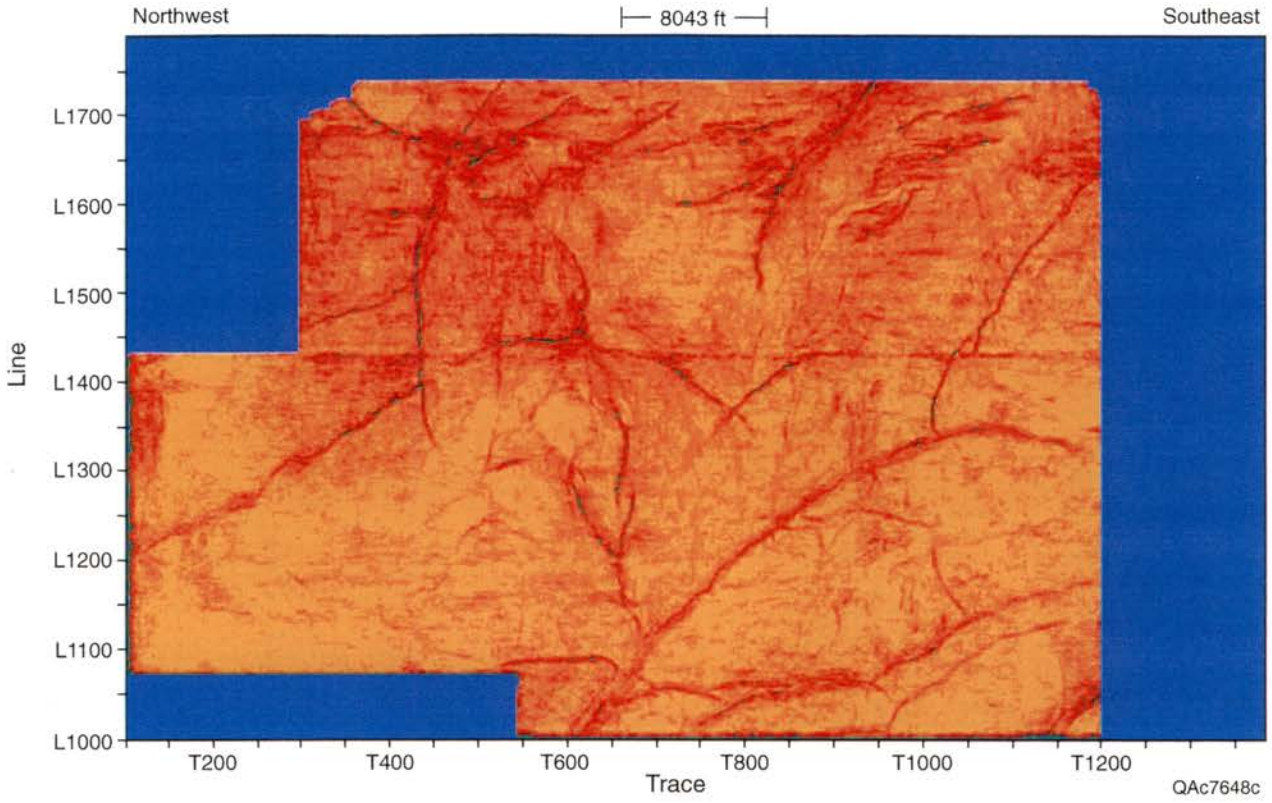

Figure 38. Coherency time slice generated at 2,000 ms revealing the areal distribution of faulting throughout the 3-D seismic study area.

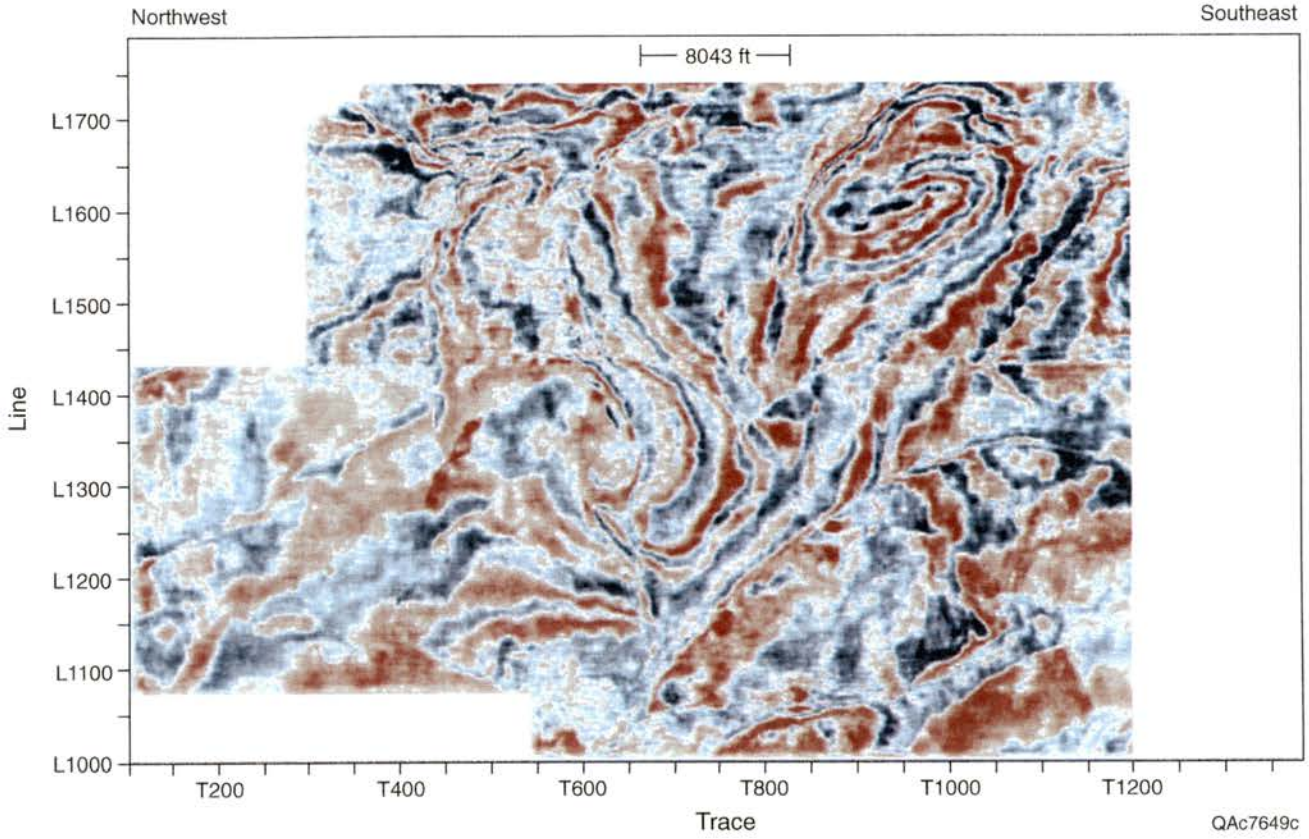

Figure 39. Conventional time slice extracted (2,000 ms) from the 3-D seismic amplitude volume.

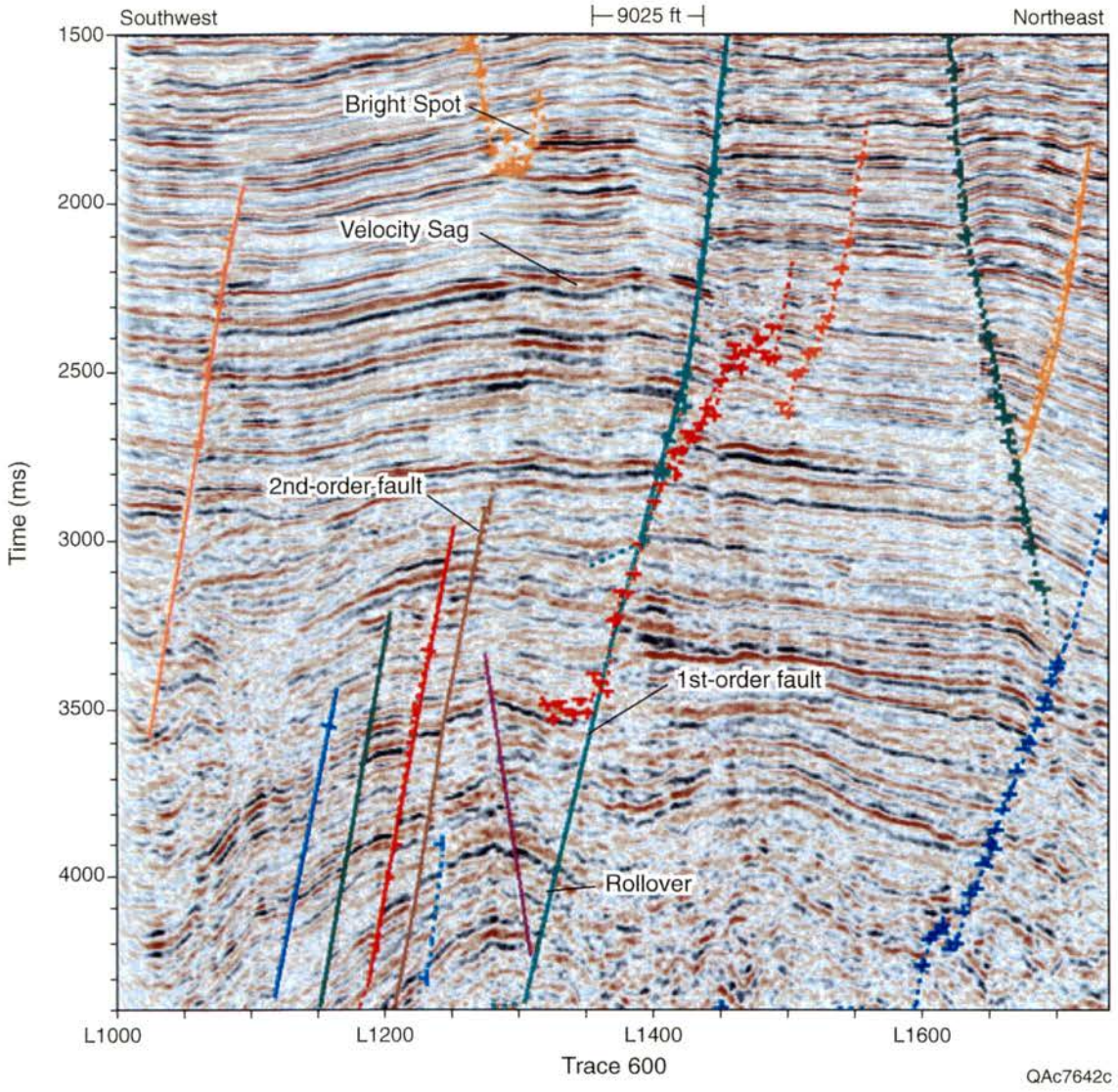

Figure 40. Vertical seismic profile showing structural (rollover), stratigraphic (bright spot), and fault interpretations of first- and second-order normal faults.

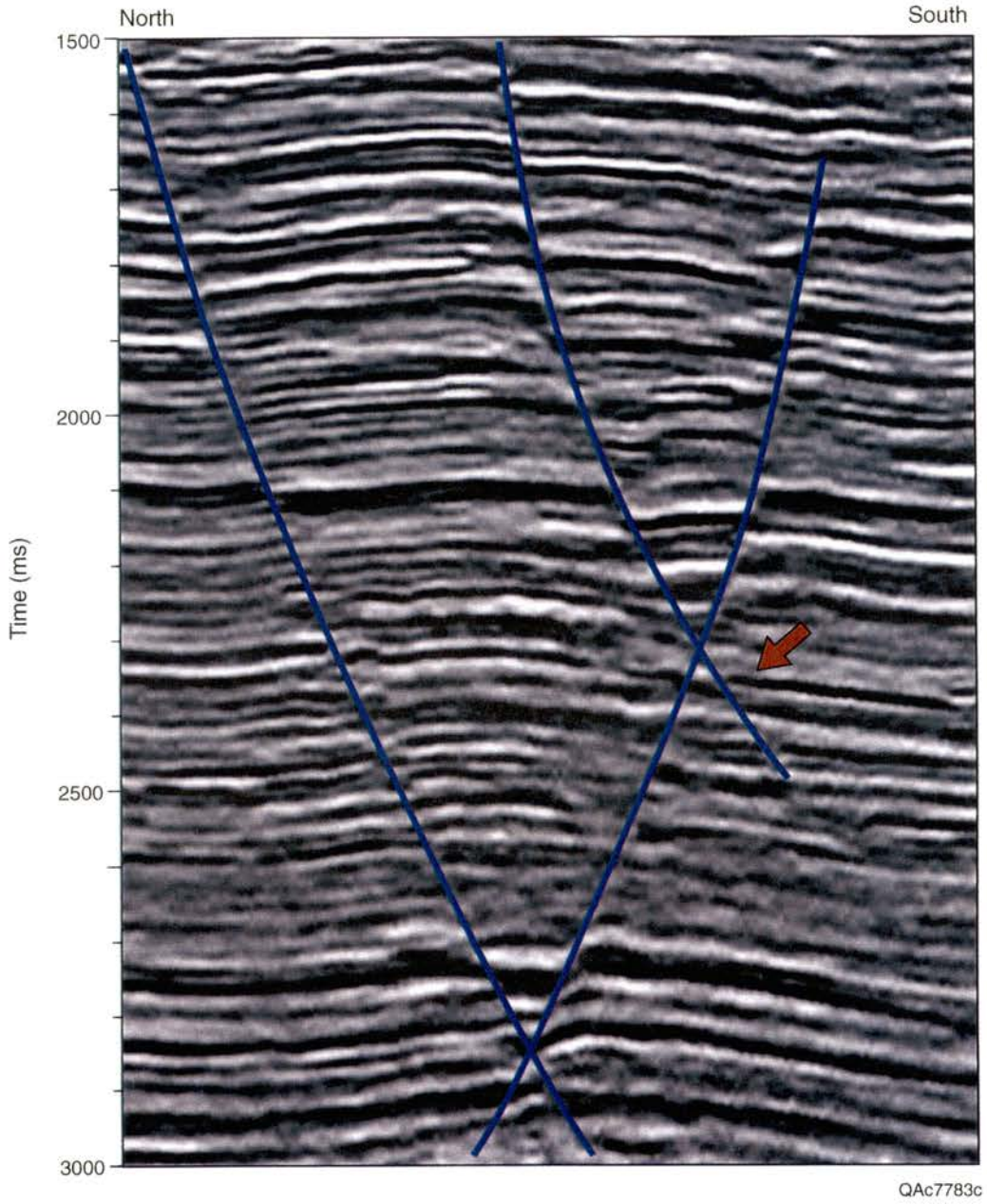

Figure 41. Vertical seismic profile showing an "hourglass" feature associated with transecting faults.

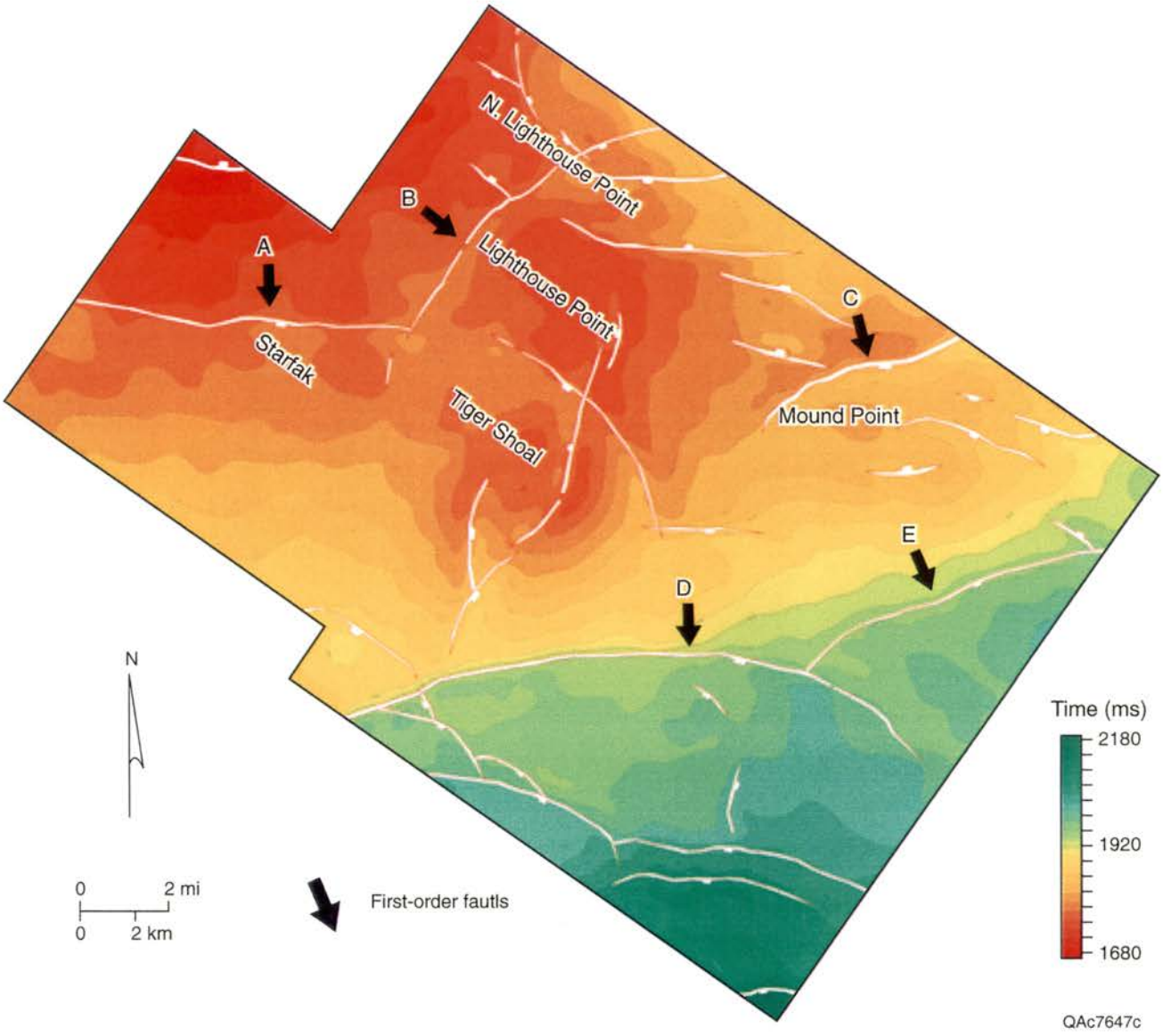

Figure 42. Time-structure map (contour interval = 20 ms) of maximum flooding surface 2 depicting the subsurface topography associated with the five major producing fields. Note the five (A, B, C, D, and E) first-order normal faults.

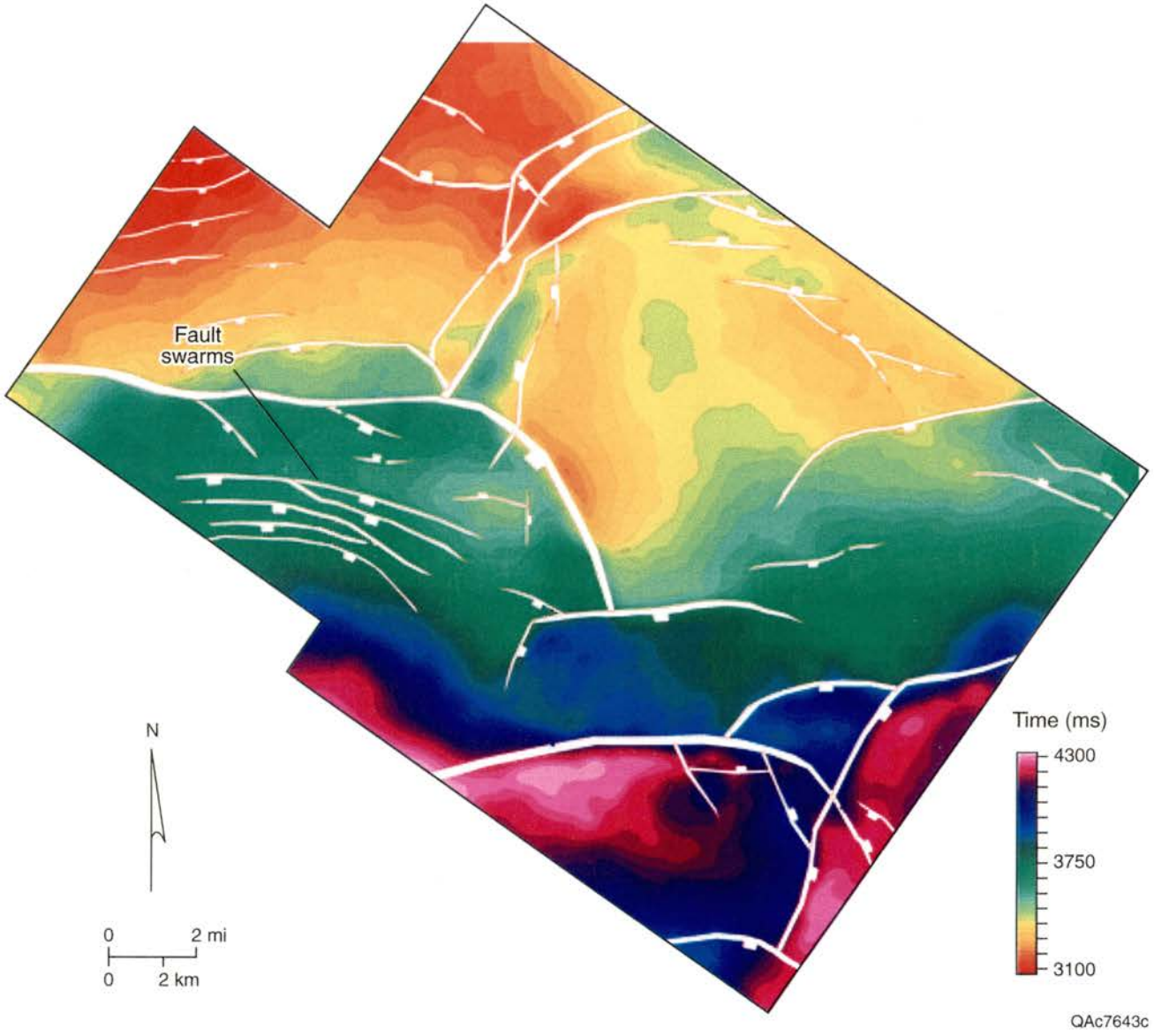

Figure 43. Time-structure map (contour interval = 25 ms) of the Robulus 4 sand with associated second-order fault swarms in Starfak field.

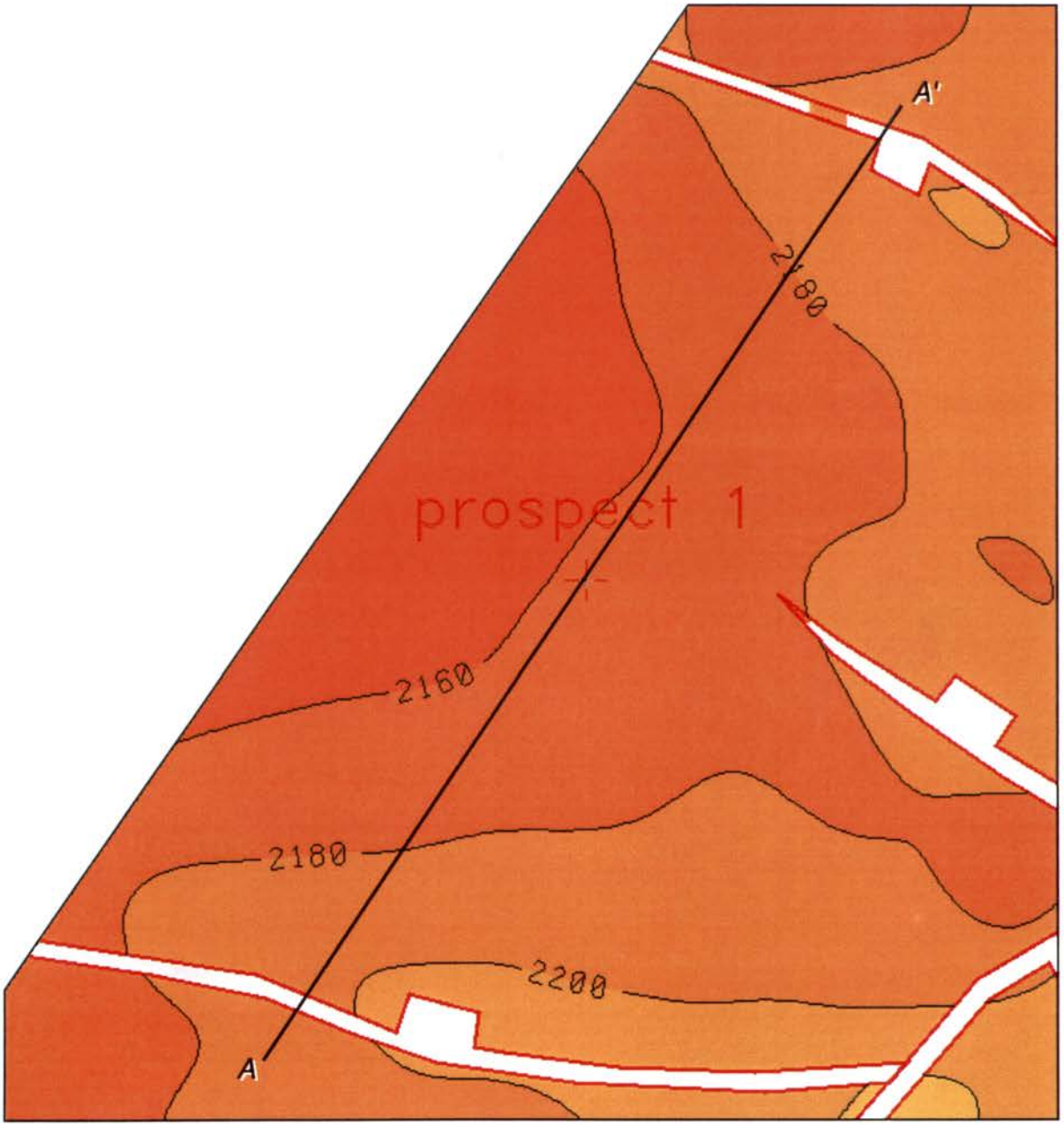

Figure 44. Prospect 1 location posted on a time-structure map of MFS16 (contour interval = 20 ms). The structure map depicts subsurface topography at the L sand reservoir level.

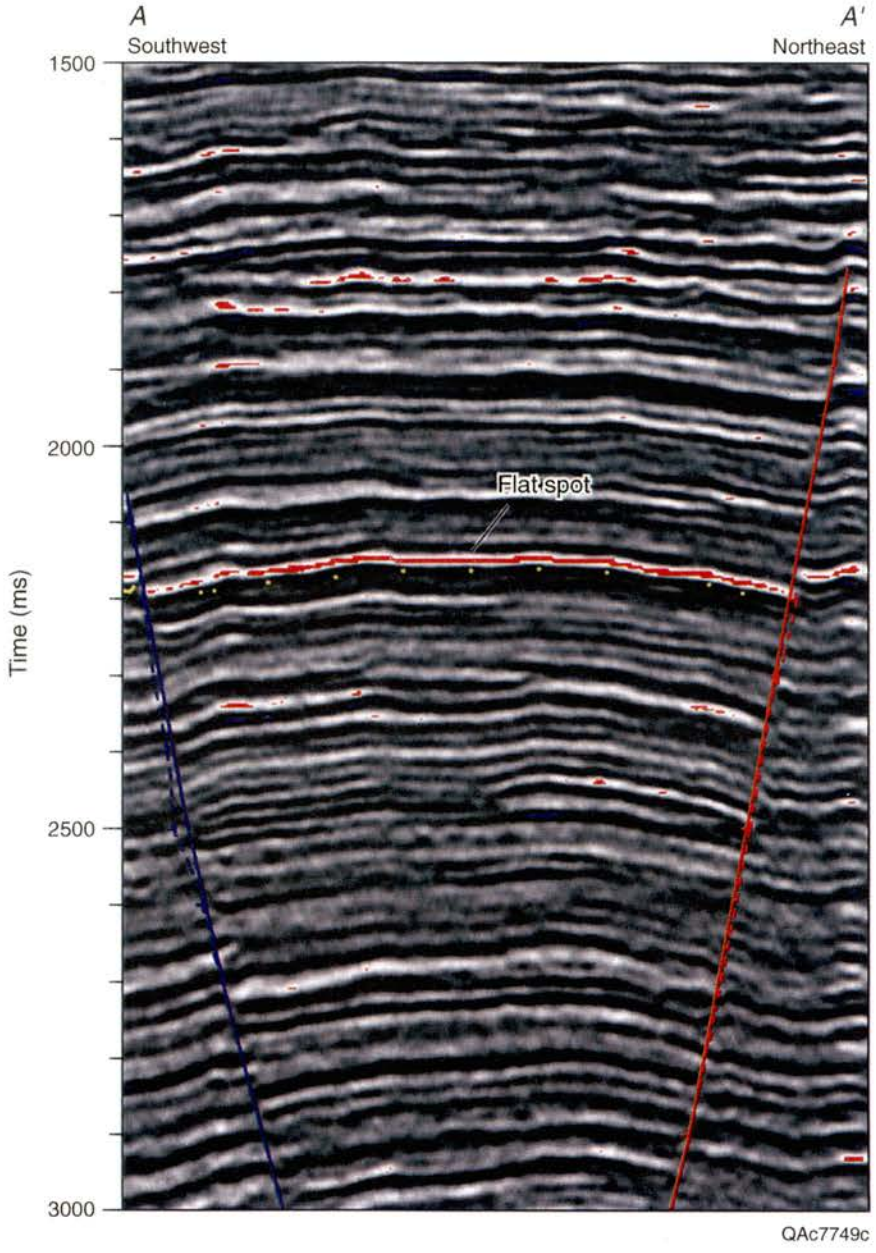

Figure 45. Vertical seismic cross section (A–A′) of prospect 1. The L sand is targeted.

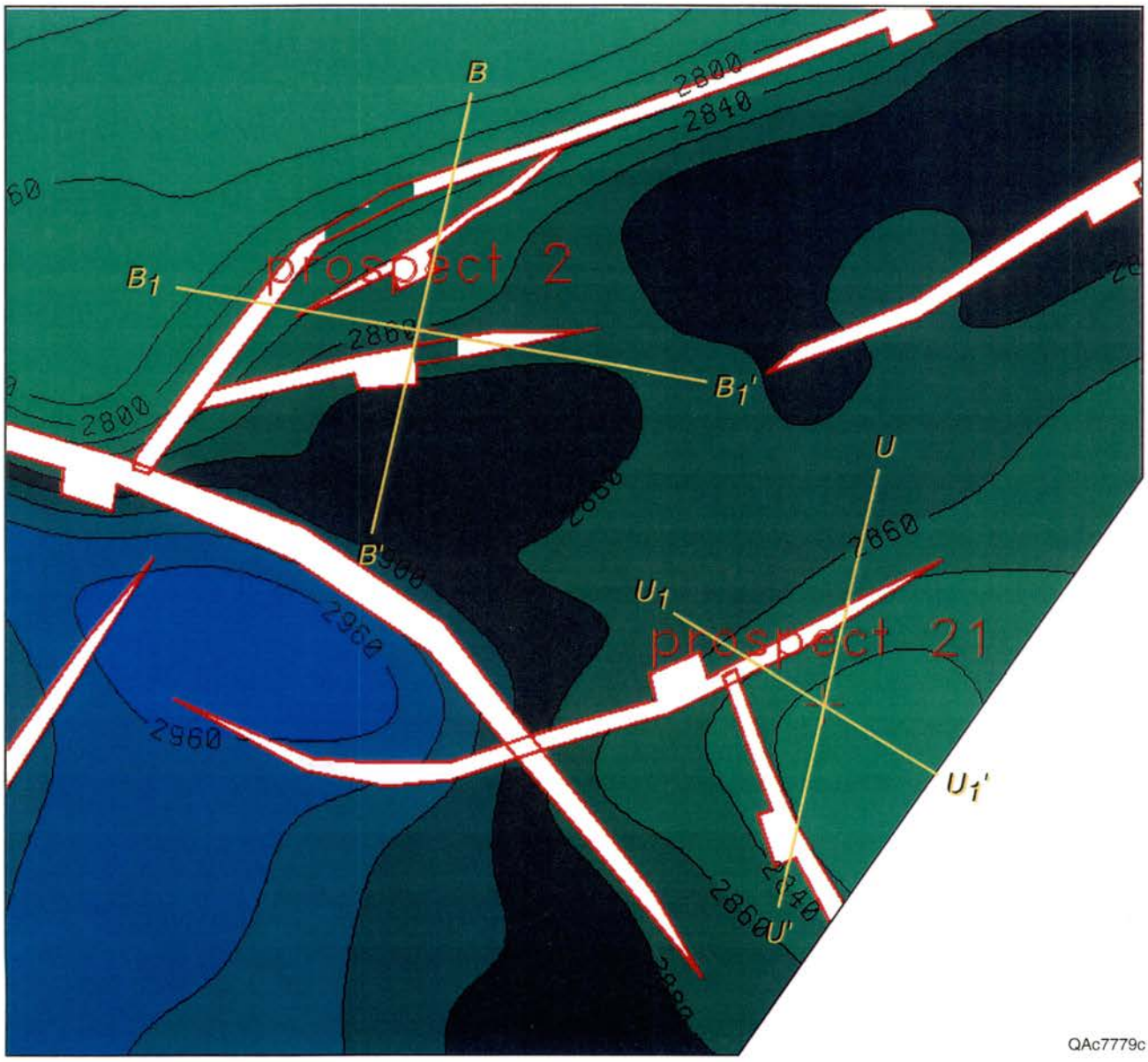

Figure 46. Prospect 2 and 21 locations posted on a time-structure map of MFS26 (contour interval = 20 ms). The structure map depicts subsurface topography at the Q sand reservoir level.

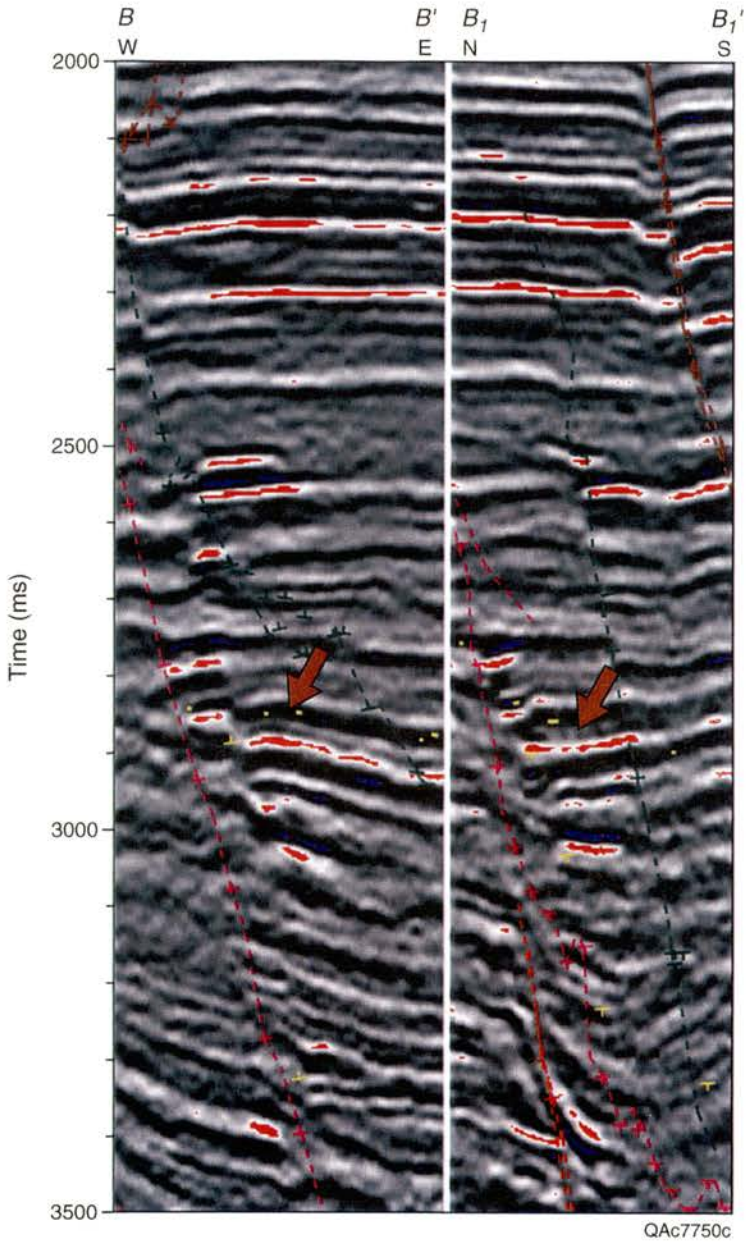

Figure 47. Vertical seismic cross sections (B–B′/B1–B1′) of prospect 2. The Q sand is targeted (arrow).

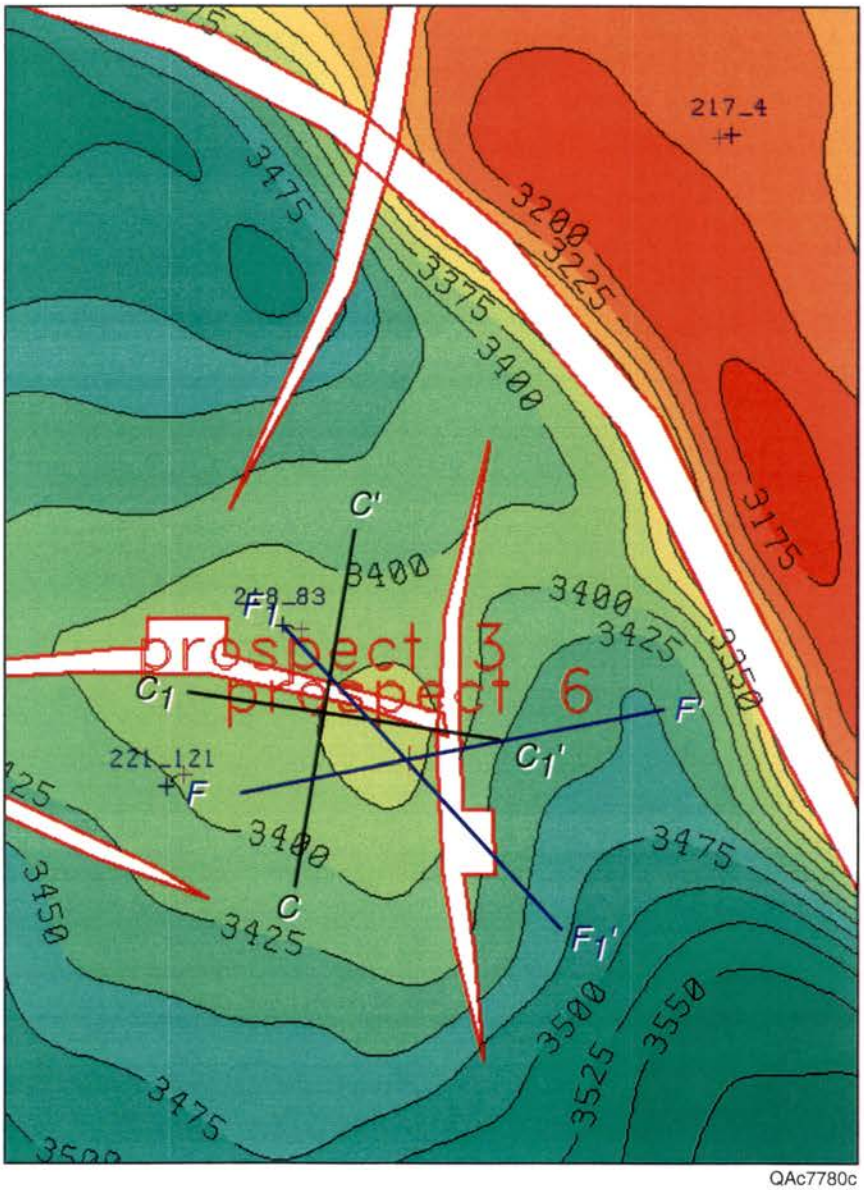

Figure 48. Prospect 3 and 6 locations posted on a time-structure map of the Robulus 2 sand (contour interval = 25 ms). The structure map depicts subsurface topography at the Robulus sand reservoir level.

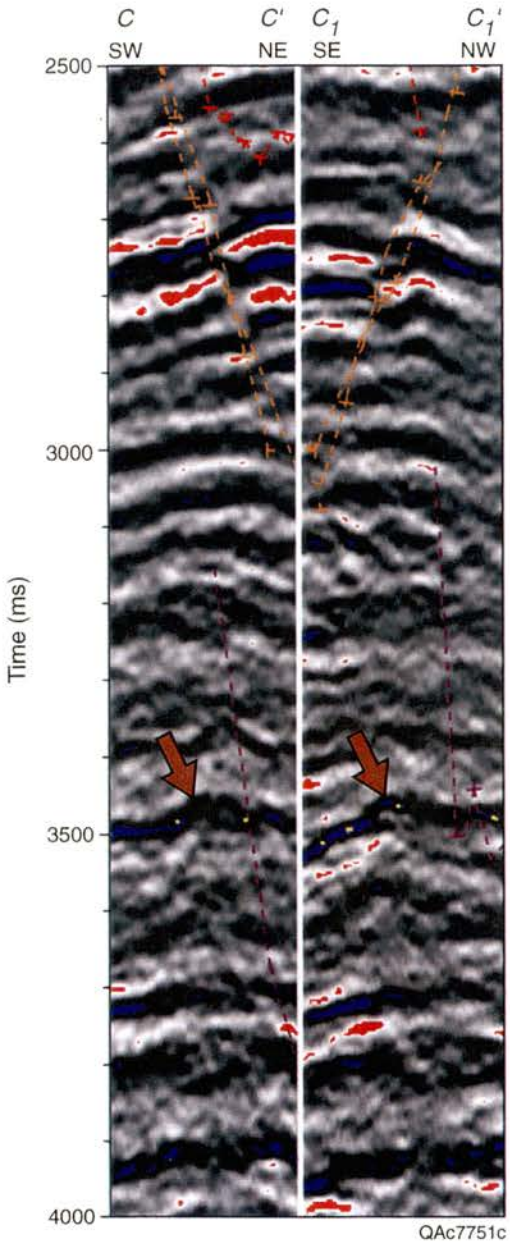

Figure 49. Vertical seismic cross sections (C–C′/C1–C1′) of prospect 3. The Robulus sands are targeted (arrow).

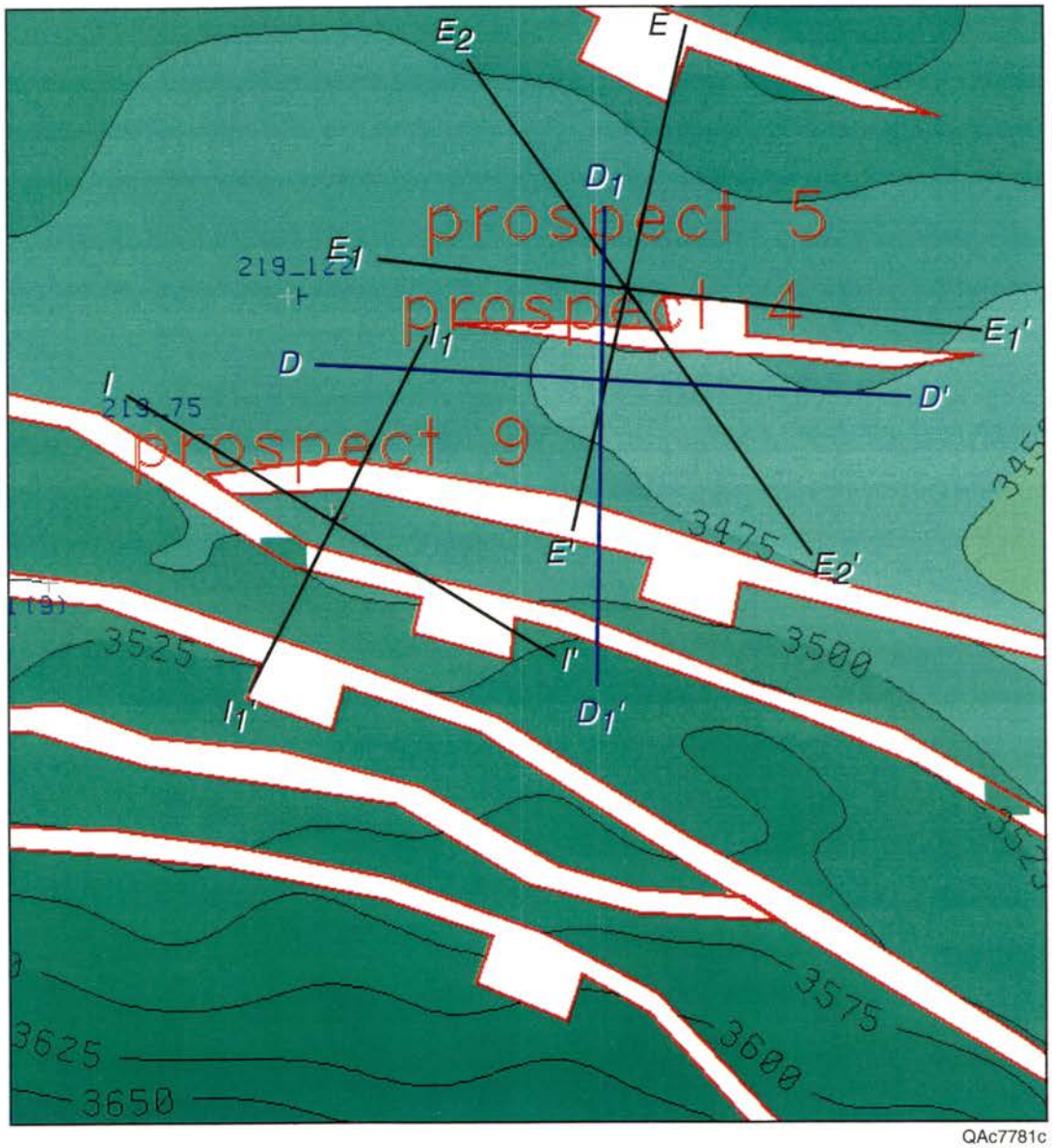

Figure 50. Prospect 4, 5, and 9 locations posted on a time-structure map of the Robulus 2 sand (contour interval = 25 ms). The structure map depicts the subsurface topography of the Robulus sand reservoir level.

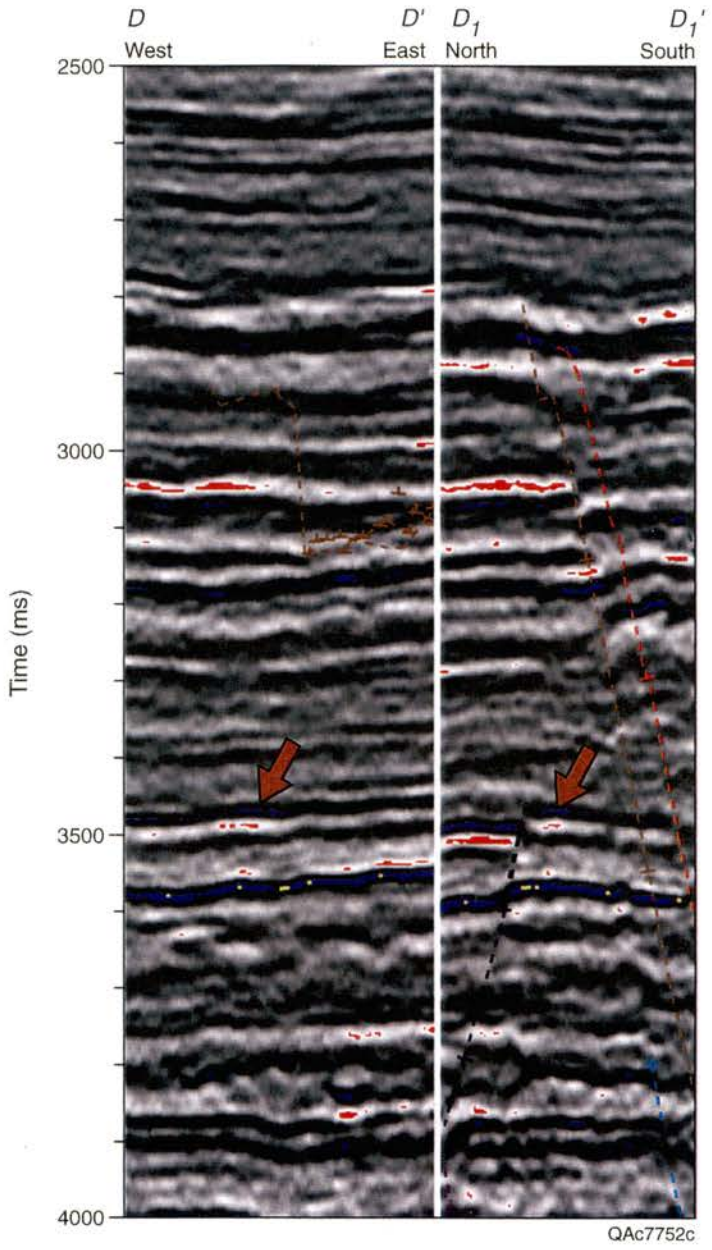

Figure 51. Vertical seismic cross sections (D–D′/D1–D1′) of prospect 4. The Robulus sands are targeted (arrow).

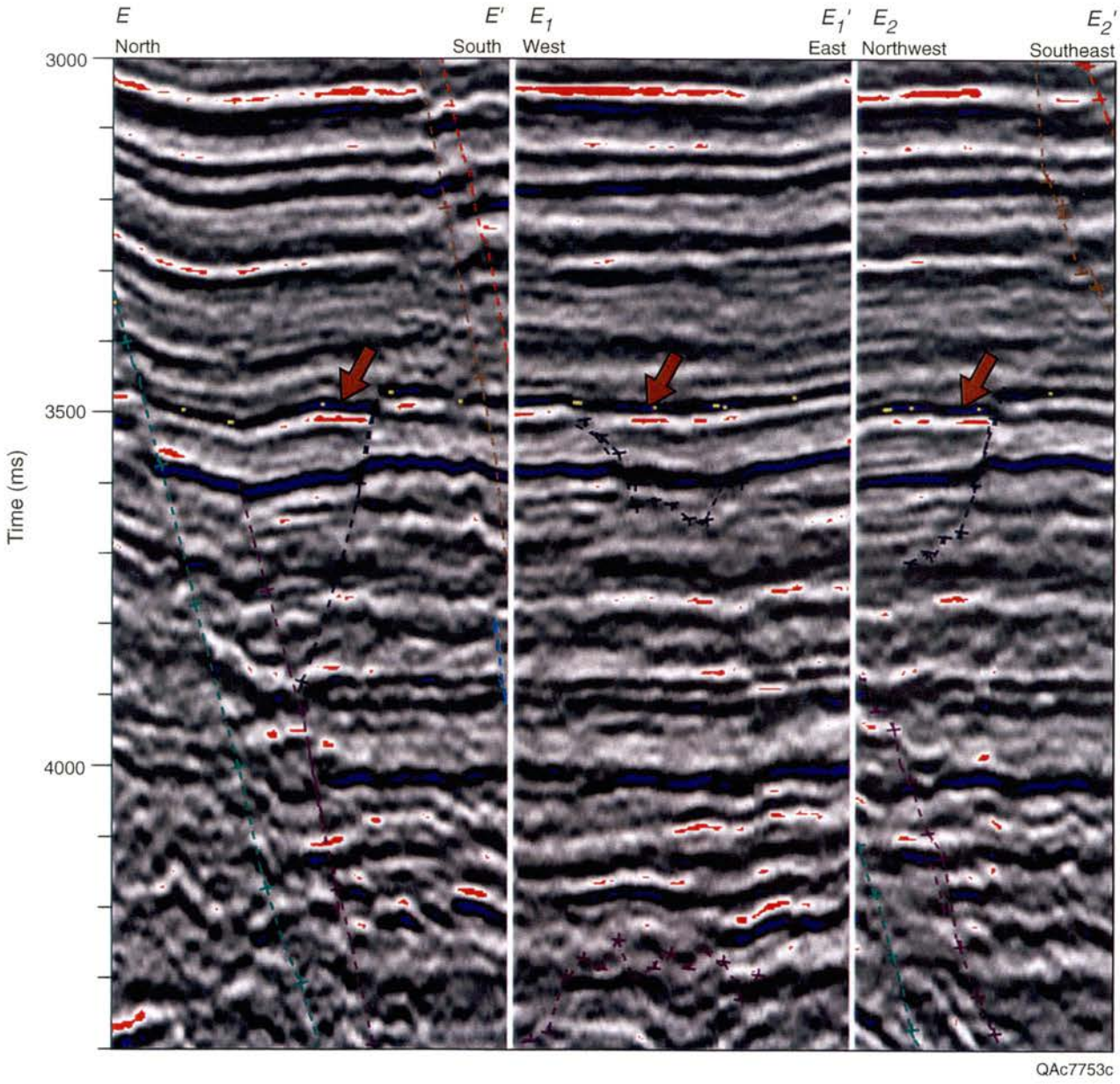

Figure 52. Vertical seismic cross sections (E–E′/E1–E1′) of prospect 5. The Robulus sands are targeted (arrow).

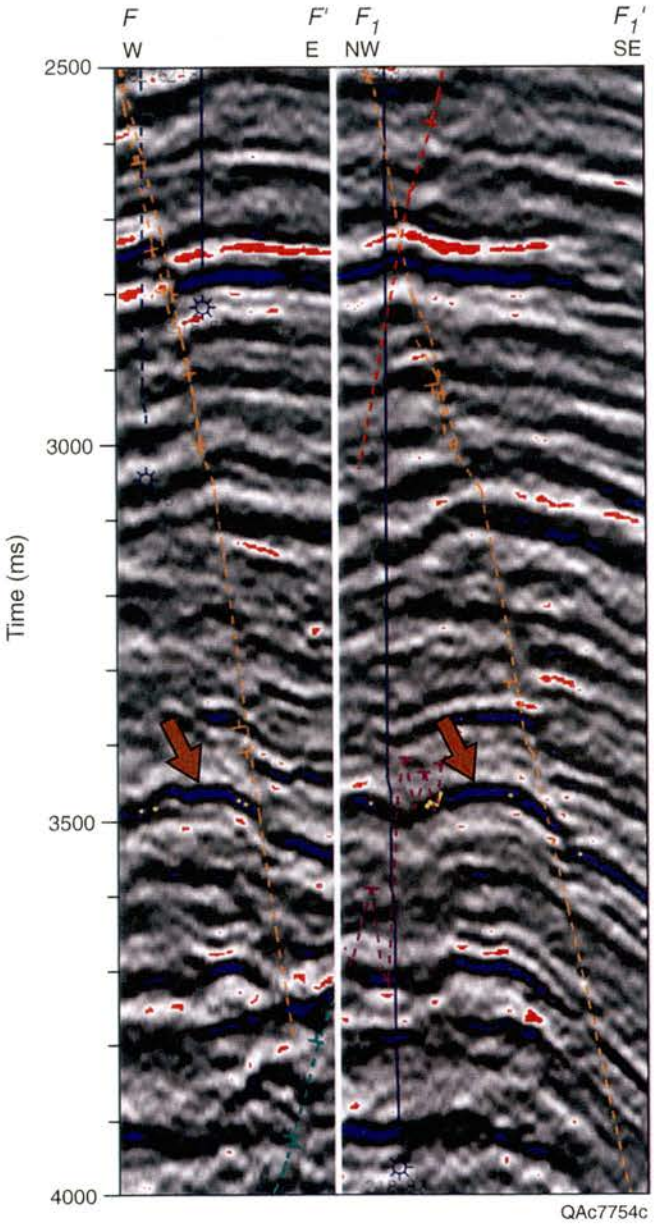

Figure 53. Vertical seismic cross sections (F–F′/F1–F1′) of prospect 6. The Robulus sands are targeted (arrow).

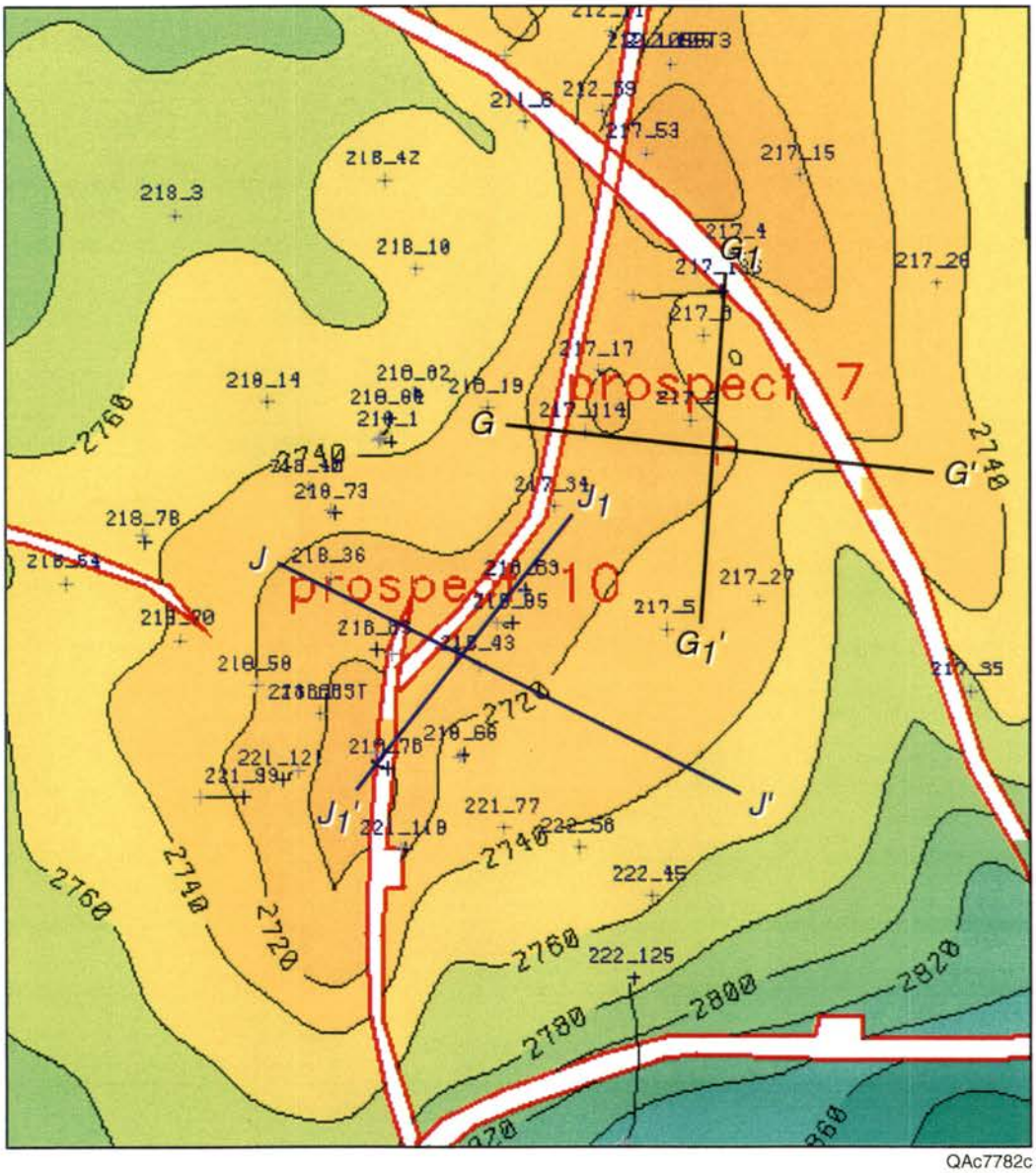

QAc7782c

Figure 54. Prospect 7 and 10 posted on a time-structure map (contour interval = 20 ms) of MFS30. The structure map depicts the subsurface topography at the T sand reservoir level.

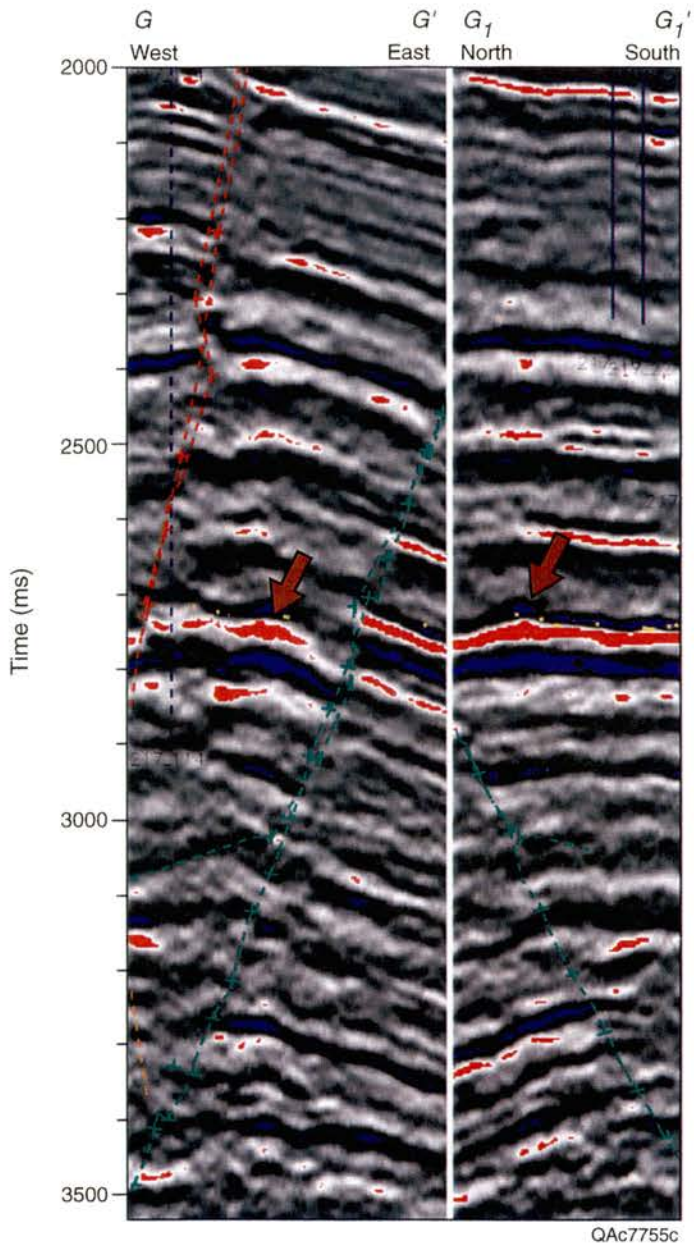

Figure 55. Vertical seismic cross sections (G–G′/G1–G1′) of prospect 7. The T sand is targeted (arrow).

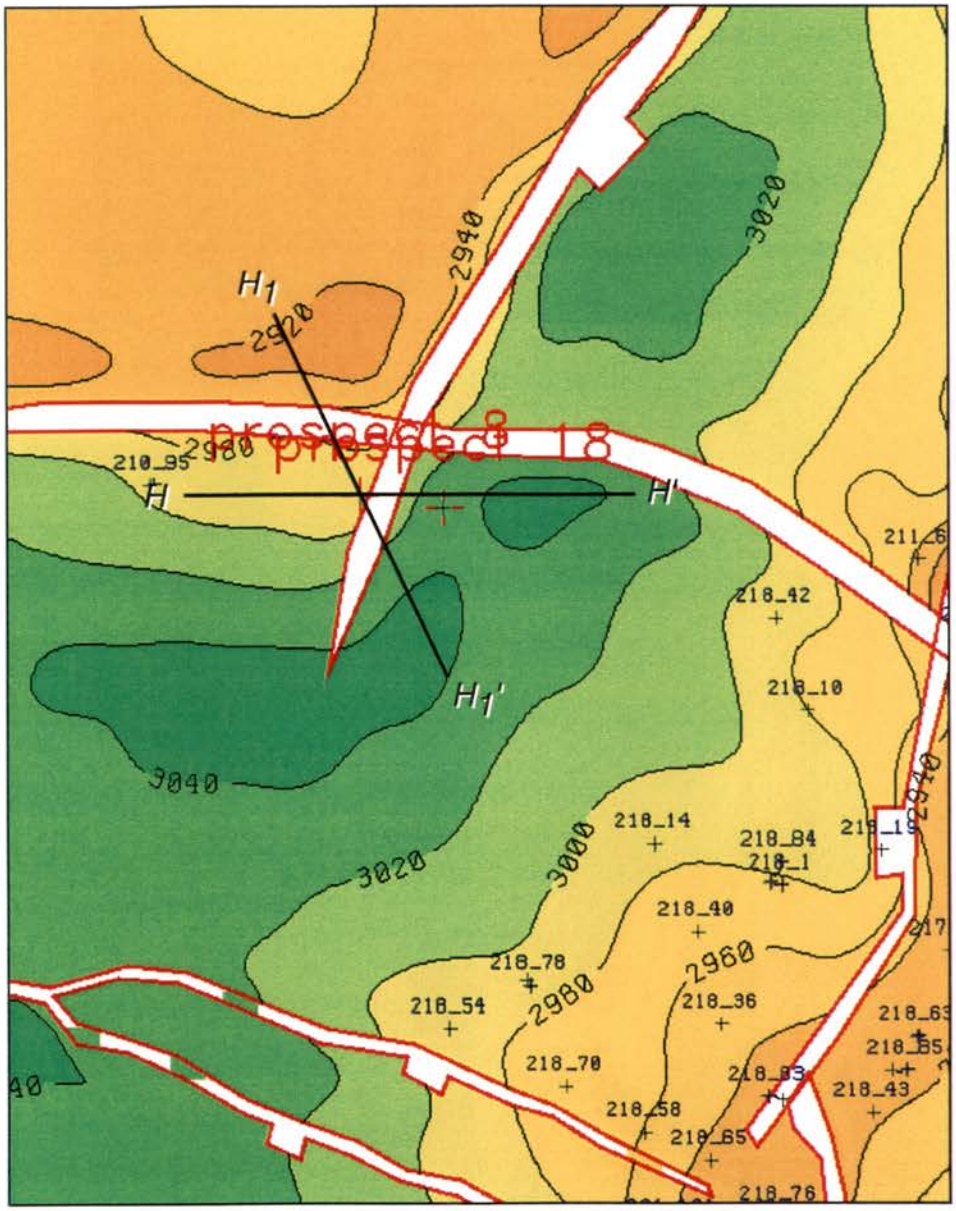

Figure 56. Prospect 8 location posted on a time-structure map (contour interval = 20 ms) of MFS40. The structure map depicts subsurface topography at the Y sand reservoir level.

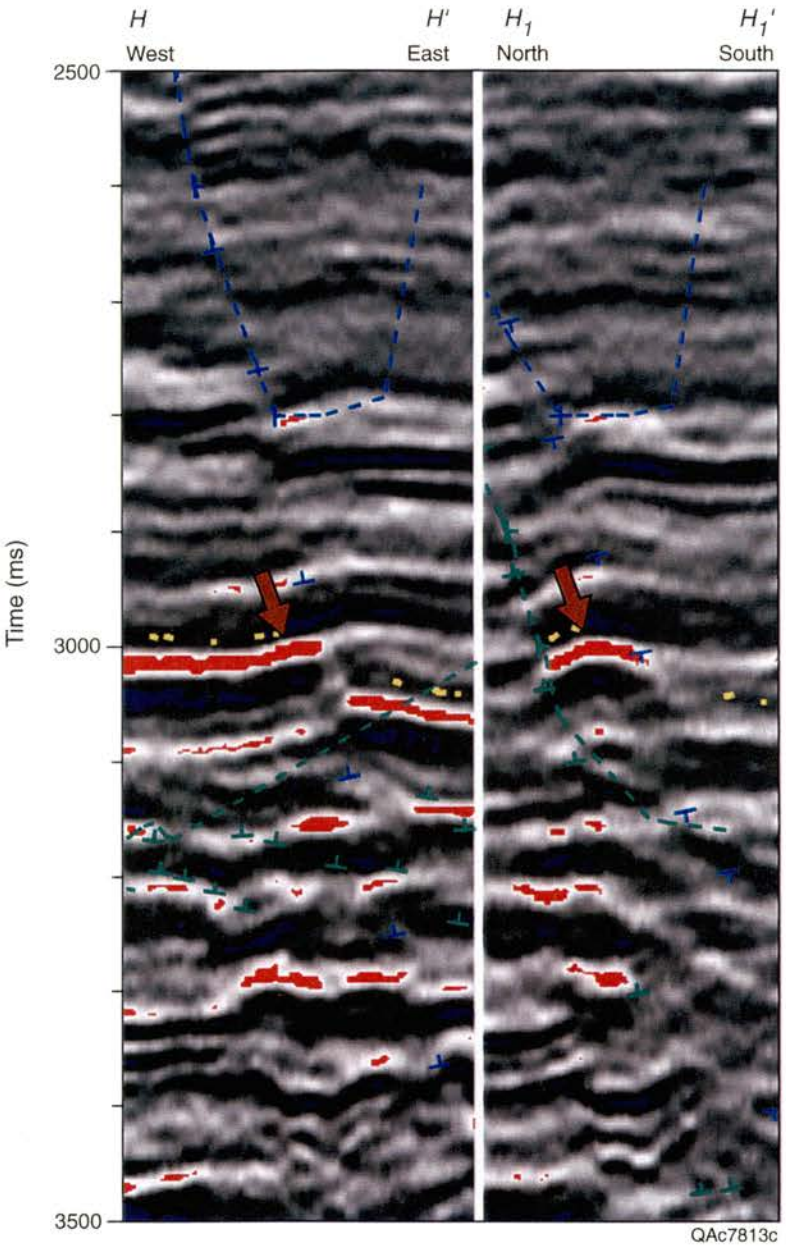

Figure 57. Vertical seismic cross sections (H–H′/H1–H1′) of prospect 8. The Y sand is targeted (arrow).

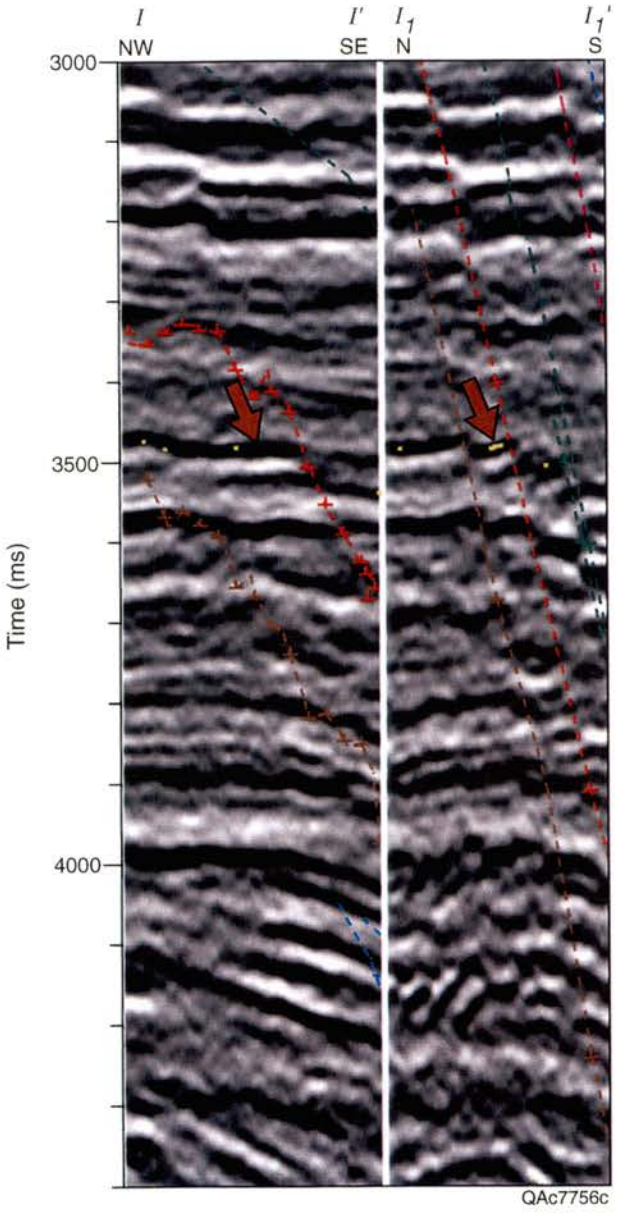

Figure 58. Vertical seismic cross sections (I–I′/I1–I1′) of prospect 9. The Robulus sands are targeted (arrow).

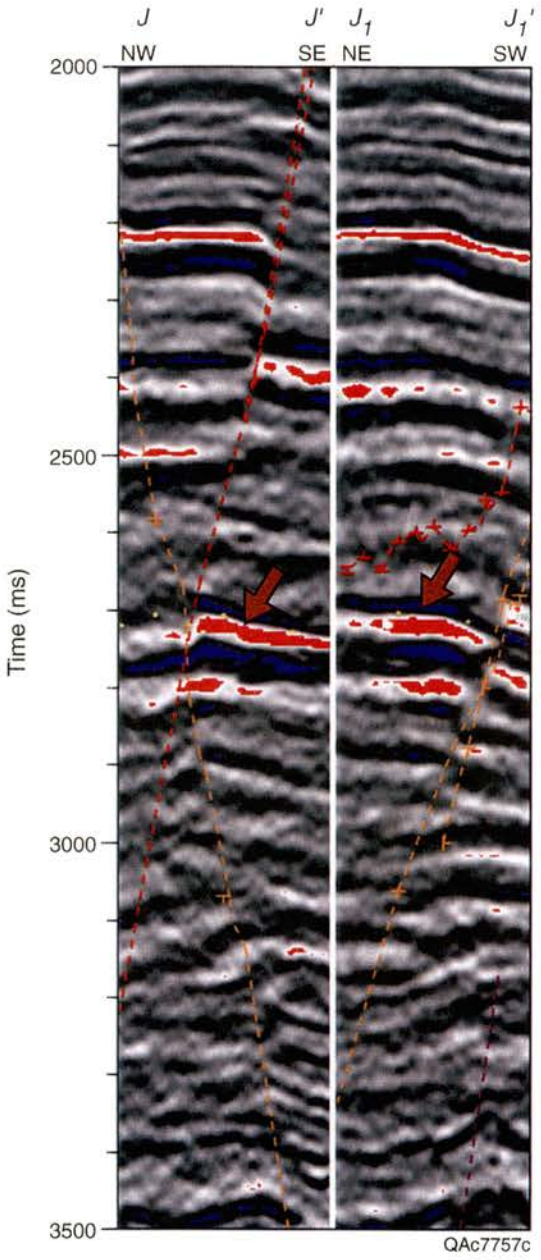

Figure 59. Vertical seismic cross sections (J–J′/J1–J1′) of prospect 10. The T sand is targeted (arrow).

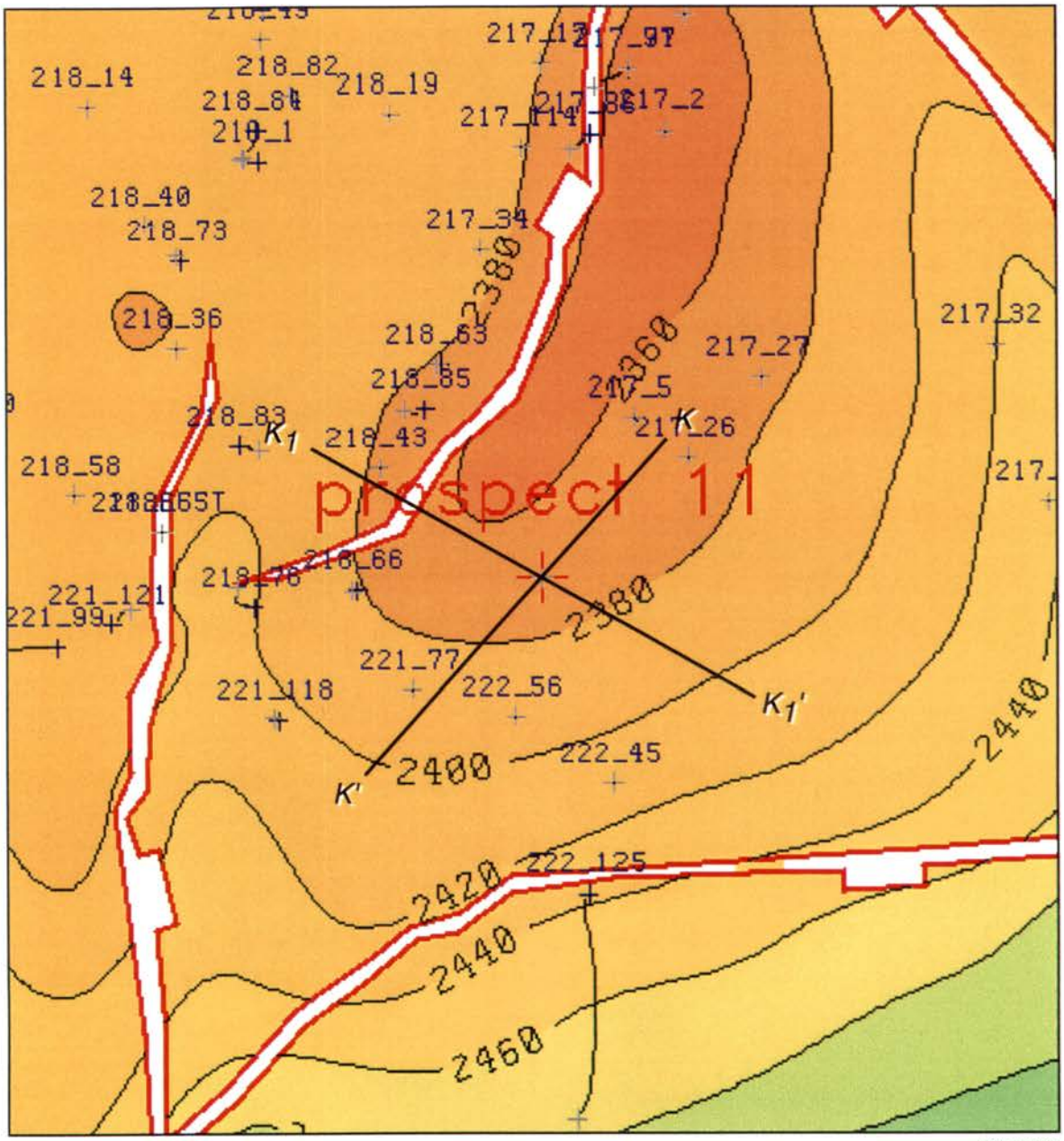

Figure 60. Prospect 11 location posted on a time-structure map (contour interval = 20 ms) of MFS24. The structure map depicts subsurface topography at the O sand reservoir level.

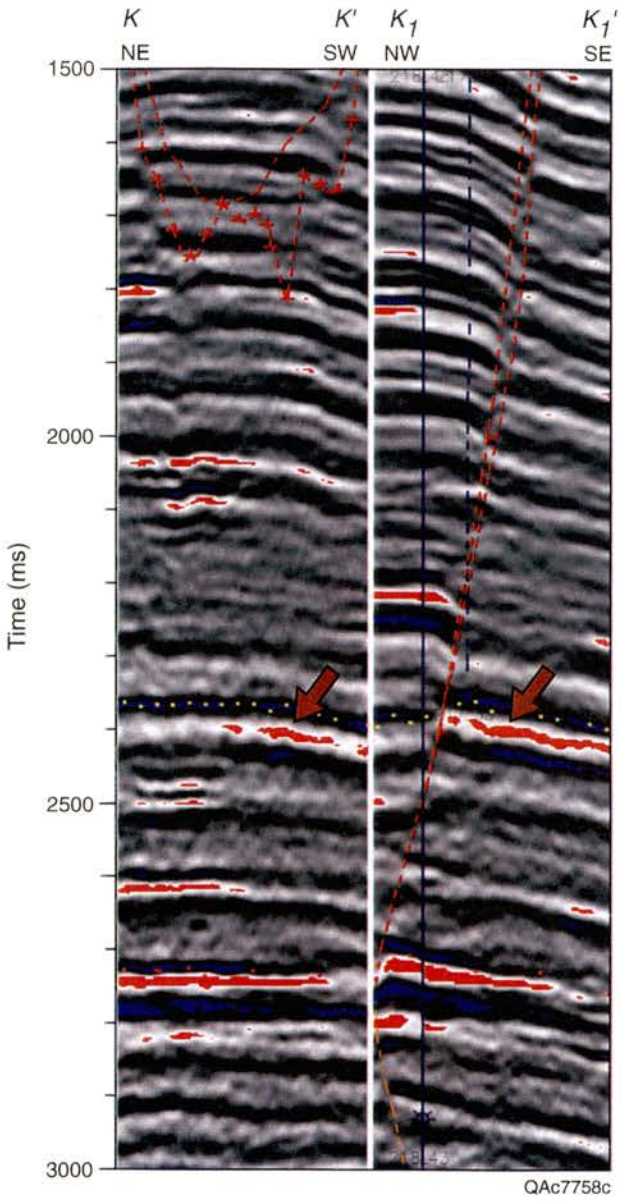

Figure 61. Vertical seismic cross sections (K–K′/ K1–K1′) of prospect 11. The O sand is targeted (arrow).

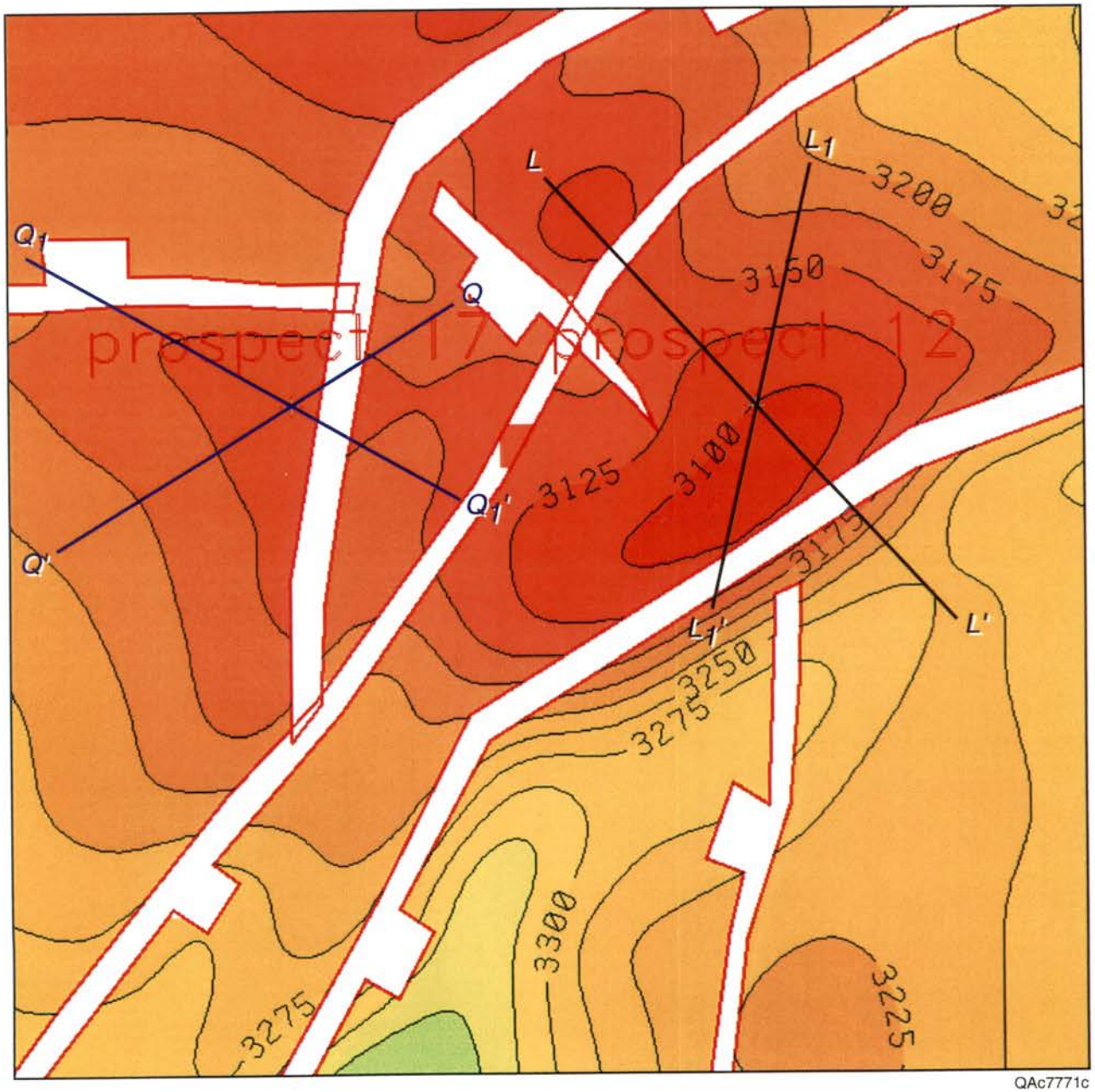

Figure 62. Prospect 12 and 17 locations posted on a time-structure map (contour interval = 25 ms) of the Robulus 2 sand. The structure map depicts the subsurface topography at the Robulus sand reservoir level.

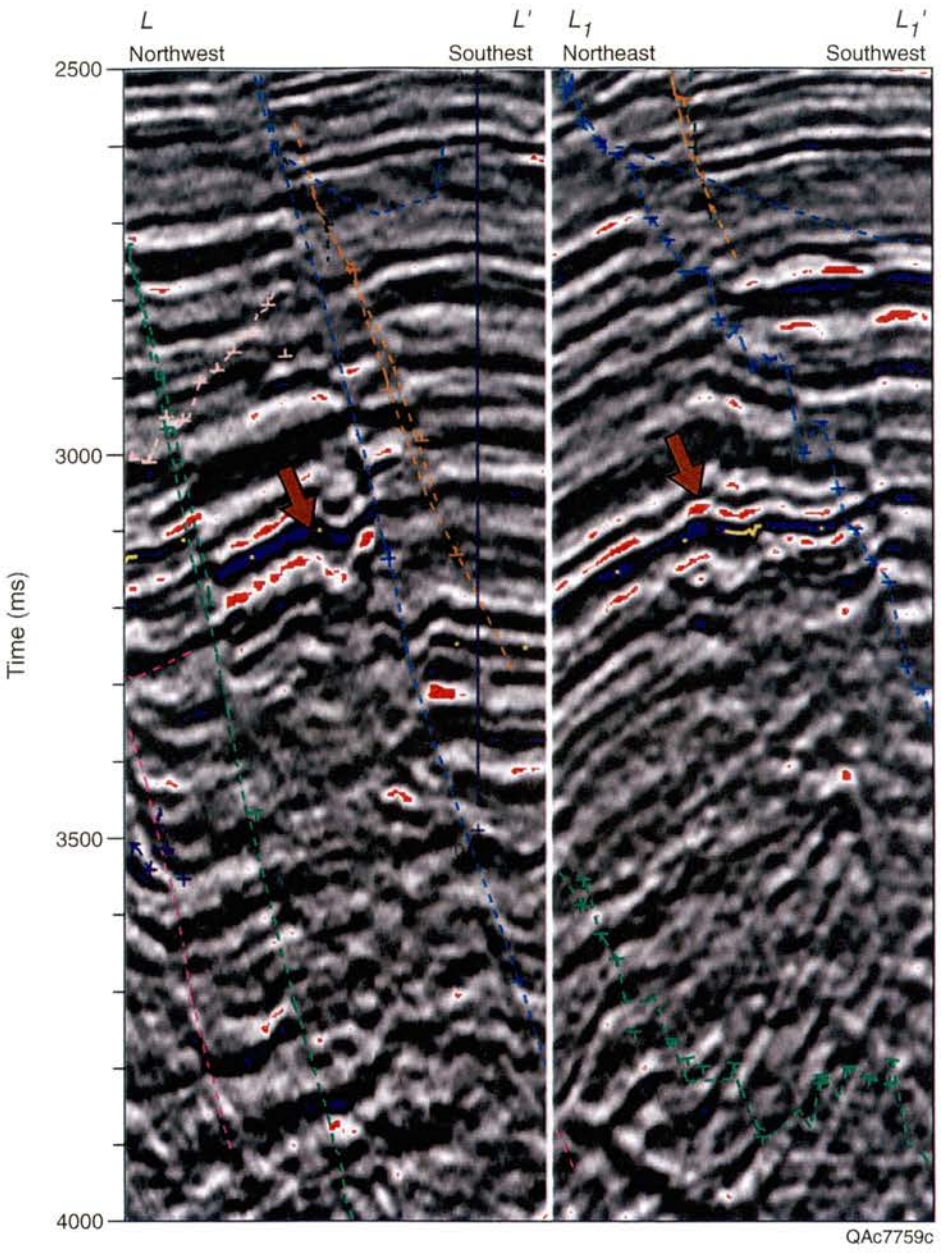

Figure 63. Vertical seismic cross sections (L–L′/L1–L1′) of prospect 12. The Robulus sands are targeted (arrow).

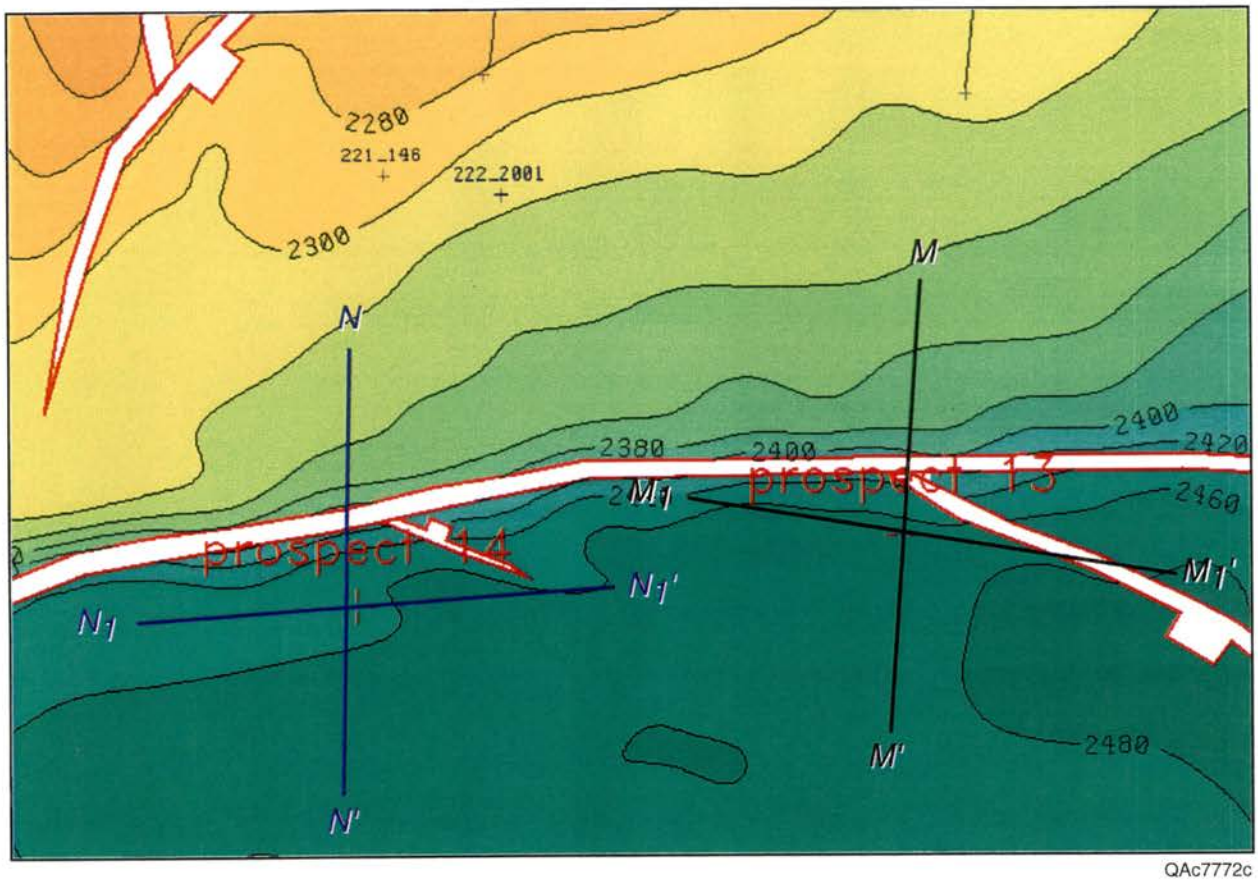

Figure 64. Prospect 13 and 14 locations posted on a time-structure map (contour interval = 20 ms) of MFS16. The structure map depicts subsurface topography at the L sand reservoir level.

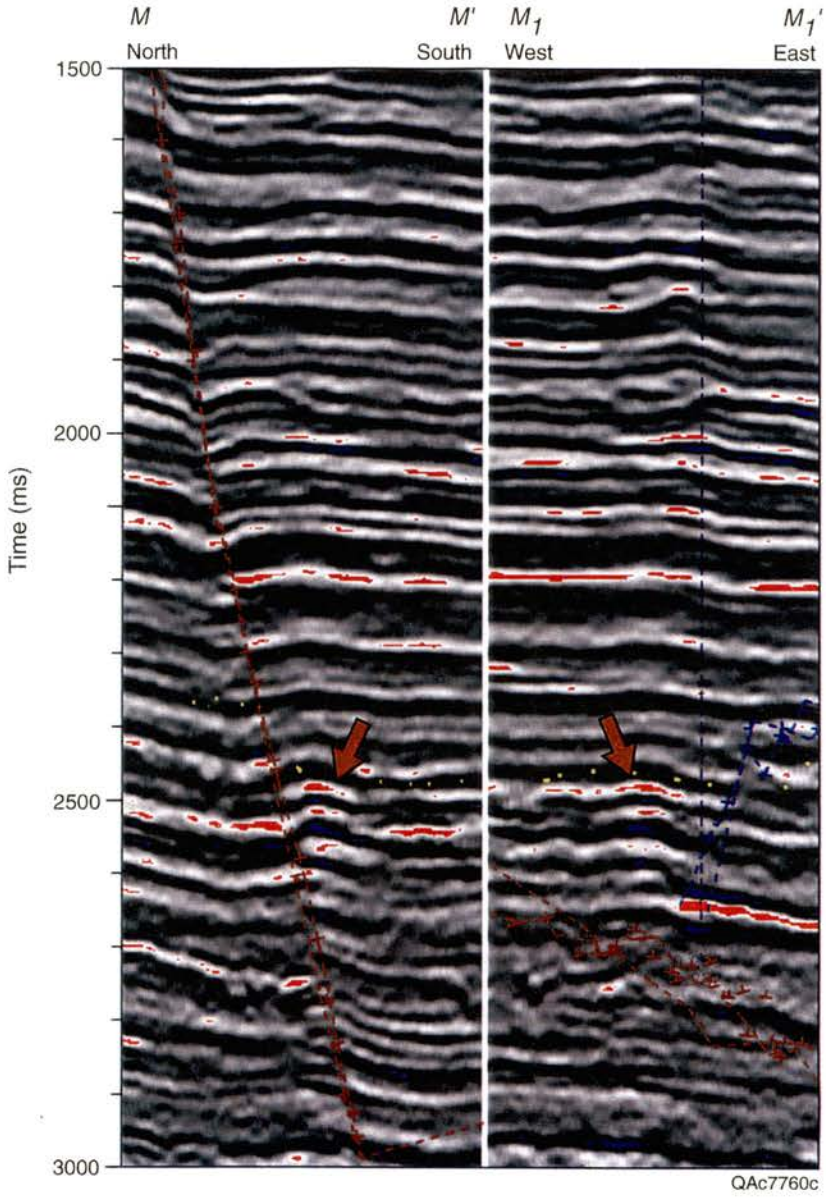

Figure 65. Vertical seismic cross sections (M–M′/M1–M1′) of prospect 13. The L sand is targeted.

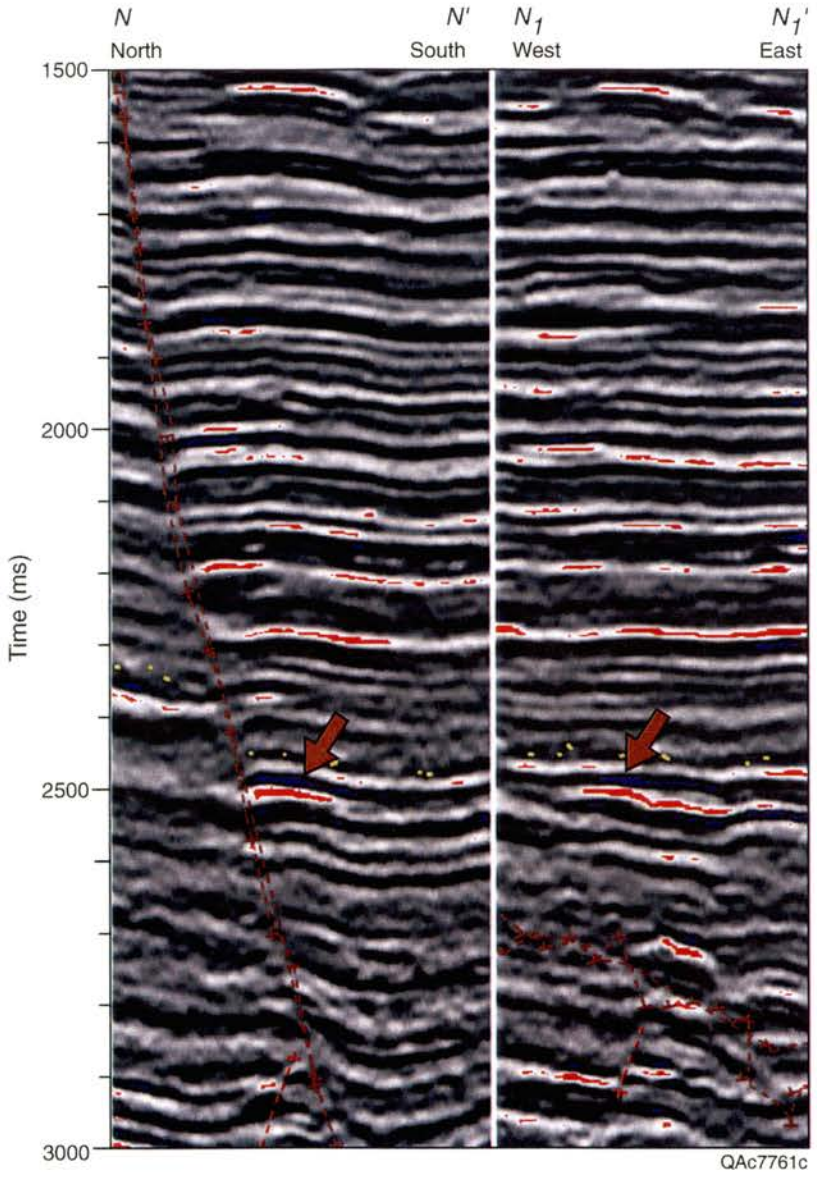

Figure 66. Vertical seismic cross sections (N–N′/N1–N1′) of prospect 14. The L sand is targeted (arrow).

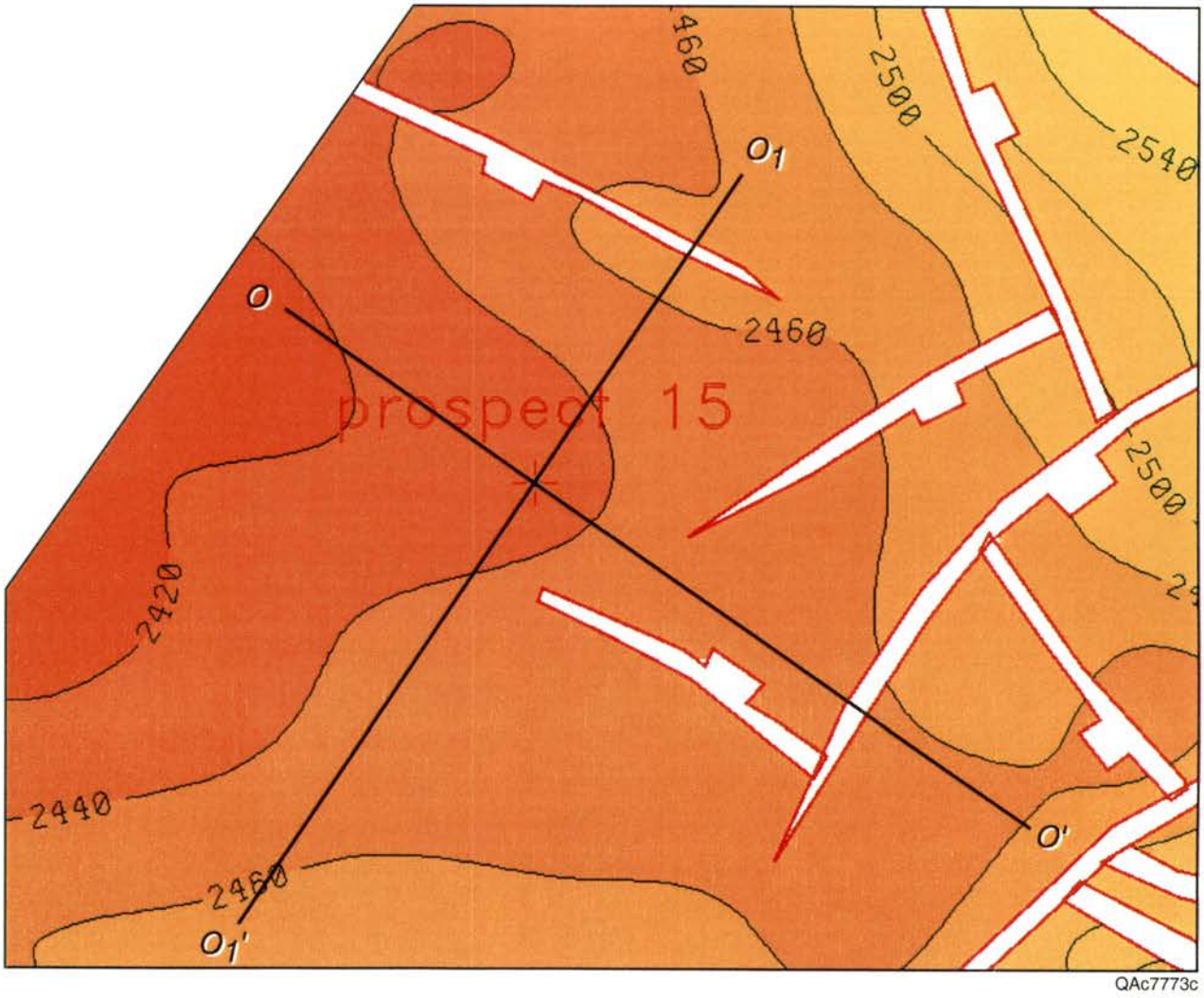

Figure 67. Prospect 15 location posted on a time-structure map (contour interval = 20 ms) of MFS26. The structure map depicts subsurface topography at the Q sand reservoir level.

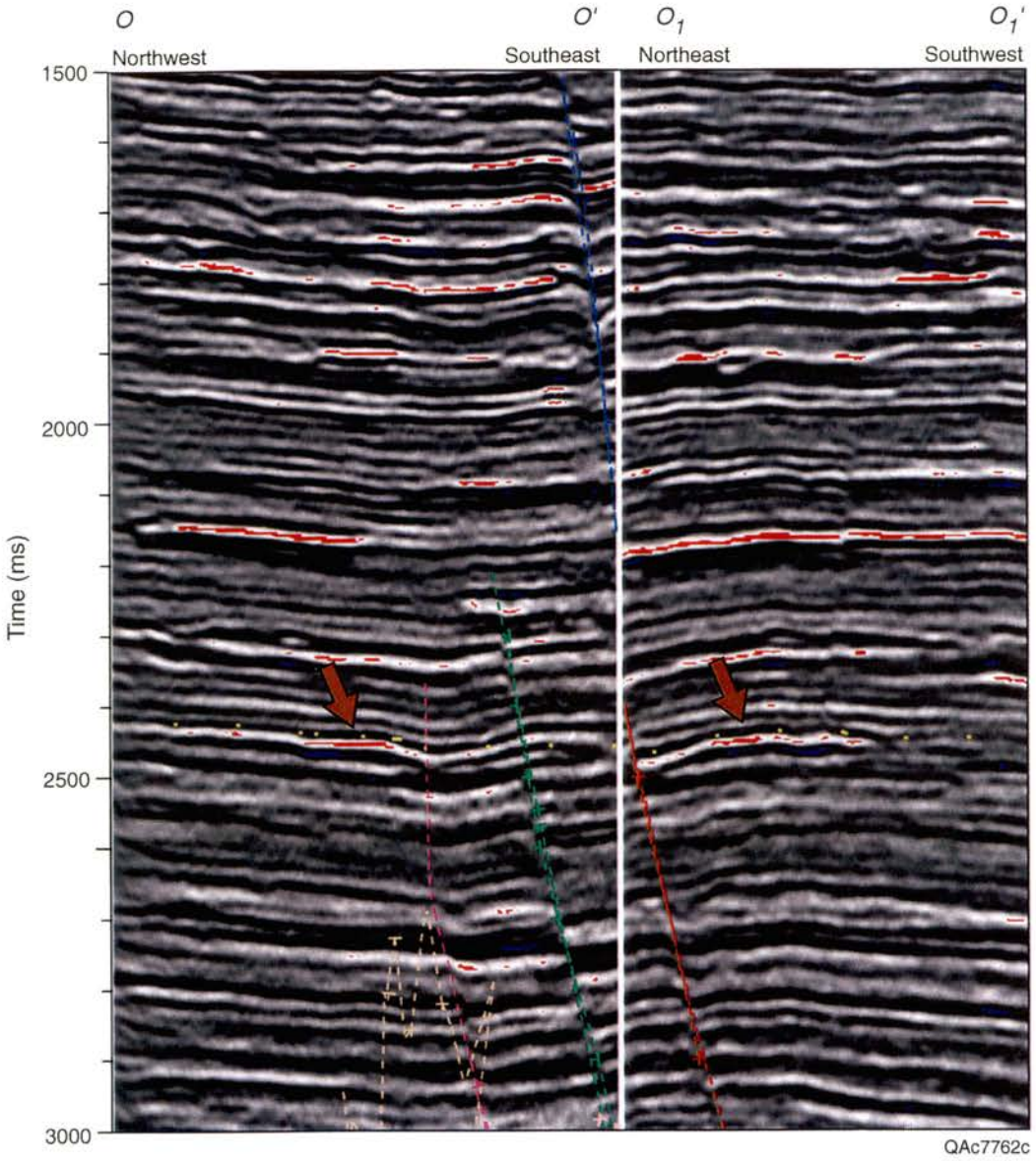

Figure 68. Vertical seismic cross sections (O–O′/O1–O1′) of prospect 15. The Q sand is targeted (arrow).

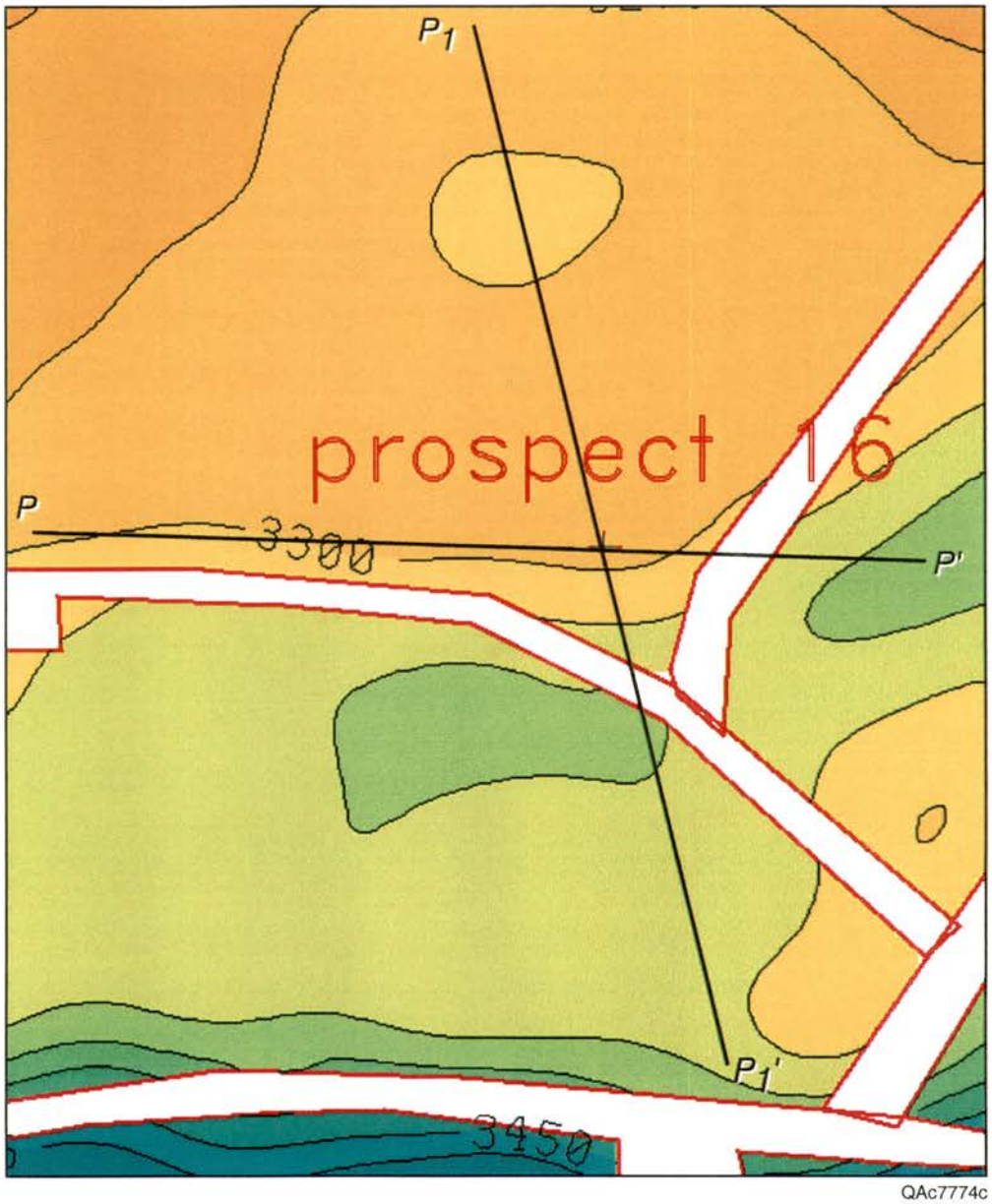

Figure 69. Prospect 16 location posted on a time-structure map (contour interval = 25 ms) of the Robulus 2 sand. The structure map depicts subsurface topography of the Robulus sand reservoir level.

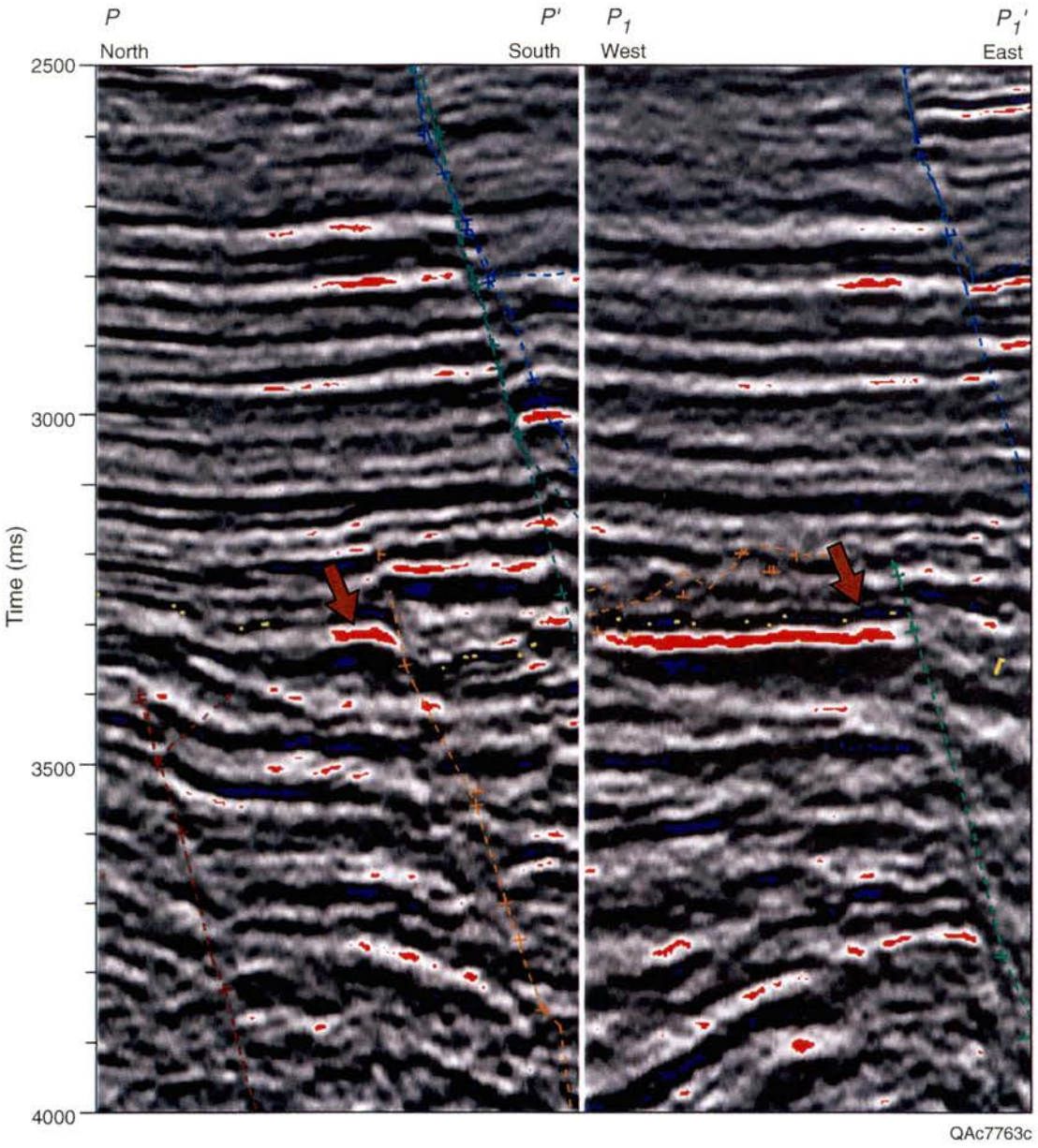

Figure 70. Vertical seismic cross sections (P–P′/P1–P1′) of prospect 16. The Robulus sands are targeted (arrow).

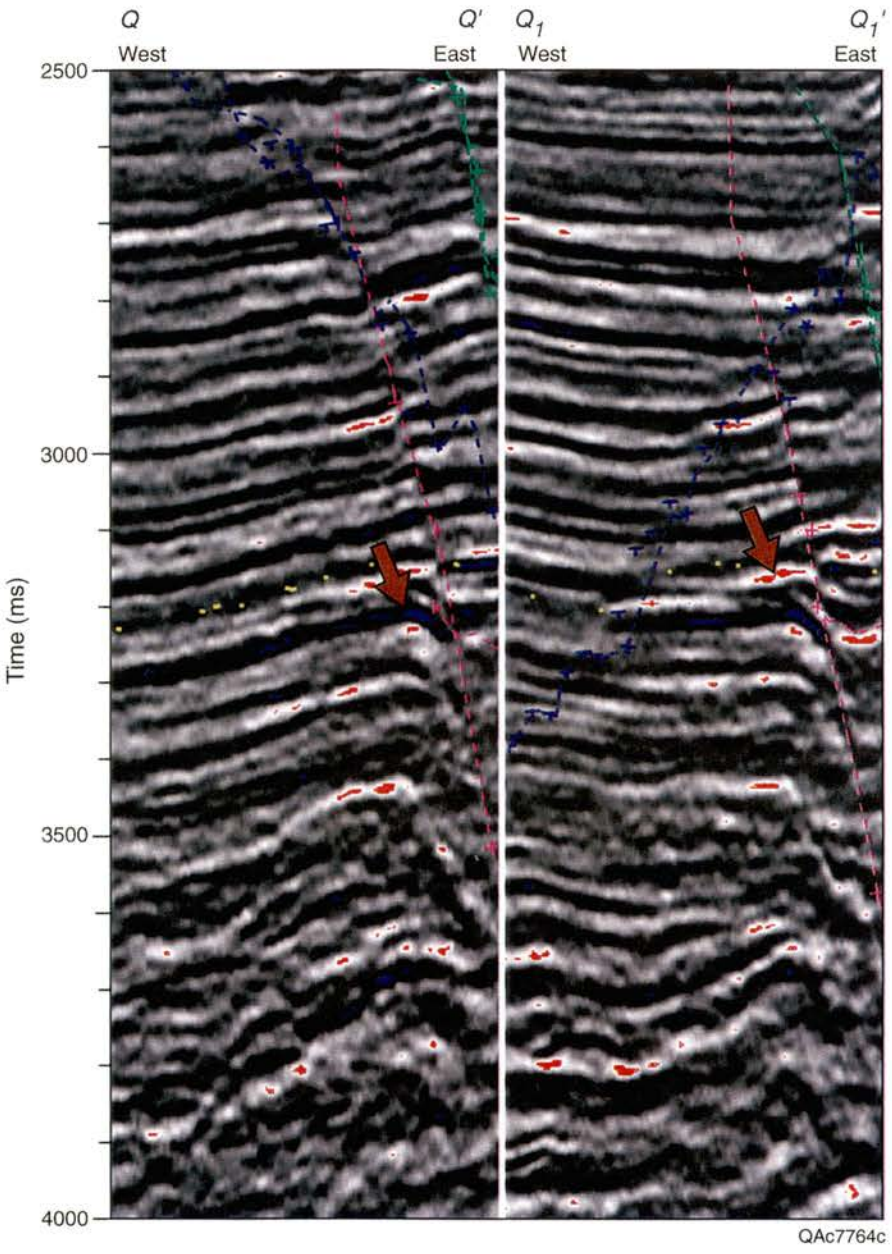

Figure 71. Vertical seismic cross sections (Q–Q′/Q1–Q1′) of prospect 17. The Robulus sands are targeted (arrow).

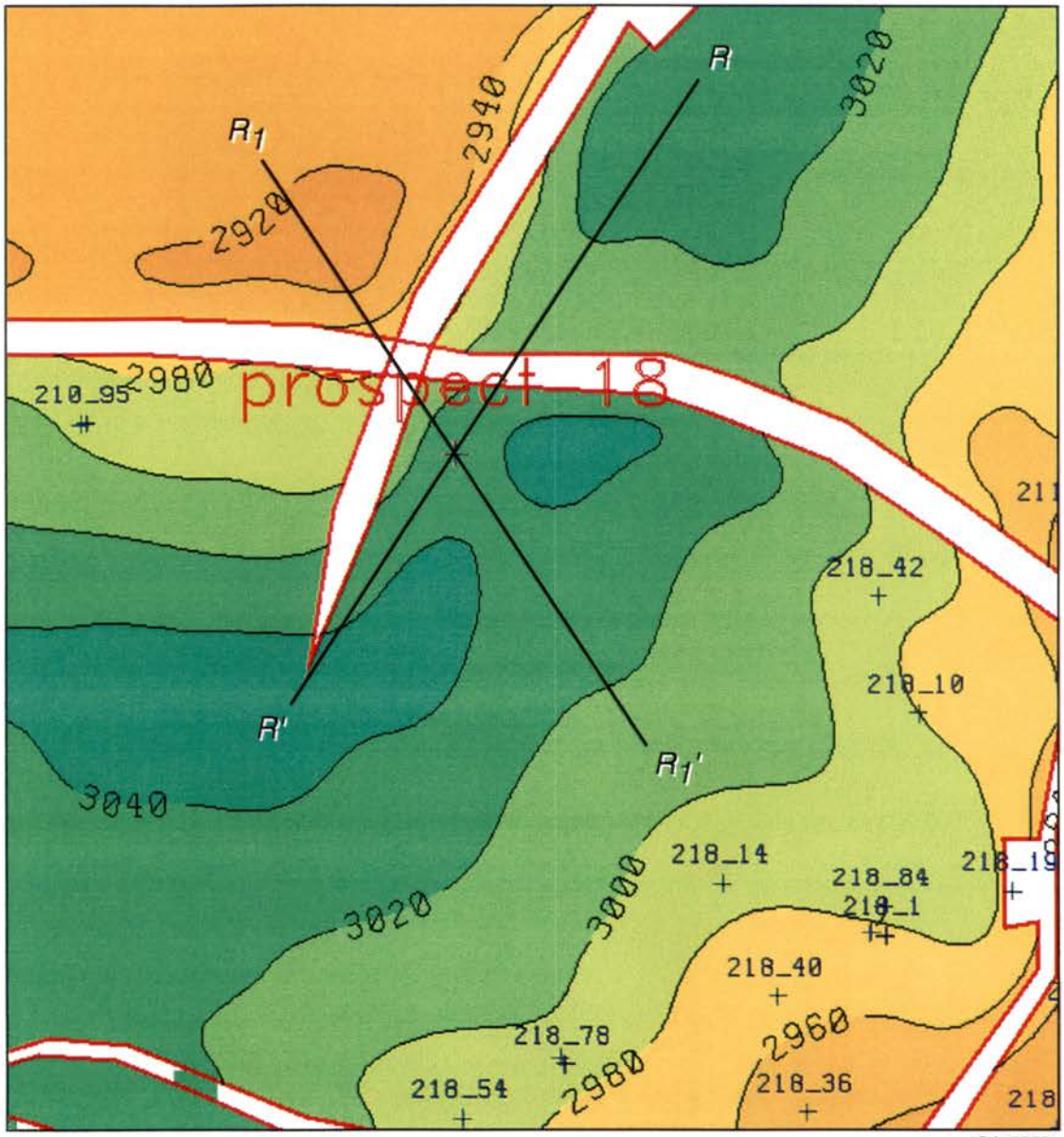

Figure 72. Prospect 18 location posted on a time-structure map (contour interval = 20 ms) of MFS40. The structure map depicts subsurface topography at the Y sand reservoir level.

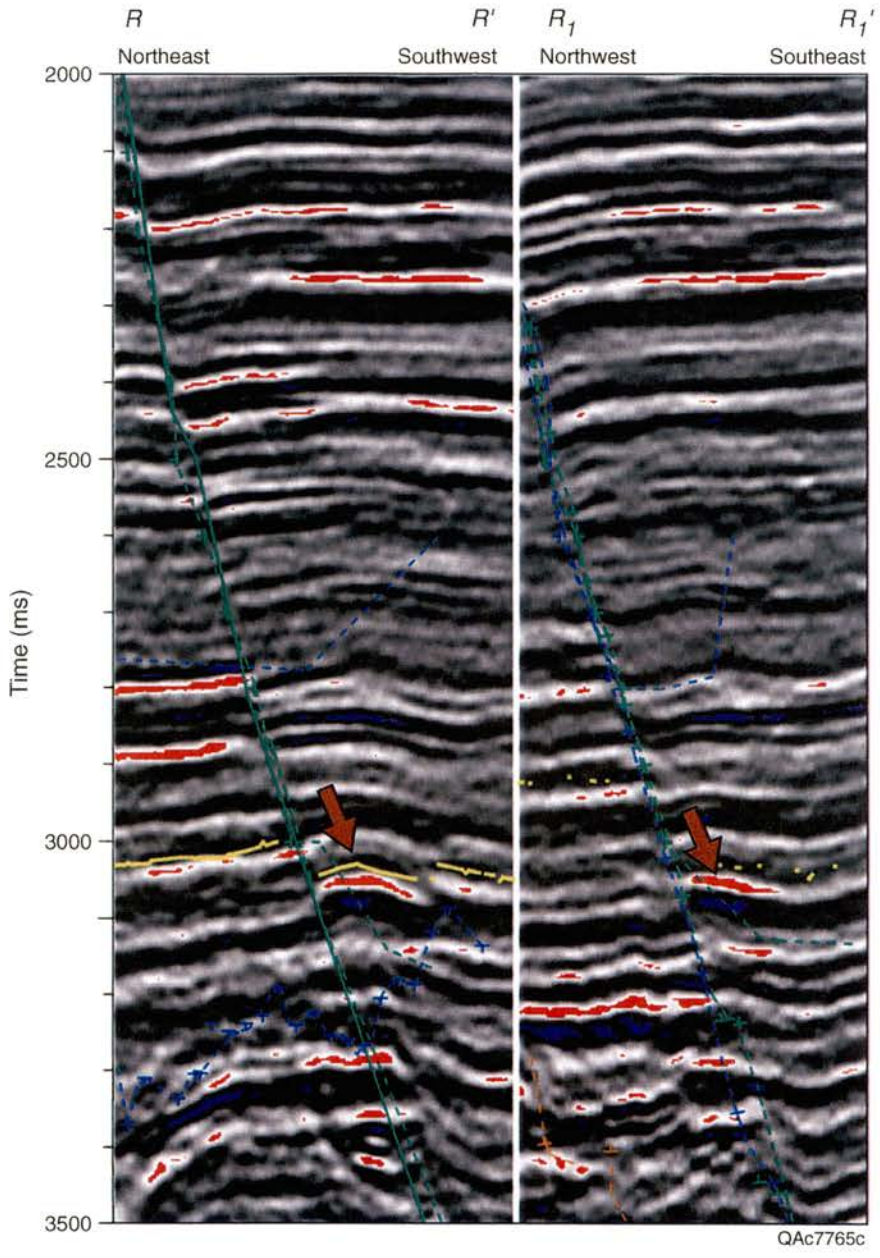

Figure 73. Vertical seismic cross sections (R–R′/R1–R1′) of prospect 18. The Y sand is targeted (arrow).

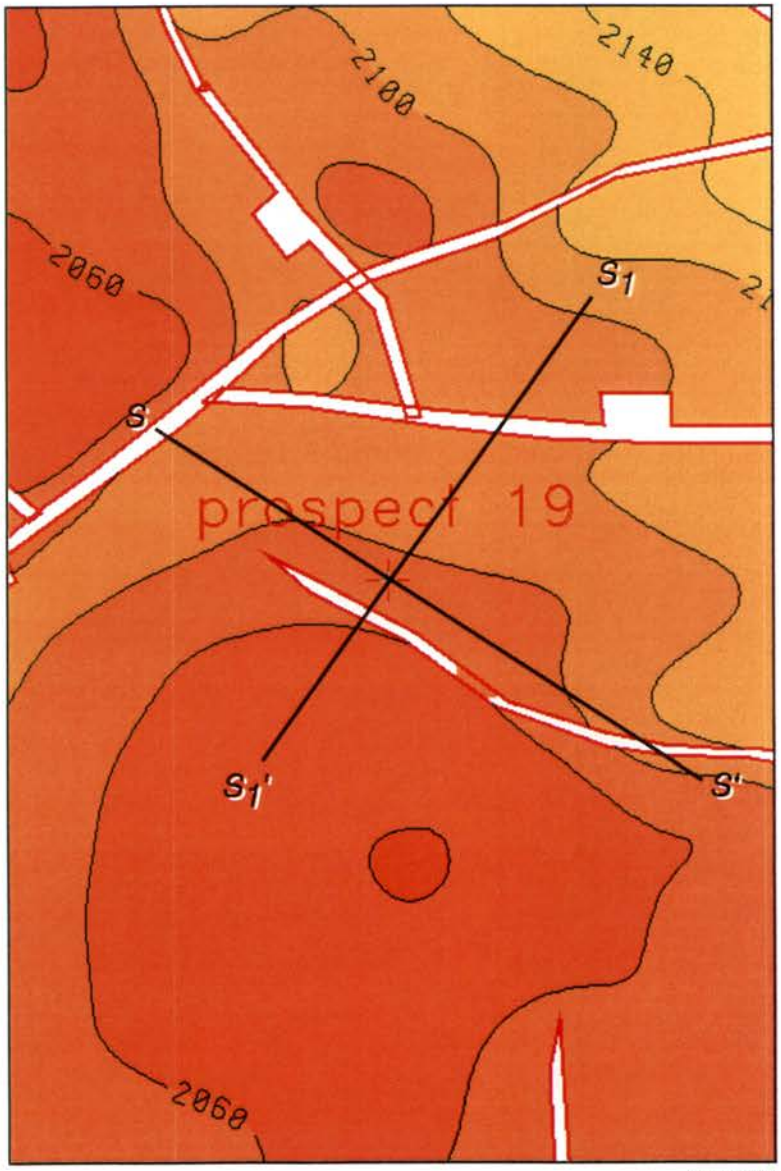

QAc7777c

Figure 74. Prospect 19 location posted on a time-structure map (contour interval = 20 ms) of MFS13. The structure map depicts subsurface topography at the J sand reservoir level.

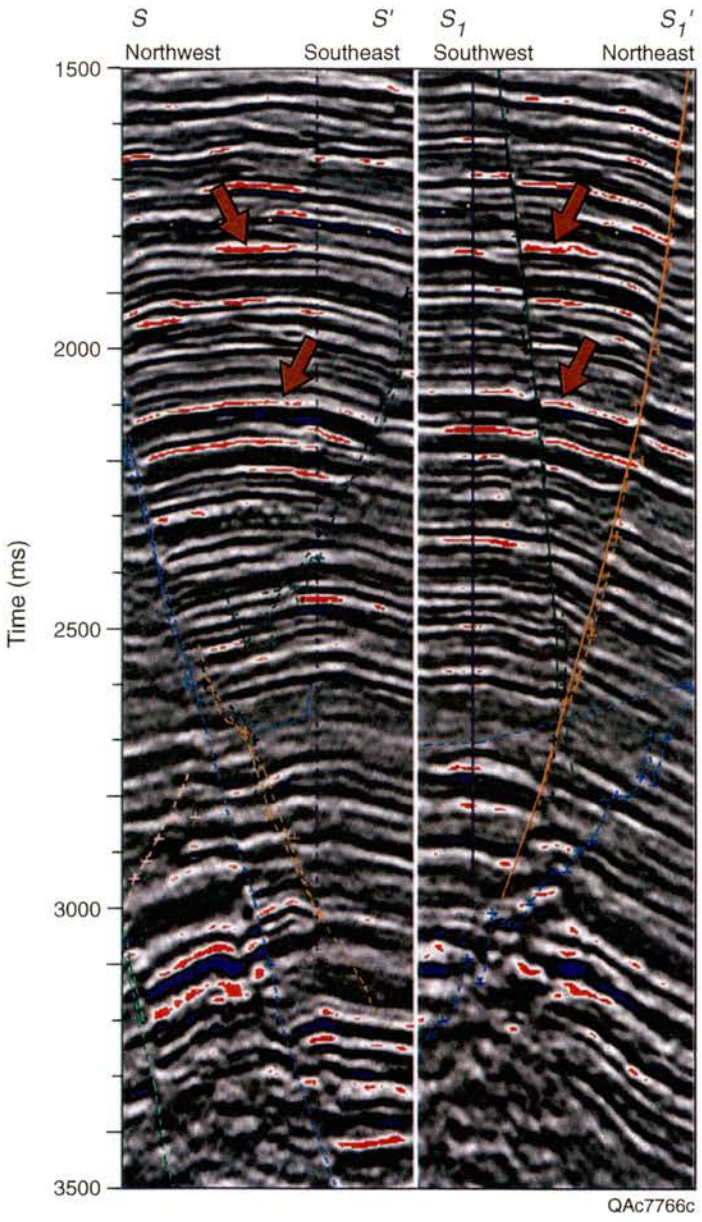

Figure 75. Vertical seismic cross sections (S–S′/S1–S1′) of prospect 19. Shallow B sand (top arrow), as well as the deeper J sand (bottom arrow), is targeted.

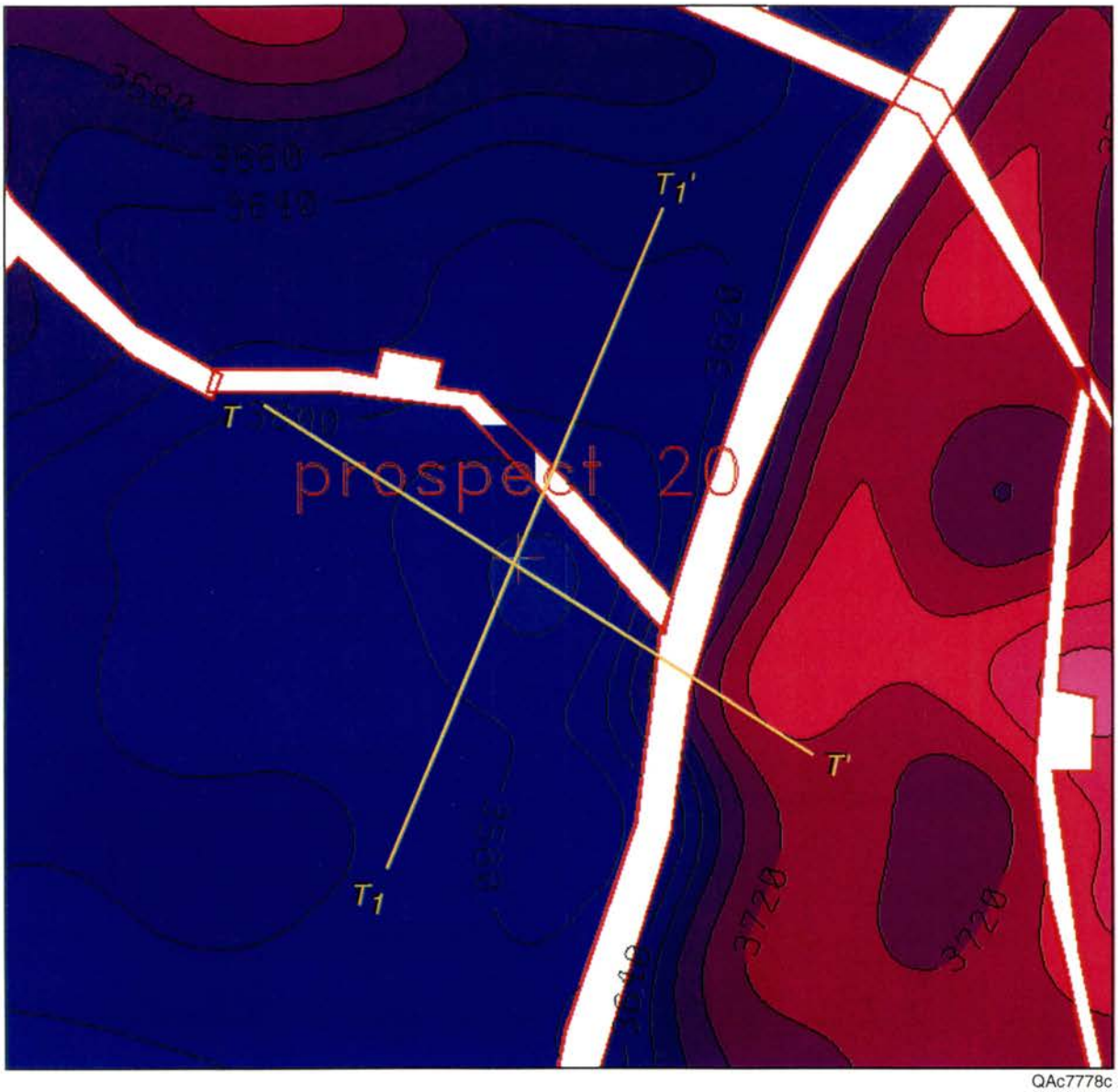

Figure 76. Prospect 20 location posted on a time-structure map (contour interval = 20 ms) of MFS45. The structure map depicts subsurface topography at the 12000A sand reservoir level.

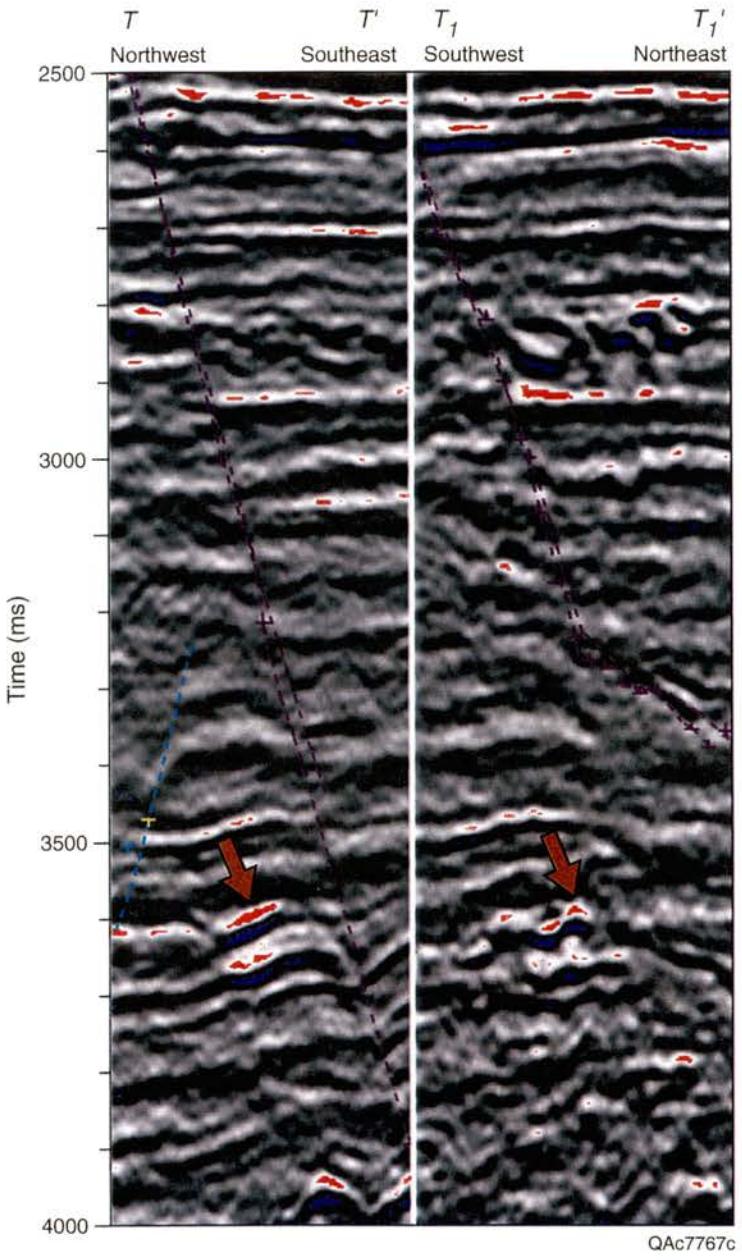

Figure 77. Vertical seismic cross sections (T–T′/T1–T1′) of prospect 20. The 12000 sand is targeted (arrow).

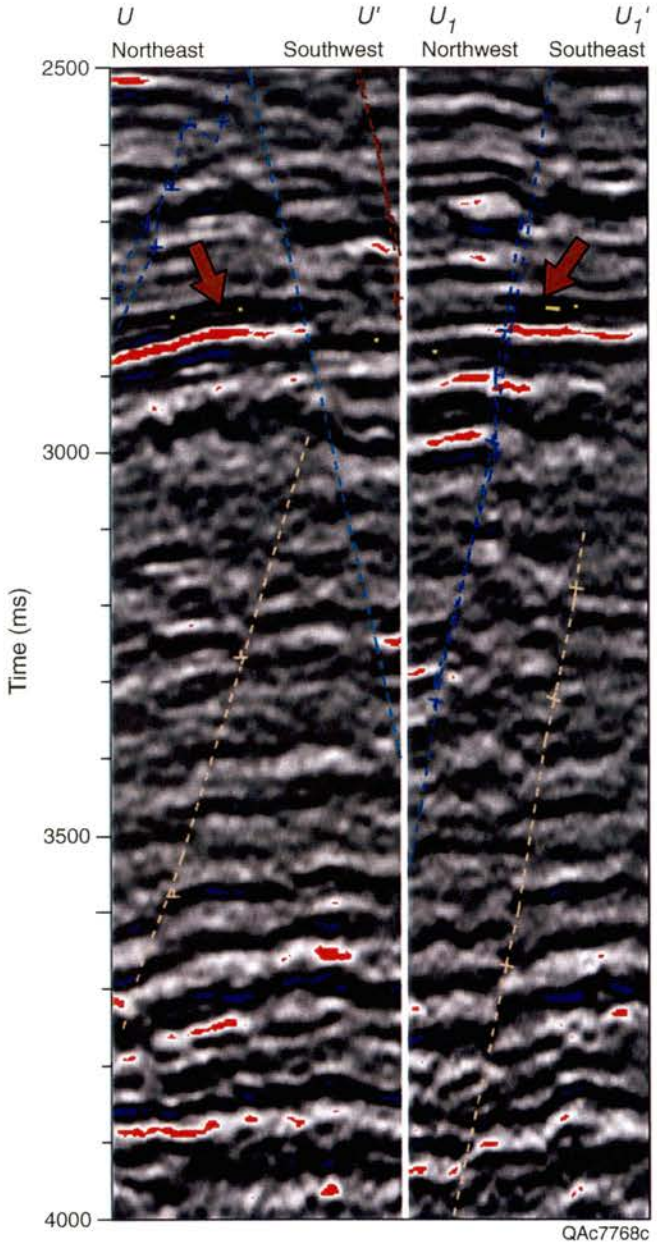

Figure 78. Vertical seismic cross sections (U–U′/U1–U1′) of prospect 21. The Q sand is targeted (arrow).

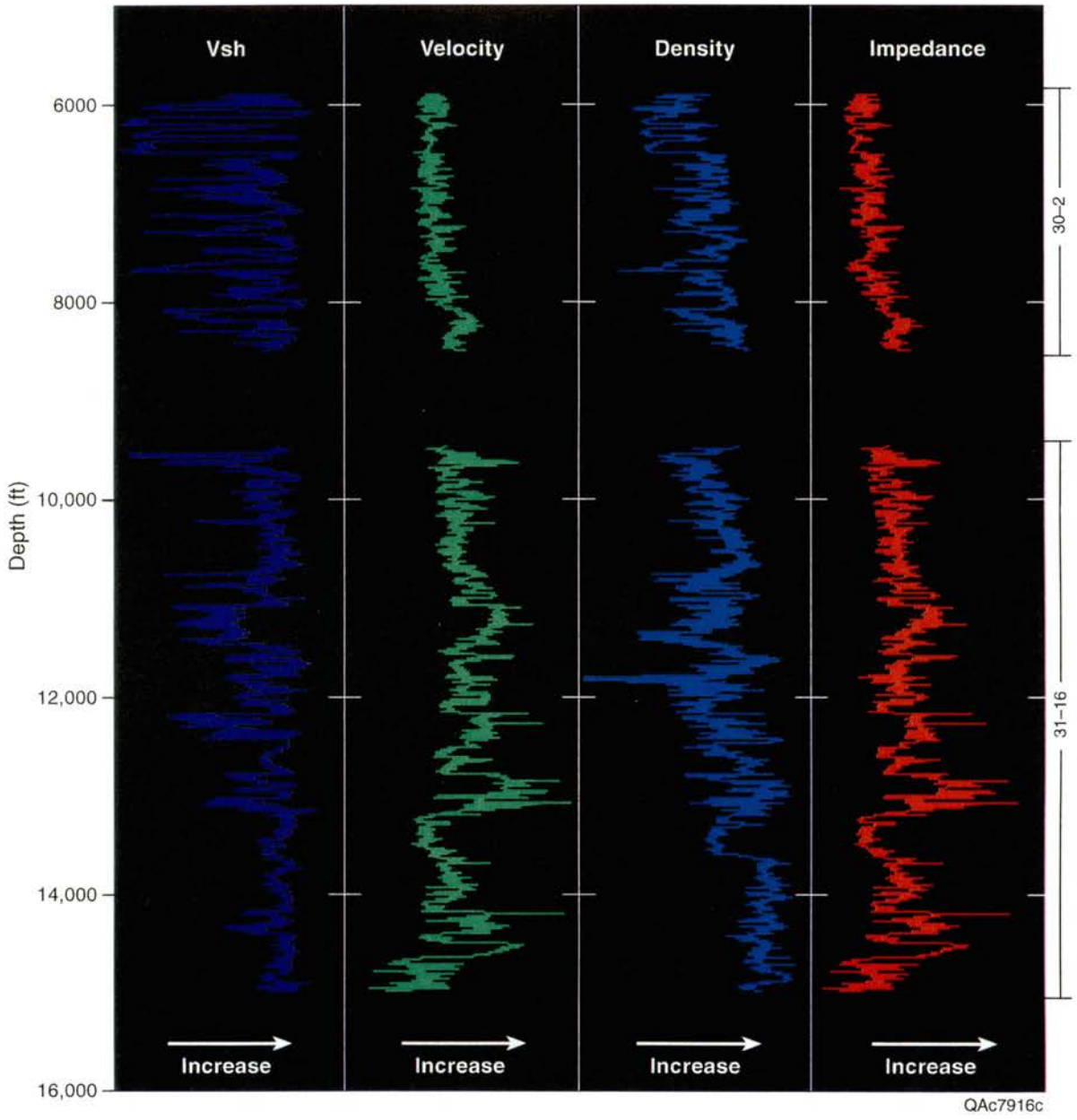

Figure 79. P-velocity (from sonic log) and density curves selected from wells 30-2 and 31-16.

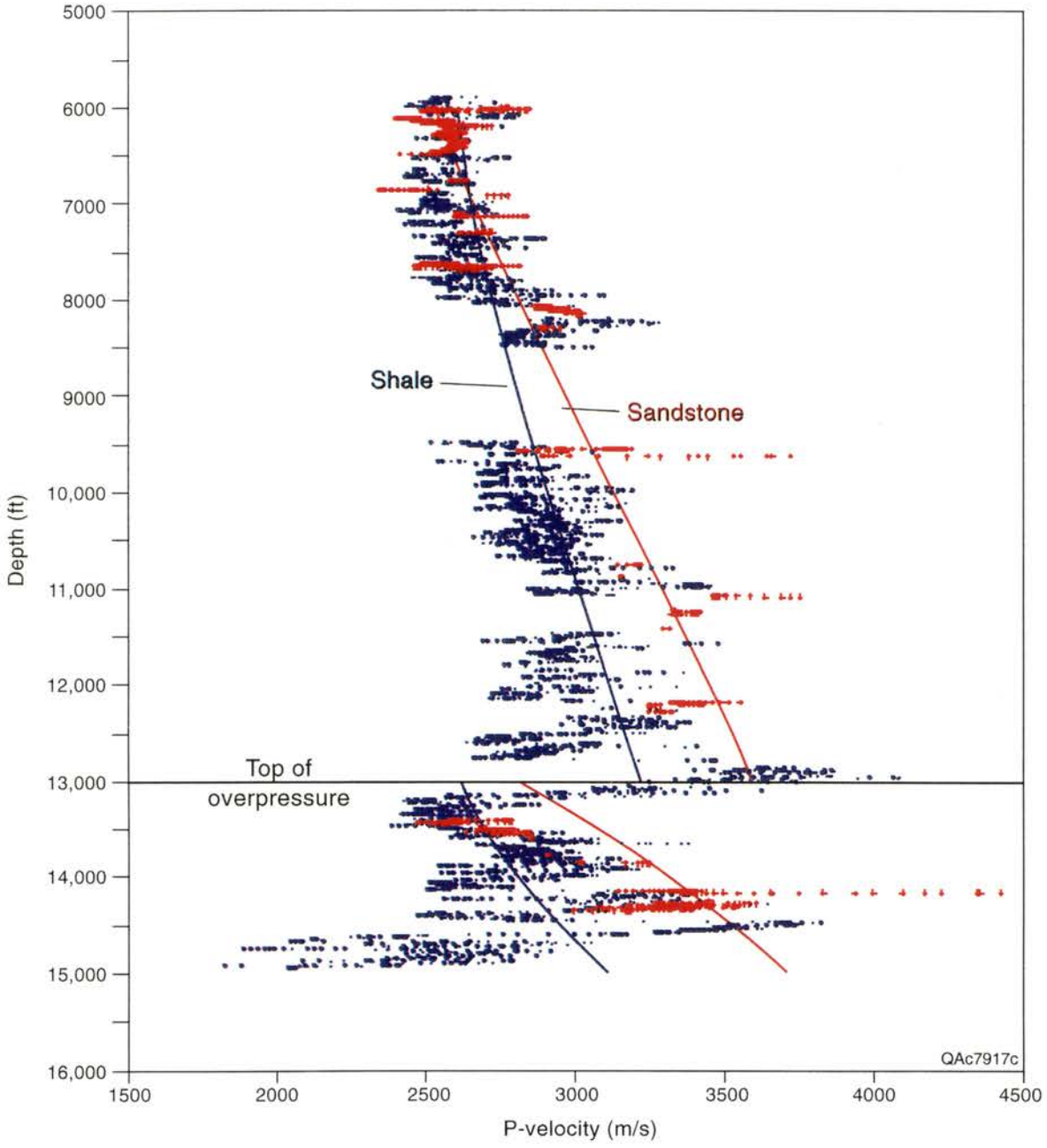

Figure 80. P-velocity of clean sandstone and shale against depth with trend lines.

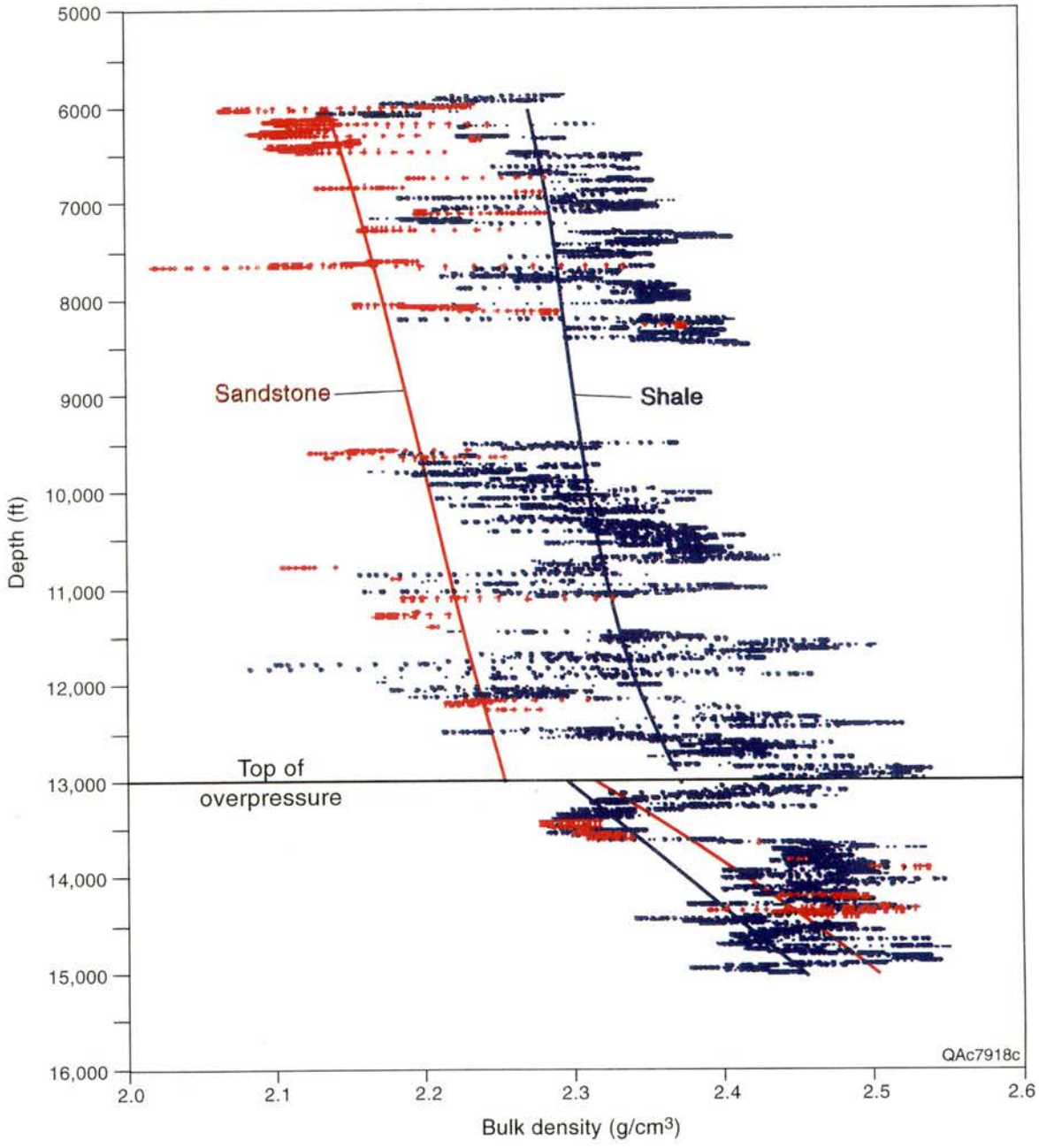

Figure 81. Bulk density of clean sandstone and shale against depth with trend lines.

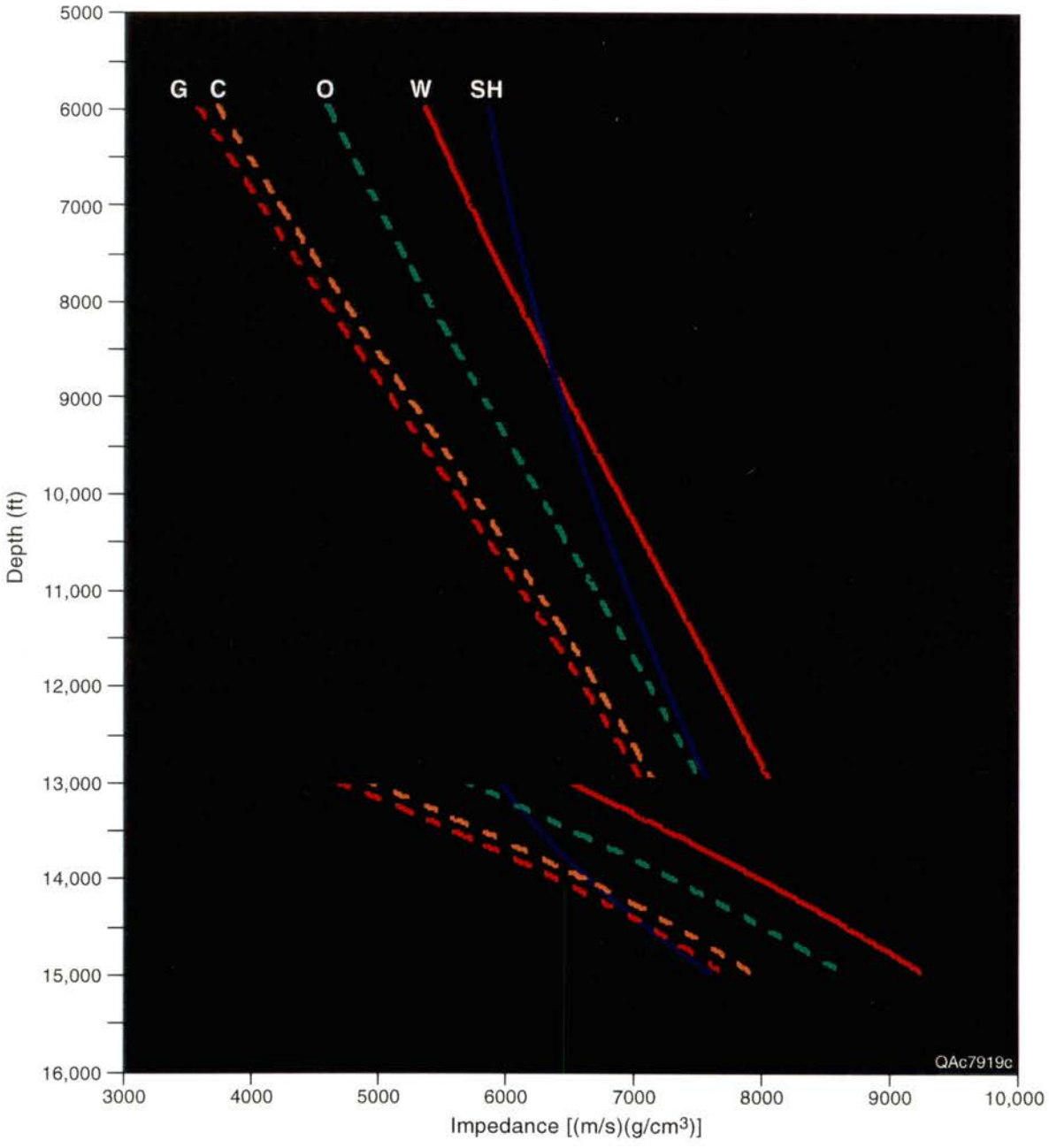

Figure 82. Acoustic impedance trend lines of brine-saturated sandstones, shale, and hydrocarbon-saturated sandstones. SH=shale, W=brine, O=oil, C=condensate, and G=gas.

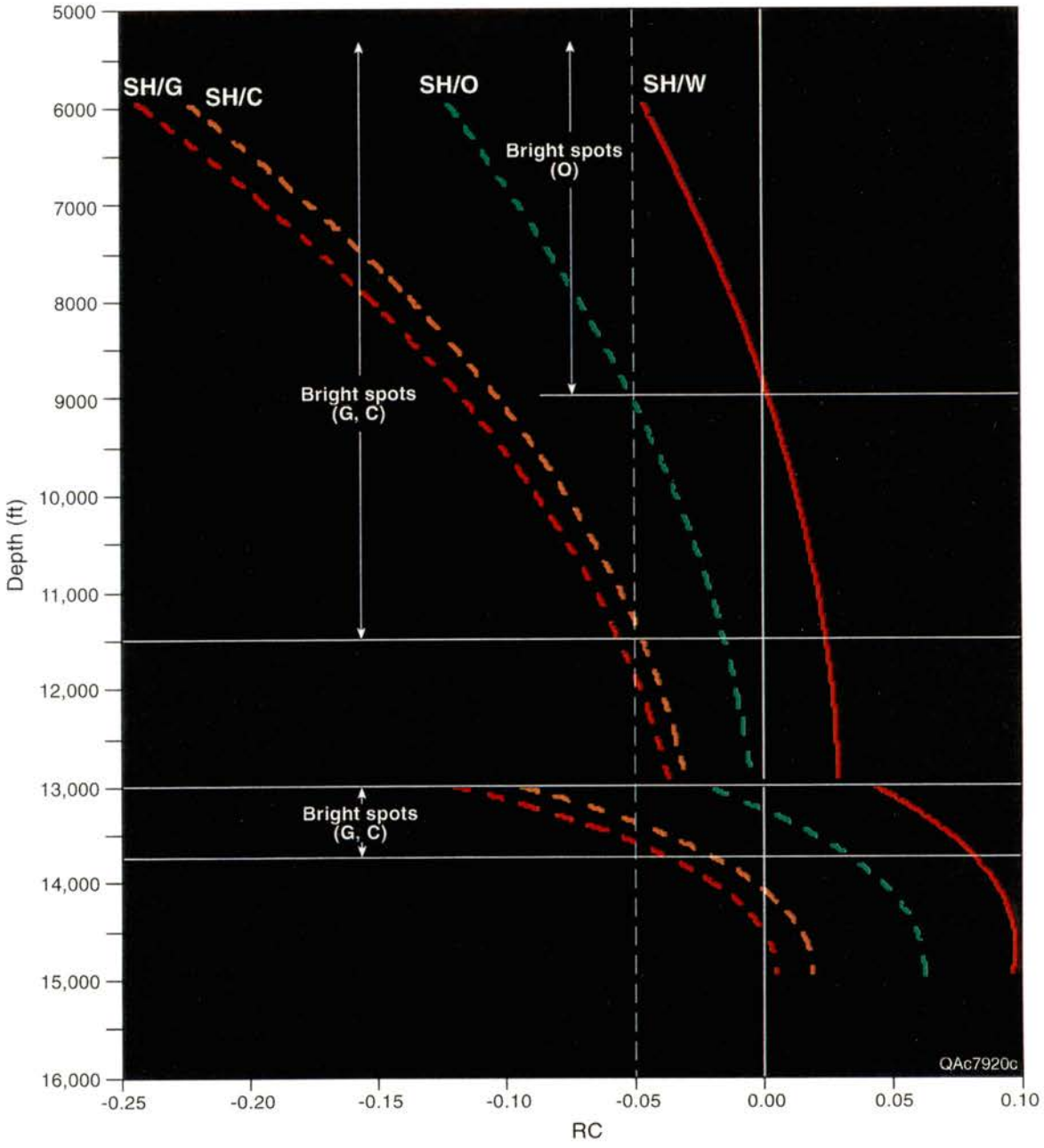

Figure 83. Reflection coefficient (RC) trend lines related to brine-saturated sandstones and hydrocarbon-saturated sandstones. SH/W=brine-saturated sandstone below shale, SH/O=oil-saturated sandstone below shale, SH/C=condensate-saturated sandstone below shale, and SH/G=gas-saturated sandstone below shale.

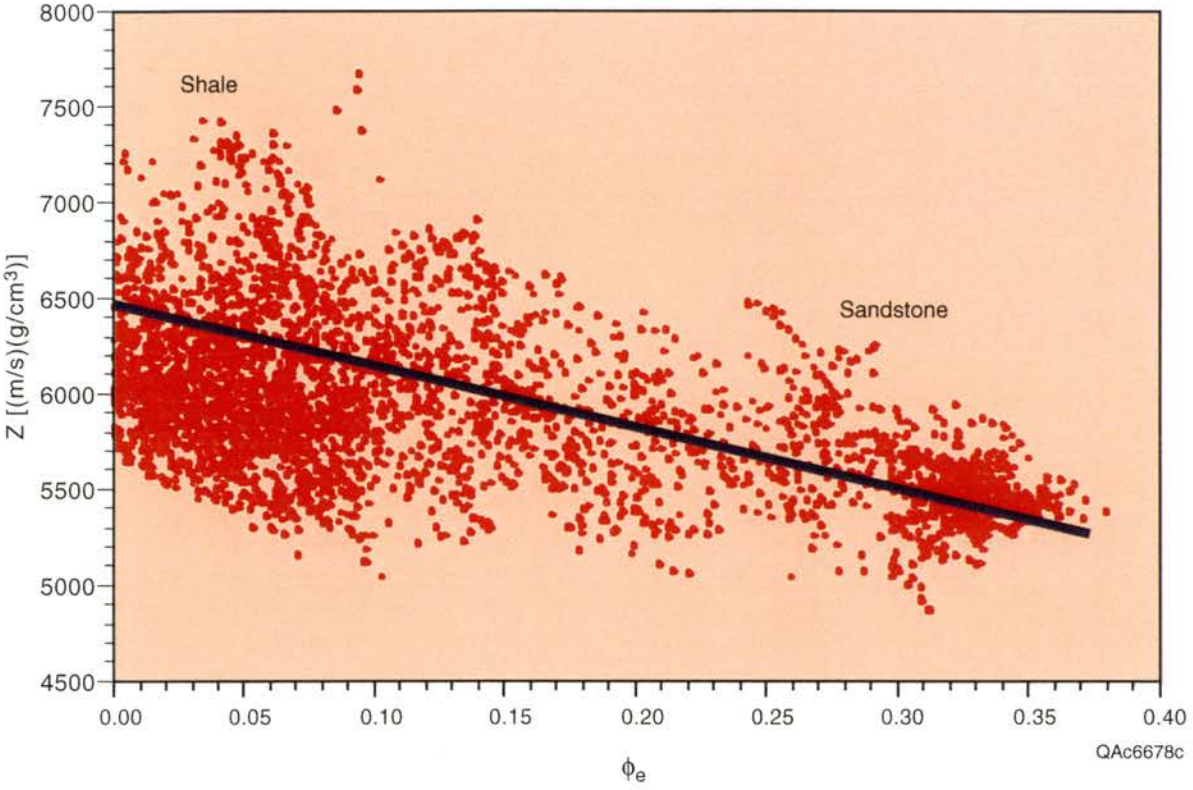

Figure 84. Acoustic impedance as an indicator of lithology (effective porosity). Data are calculated from sonic, density, and GR logs from the 2,000- to 2,700-m section (upper Miocene) in a Starfak well.

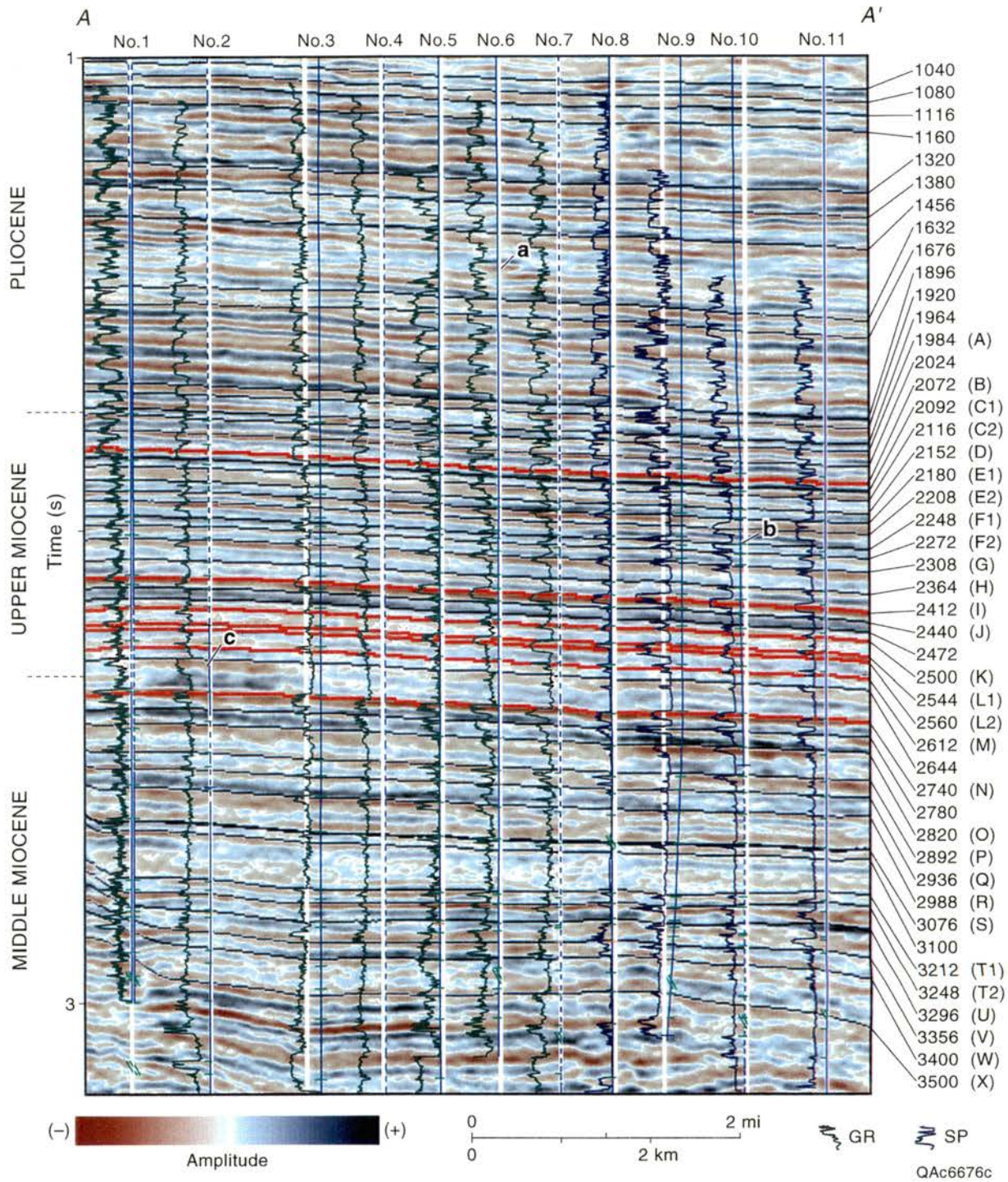

Figure 85. Cross section A–A′ in Starfak field showing well-to-seismic correlation in two-way traveltime. See figure 86a for section location. Stratal slices are numerically ordered on the right according to increasing geologic time (no scale). Texaco-designated reservoir units are identified by letters in parentheses. a, b, c = lenticular sandstones tied to patchy seismic events.

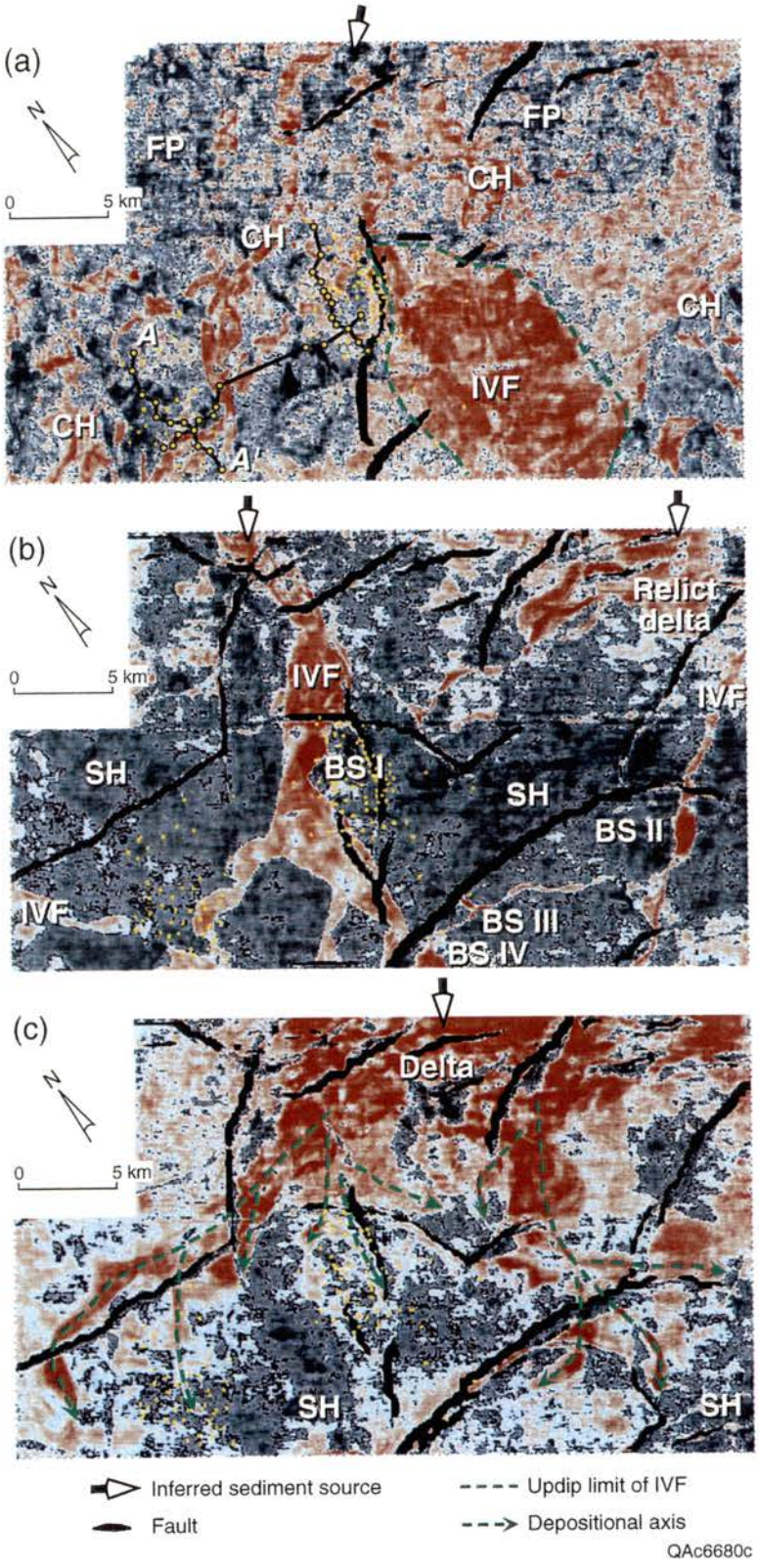

Figure 86. Amplitude stratal slices showing (a) a Pliocene coastal plain, (b) upper Miocene incised valley fill, and (c) an upper Miocene highstand-shelf delta system. See figure 33 for stratigraphic position. CH-channel; FP=floodplain; IVF=incised valley fill; SH=shelf; BS I-IV=bright spots. Cross section A–A′ shown in figure 85.

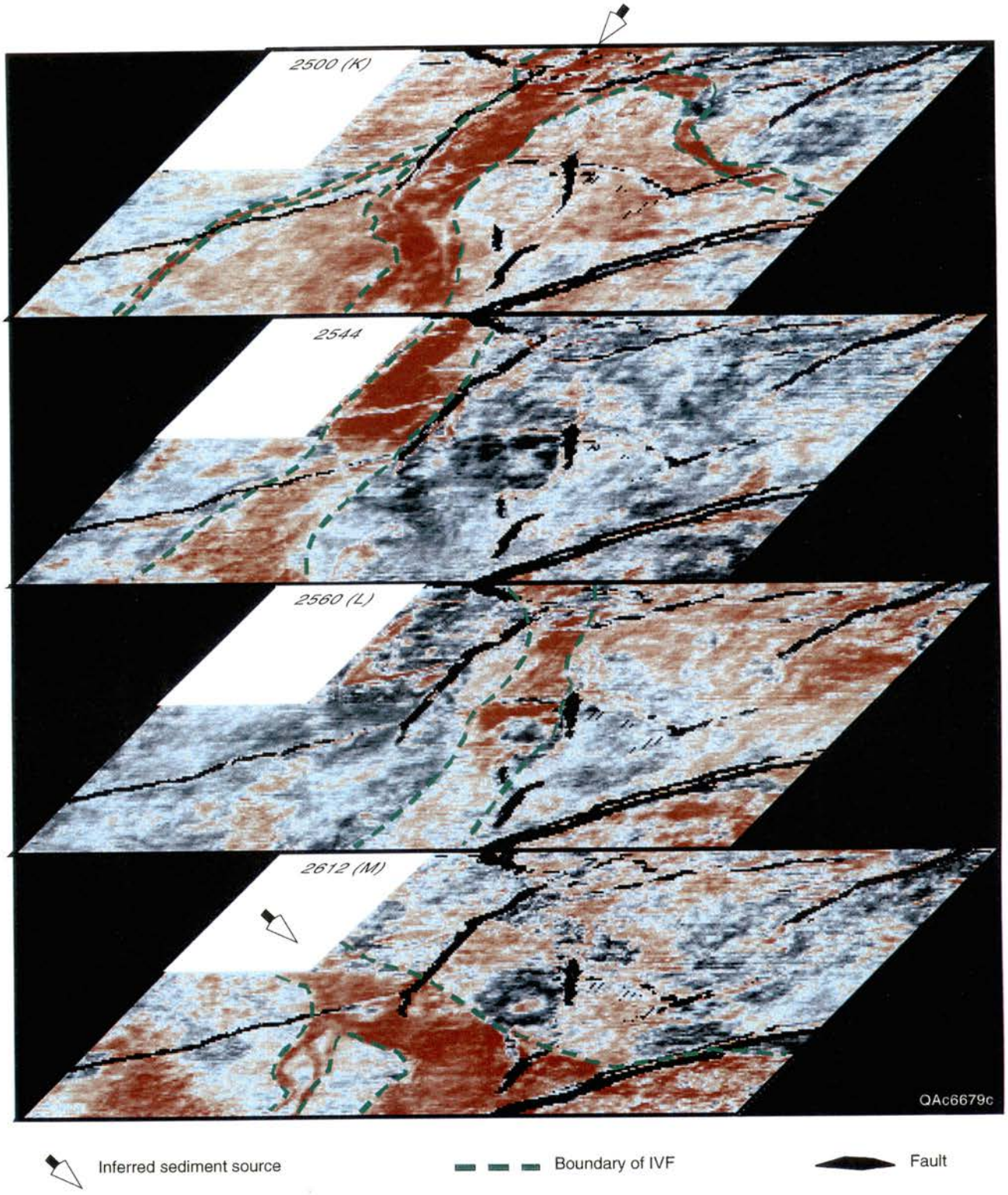

Figure 87. A four-stratal-slice series showing the migration of IVF's in geologic time (M-K sands). See figure 33 for stratigraphic position. Vertical axis not on scale.

Table 1. Distribution of reserves and production data by geologic age for the Gulf of Mexico, showing the Miocene-age reservoir resources leading all categories, including remaining proved reserves.

Age	Original proved reserves (percent)	Cumulative production (percent)	Remaining proved reserves (percent)
Pleistocene	40	41	37
Pliocene	16	16	16
Miocene	***42***	***43***	***41***
Oligocene, Cretaceous, and Jurassic	2	0	6

From Lore and others (1999)
QAc7819c

Table 2. Texaco-designated sandstone-body reservoirs in Starfak and Tiger Shoal fields.

Starfak	Tiger Shoal
M	A Stray
N	B upper
P	Big B-4
T-1	Big C
T-1A	C
T-1B	D
T-2A	E
U	E-1
W	E-2
X	F
Y	G
12000 A	G Stray
ROB L-1	H
ROB L-2	I
ROB L-5	J
	K-1
	K-2
	L
	M upper
	M-1
	M-1 lower
	M-2
	M-2 lower
	N
	N-1
	N-1 middle
	N-1 upper
	N-2
	N-3
	O
	O-2
	P
	P-2
	Q-1
	Q-2
	R
	S-2
	T-1
	T-2
	U
	V
	W
	X-1
	Y
	Z-1
	Z-2
	12000 B

Table 3. Cumulative gas (MMcf) production (through 7/1/00) from all sandstone-body reservoirs in Starfak and Tiger Shoal fields.

Reservoir	Starfak	Tiger Shoal	Total
A		37.4	37.4
B		12,237.0	12,237.0
C		54,552.9	54,552.9
D		9,427.0	9,427.0
E		50,707.7	50,707.7
F		22,102.0	22,102.0
G		3,332.9	3,332.9
H		5,064.4	5,064.4
I		1,768.9	1,768.9
J		19,260.7	19,260.7
K		26,427.4	26,427.4
L		204,499.8	204,499.8
M	1,002.9	83,491.3	84,494.2
N	11,360.0	210,210.1	221,570.1
O		72,636.9	72,636.9
P	121.5	9,153.8	9,275.3
Q		120,471.2	120,471.2
R		10,768.3	10,768.3
S		6,362.7	6,362.7
T1	28,105.5	918,215.3	946,320.8
T2	1,661.0	42,289.5	43,950.5
U	34,319.4	10,845.7	45,165.0
V		17,896.3	17,896.3
W	2,123.8	640.7	2,764.5
X	11,569.8	58.5	11,628.3
Y	17,165.0	492,211.9	509,376.9
12000A	130,768.8		130,768.8
12000B		292.5	292.5
ROB L1	9,477.5		9,477.5
ROB L2	109,312.7		109,312.7
ROB L5	244.1		244.1
TOTAL	357,231.9	2,404,962.5	2,762,194.4

Table 4. Cumulative oil (Mbbl) production (through 7/1/00) from all sandstone-body reservoirs in Starfak and Tiger Shoal fields.

Reservoir	Starfak	Tiger Shoal	Total
A		0.0	0.0
B		6.6	6.6
C		130.3	130.3
D		20.7	20.7
E		161.7	161.7
F		94.2	94.2
G		7.9	7.9
H		22.9	22.9
I		5.0	5.0
J		57.5	57.5
K		106.0	106.0
L		659.6	659.6
M	4.44	350.0	354.5
N	18.55	9,012.4	9,030.9
O		301.2	301.2
P		49.4	49.4
Q		594.1	594.1
R		48.3	48.3
S		35.7	35.7
T1		5,022.5	5,022.5
T2	601.11	357.3	958.4
U	876.49	28.9	905.4
V	4,949.45	2,058.2	7,007.6
W	50.23	4.3	54.5
X	91.42		91.4
Y	50.99	4,692.5	4,743.5
12000A	1,235.73		1,235.7
12000B		250.2	250.2
ROB L1	504.48		504.5
ROB L2	6,531.73		6,531.7
ROB L5	106.3		106.3
TOTAL	15,020.92	24,077.2	39,098.2

Table 5. Total hydrocarbons (MMboe) produced (through 7/1/00) from all sandstone-body reservoirs in Starfak and Tiger Shoal fields. For conversion of gas-volume units into barrels of oil equivalent (boe), we used the standard equation, 1 Mcf = 5.62 boe.

Reservoir	Starfak	Tiger Shoal	Total
A		0.210	0.21
B		68.772	68.77
C		306.587	306.59
D		52.980	52.98
E		284.977	284.98
F		124.213	124.21
G		18.731	18.73
H		28.462	28.46
I		9.941	9.94
J		108.245	108.25
K		148.522	148.52
L		1,149.289	1,149.29
M	5.636	469.221	474.86
N	63.843	1,181.380	1,245.22
O		408.219	408.22
P	0.683	51.444	52.13
Q		677.048	677.05
R		60.518	60.52
S		35.758	35.76
T1	157.953	5,160.370	5,318.32
T2	9.335	237.667	247.00
U	192.875	60.953	253.83
V		100.577	100.58
W	11.936	3.601	15.54
X	65.022	0.329	65.35
Y	96.467	2,766.231	2,862.70
12000A	734.920		734.92
12000B		1.644	1.64
ROB L1	53.264		53.26
ROB L2	614.338		614.34
ROB L5	1.372		1.37
TOTAL	2,007.643	13,515.889	15,523.53

Table 6. Cumulative gas (MMcf) production (through 7/1/00) from all sandstone-body reservoirs within the third-order lowstand systems tracts in Starfak and Tiger Shoal fields. The category "All others" represents cumulative production from all reservoirs that do not occur in the 10 third-order lowstand systems tracts.

Reservoir	Starfak	Tiger Shoal	Total
C		54,552.87	54,552.87
F-G		25,434.81	25,434.81
I		1,768.91	1,768.91
L-M	1,002.87	287,991.08	288,993.95
N	11,360.01	210,210.05	221,570.06
P-R	121.49	140,393.32	140,514.81
T1-V	64,085.83	989,246.69	1,053,332.52
X-Y	28,734.75	492,270.38	521,005.13
12A-B	130,768.8	292.54	131,061.29
ROB L1-5	119,034.4		119,034.38
All others	2,123.82	202,801.82	204,925.64
TOTAL	357,231.9	2,404,962.47	2,762,194.37

Table 7. Cumulative oil (Mbbl) production (through 7/1/00) from all sandstone-body reservoirs within the third-order lowstand systems tracts in Starfak and Tiger Shoal fields. The category "All others" represents cumulative production from all reservoirs that do not occur in the 10 third-order lowstand systems tracts.

Reservoir	Starfak	Tiger Shoal	Total
C		130.31	130.31
F-G		102.10	102.1
I		4.96	4.96
L-M	4.44	1,009.62	1,014.06
N	18.55	9,012.35	9,030.9
P-R		691.73	691.73
T1-V	6,427.05	7,466.87	13,893.92
X-Y	142.41	4,692.51	4,834.92
12A-B	1,235.73	250.22	1,485.95
ROB L1-5	7,142.51		7,142.51
All others	50.23	716.55	766.78
TOTAL	15,020.92	24,077.22	39,098.14

Table 8. Total hydrocarbons (MMboe) produced (through 7/1/00) from all sandstone-body reservoirs within the third-order lowstand systems tracts in Starfak and Tiger Shoal fields. The category "All others" represents cumulative production from all reservoirs that do not occur in the 10 third-order lowstand systems tracts. For conversion of gas-volume units into barrels of oil equivalent (boe), we used the standard equation, 1 Mcf = 5.62 boe.

Reservoir	Starfak	Tiger Shoal	Total
C		306.587	306.587
F-G		142.944	142.944
I		9.941	9.941
L-M	5.636	1,618.510	1,624.146
N	63.843	1,181.380	1,245.224
P-R	0.683	789.010	789.693
T1-V	360.162	5,559.566	5,919.729
X-Y	161.489	2,766.560	2,928.049
12A-B	734.920	1.644	736.564
ROB L1-5	668.973		668.973
All others	11.936	1,139.746	1,151.682
TOTAL	2,007.643	13,515.889	15,523.532

Table 9. Hydrocarbon properties from production data.

γ_{gas}= 0.6 (dry gas)
$\gamma_{condensate}$= 1.2 (treated as heavy gas)
γ_{oil}= 30° API

For depth ranging from 6,000 ft to13,000 ft:

$\rho_{gas} = -0.07392+0.004372T-0.00001804T^2$
$k_{gas} = 10.602T-199.64$
$\rho_{condensate} = -0.20672+0.012518T-0.000066582T^2$
$k_{condensate} = -964.35+57.72T-0.2733T^2$
$\rho_{oil} = 0.81503-0.0019885T$
$k_{oil} = 13,798-31.936T$

For depth ranging from 13,000 ft to 15,000 ft:

$\rho_{gas} = 0.19347+0.00051093T$
$k_{gas} = 947.57+4.8926T$
$\rho_{condensate} = 0.36345+0.00059204T$
$k_{condensate} = 6857.4-53.464T+0.1981T^2$
$\rho_{oil} = 0.7032-0.0014527T$
$k_{oil} = -8,682+330.88T-1.2921T^2$

where T is the formation temperature (°C), and

$T = 5/9*[56+0.0139*\text{depth (ft)}-32]$.

Table 10: Brine and rock properties.

Material	(g/cc)	K(GPa)
Brine	1.1	3.00
Quartz	2.65	36.47
Clay		21.42